



University of
Nottingham

UK | CHINA | MALAYSIA

New approaches to study canine and equine influenza A virus

Hope Leverett

Thesis submitted to the University of Nottingham for the
degree of Doctor of Philosophy, September 2024

Primary supervisor: Professor Janet Daly


Secondary supervisors: Dr Stephen Dunham and Dr

Toshana Foster

Declaration

I declare that the work presented in this thesis has been written by myself and not previously been submitted for any other degree. All work described was performed by me unless it is stated otherwise.

Name: Hope Leverett

Signature: 

Date: 27th September 2024

Abstract

Equine and canine influenza A viruses (IAV) have been isolated for the past 70 and 25 years, respectively. Currently, a single subtype of equine influenza A virus (H3N8) circulates. This subtype jumped species to canines in the late 1990s in the US and circulated until 2016. In 2004, an avian H3N2 subtype virus was transmitted to dogs and spread into the US where it continues to circulate. Limited research is ongoing to further understand these two neglected viruses although within the research community, new approaches are more often applied to emerging and human influenza viruses. In this research, how novel approaches can be used to generate reagents and further develop the understanding of these two viruses was investigated.

Next generation phage display was used to generate variable heavy chain (VHH) antibodies that bound to recombinant equine IAVs (eIAV) with haemagglutinin (HA) surface glycoproteins from isolates representing the two current circulating clades of equine H3N8 subtype (Florida clade 1 and clade 2). The analysis highlighted 70 potential binders and a trial number of 10 were expressed using bacterial and mammalian expression systems to produce maltose binding protein (MBP) and fragment crystallizable (Fc) fused VHH antibodies. Three of each Fc and MBP fused VHH were successfully generated. One Fc fused antibody selectively bound influenza viruses in ELISA but did not differentiate between the two clades. Nonetheless, the VHH could have

other applications in research, diagnosis or treatment of equine influenza.

Three cell lines (equine E. derm and extEqFL and canine DH82 α) were explored for suitability for researching equine and canine IAVs by titrating viruses by 50% tissue culture infectious dose and viral replication kinetics by M gene RT-qPCR. Equine and canine IAVs primarily bind to α 2,3 sialic acids (SA) so receptor staining was performed to confirm their presence on the cell lines. Generation of recombinant reverse genetics virus was undertaken to obtain the canine H3N2 subtype. Investigation into the innate immune response was completed using RNA sequencing and RT-qPCR for species specific cytokines. The extEqFL and E. derm cell lines were rejected as potential candidates due to poor lectin staining, viral replication and lack of cytokine expression. The DH82 α cell line demonstrated efficient viral replication and appropriate lectin staining. The RNA sequencing data highlighted 21 genes from the IAV pathway indicating expression with variations seen between the 6- and 24-hour samples. Cytokine responses were lower than anticipated and not all expected genes were upregulated post-infection with virus.

Receptor specificity assays were applied to determine whether changes in the HA of eIAVs aided transmission into dogs. This was investigated using solid phase binding assays and biolayer interferometry. Equine IAV pseudotype viruses (PV) with mutations in the HA were generated

however receptor binding could not be investigated with either method because of low viral titres and non-specific binding. Attempts to rescue viruses with mutated HA proteins by reverse genetics that could produce higher titres were not successful. Pseudotyped viruses were used to confirm that MDCK, DH82 α and E. derm cells did not permit virus entry with equine or canine cells.

This thesis outlines how new approaches were developed and successfully utilised to study canine and equine influenza A viruses. The generation of antibodies using next generation phage display is a promising concept, and DH82 α cells are identified as a potentially useful cell line for IAV research.

Acknowledgement

First, I want to thank Professor Janet Daly who has been the most amazing and supportive supervisor I could have ever asked for. Her never-ending patience for my stupid questions and her constant guidance has been immensely helpful over the past 4 years. Janet has encouraged me and supported me in becoming a better scientist and improving and developing my abilities to teach others. This has given me the opportunity to work with a range of undergraduates, some of who I am now grateful to be able to call colleagues.

Next up I would like to thank my secondary supervisors Dr Stephen Dunham and Dr Toshana Foster. Both of you have been there for me across the 4 years of my PhD, always happy to help or just be a listening ear and for that I am very grateful. I would also like to thank Dr Kevin Gough, for his guidance and support with the VHH chapter. I am also grateful to all the collaborators who provided reagents or protocols which were instrumental in several sections of this PhD.

I would like to thoroughly thank Dr Kieran Pitchers who I would not have got through my VHH chapter without. Kieran, you have taught me so much and supported me throughout a large proportion of my experiment setbacks.

Further thanks to Dr Karina Bingham, my desk and lab partner. I am so grateful that you became one of Janet's post docs, you have been so

amazing and supportive and have also become an incredible friend of mine during the past few years. We may thoroughly distract each other but I cannot imagine being sat with and getting to work with anyone else.

There is such a long list of people I could thank for their support and friendship over the past 4 years, so I won't include everyone. I would like to highlight; Dr Shannon Ward, Dr Meshach Mania, Dr Ola Elbohy, Dr Olaolu Tosin Olufemi, Askar Alshammari, the rest of A43 lab, Charlotte Parker, Jon Miles and Ashleigh Smith. You have all contributed to making the last 4 years, a little less stressful and a lot more enjoyable.

I would like to thank my parents and siblings for their constant support and encouragement. I am sure you are all relieved that I did not ask you to proofread my thesis, after having done so for my undergraduate dissertation. I would also like to thank Arona Jones for their support and patience whilst I completed this PhD, especially when I was getting upset with R's idiosyncrasies.

I am so grateful for the opportunity to complete this PhD and for the amazing experiences along the journey.

Abstract	3
Acknowledgement	6
Table of Figures	14
Table of Tables	17
Table of Appendices	18
Abbreviations:	19
1 Introduction:	22
1.1 Influenza A structure	24
1.2 Influenza A virus replication cycle	27
1.3 Haemagglutinin glycoprotein.....	32
1.4 Sialic acid binding	34
1.5 Neuraminidase glycoprotein.....	36
1.6 Immune response	38
1.6.1 Innate immunity	38
1.6.2 Adaptive immunity	39
1.7 Antigenic changes	41
1.7.1 Antigenic drift.....	41
1.7.2 Antigenic shift.....	42
1.8 Equine influenza	42
1.8.1 The disease.....	42
1.8.2 History and impact of equine influenza.....	43
1.8.3 Equine subtypes and lineages.....	44
1.8.4 Equine Immune response	46
1.9 Vaccines	47
1.10 Interspecies transmission.....	48
1.11 Interspecies transmission of equine influenza to dogs.....	50
1.12 Canine H3N8 lineage.....	52
1.13 Canine H3N8 mutations.....	53
1.14 Interspecies transmission of avian IAV to dogs	54
1.15 Canine H3N2 lineage.....	56
1.16 Canine H3N2 mutations.....	57
1.16.1 Sialic acid receptors in equine and canine cells	58

1.17 Potential for zoonotic transmission of influenza A viruses from companion animals	61
1.18 Current limitations to understanding interspecies transmission	63
1.19 Aims:	65
2 General Methods	66
2.1 Cell culture	66
2.1.1 Cell lines.....	66
2.1.2 Sub-culturing adherent cells	67
2.1.3 Counting cells.....	67
2.1.4 Freezing and thawing cells	68
2.1.5 Acid etched coverslips.....	69
2.2 Virology methods.....	69
2.2.1 Viruses	69
2.2.2 Growth of virus in embryonated hen's eggs	71
2.2.3 Ultracentrifugation of viruses	71
2.2.4 Sucrose gradient ultracentrifugation	72
2.2.5 Pseudotype viruses	73
2.2.6 Pseudotype virus titration	74
2.2.7 Reverse genetics.....	75
2.2.8 Haemagglutination test.....	76
2.2.9 Haemagglutination inhibition test.....	77
2.2.10 Tissue culture infectious dose 50%	78
2.2.11 Infection of cells with influenza A virus	79
2.2.12 Anti-NP ELISA.....	80
2.2.13 Receptor specificity assay	80
2.2.14 Biolayer interferometry	82
2.3 Molecular biology methods.....	84
2.3.1 Plasmid transformation.....	84
2.3.2 Plasmid DNA purification and quantification.....	85
2.3.3 RNA extraction	86
2.3.4 M gene RT-qPCR.....	86
2.3.5 Reverse transcription	87

2.3.6 Quantitative polymerase chain reaction	88
2.3.7 SDS-PAGE.....	89
2.3.8 Coomassie staining	90
2.3.9 Western blot	90
2.3.10 Bradford protein assay	91
2.4 Computational methods	92
2.4.1 Phylogenetic trees.....	92
2.4.2 Statistical analysis	92
3 Development of single domain antibodies (sdAb) for differentiation between Florida clades of equine influenza A virus	95
3.1 Introduction	95
3.1.1 Current methods used for characterising equine influenza A virus	99
3.1.2 Antibody phage display	100
3.1.3 Project background	103
3.1.4 Aim	104
3.1.5 Objectives:.....	105
3.2 Methods	105
3.2.1 Next generation phage display analysis	105
3.2.2 Expression of soluble VHH antibodies	109
3.2.3 MBP VHH ELISA.....	119
3.2.4 Haemagglutination inhibition test.....	120
3.2.5 Expression of Fc fusion VHH antibodies in mammalian cell culture	121
3.2.6 Fc Fusion VHH ELISA.....	124
3.2.7 Western blot of transfected cells	125
3.2.8 ELISA analysis using GraphPad Prism ... Error! Bookmark not defined.	
3.3 Results	127
3.3.1 NGS data analysis.....	127
3.3.2 Highest frequency analysis.....	129
3.3.3 Pilot study.....	130
3.3.4 Inverse PCR	132

3.3.5 Trial protein expression	134
3.3.6 Protein expression of retransformed samples	135
3.3.7 Protein purification of retransformed samples	136
3.3.8 VHH ELISA.....	140
3.3.9 Haemagglutination inhibition test.....	143
3.3.10 Anti-beta lactamase in pFUSE 6-well plate transfection.....	143
3.3.11 Inverse PCR VHH B, C and A in pFUSE	146
3.3.12 Transfection of anti-beta lactamase, VHH A, B and C as Fc fused VHH.....	148
3.3.13 Fc fusion VHH ELISA	149
3.3.14 Western blot of transfected cells	154
3.4 Discussion.....	155
4 Exploring the suitability of canine and equine cell lines in the investigation of the innate immune response and host interactions of influenza A viruses	163
4.1 Introduction	163
4.1.1 Primary cell and <i>ex vivo</i> culture.....	164
4.1.2 Explanted tracheal cultures	165
4.1.3 Madin-Darby canine kidney cells.....	167
4.1.4 DH82 α cells	168
4.1.5 Alternate canine cells	169
4.1.6 Equine cell lines	170
4.1.7 Human embryonic kidney 293T cells.....	172
4.1.8 Requirements of a cell line for studying canine and equine influenza A virus.....	173
4.1.9 Aim	173
4.1.10 Objectives.....	173
4.2 Methods	174
4.2.1 Cell lines.....	174
4.2.2 Viruses	174
4.2.3 Reverse genetics.....	174
4.2.4 Lectin staining	175
4.2.5 50% Tissue culture infectious dose (TCID ₅₀).....	176

4.2.6 Viral replication kinetics	176
4.2.7 Infection with influenza A virus	176
4.2.8 M gene and cytokine mRNA quantification by RT-qPCR	177
4.2.9 RNA sequencing	177
4.2.10 RNA sequencing quality and assembly	178
4.2.11 Differential expression and pathway analysis	178
4.3 Results	179
4.3.1 Lectin staining	179
4.3.2 Generation of canine H3N2 virus by reverse genetics	183
4.3.3 Cytokine response experiment	183
4.3.4 RNA sequencing experiment	188
4.4 Discussion	206
5 Potential influence of receptor binding changes on transmission of equine influenza A virus to dogs ..	219
5.1 Introduction	219
5.1.1 Canine and equine influenza receptor binding	222
5.1.2 Current methods to study receptor binding	223
5.1.3 Equine influenza pseudotype viruses	226
5.1.4 Aim	229
5.1.5 Objectives:	230
5.2 Materials and methods	230
5.2.1 Prediction of mutational effects	230
5.2.2 Molecular modelling	231
5.2.3 Cell lines	231
5.2.4 Viruses	231
5.2.5 Plasmid transformation	232
5.2.6 Plasmid DNA purification and quantification	232
5.2.7 Reverse genetics	233
5.2.8 Pseudotyped viruses	233
5.2.9 Pseudotype titration	234
5.2.10 Sucrose gradient ultracentrifugation	234
5.2.11 Receptor specificity assay	234
5.2.12 Anti-NP ELISA	235
5.2.13 Bradford protein assay	236

5.2.14 Biolayer interferometry	236
5.3 Results	240
5.3.1 Predicted effects of mutations on the protein function and structure	240
5.3.2 Reverse genetics & HA test.....	243
5.3.3 Pseudotype viruses	243
5.3.4 Receptor specificity assay results	248
5.3.5 Biolayer interferometry	249
5.4 Discussion.....	255
6 Conclusion.....	264
7 References.....	271
8 Appendix.....	326

Table of Figures

Figure 1.1. Influenza A virus naming system.....	27
Figure 1.2. Daisy-chain model.....	30
Figure 1.3. A breakdown of the influenza replication life cycle.....	31
Figure 1.4. H3 glycoprotein.	33
Figure 1.5. Illustration of the structures of α 2,3-Gal and α 2,6-Gal sialic acid linkages.....	36
Figure 2.1 Haemagglutination test.	77
Figure 3.1. Phylogenetic tree of the H3N8 HA1 sequences of equine influenza viruses.....	98
Figure 3.2. Types of antibody format used in phage display.	102
Figure 3.3. A breakdown of the phage display experiments.....	104
Figure 3.4. Flow diagram of expression of soluble VHH.....	110
Figure 3.5. Primer design:	111
Figure 3.6. Vector map for pMAL-c5x.	113
Figure 3.7. MBP fused VHH ELISA.....	120
Figure 3.8 pFUSE +ss vector map.....	122
Figure 3.9. Agarose gel of the first nine sequences with bands produced around 6 kb.....	133
Figure 3.10. Coomassie staining of trial samples after induction by IPTG.....	135
Figure 3.11. Coomassie staining of retransformed VHH B, C and A prior to and during induction.	136
Figure 3.12. Coomassie staining of purified VHH A.	137
Figure 3.13. Coomassie staining of purified VHH B.	138
Figure 3.14. Coomassie staining of purified VHH C.	139
Figure 3.15. MBP VHH ELISA against rFC2.....	141
Figure 3.16. MBP VHH ELISA against rFC1 and rFC2.	142
Figure 3.17. Coomassie stain of concentrated and purified anti- beta lactamase Fc.	144
Figure 3.18. Concentrated anti-beta lactamase Fc western blot.	145
Figure 3.19. Non-concentrated anti-beta lactamase Fc western blot.	146

Figure 3.20. Agarose gel following inverse PCR with pFUSE vector.	147
Figure 3.21. Western blots of anti-beta lactamase VHH and pFUSE VHH A, B and C from 10 cm dishes.	148
Figure 3.22. Fc fusion VHH ELISA against rFC1.	151
Figure 3.23. Fc fusion VHH ELISA against rFC1 and two additional eIAV.	152
Figure 3.24. Fc fusion VHH ELISA against rFC1, human H1N1 IAV and Schmallerberg virus.....	153
Figure 3.25. 293T/17 cells transfected with HA (H3N2), HA (H1N1), NA (H1N1) and NP (H1N1) expressing plasmids.	154
Figure 4.1. Receptor staining of the five cell lines of interest.	181
Figure 4.2. Viral replication kinetics of cIAV H3N2 and H3N8 in DH82α cells.....	186
Figure 4.3. Viral replication kinetics of cIAV H3N2 and H3N8 in extEqFL cells.	187
Figure 4.4. M gene standard curve for influenza virus.....	189
Figure 4.5. Principal component analysis (PCA) plot.....	191
Figure 4.6. Venn diagram of the differentially expressed genes.	192
Figure 4.7. Enhanced volcano plots of the two time points.....	194
Figure 4.8. Heat maps for the top 20 differentially expressed genes.	196
Figure 4.9. A dot plot of the top 20 differentially expressed genes.	197
Figure 4.10. Dot plot of the biological processes (BP) at 24 hours.	199
Figure 4.11. Dot plot of the molecular function (MF) at 24 hours.....	200
Figure 4.12. KEGG pathway analysis of the influenza A virus pathway at 24 hours post infection.	202
Figure 4.13. KEGG pathway analysis of the NOD-like receptor signalling pathway at 24 hours post infection.....	204
Figure 4.14. Cytokine response of TNF-α in DH82α cells infected with cIAV H3N2 and H3N8 at 24 hours.	205

Figure 4.15. Cytokine response of IFN- β in DH82 α cells infected with cIAV H3N2 and H3N8 at 24 hours.	206
Figure 5.1. Receptor binding sites on the H3 glycoprotein.	222
Figure 5.2. Biolayer interferometry.	225
Figure 5.3. HA alignment.	227
Figure 5.4. 3D structure of the HA glycoprotein as a trimer.	228
Figure 5.5. The titres for pseudotype viruses of Nm/1/93 and N/5/03.....	229
Figure 5.6. Receptor binding assay.	235
Figure 5.7. Mock graph of results produced from the qualitative assay by BLI.	237
Figure 5.8. Mock graph of results produced from the quantitative assay by BLI.	238
Figure 5.9. Mock graph of processed qualitative assay.....	239
Figure 5.10. Mock graph of processed quantitative assay.	239
Figure 5.11. N/1/93 3D protein structures with mutations.....	242
Figure 5.12. N/5/03 3D protein structures with mutations.....	243
Figure 5.13. Pseudotype titration of N/1/93 pseudotypes.	245
Figure 5.14. Pseudotype titration of N/5/03 pseudotypes.	246
Figure 5.15. Pseudotype virus titres in four different target cells.	247
Figure 5.16. Receptor specificity assay- receptor binding of N/5/03.	248
Figure 5.17. Receptor specificity assay- receptor binding of PR8.	249
Figure 5.18. Biolayer interferometry- receptor binding of Sussex/89.....	250
Figure 5.19. Biolayer interferometry- receptor binding of concentrated H5 pseudotype virus.....	251
Figure 5.20. Biolayer interferometry- receptor binding of Newmarket/1/93 (A) and Newmarket/5/03 (B).	254
Figure 5.21. Biolayer interferometry - receptor binding of cIAV H3N2 reverse genetics virus.	255

Table of Tables

Table 1.1. Genomic segments of influenza A virus and the major proteins encoded.	25
Table 1.2. The role of proteins secreted during the innate immune response.	39
Table 2.1 Cell lines.	66
Table 2.2. Wild type viruses.....	70
Table 2.3. Recombinant viruses.....	70
Table 2.4. Pseudotype virus transfection reagents.	74
Table 2.5. The M gene primer and probe used for M gene RT-qPCR.	87
Table 2.6. Primers used for qPCR for the target and reference genes used.....	89
Table 3.1. Sequences identified based on Z-score ≥ 10	128
Table 3.2. Highest frequency sequences.	130
Table 3.3. Trial experiment sequences and initial primers.	131
Table 3.4. The second round of primers designed.....	132
Table 3.5. The ID given to the three successful sequences VHH A-C.....	134
Table 3.6. Protein concentration of the MBP VHH.....	140
Table 3.7. Protein concentration of Fc fusion VHH.	149
Table 4.1. TCID ₅₀ /ml for each virus and cell line.	183
Table 4.2. RNA quantification.....	184
Table 4.3. RNA extraction results for RNA sequencing samples.....	188
Table 4.4. M-gene RT-qPCR results.	189
Table 4.5. Differentially expressed genes in DH82 α cells.	192
Table 5.1. HA plasmids from A/equine/Newmarket/93 and A/equine/Newmarket/5/03 with mutations introduced.	232
Table 5.2. Neuraminidase options for pseudotype viruses.	233
Table 5.3. PolyPhen-2 score results.	240
Table 5.4. SIFT results for each strain with mutations.....	241

Table of Appendices

Appendix 1. Buffers and media.	326
Appendix 2. Ion torrent barcode sequences.	329
Appendix 3. Scripts run for analysis of next generation sequencing data.	331
Appendix 4. Sequencing of inserted VHH sequence using MalEForward and MalERreverse primers.	335
Appendix 5. MBP VHH ELISA against rFC1 and rFC2 with ferret antisera diluted 1:100.	337
Appendix 6. PIP reflection statement.	338

Abbreviations:

aIAV	Avian influenza A virus
APC	Antigen presenting cells
ATCC	America type culture collection
BA	Bovine albumin
BIC	Bayesian information criteria
BLI	Biolayer interferometry
BP	Biological processes
BSL	Biosafety level
CC	Cellular component
CCL	Chemokine ligand
CDR3	Complementarity determining region 3
CD4+	T helper cells
CD8+	Cytotoxic T cells
CHO	Chinese hamster ovary cells
cIAV	Canine influenza A virus
CMAH	Cytidine monophospho-N-acetylneuraminic acid hydroxylase
CPE	Cytopathic effect
CRM1	Chromosome region maintenance 1
cRNA	Complementary RNA
Ct	Cycle threshold
CV	Column volumes
DEFRA	Department for Environmental Food and Rural Affairs
DEG	Differentially expressed genes
DMEM	Dulbecco's Modified Eagle Medium
E. derm	Equine dermal cells
eIAV	Equine influenza A virus
EMEM	Eagle's minimum essential medium
EVA	Equine viral arteritis
extEqFL	Equine lung cell line
F3	Framework 3
F4	Framework 4
Fab	Fragment antigen-binding
FBS	Fetal bovine serum
Fc	Fragment crystallizable
FC1	Florida clade 1
FC2	Florida clade 2
FFU	Focus-forming unit
FHK	Fetal horse kidney cells
GAPDH	Glyceraldehyde-3-phosphate dehydrogenase
GO	Gene ontology

HA	Haemagglutinin
HCl	Hydrochloric acid
HEF	Haemagglutinin-esterase-fusion
HEK	Human embryonic kidney
HI	Haemagglutination inhibition
HMBS	Hydroxymethylbilane synthase
HRP	Horseradish peroxidase
IAV	Influenza A virus
IBV	Influenza B virus
ICTV	International Committee on Taxonomy of Viruses
ICV	Influenza C virus
IDV	Influenza D virus
IFI44	Interferon-induced protein 44
IFITM	Interferon-induced transmembrane protein
IFN	Interferon
IFN- α	Interferon alpha
IL	Interleukin
IMS	Industrial methylated spirits
IPTG	Isopropyl β -D-1-thiogalactopyranoside
KEGG	Kyoto encyclopedia of genes and genomes
LncRNA	Long non-coding RNA
LPS	Lipopolysaccharide
LTB4	Leukotriene B4
M	Matrix
mAb	Monoclonal antibodies
MAL	<i>Maackia amurensis</i>
MBP	Maltose binding protein
MDCK	Madin-Darby canine kidney cells
MF	Molecular function
MHC	Major histocompatibility complex
MOI	Multiplicity of infection
mRNA	Messenger RNA
NA	Neuraminidase
NEP	Nuclear export protein
NES	Nuclear export signal
Neu5Ac	N-acetylneuraminic acid
Neu5Gc	N-glycolylneuraminic acid
NGS	Next generation sequencing
NLRP3	NOD-, LRR- and pyrin domain-containing protein 3
NOD	Nucleotide-binding oligomerization domain
NP	Nucleoprotein
NS	Non-structural protein
OD	Optical density
OIE	Office International des Epizooties

PA	Polymerase acidic
PAMP	Pathogen-associated molecular patterns
PBS	Phosphate buffered saline
PB1	Polymerase basic 1
PB2	Polymerase basic 2
PC	Principal component
PCA	Principal component analysis
PCV	Packed cell volume
PGE2	Prostaglandin E2
PRR	Pathogen recognition receptors
P/S	Penicillin Streptomycin
PV	Pseudotype virus
RanGTP	Ran guanosine-5'-triphosphate
RBC	Red blood cells
RBS	Receptor binding site
RIG	Retinoic acid-inducible gene
RLU	Relative light unit
RNP	Ribonucleoproteins
RT-qPCR	Reverse transcriptase quantitative polymerase chain reaction
SA	Sialic acid
ScFv	Single chain variable fragments
sdAb	Single domain antibodies
sIAV	Swine influenza A virus
SIFT	Sorting intolerant from tolerant
sLe ^x	Sialyl lewis X
SNA	<i>Sambucus nigra</i>
TBS	Tris buffered saline
TCID ₅₀	50% Tissue culture infectious dose
TLR	Toll-like receptors
TNF	Tumour necrosis factor
TM	Melting temperature
TMB	3,3',5,5'-Tetramethylbenzidine
T-MM	Trypsin maintenance medium
tRNA	Transfer RNA
VHH	Variable domain of heavy chain
vRNA	Viral RNA
vRNP	Viral ribonucleoproteins
VST	Variance stabilising transformation
VSV	Vesicular stomatitis virus
WOAH	World Organisation for Animal Health
3'SLN	3'-Sialyllactose
6'SLN	6'-Sialyl-N-acetyllactosamine

1 Introduction:

Influenza A virus (IAV), a member of the *Orthomyxoviridae* family as classified by the International Committee on Taxonomy of Viruses (ICTV), has a viral genome consisting of eight negative sense RNA segments. Influenza A virus infects humans along with a wide range of mammals. There are three other types of influenza viruses: B, C and D (IBV, ICV, IDV) that on occasion infect a smaller subset of mammals. Only IAV and IBV cause regular epidemics in humans (Chen and Holmes, 2008, Mostafa et al., 2018, Nogales et al., 2019, Osterhaus et al., 2000). Influenza C virus primarily infects humans and pigs whereas IDV infects cattle and pigs; there have been no examples of IDV infecting humans (Asha and Kumar, 2019, Foni et al., 2017, Matsuzaki et al., 2016, Su et al., 2017, Yuanji et al., 1983). Studies into IDV in horses have demonstrated that upon experimental infection respiratory disease was not observed however the virus can successfully replicate in the respiratory tract and seroconversion can occur (Sreenivasan et al., 2022). Additionally a study in the UK showed 0.3% of horses positive by HI test, however no IDV RNA was detected in respiratory samples (Daly et al., 2021). The structures of ICV and IDV are different to IAV and IBV: they have seven viral RNA segments instead of eight; the haemagglutinin (HA) and neuraminidase (NA) segments are combined and make up a segment called haemagglutinin-esterase-fusion (HEF) (Herrler and Klenk, 1991, Rosenthal et al., 1998, Su et al., 2017). At present there are 16 HA and 9 NA subtypes in water fowl, which are considered the primordial source of IAV (Webster et al.,

1992). A further two subtypes of HA and NA have been discovered (H17N10 and H18N11) but are only present in bats (Tong et al., 2013, Wu et al., 2014a).

All mammalian lineages of IAV are believed to have become established after interspecies transmission of avian influenza A viruses (aIAV) either by reassortment (i.e. exchange of gene segments) of circulating viruses or by direct transmission (He et al., 2019). This has been seen in a range of mammalian hosts including humans, horses, and pigs, where infection presents as a respiratory disease (Cullinane and Newton, 2013, Janke, 2014, Moghadami, 2017). Until the 21st century, there were no reports of IAV outbreaks in dogs; the first report of transmission from equines to canines was made in 2004 (H3N8) (Crawford et al., 2005, Yoon et al., 2005). Subsequently, there have been limited reports of IAV transmission between horses and other mammalian species (Crawford et al., 2005, Payungporn et al., 2008). A single Bactrian camel in Mongolia is recorded to have tested positive, however the camel was seemingly healthy and there were no further reports of transmission (Yondon et al., 2014). Although there are few reports of equine IAV transmission that currently circulate, an outbreak of H3N2 canine influenza A virus (cIAV) originally from birds has continued to circulate to date (Zhu et al., 2015).

Human and avian influenza A viruses show a preference for one of two galactose sialic acid (SA) receptors; α 2,6 or α 2,3 respectively

(Gambaryan et al., 2002, Ito et al., 1998, Kuchipudi et al., 2009). Respiratory epithelial cells of pigs have both $\alpha 2,3$ and $\alpha 2,6$ sialic acid receptors, meaning that they can be infected with both avian and human influenza viruses and act as a mixing vessel for reassortment of influenza A viruses (Chan et al., 2013a, Webster et al., 1997). The 2009 H1N1 pandemic was an example of this, stemming from a reassortment of three influenza viruses: classical swine H1N1 pandemic virus, avian-like Eurasian swine H1N1 and the North American H3N2 triple-reassortant in pigs. Thus, the first human pandemic of the 21st century originated from the transmission of the triple reassortant virus from pigs (Dawood et al., 2009, Girard et al., 2010). Researchers have raised some concerns that dogs may act as mixing vessels due to their ability to be infected with both avian and human influenza viruses as seen in pigs and produce a novel reassortant virus that could be a risk to public health (Gonzalez et al., 2014, Sun et al., 2017, Zhu et al., 2015).

1.1 Influenza A structure

The virion of influenza A has a host-derived lipid bilayer envelope; embedded within that bilayer are two abundant glycoproteins (HA and NA); as well as a smaller amount of matrix (M) 2 protein. The ratio of HA to NA is around four to one, whereas the ratio of M2 to HA is one M2 to every 10 to 100 HA molecules (Zebedee and Lamb, 1988). In addition to these three integral membrane proteins, the matrix 1 protein is also present and forms a shell at the inner surface, surrounding the genetic material. The genome segments are numbered in decreasing

length order with segments 1–6 encoding a single major viral protein as shown in Table 1.1 (Bouvier and Palese, 2008). Each protein plays a key role in the replication cycle of IAV. Along with the core gene products, there are additional accessory proteins that have been identified and are expressed from these gene segments: 1, 2, 3, 5, 6, 7 and 8 (Pinto et al., 2021). The accessory proteins are not present in all influenza A viruses and are not essential for viral replication, but they have been shown to affect virus pathogenicity.

Table 1.1. Genomic segments of influenza A virus and the major proteins encoded. Adapted from Bouvier and Palese (2008).

Gene segment	Typical length (bp)	Major protein (s) encoded	Abbreviation
1	2,309	Polymerase basic 1	PB1
2	2,308	Polymerase basic 2	PB2
3	2,200	Polymerase acidic	PA
4	1,728	Haemagglutinin	HA
5	1,529	Nucleoprotein	NP
6	1,424	Neuraminidase	NA
7	991	Matrix 1 and 2	M1/ M2
		Non-structural 1 and	NS1,
8	855	Nuclear export protein*	NEP/NS1

Base pairs (bp), * previously called non-structural protein 2

The naming system for influenza A viruses is demonstrated in

Figure 1.1. If the IAV is non-human then it includes the species, this system is similar for other types of influenza virus. IAVs circulating in mammalian species at present only make up a small number of the HA subtypes that have been identified; an example of this can be seen in humans, only three HA subtypes have caused epidemics: H1, H2 and H3 (Bouvier and Palese, 2008). The HA and NA can be split into two groups as demonstrated in Figure 1.1 B. However, H17, H18, N10 and N11 do not have corresponding structures or functions to typical influenza A viruses (Hussain et al., 2017, Wu et al., 2014b). There is also a potential H19 subtype identified in birds in Kazakhstan (Fereidouni et al., 2023). Two more avian IAV sequences have been identified as being genetically similar to H19, although they were detected in America in surveillance data from 2010–2013 (Karakus et al., 2024) suggesting that the identification of a substantially different virus in Kazakhstan was not an isolated event.

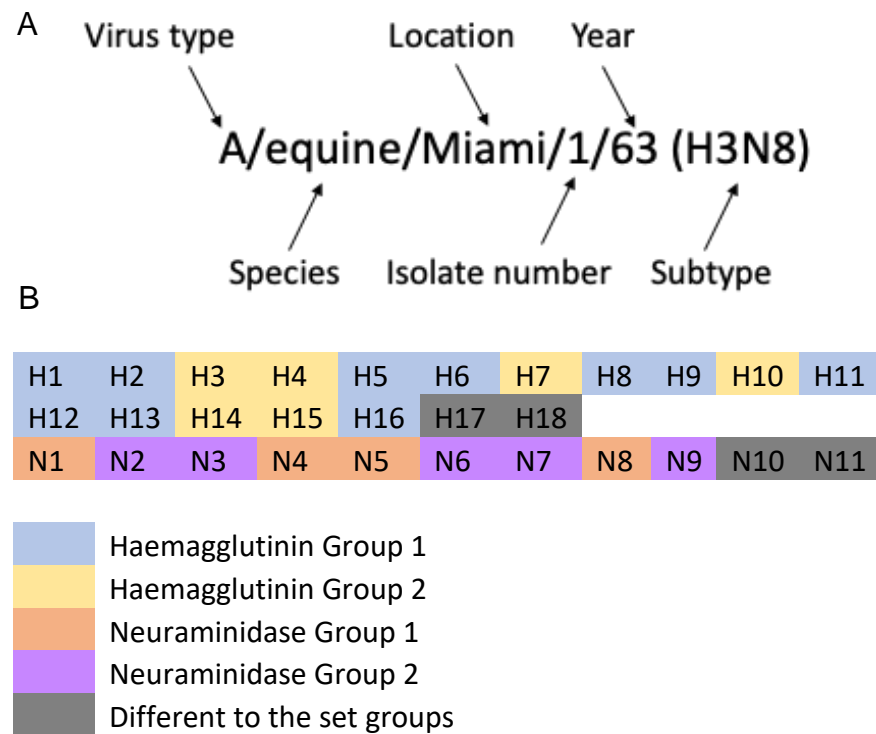


Figure 1.1. Influenza A virus naming system. A). A breakdown of the influenza A virus naming system using an example from an equine influenza A virus. (B). The groups that HA and NA can be divided into.

The HA glycoproteins are initially synthesised as a single protein (HA0) and the virus only becomes infectious after the HA0 has been cleaved by specific cellular proteases into two chains (HA1 and HA2). The HA1 and HA2 chains are connected by disulphide bonds, these monomers then associate noncovalently to form the trimer structure. The HA glycoproteins bind to sialic acids on the host cell surface. The virus is then endocytosed via receptor-mediated endocytosis and enters the

host cell in an endosome. This is followed by uncoating of the virus by two processes: firstly, a drop in pH triggering a conformational change in the HA and secondly an increase in hydrogen ions in the virus particle. When the pH is lowered it exposes the fusion peptide (Bullough et al., 1994, Lakadamyali et al., 2003, Pinto and Lamb, 2006, Stegmann, 2000, White et al., 1982) on the hydrophobic N-terminal of the HA2 which is then inserted into the membrane of the endosome. The C-terminal domain anchors the HA2 and creates a hairpin, then the HA trimer folds back causing the two membranes to be drawn together and to fuse (Dou et al., 2018). The process of entry and fusion occurs relatively quickly, taking approximately 10 minutes (Dou et al., 2018). During this time the M2 ion channel activates and once opened it acidifies the inside of the virus particle; this releases individual viral ribonucleoproteins (vRNPs) from the M1. Viral RNPs are made up of eight segments of genomic RNA each, of which is bound to a viral polymerase complex and numerous copies of the viral nucleoprotein (Eisfeld et al., 2015b). The vRNPs are then transferred to the host cytoplasm after HA-mediated fusion (Bui et al., 1996, Martin and Helenius, 1991). The current model for genome trafficking is that the vRNPs use an importin- α -importin- β import pathway to enter the nucleoplasm of the host cell (Chou et al., 2013, Cros and Palese, 2003). The process of vRNP delivery from the cell surface to the nucleus takes approximately one hour, significantly longer than the time for fusion and entry (Dou et al., 2018).

Once inside the nucleus, viral RNA-dependent RNA polymerase carries out viral RNA (vRNA) transcription and replication. Negative sense vRNAs are used as a template to synthesise messenger RNA (mRNA) templates for the synthesis of viral proteins. The influenza genome requires a two-step replication process for production of new vRNAs; first complementary RNAs (cRNAs) undergo transcription, then the cRNAs are used as a template for transcription of new vRNAs (Dou et al., 2018). Before the mRNAs can be exported and translated, they must be capped and polyadenylated. The viral RNA polymerase, made up of polymerase basic 1 (PB1), polymerase basic 2 (PB2) and polymerase acidic (PA), transcribe the segmented genome of the virus into mRNA containing the poly (A) tail (te Velhuis, 2019). The final step before export is cap snatching; this is when the PB1 and PB2 proteins steal primers from the host pre-mRNA transcripts to initiate synthesis of viral mRNA (De Vlugt et al., 2018, Krug, 1981).

The viral mRNA can then be exported from the nucleus and translated in the same way as host mRNA. The vRNA are exported in a separate manner; the M1 protein interacts with the vRNP and nucleoprotein (NP), bringing these components together. The M1 also interacts with the nuclear export protein (NEP) and the combination of these interactions allow for mediation of the export of vRNA segments via nucleoporins in the cytoplasm (Bouvier and Palese, 2008). The mechanisms behind these interactions are not clear, but a 'daisy-chain model' has been proposed (Figure 1.2) (Eisfeld et al., 2015a). An alternative mechanism

has also been proposed that suggests NP directly interacts with the chromosome region maintenance 1 (CRM1) (Chutiwitoonchai and Aida, 2016, Elton et al., 2001).

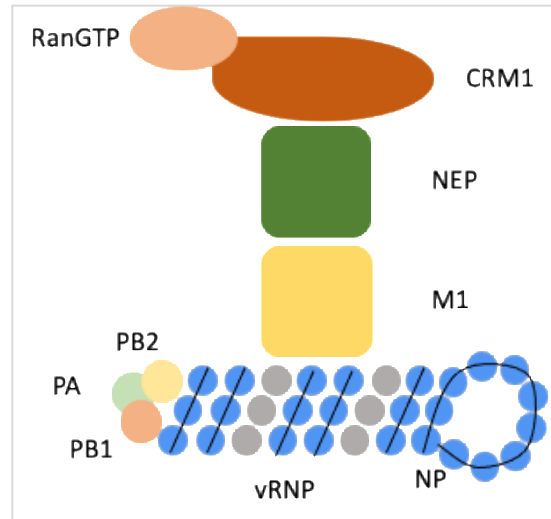


Figure 1.2. Daisy-chain model. The proposed daisy-chain model for the interaction between the NEP and matrix 1 (M1) and then subsequently the vRNPs. The NEP acts as an adaptor between the trimeric complex (chromosomal maintenance 1 (CRM1), ran guanosine-5'-triphosphate (RanGTP) and nuclear export signals (NESs) in the nucleoplasm) and M1-vRNP complexes. Adapted from Brunotte et al. (2014).

The HA, NA and M2 envelope proteins are synthesized from mRNA on ribosomes bound to the membrane in the endoplasmic reticulum where they are folded and then transported to the Golgi apparatus for modifications. There are two theories proposed for packaging of RNPs: selective-incorporation model and the random-incorporation model (Li et al., 2021a, Shafiuddin and Boon, 2019). Evidence suggests that it is selective, and packaging signals on the vRNA segments ensure that a

full genome is integrated into the virus particles (Bancroft and Parslow, 2002, Fujii et al., 2003). The final step is budding and release. This occurs at the cell membrane, most likely initiated by the M1 protein. Once budding is complete, the HA continues to bind to the sialic acid on the cell surface until sialidase activity of the NA protein causes release of virus particles (Dou et al., 2018). Figure 1.3 gives an overall breakdown of the process of replication of an influenza virus.

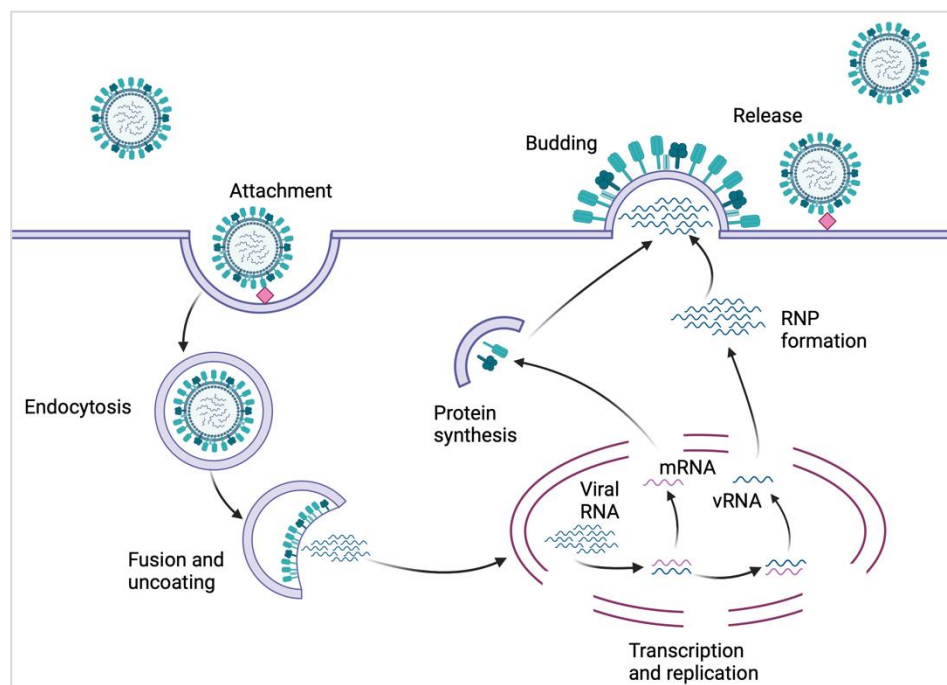


Figure 1.3. A breakdown of the influenza replication life cycle. A simplified version of the influenza replication life cycle, including transcription and replication of viral RNA (vRNA) to messenger RNA (mRNA) and vRNA to ribonucleoproteins (RNPs) for budding and release. Adapted from Herold et al. (2015). Image created using BioRender.

1.3 Haemagglutinin glycoprotein

As described above, the HA glycoprotein plays a vital role in the early stages of the virus replication life cycle. Cleavage of HA0 into HA1 and HA2 by specific cellular proteases is essential for virus infectivity as it enables the conformational change that exposes the fusion peptide from its position in the interior of the trimer. The HA1 subunit contains the sialic acid binding site and is responsible for binding of the virion to receptors on the host cell surface. The HA2 subunit is the portion thought to mediate fusion of the envelope with the target cell membrane (Hamilton et al., 2012, Steinhauer, 1999). There are four structural features that make up the receptor binding site (RBS), the 190- α helix, the 130-loop, the 220-loop and the 150-loop (Figure 1.4). Additionally, there is a network of amino acids at positions 98, 153, 183 and 195 corresponding to the H3 subtype that are hydrogen bonded to the sialic acid moiety of the receptor (Shi et al., 2014, Weis et al., 1988, Wilson et al., 1981). These four amino acids make up a depression at the bottom of the binding site. Whilst all HA subtypes have these four structural elements, they vary amongst the strains in length and amino acid composition, which may determine which receptor type they recognise (Lazniowski et al., 2018).

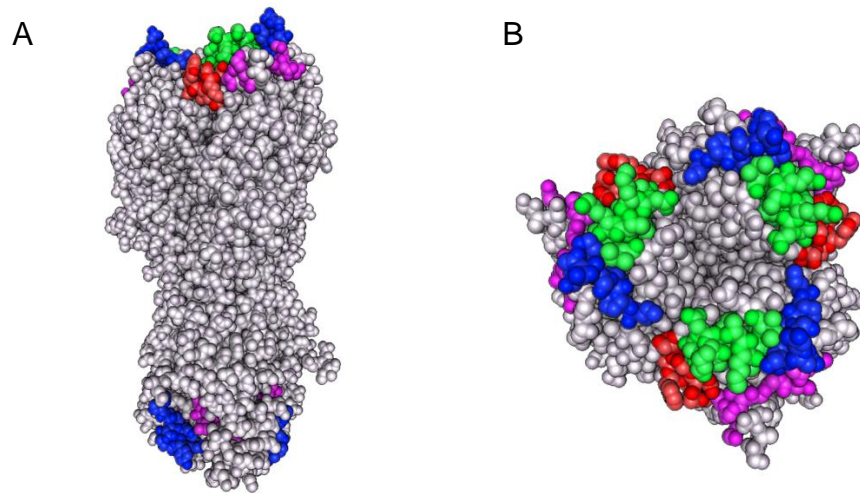


Figure 1.4. Haemagglutinin 3 glycoprotein. The 3D protein imaging model of H3 trimer (2HMG.pdb) with the 4 loops that make up the receptor binding site. A) side view B) top-down view. The pink denotes the 130-loop, the dark blue the 150-loop, the green the 190-loop and the red the 220-loop.

The RBS has been an area of interest since it was first identified and has been considered for several applications including as a site for sialic acid analogues to act as inhibitors and as a site for antibody attachment (Matrosovich and Klenk, 2003, Xu et al., 2013). The RBS modulates influenza virus affinity for specific sialic acid receptors; it is a shallow pocket that can expose modified glycosylation on the head of the HA if single amino acids changes occur within the pocket or around the rim (Matrosovich et al., 2015). Other changes that can occur include alterations in the general shape of the RBS and changes in glycan attachment that expose or hide the underlying amino acids allowing the virus to be recognised or hidden to antibodies raised against it. The

RBS is often targeted during vaccine design as it elicits humoral immunity however mutations occur regularly within that area resulting in vaccine mismatch and antigenic drift, commonly observed with H3N2 IAVs (Chiba et al., 2023).

1.4 Sialic acid binding

Influenza A viruses recognise sialic acid receptors on the target cell surface; these receptors appear with two different linkages. The terminal sialic acid has a carbon-2, this either binds to the carbon-3 or carbon-6 of the adjoining galactose, forming $\alpha 2,3$ (Neu5Ac $\alpha 2 - 3$ Gal) or $\alpha 2,6$ linkages (Neu5Ac $\alpha 2 - 6$ Gal). The two different terminal linkages can be seen in Figure 1.5. In aquatic bird species there are predominantly $\alpha 2,3$ linkages in the intestinal and respiratory tract unlike in humans where there are predominantly $\alpha 2,6$ linkages on the epithelial cells in the airway (Gambaryan et al., 2002, Ito et al., 1998, Kuchipudi et al., 2009, Pillai and Lee, 2010, Shinya et al., 2006). Pig and chicken trachea have both $\alpha 2,3$ and $\alpha 2,6$ linkages giving them the capability to act as mixing vessels; this can facilitate generation of novel pandemic strains (Chan et al., 2013a, Kuchipudi et al., 2009, Webster et al., 1997). As avian epithelial cells have $\alpha 2,3$ linkages, avian influenza viruses preferentially recognise $\alpha 2,3$ sialic acids and, similarly for human influenza viruses and human epithelial cells, they have matching $\alpha 2,6$ sialic acid preferences and linkages' respectively (Gambaryan et al., 2002, Ito et al., 1998, Kuchipudi et al., 2009, Shinya et al., 2006). The reality is more complicated than this outline and there

are some variations in the number and the type of sialic acids present on the epithelial cells and in glycan preference. Equine tracheal epithelial cells demonstrate staining for both $\alpha 2,3$ and $\alpha 2,6$ sialic acid, which partially matches with equine influenza virus preferential binding to $\alpha 2,3$ sialic acids (Feng et al., 2015). This infers that IAVs potentially bind more than one receptor during transmission or there is an alternate mechanism not yet identified (Dou et al., 2018). This theory may help explain why it is not yet fully understood the extent to which variations in the number and type of sialic acids influence interspecies transmission events of influenza virus.

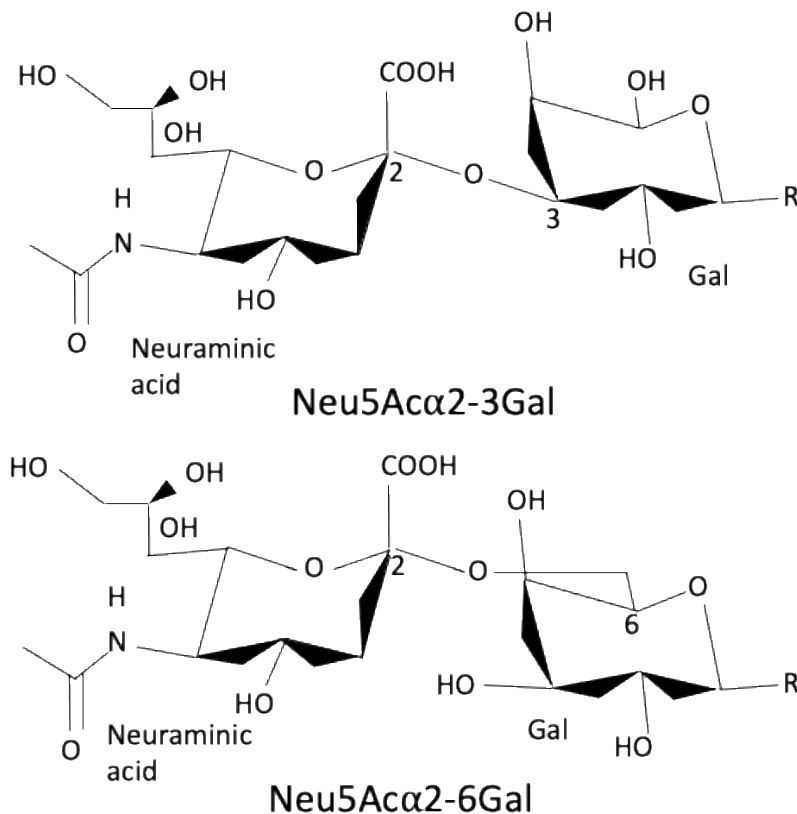


Figure 1.5. Illustration of the structures of α 2,3-Gal and α 2,6-Gal sialic acid linkages. The neuraminic acid and gal molecules are labelled and the numbers demonstrate where the linkages occur. R indicates a variable region at the end of each molecule. Adapted from Byrd-Leotis et al. (2017).

1.5 Neuraminidase glycoprotein

As outlined above NA, is the second surface glycoprotein embedded in the envelope of IAVs. The NA is composed of four distinct structural domains made up of four monomers. The four domains are: the catalytic head, the stalk, the transmembrane region and the cytoplasmic tail (McAuley et al., 2019). The most important role that NA plays is its role as a sialidase enzyme. It works by cleaving sialic acids from

respiratory mucin, cilia, virus receptors and the cell surface (Matrosovich et al., 2004, Wagner et al., 2002, Yang et al., 2014). This encourages virus migration, fusion and the release of progeny virus, demonstrating its varied roles in the influenza A virus replication cycle. Whilst the other roles of NA are not fully understood, it has been shown to increase the effectiveness of viral infection and virus attachment to host cells.

Antivirals have been generated that inhibit the activity of NA by targeting this glycoprotein. Neuraminidase inhibitors work by competing for the enzyme-binding site on the glycoprotein. There are three well known examples; zanamivir, oseltamivir and peramivir, which have been shown to work effectively against 9 NA subtypes (Govorkova et al., 2001). Both oseltamivir and zanamivir have been trialled in horses but oseltamivir needs to be administered twice daily for 5 days and zanamivir must be inhaled, making these impractical for use in equids (Yamanaka et al., 2006, Yamanaka et al., 2012a) or other veterinary species. The use of these neuraminidase inhibitors in dogs is not recommended as the safety and efficacy against cIAV is unknown (Dubovi and Njaa, 2008). It has been used in the treatment of canine parvovirus, however there is no clear understanding of how it works given canine parvovirus does not contain NA (Mercer, 2022). The use of oseltamivir in particular should be limited to human populations to reduce the potential for resistance (Ashton et al., 2010).

1.6 Immune response

Immune response is split into two phases; the innate and the adaptive and they perform different functions. Innate immunity is non-specific and is the first line of defence, activating immediately or within a few hours of encountering the antigen (Marshall et al., 2018). Adaptive immunity is the second line of defence, it takes time to activate because it is antigen specific and antigen dependent. Although adaptive immunity takes time it can remember previously encountered antigens and mount a quicker response on subsequent exposure to the antigen, providing a long-term defence resource.

1.6.1 Innate immunity

There are four types of barriers: anatomic, physiologic, endocytic and phagocytic and inflammatory. The innate system requires pathogen recognition receptors (PRRs) to recognise pathogen-associated molecular patterns (PAMPs), a limited range of common structures that pathogens share (Marshall et al., 2018). There are three classes of PRRs that are used to recognise influenza viruses: Toll-like receptors (TLR) (TLR3, TLR7 and TLR8), retinoic acid-inducible gene 1 (RIG-1) and NOD-like receptor family member NOD-, (LRR- and pyrin domain-containing 3 (NLRP3)) (Iwasaki and Pillai, 2014). The viral RNA in infected cells is recognised by the PRRs as foreign and the host starts to secrete chemokines, pro-inflammatory cytokines, eicosanoids, and type 1 interferons (IFNs). Table 1.2 demonstrates the different roles each of these proteins play in the innate immune response. If the innate

immune response is not sufficient then the adaptive immune response will take over after being signalled by pro-inflammatory cytokines.

Table 1.2. The role of proteins secreted during the innate immune response. Included are a few examples for each type of protein and a description of the role they play in the innate immune response.

Chemokine (C-C motif) ligand (CCL), interleukin (IL), tumour necrosis factor (TNF), prostaglandin E2 (PGE2), leukotriene B4 (LTB4) and interferon alpha (IFN- α).

Protein type	Role of protein	Examples
Chemokine	Recruit additional immune cells such as neutrophils, monocytes and natural killer cells to the site of infection	CCL3, CCL4 and CCL5
Pro-inflammatory cytokine	Contribute to inflammation during infection, recruit leukocytes, activate the epithelium and signal the adaptive immune response.	IL-6, TNF- α IL-1
Eicosanoid	Effect induction and resolution of inflammation	PGE2, LTB4
Type 1 interferon	Stimulate genes in neighbouring cells inducing an antiviral state that interfere with the replication cycle of the virus	IFN- α

1.6.2 Adaptive immunity

The adaptive immune system is signalled and aided by the innate immune system, and it is made up of T cells (CD8+, CD4+ and Treg cells) and B cells (memory B cells or antibody-secreting plasma cells). Both cell types are created from haematopoietic stem cells and then either travel to the thymus (T cells) or the bone marrow (B cells) to mature (Jenkinson et al., 2006).

Each T cell expresses a single T cell receptor and can generate more of itself when activated by the right signals, but to recognise a specific antigen it requires antigen presenting cells (APC) (dendritic cells or macrophages). APCs have either class I or class II major histocompatibility complexes (MHC); class I MHCs present endogenous peptides and class II present exogenous peptides to T cells (Janeway et al., 2001a, Janeway et al., 2001b). When the T cells encounter APCs with the correct MHC it differentiates into a cytotoxic T cell (CD8+) or T helper cell (CD4+). CD8+ cells are primarily involved in the destruction of infected cells or the production of effector cells that induce apoptosis. CD4+ cells help establish and maximise the immune response: they do not perform cytotoxic or phagocytic actions, they direct other cells to perform that function (Marshall et al., 2018). T helper cells are activated through the interaction with class II MHCs. The final type of T cell is the T regulatory cell that suppresses or promotes the immune response to the level of infection.

Alternatively, there are B cells that do not require APCs as they interact directly through antibodies on their cell surface and differentiate when they come in contact with foreign antigens that correspond with the specific antibody that is presented. B cells differentiate into either antibody-secreting plasma cells or memory B cells. The plasma cells produce large quantities of antibodies that enter the blood stream to protect against pathogens. Memory B cells that express virus-specific

antigen binding receptors are retained from past infections (Marshall et al., 2018).

1.7 Antigenic changes

1.7.1 Antigenic drift

Antigenic drift is the introduction of point mutations into the viral epitope (Kim et al., 2018a). Selection pressure from natural infection or vaccination causes selection for antigenic variants that facilitate escape from the immune response, particularly in the RBS (Smith et al., 2004). In IAVs this is common due to the lack of proof-reading mechanisms in the replication cycle (Shao et al., 2017). Some mutations have no impact whilst others may alter the HA and/or NA glycoproteins and allow the virus to evade the host immune response (Koelle et al., 2006, Wille et al., 2022). Viruses that contain these epitope altering mutations are selected by host immunity which in turn encourages antigenic drift to occur (Webby and Webster, 2001). The introduction of a single or multiple mutations at the antigenic sites can create virus strains that may no longer be neutralised by host antibodies (Bouvier and Palese, 2008). The antigenic sites for influenza virus surround the receptor binding site so point mutations in this area may alter the ability of the virus to bind. Human and animal influenza epidemics have the possibility to occur because of these slight but significant mutations.

1.7.2 Antigenic shift

Whilst antigenic drift results from minor changes to the viral genome, antigenic shift results from major changes and in which one viral gene segment is exchanged for another. This can occur among IAVs due to the extensive number of animal reservoirs providing many sources of antigenically distinct viruses (Kim et al., 2018a). Antigenic shift occurs shortly after co-infection of a single cell where gene segment exchange takes place, generating a reassortant virus. The impact of antigenic shift is more significant because a population will have limited immunity to a novel virus, so there will likely be increased transmission and the greater potential for a pandemic to break out (Kim et al., 2018a). This is part of the reason there is such rigorous monitoring of IAVs globally and novel subtypes are thoroughly investigated.

1.8 Equine influenza

1.8.1 The disease

Equine influenza A virus (eIAV) is highly contagious in all equine species. Disease transmission occurs by inhalation of droplets in the air. The droplets can travel up to 2 km (Davis et al., 2009) and this plays a major role in transmission between individuals. Transmission between horses is relatively rapid, influenza spreads faster than any other respiratory infection in equids. The virus can survive in the environment for around 3 days, helping to further facilitate transmission. Individuals have also been identified as being able to shed the virus for up to 10 days after initial identification. The incubation period for this virus is 1 to

3 days which is one of the shorter incubation periods for equine respiratory viruses, especially when compared to equine viral arteritis (EVA) which has the longest incubation period ranging from 2 to 14 days (Lattimer et al., 2020).

Equine influenza presents as a dry hacking cough, fever, loss of appetite, muscular soreness and tracheobronchitis (van Maanen and Cullinane, 2002, Slater and Hannant, 2000, Stack et al., 2013, Yin et al., 2014). The H3N8 subtype of eIAV currently circulating produces similar clinical signs to H7N7 eIAV, the equine influenza A virus previously circulating in horses, but the clinical signs are more severe (Chambers, 2020a). Bronchopneumonia comes secondary to equine influenza infections caused by bacterial infections such as β -haemolytic streptococci and *Actinobacillus* spp. There is only one neurological disease reportedly involved with equine influenza virus infection: it is non-suppurative encephalitis, which is rarely observed (Daly et al., 2006). Cases of this were observed during the 2003 eIAV epidemic, during the same time period that transmission of H3N8 eIAV to canines was observed.

1.8.2 History and impact of equine influenza

Equine influenza has been observed for hundreds of years; it is even thought to have been around at the time of Homer's writing of the Iliad (Morens and Taubenberger, 2010). Since 1956, eIAV outbreaks have occurred almost worldwide; Europe and North America are the most

endemic regions however developing countries have been severely impacted too (Singh et al., 2018). The role horses have played in the lives of humans has changed in the past few centuries, with a shift from working animals, to racehorses and then towards companion animals. All these roles rely on healthy horses, therefore an outbreak of equine influenza has as much of an impact now as it did when they were primarily work animals. There has been a severe economic impact on the equine industry from outbreaks of equine influenza, such as in South Africa in 1986, Hong Kong in 1992, Australia in 2007–2008 and in the United Kingdom in 2019 (Guthrie et al., 1999, Powell et al., 1995, Rendle et al., 2019). The economic impact has been reduced in recent years due to improvements in control methods, however recent outbreaks in the racing industry still have an economic impact. In developing countries, the economic impact of equine IAV outbreaks is serious because control methods are not as well implemented. In India, horses are a sole source of income for some farmers and nomads; in 2008 the number of horses performing this role was 1.58 million (Virmani et al., 2010). In the United Kingdom, the equine industry is different; much of the impact is on the companion animal industry where there is a greater emotional connection.

1.8.3 Equine subtypes and lineages

The first isolation of equine influenza H7N7 was in 1956 (Driskell, 2014), although it was not until 1963 when the second subtype (H3N8) was isolated (Waddell et al., 1963). They were previously described as

equine 1 and equine 2 however since the 1980s they have been classified as H7N7 and H3N8, respectively (Webster et al., 1992). H7N7 has not been isolated since 1977; therefore, it has been concluded that this subtype no longer circulates. Transfer RNA (tRNA) isotypes, which are RNAs involved in translation and protein synthesis and are a key molecule in deciphering the genetic code. In H7N7 eIAVs tRNA was found to be less adapted to equine cells than the H3N8 subtype currently circulating (Kumar et al., 2016). Since H7N7 was less adapted to the most frequently used tRNA isotypes, it would have been at a genetic disadvantage and been less likely to replicate successfully in equine cells. The H7N7 codon usage bias was compared with that of H3N8 and it was shown to have higher codon usage bias and a low mutation pressure, reducing the chances of the subtype being able to adapt potentially explaining why it is believed to have died out (Kumar et al., 2016). Whilst H7N7 and H3N8 were circulating at the same time for a period of 15 years, the two subtypes reassorted with each other several times (Bean, 1984, Ito et al., 1999, Murcia et al., 2011). This reassortment was likely the cause of the prolonged survival of the H7N7 subtype because the reassortant virus replaced the original H7N7 Prague/56 strain (Ito et al., 1999).

Between 1963 and 1990, H3N8 eIAV evolved as a monophyletic lineage, it was after this point that H3N8 started to diverge (Daly et al., 1996). Equine influenza H3N8 split into two lineages: the American and the Eurasian. The American lineage has since split into four, including

Florida clades 1 and 2 (Bryant et al., 2009, Daly et al., 1996, Murcia et al., 2011). Although eIAV H7N7 and H3N8 circulated at the same time, there was another IAV outbreak brought about by a single transmission event in 1989; avian influenza virus (aIAV) into horses (Guo et al., 1992). Genetic analysis of eIAV and aIAV showed a close relationship between the two IAVs and added evidence that the two circulated simultaneously. The ratio of nonsynonymous and synonymous nucleotide substitutions for each gene of eIAV H3N8 were estimated by Murcia et al. (2011). All values were less than 1, which is consistent with purifying selection, the highest ratios were observed in HA, NA and NS1, 0.26, 0.25 and 0.3 respectively which was indicative of localized adaptive evolution. The ratio of nonsynonymous to synonymous substitutions was also investigated by He et al. (2019) however they compared eIAV H3N8 and cIAV H3N8. The gene segments all had higher ratios for cIAV than eIAV indicating that there were more nonsynonymous substitutions after transmission into canines. As seen by Murcia et al. (2011) the highest ratios were observed in HA, NS1 and NA but also M1 where the ratio for cIAV was double that of eIAV. The heightened ratio of the NS1 suggests an adaption to the host innate immune response was required for transmission into dogs.

1.8.4 Equine Immune response

In equids the virus is detected in the respiratory tract 3–7 days after infection. The virus induces death of the cilia which stops the horse from eliminating foreign substances that enter via the respiratory tract.

Viral infection causes inflammation, death of epithelial cells, oedema and removal of the intricate barrier provided by the epithelial cells (Dionísio et al., 2021). At the same time, type 1 interferons and IL-6 are induced and activated, which the virus can inhibit and then go on to attenuate host expression (García-Sastre, 2006, Mibayashi et al., 2007, Noah et al., 2003, Wattrang et al., 2003). *In vitro* studies looking at the immune response to equine influenza virus are completed in peripheral blood lymphocytes in response to infection of naïve horses (Adeyefa et al., 1997). At the time of writing there are no studies that compare the immune response seen in immortal cell lines to the typical response seen in equids.

1.9 Vaccines

Vaccines against IAV in humans were first commercialised in 1945 to reduce the burden of epidemics and pandemics (Kim et al., 2018a). Vaccines against equine influenza were not available until 1960s, and inactivated vaccines remained in use for several decades. In the US inactivated and attenuated virus vaccines are currently on the market against eIAV however in other parts of the world alternative vaccine types are licensed such as viral vectored and subunit (Oladunni et al., 2021). Each type of vaccine has advantages and disadvantages including risk of side effects, ease of transport and storage, booster vaccine requirement, length of immunity and cost (Oladunni et al., 2021). There can be issues when developing vaccines for any influenza A virus because of antigenic drift and shift. Mutational changes in

seasonal H3N2 have led to the development of a clade numbering system, which has assisted in the choosing of vaccine strains (Allen and Ross, 2018). For equine influenza the focus is on antigenic drift as there have only been two subtypes of equine influenza. Whilst the WOA (World Organisation for Animal Health), founded as OIE (Office International des Epizooties), publishes their conclusions and recommendations annually there is no obligation for companies that develop vaccines to update them according to these recommendations. Since H3N8 diverged into the Eurasian and American sublineages the WOAs recommendations have been to include strains from each lineage as they both continue to circulate worldwide. The focus of vaccine research has been on antigenic drift in the HA glycoprotein as that is where the antigenic sites are found. Although NA is subject to antigenic drift its significance in eIAV vaccines is still not well understood (Murcia et al., 2011, Oladunni et al., 2021). Antibodies to NA are becoming increasingly recognised as important in the development of human influenza A vaccines (Wu and Ellebedy, 2024).

In the US, there are currently vaccines available for both H3N8 and H3N2 cIAV individually as well as a combined vaccine (Tonozzi, 2022). In the UK there are no vaccines available against cIAV.

1.10 Interspecies transmission

There are three stages of viral disease emergence that lead to a host switching event being successful: (i) initial infection of a single individual

from a new host with no onward transmission, (ii) the event then causes local transmission chains in the new host population (iii) finally epidemics or continued transmission endemically from host to host within the new population. There is a range of factors that explain the low percentage of successful species barrier jumps in IAV infection. These factors typically fall into three categories; ecological, genetic and immunological barriers (Zhu et al., 2019). An example of an ecological barrier is the lack of sufficient contact between infected and non-infected individuals for long-term transmission. The virus can also lack adaptations required for interspecies transmission, such as the requirement for species-specific balance between the HA and NA glycoproteins, acting as a genetic barrier (de Vries et al., 2020). An example of an immunological barrier would be haemagglutinin imprinting, a process in which the first IAV infection causes cross-protection against further IAV infections because the HA is from the same phylogenetic group (Gostic et al., 2016).

In mammalian IAVs interspecies transmission came about by transmission of aIAV either by reassortment of circulating viruses or by direct transmission (He et al., 2019). Horses have undergone four major IAV introductions: one of unknown subtype in 1872, a H7N7 epidemic in Czechoslovakia in 1956, which died out in 1970 (Zhu et al., 2019); one in 1963 of the H3N8 origin, which still circulates today; and another of H3N8 origin in Jilin, China in 1989. This second H3N8 strain only circulated for a couple of years before dying out (Guo et al., 1992, Guo

et al., 1995). Zhu et al. (2019) showed that avian H3N8 viruses can replicate in explanted equine trachea, but they do so without the ability to cause damage to the tissue, unlike eIAV infections. This suggests that aIAV transmission to horses may happen more often than originally thought but it is likely to go undetected due to an absence of clinical signs (Chambers, 2020b, Zhu et al., 2019). The H3N8 aIAVs used in the study by Zhu et al. (2019) were compared to the A/equine/Jilin/98 virus and due to similarities between five of the eight segments it could be concluded that there would be a minimal mutational hurdle for the aIAV to adapt to an equine host. There have been four human influenza pandemics associated with emergence of a new IAV subtype in 1918, 1957, 1968 and 2009, all thought to be caused by aIAV or swine influenza virus (sIAV). For this to occur the viruses will have had to acquire virulence factors through adaptive mutations or reassortment with human influenza viruses to overcome the species barrier (Sun et al., 2020). There is a requirement to understand interspecies transmission, including unsuccessful long-term transmission to monitor and be prepared for future spillover and emerging outbreaks.

1.11 Interspecies transmission of equine influenza to dogs

Canine influenza A virus (cIAV) (H3N8) was first identified in 2004 in racing greyhounds in Florida (Crawford et al., 2005). It then spread across the United States with greyhounds acting as a host species for the virus. In 2005, samples from an outbreak of an unknown respiratory

virus in foxhounds in the United Kingdom in 2002 were retrospectively investigated (Daly et al., 2008). This study showed that there was the opportunity for an independent transmission event of equine influenza virus into dogs; this event was not directly linked to the one in Florida in 2004 (Daly et al., 2008). Canine IAV H3N8 emerged from eIAV H3N8 Florida clade 1 sub-lineage; however, the reason behind the sporadic appearance of outbreaks since it was first isolated is likely due to endemic hotspots in large animal shelters in USA (Crawford et al., 2005, Dalziel et al., 2014, Payungporn et al., 2008). After the initial transmission event into greyhounds in Florida, cIAV spread to other regions in the US including Denver, New York City and Philadelphia in animal shelters, kennels and canine day care, likely due to cross country movement of infected greyhounds (Hayward et al., 2010). Canine IAV and eIAV share over 96% of their nucleotide sequence suggesting that this transmission was direct and not through a reassortment event with other strains leading to the conclusion that the entire genome of the equine influenza virus was transmitted into dogs (Crawford et al., 2005). The genes from the canine isolate shared 94% identity with those of other influenza A virus isolates (avian, swine and human origin) (Crawford et al., 2005). The H3N8 cIAV has not been reported as causing infection since 2016, however, as transmission events occur sporadically there is the chance that another event could occur in the foreseeable future (Borland et al., 2020). The clinical signs of cIAV are similar to those of eIAV: fever, cough, anorexia, nasal discharge and lethargy (Dubovi and Njaa, 2008). There has been close

contact between horses and dogs for many years, but only recently has a transmission event occurred.

1.12 Canine H3N8 lineage

He et al. (2019) suggested that H3N8 cIAV could be split into six major clades, with the first clade consisting of viruses isolated in Florida in 2004. Clades were defined by WHO, OIE and FAO as sharing a common node in the phylogenetic tree, monophyletic grouping with a bootstrap value of ≥ 60 at the defining node and average pairwise distances between and within clades of $>1.5\%$ and $<1.5\%$, respectively for H5 (WHO et al., 2011). The other five clades cover the years 2006 to 2016; each clade has isolates from different states across the United States. This study not only covers the divergence of cIAV and eIAV but also the divergence of the internal genes of H3N8 cIAV and their rate of evolution. Almost all the segments were calculated as having their most recent common ancestor from 2002 which aligns with the emergence of cIAV and therefore after that point they would have to adapt and evolve. Interestingly, the NS1 appeared to have diverged earlier, between 1999 and 2002. This coincides with ideas put forward by Barba and Daly (2016) that changes in the NS1 could be an example of adaptive mutation to switch hosts. When cIAV emerged in 2002, it was a unique event. The similarities between the cIAV and eIAV Florida 1 clade combined with the geographic position demonstrates the emergence was likely a result of a host range shift event (He et al., 2019).

1.13 Canine H3N8 mutations

Several mutations have been identified in the HA of H3N8 cIAV that are not present in equine influenza. Five of these mutations are suggested to be candidates for conferring the ability to facilitate establishment of canine-to-canine transmission; N54K, N83S, I328T, W222L and N483T (Crawford et al., 2005, Payungporn et al., 2008). The W222L substitution helped to improve binding avidity of cIAV H3N8 to receptor glycans with the specific motifs sialyl Lewis X (sLe^x) and N-glycolylneuraminic acid (Neu5Gc) (Wen et al., 2018b). The sLe^x glycan is included in glycan microarray analysis because H7 demonstrates higher preferential binding to sLe^x and therefore that could be the case for other subtypes (Guan et al., 2022). The W222L mutation was thought to be the key for transmission of H3N8 to respiratory epithelial cells that were missing the cytidine monophospho-N-acetylneuraminic acid hydroxylase (CMAH). The CMAH gene produces Neu5Gc by facilitating hydroxylation of Neu5Ac, therefore the mutation may promote binding when there is a reduction in Neu5Gc produced. Although further research is needed to understand these mutations, similar amino acid substitutions have been seen in other interspecies transmission events between the HA of avian influenza viruses and human hosts from varying subtypes (H1, H2 and H3) (Matrosovich et al., 2000, Vines et al., 1998).

Analysis of whole genome eIAV and cIAV samples from 1990–2011 and 2003–2013 identified the specific amino acid changes that

happened within those intervals (Feng et al., 2015). A selection of the mutations only occurred between eIAV and cIAV sequences isolated in 2003–2007 whereas others were present in the cIAV sequences isolated between 2003–2007 and 2008–2013. In this project, HA contained the highest number of mutations, including mutations at residues; 54, 75, 83, 92, 159 and 216 in the HA1 as well as residues 222 and 223, which are all part of the RBS. There were also mutations of note at residues 328 and 483 in HA2 that may impact the HA cleavage site (Feng et al., 2015). The mutations identified at residues 83 and 222 were demonstrated to have a significant effect on replication and receptor binding however the mutation at 54 had no significant result (Wen et al., 2018a). The other identified mutations have not been studied precluding comment on the effect that these mutations may have.

1.14 Interspecies transmission of avian IAV to dogs

At a similar time to the isolation of H3N8 cIAV, a H3N2 cIAV subtype was isolated in China and Korea (2004–2005). This isolate was most closely related to H3N2 aIAVs circulating at the time (Zhu et al., 2015). By 2006, this subtype was present in dogs in China and Korea, spreading throughout both countries (Wasik et al., 2021). In 2015, H3N2 cIAV isolates from the United States were analysed, concluding that they originated from South Korea. Dogs from South Korea were being rescued and brought back to America so they would not be sold for human consumption (Voorhees et al., 2017). This led to a

continuous spread of H3N2 cIAV infections across America. These outbreaks each appeared and died out within a couple of weeks (Wasik et al., 2021). The only place thought to have undergone sustained infections was in Chicago where there were ongoing low rates of infection for a few years (Newbury et al., 2016, Voorhees et al., 2017). As of 2018 only A/canine/California/84315/2017 (H3N2) viruses were being isolated from clinical samples and all other H3N2 outbreaks in the United States had demonstrated the burst-fade-out evolutionary dynamic often seen in IAVs (Voorhees et al., 2018). For the next 5 years there was a decrease in prevalence in the US. However, from the end of 2022 into the beginning of 2024, 14 states reported cases of cIAV (Oduoye et al., 2023, ProMED, 2022, ProMED, 2023f, ProMED, 2023e, ProMED, 2023d, ProMED, 2023c, ProMED, 2023b, ProMED, 2023a, ProMED, 2024). The clinical signs attributed to cIAV H3N2 are similar to the H3N8 subtype: mild upper respiratory tract disease, along with fever, lethargy, anorexia and frequent coughing (Pulit-Penalosa et al., 2017, Song et al., 2011). A recent review undertaken by Leung et al. (2024) demonstrated that whilst cIAV was circulating globally the majority of strains of H3N2 and H3N8 were observed in China. The arrival of H3N8 cIAV was from a single transmission event from horses, however the H3N2 subtype arose from an avian reservoir, however they were both associated with similar clinical signs (Parrish and Voorhees, 2019). The H3N8 virus was restricted to canines however the H3N2 demonstrated limited transmission in cats, which was confined to shelters (Jeoung et al., 2013, Yamanaka et al., 2012b).

It has also been shown repeatedly that dogs can be infected with avian origin H5N1 (Chen et al., 2010, Maas et al., 2007). In Thailand, H5N1 was isolated from a dog that had ingested several duck carcasses from an area that was H5N1 positive, although the closest genetic relative was A/tiger/Suphanburi/Thailand/Ti-1/04 rather than an avian sequence (Songserm et al., 2006). Additionally, an unpublished study identified 160 dogs that had antibodies to avian H5N1 suggesting a past or current infection (Butler, 2006). The recent outbreak of avian origin H5N1 in cattle in the US and initially into a single dairy farm worker demonstrates how quickly and easily transmission can happen (Uyeki et al., 2024). As of 28/06/24 there have been three cases of infection among farm workers (CDC, 2024), with cases also observed in cats.

1.15 Canine H3N2 lineage

At the time of writing there has only been a single study investigating a diverged lineage of cIAV H3N2 by separation into distinct clades as seen with H3N8 (Chen et al., 2023). Chen et al. (2023) suggested that cIAV H3N2 could be split into 6 clades from 2006 to 2019. The most recent clade, 5.1, consists of sequences isolated solely in China and the surrounding regions however there is clustering with the more recently identified sequences in America. Additionally, and unlike eIAV, very little clade-specific geographical segregation has been observed. Sequences identified in China were found alongside sequences identified in America (Li et al., 2021c), although the HA of the canine

sequences are distinct from avian and environmental sequences (Yao et al., 2022). The study by Yao et al. (2022) showed that some studied avian PB1 and PB2 sequences clustered with canine H3N2 PB1 and PB2 sequences. A distinction from the H3N8 lineage is that transmission has continually been noted in America and southeast Asia, whereas with cIAV H3N8 continued transmission was only seen in America and has since died out (Wasik et al., 2023).

1.16 Canine H3N2 mutations

There has been a range of mutations identified that may play a role in the adaption of the avian H3N2 influenza virus into canines. Similarly to canine H3N8, a mutation in residue 222 in the HA was identified. This was a tryptophan (W) amino acid in the avian H3N2 but became a leucine (L) in the canine H3N2 sequences (Li et al., 2010). As discussed in 1.13, residue 222 is found in the receptor binding site of the HA glycoprotein. This was thought to be the only residue in the RBS that was different to its avian precursor (Yang et al., 2013). This was proven incorrect by Li et al. (2021b) who completed a more recent study to look at host adaptive signatures in the canine H3N2 virus. The study identified a mutation at residue 196, within the 190 helix of the RBS. Additionally, a study completed by Guo et al. (2021) identified 54 genetic substitutions that were fixed in canine H3N2. By comparison the study by Li et al. (2021b) only identified 5. The sequencing variations between the two studies are likely due to the varying methods used and the different targets of their analyses. Guo et al. (2021) performed

sequence analysis using rates of non-synonymous and synonymous substitutions whereas Li et al. (2021b) used entropy value computing, setting mutational thresholds for the entropy value. Guo et al. (2021) also focused only on H3N2 CIV, AIV and H3N8 CIV, whereas Li et al. (2021b) focused on specific species transmissions such as avian-canine H3N2 and avian-human H3N2.

1.16.1 Sialic acid receptors in equine and canine cells

When Daly et al. (2008) first compared equine and canine tracheas they performed lectin staining using *Sambucus nigra* (SNA) and *Maackia amurensis* (MAL) to identify α 2,3 and α 2,6 sialic acid receptors. This experiment demonstrated the presence of α 2,3 sialic acid receptors in both equine and canine trachea cells. The equine trachea only showed the presence of α 2,3 SA receptors however the canine tissue predominantly stained for α 2,3 with minimal staining for α 2,6 SA receptors. This study revealed that canine trachea had the correct receptors for equine influenza to bind.

A different study was performed by Ning et al. (2012) where they completed a lectin staining study looking at tissues from the respiratory and gastrointestinal tracts of beagles. Goblet cells found in the trachea demonstrated the presence of α 2,3 SA receptors and α 2,6 SA receptors. The α 2,6 SA receptors demonstrated a lower level of staining and were less abundant in the goblet cells than the α 2,3 SA receptors. These results are similar to those of Daly et al. (2008). Non-ciliated and

ciliated cells within the respiratory tract were also stained and they were all positive for $\alpha 2,3$ SA receptors. The same cells also demonstrated little to no staining of $\alpha 2,6$ sialic acid receptors albeit with areas of weak focal staining. The study also examined the distribution of receptors in the gastrointestinal tract of dogs; as the presence of $\alpha 2,3$ and $\alpha 2,6$ SA receptors in the gastrointestinal tract provide an alternative area for avian influenza virus infection, replication and disease transmission. The results showed that most endothelial cells of the gastrointestinal tract did not express $\alpha 2,3$ SA and weak for $\alpha 2,6$, however in the glands there was strong positive staining for $\alpha 2,6$ and minimal for $\alpha 2,3$. This suggested that experimentally infecting dogs with avian influenza virus would be possible, but it would not be possible with human influenza virus.

One of the key differences between the two studies is the breed in which the study was completed. The study done by Ning et al. (2012) was done on beagles whereas the studies done by Daly et al. (2008) was done on respiratory tract tissue of greyhounds. Although these studies were done on different breeds both showed that *Sambucus nigra* lectin was able to bind to some $\alpha 2,6$ SA receptors on the canine epithelium (Daly et al., 2008, Ning et al., 2012). To better understand the presence of receptors within canines, a broader study of a variety of size breeds would be beneficial. Both experiments used the same stains *Sambucus nigra* for $\alpha 2,6$ Gal SA and *Maackia amurensis* specific for $\alpha 2,3$ Gal SA, however the experiment completed by Daly et al.

(2008) was done using immunofluorescence, which can improve sensitivity and specificity producing cleaner and clearer results.

A similar immunohistochemical examination was performed in the trachea, bronchus, and bronchioles of dogs experimentally infected with H3N2 cIAV by Song et al. (2008). The lectin staining for α 2,3 SA bound positively in canine trachea, bronchus, and bronchioles however lectin staining for α 2,6 SA was not present. This study performed staining on both dogs and pigs using pigs as a positive control to confirm that both the α 2,3 and α 2,6 reagents were working.

As mentioned in 1.14, H5N1 avian influenza viruses are known for being able to infect humans and canines, specifically within the gastrointestinal tract of humans and, as demonstrated by Maas et al. (2007), the respiratory tract in dogs. This study showed H5N1 binding to cells along three regions of the respiratory tract and then that binding to α 2,3 SA receptors were blocked by *Maackia amurensis* lectin. This study did not look at α 2,6 SA receptors, likely because H5N1 is of avian origin and therefore you would not expect to see binding to the α 2,6 receptors.

1.17 Potential for zoonotic transmission of influenza A viruses from companion animals

A pandemic event caused by interspecies transmission from a companion animal could feasibly have the kind of socioeconomic impact that was observed during the COVID-19 pandemic.

Currently there have been no clinical cases of equine influenza in humans, however there is still the possibility in the future that subclinical eIAV infections could occur. We know that equine influenza virus can infect humans if there is enough virus present. This has been demonstrated by Alford et al. (1967) who infected participants with equine influenza virus. If this is possible, then infection could lead to reassortment with human influenza virus thereby risking production of a novel strain. Equine IAV HA shows preferential sialic acid binding to $\alpha 2,3$ Gal unlike human influenza viruses, however in the respiratory tract of horses >90% of the total sialic acids are NeuGc instead of N-acetyl-neuraminic (NeuAc). NeuGc was thought to be absent from human tissues due to an exon deletion that meant that humans were unable to synthesize it (Springer et al., 2014, Suzuki, 2006). A study done by Bardor et al. (2005) demonstrated that Neu5Gc that is present in human tissues is from ingestion of red meats and milk products. The eIAV H3 and H7 subtypes bind both NeuGc and NeuAc, with H7 showing an increased avidity for NeuGc than NeuAc (Gambaryan et al., 2012). Broszeit et al. (2019) suggested that the increased avidity for NeuGc could explain why H7N7 is no longer circulating additionally at

the time of publishing this paper suggested that no viruses circulated that bound to NeuGc. The small change between NeuGc and NeuAc stops certain influenza viruses from binding. This comes as a benefit to humans since it reduces the chance of infection.

The existence of cIAV and influenza viruses in cats means that there is a chance for zoonotic transmission into humans, however feline influenza viruses do not demonstrate sustained transmission. In canines we are beginning to see sustained transmission of H3N2 influenza virus, however, there have currently been no cases of transmission into humans. There already exists a specific host barrier that is blocking the transmission between dogs and humans, the human immune response (Cauldwell et al., 2014, Jimenez-Bluhm et al., 2021). On infection, there would be activation of RIG-I by binding of viral RNA, causing ubiquitination of IFN-inducible E3 ubiquitin ligase, TRIM25, additionally RIG-I can start signalling cascades leading to transcription of proinflammatory cytokines and chemokines mounting an antiviral response (Van de Sandt et al., 2012b). There is additionally a shortage of surveillance being performed on companion animals, as well as a lack of forethought on vaccines or rapid testing in case of an outbreak (Borland et al., 2020). Although zoonotic transmission from companion animals may never occur it remains important to be able to identify risk factors and understand all transmission events.

1.18 Current limitations to understanding interspecies transmission

Although research and technology development is continually happening, there are still limitations to performing research and improving our understanding of interspecies transmission. To research IAVs the standard cell line used is Madin-Darby canine kidney cells (MDCK). This cell line is used regularly to research human IAV however eIAV does not replicate well in MDCKs (Ilobi et al., 1998, Chambers and Reedy, 2014). Since a home office licence is required in the UK to grow viruses in embryonated hen's eggs, MDCK cells are typically used to passage viruses, however after serial passaging into the cells, the virus will select mutations that improve their replication (Barnard et al., 2020). This means that eIAVs must be grown in embryonated hens' eggs which introduces some ethical concerns as well as issues connected to the availability of hens' eggs. The limitations of using MDCK cells include the variation in infectivity between influenza strains and greater heterogeneity seen when eIAVs are grown (Ilobi et al., 1994). Although eIAV cannot easily infect humans, research with infectious virus must be done at the correct containment level. The alternatives are to generate reverse genetics viruses however to produce and generate them, MDCK cells or embryonated hens' eggs are required and so the same limitations as above apply.

Due to the COVID-19 pandemic, pseudotyped viruses, which are mimic viruses made with a combination of a foreign viral envelope, a retroviral

core and a report gene, have come to the fore front as studies originally done at biosafety level (BSL) 3 can now be done at BSL-2 (Fujioka et al., 2022). Pseudotype viruses allow easy introduction of mutations in the HA and NA glycoproteins, meaning studies looking at receptor binding can be completed in a shorter time frame. There is a difference of two to three weeks in the time it takes to generate pseudotype viruses in comparison to reverse genetics viruses.

Another limitation in understanding interspecies transmission is the shortage of antibodies available and the ethical concerns related to generating more. This can be overcome by using phage display libraries to identify potential binders to target antigens. Phage display libraries can be generated as immune, naïve or synthetic. There are also an array of antibody fragments that can be used including Fab (antigen binding fragment), scFv (single chain fragment variable) and VHH (variable domain of heavy chain) (Bazan et al., 2012). VHH, which are used in this study are small in size (15 kDa), easy to produce, with a low production cost and have been used in biotechnology, diagnostics and therapeutics (Nakakido et al., 2024). Muyldermans (2021a) discusses VHH emergence, identification and further uses in detail.

Equine and canine influenza viruses are considered to be neglected influenza viruses and therefore research and development of tools to study them are not a key priority, especially in comparison to human influenza virus research.

1.19 Aims:

- To develop single domain antibodies to differentiate between Florida clades of Equine influenza A virus
- To explore the suitability of canine and equine cell lines for influenza A virus research
- To investigate whether amino acid changes in the HA of recent equine influenza A viruses modify receptor binding and enable interspecies transmission

2 General Methods

2.1 Cell culture

2.1.1 Cell lines

Table 2.1 Cell lines.

Cells	Notes	Media
293Ts	Human kidney, epithelial-like cells	Dulbecco's Modified Eagle Medium (DMEM)
293T/17s	Highly transfectable 293T cells	DMEM
MDCK	Madin Darby canine kidney cells	DMEM
DH82 α	Macrophage-like cells from a dog	DMEM
E. derm	Equine dermal fibroblast cells (NBL-6)	Eagle's Minimum Essential Medium (EMEM)
extEqFL	Immortalized equine lung cells	DMEM

All cell lines were grown in either Nunc Nunclon Delta 25cm or 75cm EasYFlask Filter Cap at 37°C in 5% CO₂. Dulbecco's Modified Eagle Medium (DMEM, Gibco, Cat no. 41966-029) supplemented with 10% heat inactivated fetal bovine serum (FBS, various sources) and 1% (v/v) penicillin-streptomycin made up of 10,000 U penicillin and 10 mg/ml streptomycin (Sigma Aldrich), and 1% (v/v) L-glutamine (Gibco). The E. derm cells were cultured in Eagle's Minimum Essential Medium (EMEM, Sigma Aldrich, Cat no. M2279-500ML) supplemented with 10% FBS, 1% (v/v) penicillin-streptomycin (P/S) made up of 10,000 U penicillin and 10 mg/ml streptomycin, 1% (v/v) L-glutamine and 1% non-essential amino acids. Complete medium refers to either of the two cell culture media with 10% FBS.

2.1.2 Sub-culturing adherent cells

Growth media was discarded, and cells were washed with pre-warmed phosphate-buffered saline (PBS). An appropriate amount of trypsin (Merck) was added to cover the cell monolayer and to detach cells from the flask surface. An equal volume of complete media was added to neutralise the trypsin and then the cell suspension was transferred to a 15 ml V-bottomed tube and centrifuged for 5 minutes at 2500 rpm. The supernatant was discarded, and the cell pellet was resuspended with complete media. The correct seeding density was based on the useful numbers for cell culture (Thermo Fisher Scientific, 2024), and the appropriate amount was added into a new flask containing the appropriate volume of complete media. The flasks were then returned to the 37°C incubator.

For the MDCK cells the same process was followed but with an additional wash with 3 ml of versene (1X, Gibco) prior to the addition of trypsin to assist in the detachment of cells from the flask surface. For the E. derm cells the same process was followed including the additional versene wash step used with MDCK cells but with EMEM.

2.1.3 Counting cells

The cell suspension was prepared in the same way as 2.1.2. The haemocytometer and coverslip were cleaned with 70% industrial methylated spirits (IMS) prior to use. The coverslip was applied to the haemocytometer and the cell suspension was gently swirled to ensure

the cells were evenly distributed. Ten μ l of cell suspension was added to one of the chambers and allowed to be drawn inside. The cells were then either counted using the Countess 3 Automated Cell counter (ThermoFisher Scientific) or under a light microscope with 10X magnification. When counted under the microscope, the cells were counted by only including cells that were within the squares and that touched the left hand and bottom lines.

2.1.4 Freezing and thawing cells

The cell suspension was prepared the same way as 2.1.2 and then counted as described in 2.1.3. The suspension was then centrifuged again and resuspended in the appropriate volume of freezing media (Appendix 1). This was then aliquoted into 1.8 ml cryotubes with 1 ml of freezing media and then placed into Mr Frost cell freezing containers. These were moved to -70°C freezers and left overnight and then transferred into liquid nitrogen storage the next day.

Cells were removed from liquid nitrogen and then briefly thawed in a water bath until the suspension turned liquid. The cryotube was cleaned with 70% IMS before being opened in a tissue culture hood. The suspension was immediately transferred into a 15 ml V-bottomed tube with 3–4 ml of pre-warmed appropriate media. The cells were then centrifuged at 2500 rpm in a Sorvall Legend RT + BIO1000 shield rotor (Thermo Fisher Scientific) for 5 minutes and the supernatant was removed. The pellet was resuspended with fresh complete media and

transferred into the appropriately sized flask and then placed into the 37°C incubator at 5% CO₂.

2.1.5 Acid etched coverslips

A 1M solution of hydrochloric acid (HCl) was made up and pipetted into a beaker. Coverslips were carefully placed into the beaker and the beaker was then covered with cling film and placed into a water bath set to 50°C. The coverslips were incubated for either 4 hours or overnight and then removed from the water bath and left to cool. Once cool the coverslips were placed into a clean beaker with double distilled water and rinsed. This was repeated two more times and then the coverslips were placed into a sonicating water bath for 30 minutes. The coverslips were briefly rinsed with 100% ethanol and then stored in a 50 ml V-bottomed tube at room temperature.

2.2 Virology methods

2.2.1 Viruses

All equine influenza viruses, including the recombinant viruses were obtained from the Animal Health Trust. The sources of other viruses are provided in Table 2.2 and Table 2.3.

Table 2.2. Wild type viruses.

Isolate	Use
A/Puerto Rico/8/34 (H1N1)	Receptor specificity assay and Biolayer interferometry
A/equine/Shropshire/10	Receptor specificity assay
A/equine/Newmarket/5/03	Receptor specificity assay, RT-qPCR and Biolayer interferometry
A/equine/Newmarket/1/93	RT-qPCR, sucrose gradient ultracentrifugation and Biolayer interferometry
A/equine/Newmarket/2/93	RT-qPCR, sucrose gradient ultracentrifugation and Biolayer interferometry
A/equine/Sussex/89	RT-qPCR and Biolayer interferometry
A/canine/New York/51864/2008 (H3N8) ¹	RT-qPCR

¹ Professor Edward Dubovi, Cornell University.

Table 2.3. Recombinant viruses.

Name	Use
A/equine/Devon/1/2011	VHH ELISA
A/equine/Kentucky/1/2014	VHH ELISA
A/canine/Illinois/41915/2015 (H3N2) ²	Reverse genetics, RT-qPCR and Biolayer interferometry
A/Puerto Rico/8/34 (H1N1) ³	Reverse genetics
A/equine/Sussex/89	RT-qPCR

² Professor Colin Parrish, Cornell University, ³ Dr Holly Shelton, previously at The Pirbright Institute.

2.2.2 Growth of virus in embryonated hen's eggs

Embryonated white hen's eggs (Henry Stewart Ltd) were received at day 0 and placed pointed end down in an egg incubator at 37°C and 40–50% humidity. The eggs were monitored daily and at day 9/10 the eggs were candled, the process of shining a light at the bottom of the egg in a dark space to check for growth, cracking and infertility (Brauer and Chen, 2015). The fertilised eggs were marked on the air sac and at the top. Seed virus was thawed and diluted 1:100 in diluting fluid (Appendix 1) to avoid generation of defective interfering particles (OIE, 2024) and filtered through a 0.22 µm filter. Holes were pierced where the marks were and a 1 ml syringe with a 25 G needle were prepared so 0.1 ml of diluted virus could be injected 2 mm into the allantoic cavity. The holes were sealed with a small amount of wax and then transferred back into the egg incubator for 72 hours. The eggs were then removed and placed in a 4°C cold room overnight to kill the embryos and to contract the blood vessels. The tops of the shell were removed using scissors and then the allantoic fluid was harvested and put on ice. The allantoic fluid was briefly centrifuged at 2,500 rpm for 5 minutes and then aliquoted for storage at -70°C.

2.2.3 Ultracentrifugation of viruses

Allantoic fluid was thawed or ultracentrifuged straight from collection, by adding fluid into ultracentrifuge tubes (Hitachi) and topping up until the tubes were balanced. The tubes were then inserted into the P28S swinging bucket rotor and placed into the Himac ultracentrifuge

CP80NX (Hitachi) and spun down at 19,000 rpm for 3 hours at 4°C.

Once the ultracentrifuge was stopped, the tubes were removed, and the supernatant was pipetted off. The chosen volume of PBS was added to the tubes which were then placed into the fridge overnight to loosen the pellet. The next day the pellet was resuspended and stored at -70°C until further use.

2.2.4 Sucrose gradient ultracentrifugation

In 50 ml V-bottomed tubes, sucrose solutions varying from 60% to 30% w/v were made up with PBS. They were placed on a roller and left to dissolve before being passed through a 0.45 µm filter with a syringe into new 50 ml tubes. To make up 35, 45 and 55% w/v solutions equal amounts of the other solutions were added together. All solutions were then transferred to the fridge to be stored at 4°C prior to ultracentrifugation. To layer the solutions, 16 ml ultracentrifugation tubes (Hitachi) were tilted to 45° and each new layer was pipetted into the meniscus against the far tube wall. The most concentrated solution was added first and then the other solutions were added 2 ml at a time and ~ 2 ml of virus was added to the top. The tubes were balanced and then placed into the P28S swinging bucket rotor and put into the Himac ultracentrifuge CP80NX (Hitachi) and spun at 28,000 rpm for 150 minutes at 4°C.

After ultracentrifugation a milky white band should be visible, all liquid above the band was carefully removed. The milky band was then

pipetted up using a needle and syringe and was added to the top of a tube containing PBS to be spun down again. The tube was ultracentrifuged at 30,000 rpm for 60 minutes at 4°C in the P55ST2 swinging bucket rotor. The supernatant was removed, and the pellet was resuspended in PBS and stored at -70°C.

2.2.5 Pseudotype viruses

Influenza pseudotyped lentivirus particles that express firefly luciferase reporter gene were generated using a selection of plasmids. The 293T cells were seeded in 6-well plates at 6×10^5 cells per well in 2 ml of media and incubated overnight at 37°C and 5% CO₂. Around 1–4 hours prior to transfection, the complete media was replaced with serum free media. A mix of lipofectamine 2000 (Thermo Fisher Scientific) and OptiMEM (Thermo Fisher Scientific) was created with 7 µl of lipofectamine 2000 per 100 µl of OptiMEM. Separate tubes were made up for each influenza pseudotype virus as well as vesicular stomatitis virus G (VSV-G, provided by Professor Cinzia Allegrucci, University of Nottingham) and Δ envelope as positive and negative controls respectively. The OptiMEM and lipofectamine mix was distributed amongst the tubes and the combined mixture was added to the corresponding wells. After either a four-hour incubation or an overnight incubation the transfection media was replaced with reduced FBS DMEM. After 48–72 hours the cells were checked under the microscope and the supernatant was harvested by passing it through a 0.45 µm

filter attached to a 5 ml syringe and then pseudotype viruses were stored at -80°C or immediately used to infect target cells.

Table 2.4. Pseudotype virus transfection reagents.

Transfection reagent required, and the quantity of each reagent for transfections in two different size culture plates including optional use of NA and protease plasmids.

Transfection reagent	Quantity of reagent	
	6-well plate	10 cm dish
Lipofectamine 2000	7 µl	14 µl
OptiMEM	100 µl	200 µl
PI.18-HA	500 ng	1 µg
PI.18-NA	125 ng	250 ng
PCSFLW ¹	1 µg	2 µg
psPAX2 ²	500 ng	1 µg
PCAGGS-HAT ³	125 ng	250 ng
p8.91 ⁴	500 ng	1 µg

^{1, 4} Professor Nigel Temperton, University of Kent, ² Professor Cinzia

Allegrucci, University of Nottingham, ³ Professor Eva Friebertshaeuser,

Philipps-Universität Marburg

2.2.6 Pseudotype virus titration

In a 96-well cell culture plate, 100 µl of neat pseudotyped virus (PV) was added in duplicate in row H. This was diluted up the plate and the final column was used as a cell-only control. Target cells were added at 1×10^4 cells in 50 µl complete DMEM, and the plate was incubated for 48 hours at 37°C and 5% CO₂. The contents of the plate was removed and 50 µl per well of Steady-Glo luciferase assay (Promega) was added and

left to incubate for 10 minutes. The luciferase activity of the plate was read using a Glomax Explorer (Promega).

2.2.7 Reverse genetics

Prior to transfection, two 100 mm dishes of 293T and MDCK cells were seeded to be 80–90% confluent the next day. For every 250 µl of OptiMEM media, 7 µl of lipofectamine 2000 was required and added into a separate tube, this was left to incubate for 5–10 minutes. During this time an 1.5 ml tube was prepared with 50 µl of OptiMEM and 1 µg of each plasmid required per rescue (Table 2.3

A/canine/Illinois/41915/2015 (Rodriguez et al., 2017) and A/Puerto Rico/8/34 systems). A reaction's worth of the OptiMEM Lipofectamine mix was added into each tube with the plasmid mixture in and left to incubate for 20–30 minutes. The two plates of 239T and MDCK cells were washed, trypsinised and resuspended in 10 ml of complete DMEM. Once spun down at 2,500 rpm for 3 minutes they were resuspended in 3 ml of complete DMEM, and the two cell suspensions were combined and the mixture was distributed between 10–12 wells across two 6-well plates. After the combined mixtures finished incubating, they were added to the wells and left overnight to incubate at 37°C and 5% CO₂.

After 16–24 hours the media was changed to DMEM with 0.3% BA, 1% P/S and 1 µg/ml of TPCK-Trypsin for 48 hours. The role of TPCK-trypsin was to assist in the cleavage of the virus particle. The

supernatant was harvested and centrifuged for 1–2 minutes at 2,500 rpm to remove cell debris in preparation for infecting embryonated hen's eggs (Henry Stewart Ltd) (2.2.2). Alternatively, MDCK cells were passaged in 100 mm dishes and left overnight to create a monolayer. The cells were washed twice with 1x PBS and then infected with 800 µl of centrifuged tissue culture supernatant. The supernatant was incubated for an hour and the dishes were rocked every ten minutes. At the end of the hour the supernatant was removed and 12 ml of DMEM with 1% P/S, 0.3% bovine albumin (BA) and 1 µg/ml of TPCK-Trypsin was added. The cells were then left for 48–72 hours before harvest.

2.2.8 Haemagglutination test

Chicken red blood cells in Alsever's solution (RBC) (TCS Biosciences Ltd) were washed in PBS and centrifuged for 1 minute at 2,500 rpm. This was performed a maximum of three times to remove any leftover Alsever's solution. A sample of this was spun in a haematospin 1300 (Hawksley) to obtain the packed cell volume (PCV) from which a 1% solution was calculated and was then made up with PBS. In a 96-well V-bottomed microtitre plate 25 µl of PBS was added in rows 2–12 and then 25 µl of the chosen virus was titrated across the plate in rows 1–11 with a control in row 12. Finally, 25 µl of 1% RBCs were added to all wells and left to incubate at room temperature for 30 minutes. If successful haemagglutination then there should be a sedimented drop of blood cells in the PBS and a diffuse red well where virus is present

until cut off dilution where it will pinpoint (Figure 2.1). The virus titre is measured at the final well diffuse well.

2.2.9 Haemagglutination inhibition test

Chicken red blood cells were washed and the PCV was performed as described in 2.2.8. In a 96-well V bottomed microtitre plate, 25 µl of PBS was added in rows 2–12 and then 25 µl of chosen antisera was titrated across the plate in rows 1–11 with an additional 25 µl of PBS added to row 12 as control. Then 25 µl of 4 HA units of virus was added from row 1–11. Finally, 50 µl of 1% RBCs were added to all wells and left to incubate at room temperature for 30 minutes. In the control well there will be a sedimented drop of blood, in wells with virus and antibody there will be a sedimented drop until cut off where the antibody is too diluted and then it will appear as a diffuse red well (Figure 2.1).

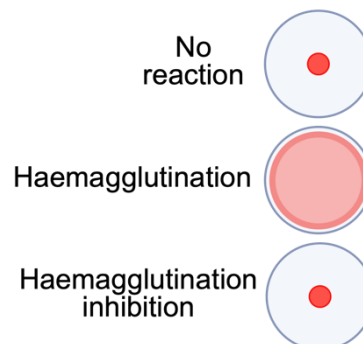


Figure 2.1 Haemagglutination test.

An image of haemagglutination test results, for both HA tests and HI tests. Image created using BioRender.

2.2.10 Tissue culture infectious dose 50%

The chosen cells were seeded at 1×10^4 cells per well in a 96-well-flat bottomed tissue culture plate and left to incubate at 37°C with 5% CO_2 overnight until the cells were 80–90% confluent. Dilutions of the chosen viruses were prepared starting with 10^{-1} down to 10^{-10} in sterile bijoux with serum-free DMEM as the dilutant. The media from the overnight incubation was discarded and the plate was tapped onto tissue paper to remove all excess media. The plate was then made up with 50 μl /well of serum-free DMEM in columns 11 and 12 and then 50 μl /well of the 10^{-10} dilution was added to column 10 down to the 10^{-1} dilution in column 1. The plate was left to incubate at 37°C with 5% CO_2 for an hour after which the serum-free media was discarded and replaced with 100 μl /well of trypsin maintenance medium (T-MM; 100 ml serum free DMEM and 1 ml of 125 $\mu\text{g}/\text{ml}$ TPCK treated trypsin). The plate was left to incubate for 3 days at 37°C and 5% CO_2 with any observations of cytopathic effect (CPE) noted each day. On day 3 the dilutions were transferred to a V-bottomed 96-well plate and a HA test was performed (2.2.8). The Kärber formula was used to calculate the TCID_{50} . It was expressed as follows:

$$\text{Log}_{10} \text{TCID}_{50} = -[X_{p=1} + 0.5d - d(\text{Sum of } p)]$$

' $X_{p=1}$ ' is the highest dilution giving 5/5 wells positive for infection. 'd' is \log_{10} dilution interval which in this case is 1 as there are 10-fold dilutions, 'p' is the proportion positive for infection at any given dilution and 'Sum of p' is the sum of all p values.

2.2.11 Infection of cells with influenza A virus

The 24-well plates were seeded with the chosen cells at 2×10^5 cells/well with 1 ml/well and were left to incubate overnight until the cells were 80–90% confluent. The media was changed from complete DMEM to serum free DMEM 1–4 hours prior to infection. The viruses were diluted in media containing 1.25 µg/ml TPCK-trypsin to varying concentrations dependent on the TCID₅₀ results. A mock infection was performed using media and then 500 µl of each dilution were added per well and a mock well was included for each dilution, time point and virus. The plate was left to incubate for an hour at 37°C and 5% CO₂. The supernatant was discarded and replaced with serum-free media and returned to the incubator until the chosen time points.

2.2.11.1 Harvest of cell suspension, supernatant and storage

Three time points were selected to harvest the cells and supernatant: 6-, 12- and 24-hours post-infection. The supernatant was harvested and transferred into 1.5 ml microtube and then stored at -20°C until required. The cells were trypsinised with 500 µl of 1x trypsin and then centrifuged at 11,000 *g* for 1 minute. The supernatant was removed and then the cells were either frozen as a pellet for later analysis or were resuspended in 100 µl of PBS and 500 µl of RNALater (Sigma-Aldrich) to preserve the cells. They were then stored at -20°C until further processing.

2.2.12 Anti-NP ELISA

Maxisorb ELISA plates were coated with virus serially diluted two-fold in coating buffer (Appendix 1). The plate was left to incubate overnight at 4°C in a covered box with a plate sealer to prevent the plate drying out. The virus was then permeabilised by adding 200 µl 0.2% Triton X-100 (Appendix 1) for 30 minutes at RT. The plate was then washed four times with 100 µl PBST and 50 µl of blocking buffer (Appendix 1) was left to incubate for an hour at RT. The blocking buffer was removed by tapping the plate out onto white roll. Then 50 µl of #58 anti-NP antibody clone HB65 kindly provided by Professor Munir Iqbal of The Pirbright Institute was diluted 1:3000 in blocking buffer and was then added and left to incubate for an hour at RT. The wash step was performed as described above and then 50 µl anti-mouse IgG HRP antibody (Cell Signalling Technology #7076) was diluted 1:3000 in blocking buffer and left to incubate for an hour at RT. The wash step was repeated as described above then 50 µl of 1 step Ultra TMB ELISA substrate solution (Thermo Fisher Scientific) was added and left to incubate for 10 minutes at RT. To stop colour development 50 µl of 2M sulphuric acid was added and then the plate was read at 450 nm on a Promega Glomax Explorer.

2.2.13 Receptor specificity assay

Prior to performing the assay, fetuin coated ELISA plates were made using 10 µg/ml of fetuin in PBS to help with virus binding. The diluted fetuin was added to a 96-well ELISA plate by adding 200 µl per well and

left to incubate overnight at 4°C. The next day leftover liquid was discarded, and the plates were rinsed three times with tap water and once with distilled water. The plates were left to dry for 3 hours at room temperature on a clean bench and stored in a dark, cool place.

The viruses were diluted 1:50 in TBS and 50 µl/well was added in duplicate across two rows of a 96-well fetuin coated ELISA plate. An additional two rows of only tris buffered saline (TBS) were added to act as controls. The plate was sealed and left to incubate overnight at 4°C and washed three times with 200 µl PBS/well the next day. The plate was then blocked with 200 µl blocking buffer either overnight at 4°C or for an hour at RT. After the incubation the plate was washed twice with 4°C wash buffer 200 µl/well. Eight-two-fold dilutions of each lectin 3'-Sialyllactose and 6'-Sialyl-N-acetylactosamine (3' SLN-biotin and 6'SLN biotin) (Dextra, UK) were prepared in reaction solution (Appendix 1) starting at 1 µM. The plate was divided into two with each biotinylated SLN covering half a plate, 50 µl/well was added and the plate was left to incubate for an hour at 4°C. During this incubation step peroxidase labelled streptavidin (Thermo Fisher Scientific #1859400) was diluted 1:1000 in reaction solution so it could be added at 50 µl/well after washing the plate three times with 4°C wash buffer. This was left to incubate for 1–2 hours at 4°C and then washed and 100 µl/well of SIGMAFAST pNPP tablets (Sigma) made up according to the manufacturer's instructions was added. It was then incubated for 30 minutes at RT, away from direct light before 50 µl of 3M sodium

hydroxide solution was added. The plate was read at 405 nm on the Labtech LT-400 microplate reader.

Variations were made to the protocol to improve results; the peroxidase-labelled streptavidin was changed to streptavidin horseradish peroxidase (HRP) (Proteintech #SA00001-0) but used at the same volume and dilution. This was left to incubate for an hour before being washed and then 50 µl 3,3',5,5'-tetramethylbenzidine (TMB) was added per well and left for 15–30 minutes after which 2M sulphuric acid was added, and the plate was read at 450nm.

2.2.14 Biolayer interferometry

The octet is an optical technique used for measuring the presence of protein interactions by analysing interference patterns of white light that reflects from the sensor tip. The sensors have a molecule immobilized to them, this is then dipped into the well and binding is measured, this is repeated until all wells have been dipped into and the changes in the number of molecules bound to the tip are recorded in real-time (Sartorius).

2.2.14.1 Qualitative assay

Prior to performing the assay, streptavidin coated biosensors were hydrated in HBS-EP buffer (10 mM HEPES pH 7.4, 150 mM NaCl, 3 mM EDTA and 0.005% tween-20, Bio-world) for a minimum of 10 minutes at room temperature. A 96-well black flat-bottomed plate was

made up with HBS-EP buffer in column 1, the lectins and 2 control wells in column 2, HBS-EP buffer and drugs in column 3 and finally the virus/pseudotype virus and controls in column 4. The two lectins: 3'-Sialyl-N-acetyllactosamine-biotin and 6'-Sialyl-N-acetyllactosamine-biotin (Dextra), were diluted down to 0.2 µg/ml. The viruses used were diluted to 15 µg/ml based on a Bradford protein assay (2.3.10) in HBS-EP containing 100 µM oseltamivir carboxylate (Aobious AOB 5627) and zanamivir (Sigma Aldrich, SML0492) which were added to inhibit neuraminidase. Optimisation was performed for both assays. The timings used were:

Baseline – 240s

Loading – 300s

Wash buffer – 240s

Association – 1800

Dissociation – 1800s

2.2.14.2 Quantitative assay

Prior to performing the assay, streptavidin coated biosensors were hydrated in HBS-EP buffer (10 mM HEPES pH 7.4, 150 mM NaCl, 3 mM EDTA and 0.005% tween-20) for a minimum of 10 minutes at room temperature. A 96-well black flat-bottomed plate was made up with HBS-EP buffer in column 1, the diluted lectin and a control well in column 2, HBS-EP buffer and drugs in column 3 and finally the virus/pseudotype virus in column 4. The two lectins; 3'-Sialyl-N-acetyllactosamine-biotin and 6'-Sialyl-N-acetyllactosamine-biotin

(Dextra) were diluted down to 0.2 µg/ml and then down by x1.75. The viruses were diluted to 15 µg/ml based on a Bradford protein assay in the same buffer containing the same concentration of drugs. The same timings were also used in this assay.

2.2.14.3 Basic octet data analysis

Analysis was done using Octet Analysis Studio 13.0.0.32, which automatically received the data once the assay was complete. The first step in processing the data was to select the reference sensor (the non-specific binding control) and subtract that from all wells by average. Then the reference sample was selected (the baseline drift control) and subtracted from the remaining samples. The data was then corrected, using the average of the baseline step to align the samples on the y axis. Then the previous steps were shifted to the end of the dissociation step to correct for the interstep and finally Savitzky-Golay filtering was applied to remove high frequency noise from the data. The next step was to open the kinetic analysis tab which applied the subtractions and corrections and produced graphs plotting the time vs the absorbance (nm). This also calculated the kinetics for each interaction, including the dissociation rate constant (k_{dis} (1/s)).

2.3 Molecular biology methods

2.3.1 Plasmid transformation

Plasmids were transformed using Subcloning Efficiency DH5α chemically competent cells (Fisher Scientific UK Ltd). An aliquot (50 µl)

was thawed on ice before 2 µl of DNA was added, mixed and left to incubate on ice for 30 minutes. The cells were then heat shocked in a heat block at 42°C for 20 seconds and then incubated on ice for 2 minutes. The cells were added to a 950 µl aliquot of warmed LB broth (Sigma, Cat no. L3522) for maximum transformation efficiency before being placed in a shaking incubator for one hour at 37°C at 220 rpm. LB agar plates (Merck Life sciences) were made following manufacturer guidelines by adding ten 1.68 g tablets to 483 ml of ddH₂O with an additional 100 µg/ml of ampicillin. Next 200 µl of the LB broth containing transformed cells was plated and incubated at 37°C overnight. The following afternoon, colonies were picked and inoculated in 4 ml of LB media containing 100 µg/ml of ampicillin and left to grow overnight (16–18 hours) at 37°C and 220 rpm.

2.3.2 Plasmid DNA purification and quantification

Extraction and purification of plasmid DNA from the transformed cells was carried out using the Qiagen Spin Mini Prep kit (QIAGEN). Manufacturer's guidelines were followed except for the addition of a 2-minute incubation at 60°C before the final spin step. The final elution was also eluted twice through the spin column to maximise the DNA yield. The concentration and purity of the DNA was measured using the NanoDrop 2000 spectrophotometer.

2.3.3 RNA extraction

The cell pellets collected were thawed and 500 µl of PBS was added. The solution was centrifuged for 2 minutes at 13,000 rpm on a benchtop centrifuge and the appropriate volume of ethanol and lysis buffer was added. Then either the Qiagen RNAeasy kit or the Macherey-Nagel NucleoSpin RNA kit were used for the remainder of the RNA extraction following the manufacturer's guidelines. For extraction of viral RNA from collected supernatant the Qiagen Viral RNA kit was used with the spin protocol, following the manufacturer's guidelines. The RNA concentration was measured using a Nanodrop 2000 spectrophotometer.

2.3.4 M gene RT-qPCR

The M gene RT-qPCR was run using the 2x SensiFAST Probe No-ROX One-Step mix (Bioline). The master mix was made up with the following components: 10 µl 2x SensiFAST Probe No-ROX One-Step mix, 0.8 µl of 10 µM forward and reverse primers, 0.2 µl of probe, 0.2 µl reverse transcriptase (Bioline), 0.4 µl RiboSafe RNase Inhibitor (Bioline) and H₂O to make each reaction up to 16 µl. Finally, 4 µl of template was added per reaction once plated up. Two non-template controls were also included. The RT-qPCR was set up with the following parameters: reverse transcription: 45°C for 15 minutes, polymerase activation: 95°C for 2 minutes and then 45 cycles of 95° for 5 seconds and then 60°C for 30s for the denaturation and annealing/ extension. A standard curve

was produced using M gene RNA produced by in vitro transcription (kindly gifted by Dr Suresh Kuchipudi) to provide a known copy number.

Table 2.5. The M gene primer and probe used for M gene RT-qPCR.

The primers amplified a 101 bp region of the M gene.

Primer/ Probe	Sequence (5'-3')
M gene Forward	AGATGAGTCTTCTAACCGAGTCG
M gene Reverse	TGCAAAAACATCTTCAAGTCT
Hydrolysis probe	[6FAM] TCAGGCCCCCTCAAAGCCGA [BHQ1]

2.3.5 Reverse transcription

A master mix was made up with the following components: 1 µl 50 µM Oligo d(T)₂₀ primer or 50 µM random hexamers, 1 µl 10 mM dNTP mix and 13 µl nuclease free water per reaction. The master mix was mixed and centrifuged for 15 seconds at 8,000 g. Then 15 µl of the master mix was added to 10 µl of template RNA in individual tubes and centrifuged for 15 seconds at 8,000 g. Each tube was then individually heated to 65°C for 5 minutes and then incubated on ice for 1 minute. A second master mix was made up containing: 4 µl 5x SSIV buffer, 1 µl 100 mM DTT, 1 µl RNaseOut Recombinant RNase inhibitor and 1 µl SuperScript IV reverse transcriptase per reaction which was then mixed and centrifuged for 15 seconds at 8,000 g. Once centrifuged 7 µl of the master mix was aliquoted into the previous tubes and because random hexamers were used the mixture was left to incubate at 23°C for 10 minutes. The samples were then moved to a heat block to be incubated at 55°C for 10 minutes and then inactivated at 80°C for a final 10

minutes. Samples were then either stored at -20°C until further use or processed straight away.

2.3.6 Quantitative polymerase chain reaction

Quantitative polymerase chain reaction (RT-qPCR) assay was carried out using a CFX connect real time PCR detection system (Bio-Rad). Gene specific primers were used to select certain cytokines based on the species of the cell line (IL-6, TNF- α , IFN- α and IFN- β) primer sequences can be seen in Table 2.6 along with hydroxymethylbilane synthase (HMBS) or β -actin which were used as a reference gene as an internal control. A master mix for each cytokine included the following: 10 μ l SYBR Green Master mix, 7 μ l of water, 1 μ l forward primer and 1 μ l reverse primer. Into a 96-well plate, 19 μ l of the master mix was aliquoted into each well and then 1 μ l of template was added afterwards. The plate layout was altered to accommodate additional virus dilutions performed and to increase the number of cytokines that could be observed per plate.

The plate was centrifuged for 2 minutes at 2000 rpm and then a 3-step cycling protocol was followed in the thermocycler. The first step was for the plate to be heated at 95°C for 2 minutes. The next three steps were repeated 40 times, 95°C for 5 seconds, 60°C for 10 seconds and finally 72°C for 10 seconds. At the end of each cycle the fluorescence was read, and the melting curve analysis was performed from 65–95°C every 2.2°C increase in temperature. A cycle threshold (Ct) value was

calculated for each sample and all samples were run in duplicate or triplicate depending on plate space.

Table 2.6. Primers used for qPCR for the target and reference genes used.

Gene	Primer	Sequence (5'-3')	TM (°C)
Canine TNF α	F	ACCACACTCTTCTGCCTGCT	61.4
	R	CTGGTTGTCTGTCAGCTCCA	59.6
Canine IFN β	F	CCAGTTCAGAAAGGAGGACA	58.7
	R	TGTCCCAGGTGAAGTTTTCC	57.6
HMBS	F	TCACCATCGGAGCCATCT	57.6
	R	GTTCCCACCACGCTCTTCT	59.6
GAPDH	F	GAGAAAGCTGCCAAATATG	57.5
	R	CCAGGAAATGAGCTTGACA	61.5
Beta Actin	F	GGCATCCTGACCCTCAAGTACC	67.8
	R	GCTCGTTGTAGAAGGTGTGGTG	65.8
Equine IL-6	F	GGATGCTTCCAATCTGGGTTCAAT	69.7
	R	TCCGAAAGACCAGTGGTGATTTT	67.5
Equine TNF α	F	TTACCGAATGCCTTCCAGTCAAT	67.3
	R	GGGCTACAGGCTTGCTCACTT	63.2

Melting temperature (TM), tumour necrosis factor (TNF), interferon (IFN), hydroxymethylbilane synthase (HMBS), glyceraldehyde-3-phosphate dehydrogenase (GAPDH) and interleukin (IL)

2.3.7 SDS-PAGE

Samples were diluted in 2x Laemmli Buffer (Merck) and heated at 98°C for 5 minutes. Whilst heating, 12% precast protein gels (several suppliers used) were prepared and placed into a gel tank and appropriate running buffer was added to cover the wells and half fill the

tank. Once heated 10 µl of each sample was added per well and 7–10 µl of Prestained protein ladder (several suppliers used) was applied to the first well. The lid was added to the gel tank then it was plugged into the power supply. The gel was electrophoresed at 200V for 40–60 minutes and then the gel case was prised open and briefly rinsed with de-ionised water.

2.3.8 Coomassie staining

Once rinsed the gel was placed into a clear tub and Coomassie stain (several suppliers used) was added to cover the gel and left to incubate on a plate shaker for 20–60 minutes. Once sufficiently stained, the stain was removed and replaced with de-ionised water and left overnight to de-stain. The next day the gel was imaged using the iBright 750 imager (ThermoFisher).

2.3.9 Western blot

Alternatively, a western blot was performed. Prior to the SDS-PAGE finishing, five sponges and two pieces of filter paper were soaked in transfer buffer and pressure was applied to remove excess bubbles from the sponges. Simultaneously the membrane (several suppliers used) was soaked in methanol in preparation for transfer. Once the gel had finished, the western blot was layered by placing three sponges against the cathode. The case surrounding the gel was broken open and the foot and wells of the gel were removed. One of the pieces of filter paper was placed on top of the gel and then transferred onto the

layered sponges. The membrane was removed from the methanol and briefly rinsed in transfer buffer before being carefully placed on top of the gel and then carefully pushed against to remove any bubbles. The final piece of filter paper was added and then the two remaining sponges were placed on top. Finally, the anode was put on, and the apparatus was placed into a gel tank. The central area of the tank was filled with transfer buffer until the sponges were covered and the space outside of it was filled with RO water. The gel tank was plugged into the power supply and run at 30V for 1 hour.

Once the gel had finished transferring to the membrane the apparatus was opened, and the membrane was placed into blocking buffer overnight. The next day the membrane was placed into a 50 ml tube with the chosen antibody diluted in PBS-T for an hour at room temperature and rolling. After the hour was up, the antibody was removed and five washes with PBS-T were performed over 25 minutes in total. Once the washes were completed One Step NBT/BCIP (ThermoFisher) was added, and it was left to incubate for 5–10 minutes until colour had developed. The membrane was rinsed with RO water and then visualised using an iBright 750.

2.3.10 Bradford protein assay

Bradford reagent (Merck) was gently mixed and brought up to room temperature. BA standards were prepared at 1.4 mg/ml, 1.0 mg/ml, 0.5 mg/ml, 0.25 mg/ml and 0.125 mg/ml. In a 96-well U bottomed plate, 5 µl

of each protein standard and sample was added in duplicate. Then 250 μ l of Bradford reagent was added per well and the plate was placed onto a shaker for 30 seconds. The samples were left to incubate for 15 minutes and then the absorbance was measured at 595 nm. The absorbance and the protein concentrations were plotted on a graph and a standard curve was plotted. The samples were then plotted onto the graph and the concentration was calculated based on the standard curve.

2.4 Computational methods

2.4.1 Phylogenetic trees

All phylogenetic trees were generated using MEGAX with nucleotide sequences downloaded primarily from GenBank but additionally from GISAID. Sequences were aligned by ClustalW and then the model function was used to suggest the best maximum likelihood tree. The model with the lowest Bayesian information criteria (BIC); Hasegawa-Kishino-Yano with discrete gamma distribution was chosen as the substitution model. This was then applied to construct the maximum likelihood tree using 200 bootstrap approximations. To root the tree, A/equine/Miami/1963 was chosen, and any additional labels/ highlighting was performed using FigTree v1.4.4.

2.4.2 Statistical analysis

All statistical analysis and generation of graphs was completed using GraphPad prism (varying versions).

For ELISA results the data was added to GraphPad in duplicate and then was baseline corrected, and column math was applied to calculate the mean and standard error mean. These were then plotted onto grouped, summary data graphs with absorbance on the y axis and virus or VHH on the x axis.

For the viral replication curves, the ct values were added in duplicate per time point and per virus (separate columns). The mean and error (as standard deviation) was then plotted on XY graphs with connected lines plotted. The ct value was plotted on the y axis and time on the x axis.

The cytokine results were calculated on Microsoft excel using two housekeeping genes that were averaged. The averages were added together and multiplied by 0.5. This was labelled the reference ct, which was then subtracted from the averaged gene of interest ct value to calculate the Δ ct. Each virus was tested in duplicate and using GraphPad prism, the mean and standard deviation were plotted on a grouped, summary data graph. An unpaired T test was performed between each virus and the mock assuming gaussian distribution and the statistical results were plotted onto the graphs.

The pseudotype titres were added to GraphPad prism in single or duplicate and were then plotted on a grouped summary data graph. The

bars are representative of the mean and the error bars of the standard error of mean.

3 Development of single domain antibodies (sdAb) for differentiation between Florida clades of equine influenza A virus

3.1 Introduction

Viruses of the H3N8 subtype of equine influenza A virus (eIAV) are currently circulating almost worldwide; however, the subtype has diverged into distinct lineages, because of antigenic drift. Antigenic drift introduces minor changes across the envelope protein on the viral epitopes, including at antigenic sites surrounding the receptor-binding site. In influenza A viruses (IAVs) antigenic drift is common because RNA dependent RNA polymerase has no proof reading mechanism in the replication cycle (Steinhauer et al., 1992). The surface glycoprotein, haemagglutinin (HA), is susceptible to rapid evolution resulting in potential changes to crucial viral functions (Zolotarova et al., 2019). Alterations in the HA can lead to vaccine failure as they may allow the virus to evade the host's immune response due to impairing antigen recognition (van de Sandt et al., 2012a). These alterations mean that HA is the focal point in the surveillance of equine influenza virus and in subsequent vaccine design (Lewis et al., 2011). Compared to human IAV, eIAV has been observed to undergo antigenic drift at a slower rate so changes to vaccine composition are required less frequently (Murcia et al., 2011).

The two lineages of equine H3N8 IAV are named Eurasian and American according to the geographic origin of the earliest strains. Two clades descended from the American lineage, Florida clade 1 (FC1) and Florida clade 2 (FC2) as demonstrated in Bryant et al. (2009) (Figure 3.1). Both clades spread internationally but each clade circulated in specific continents. Florida clade 1 predominantly circulated in America and clade 2 in Europe and Asia (Ahmed et al., 2022). Whilst they predominantly circulate in these continents, both clades have caused outbreaks in Europe, Africa, South America, and Asia (Ahmed et al., 2022, Cullinane and Newton, 2013, Diallo et al., 2021). The prototype strain for FC2 in the UK was A/equine/Newmarket/5/2003, but the representative strain for inclusion in equine influenza vaccines was updated to A/equine/Richmond/2007 (OIE, 2022). The FC1 clade currently recommended for inclusion in vaccines is A/equine/South Africa/2003. The two clades are still circulating at the time of writing, but clade 1 viruses are now predominantly circulating in Europe (OIE, 2022). In 2019, there was an outbreak across Europe affecting 228 horse premises in the UK, 80 premises in Ireland and 60 in France (OIE, 2020). This outbreak affected both vaccinated and unvaccinated horses, with vaccinated horses showing reduced clinical signs. This indicates the need to ensure vaccines used are protective against the currently circulating strains as vaccine breakdown may have been the reason for clinical manifestation in vaccinated horses (Oladunni et al., 2021).

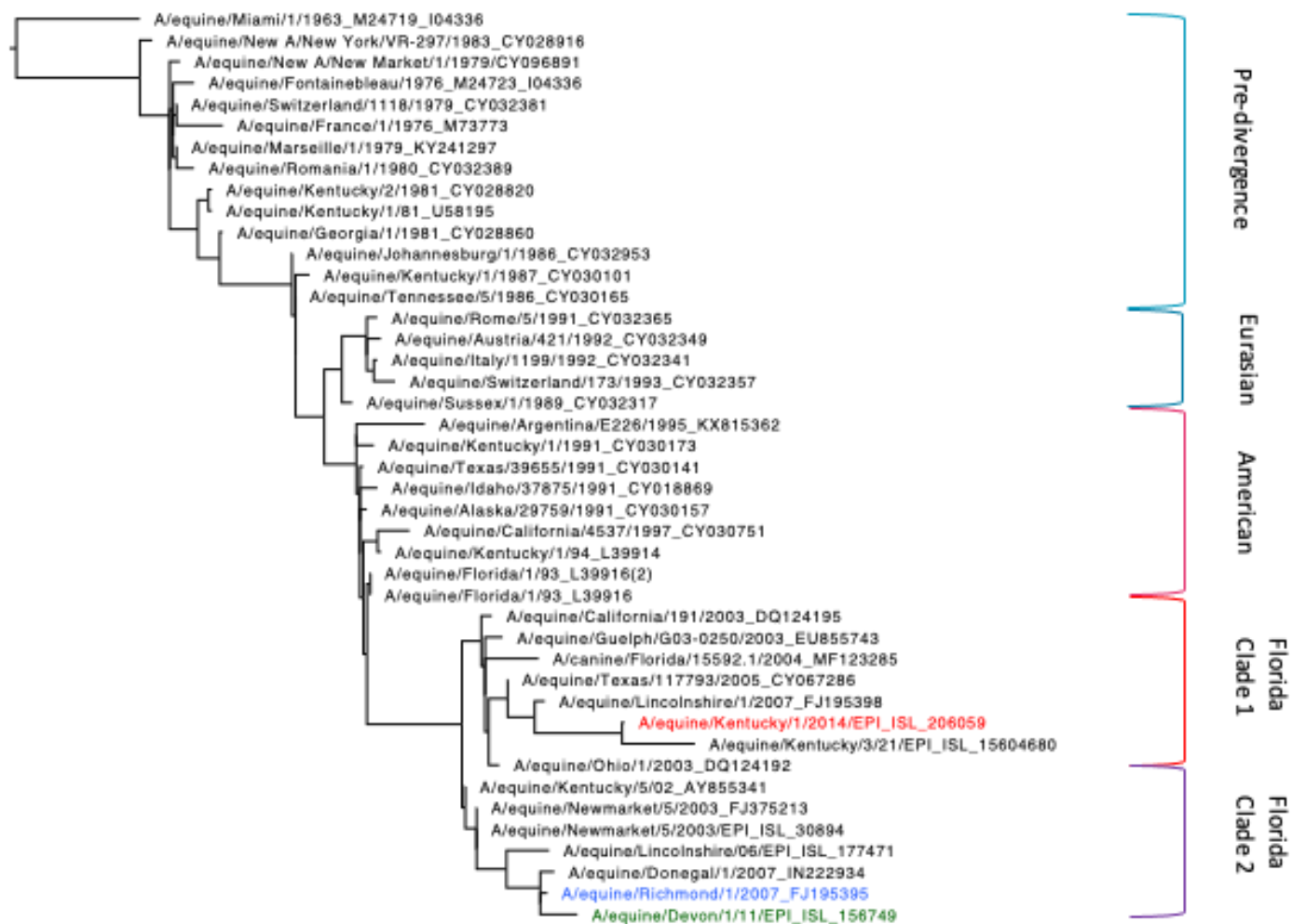


Figure 3.1. Phylogenetic tree of the H3N8 HA1 sequences of equine influenza viruses. Maximum likelihood phylogenetic tree constructed at 200 bootstrap approximations using equine influenza A virus nucleotides sequences downloaded from GenBank and GISAID on MEGAX and Hasegawa-Kishino-Yano model with gamma distribution. The tree is rooted on A/equine/Miami/1/1963. The three viruses central to this study are highlighted A/equine/Kentucky/1/2014- red, A/equine/Richmond/1/2007- blue and A/equine/Devon/1/11- green. Adapted from Wu (2020) .

3.1.1 Current methods used for characterising equine influenza A virus

Currently, one of the main methods for characterising eIAV is the haemagglutinin inhibition (HI) test (OIE, 2024). The HI test can distinguish between different influenza strains of the same subtype using antisera from animals.

The HA sequences of the two Florida clade viruses originally differed by two residues at positions 159 and 78 (Bryant et al., 2009) but since 2011 a variation in position 144 has been observed in FC2 clade viruses (Nemoto et al., 2019, Yamanaka et al., 2015). The 2019 outbreak mentioned above was significant because there were not any antigenic differences in the virus strains that could be attributed to the large-scale outbreak when standard HI testing was performed (OIE, 2020). Nemoto et al. (2021) used a virus neutralisation test because it has been shown to have higher sensitivity to differences in the antigenic sites using equine antisera compared to an HI test. The results from the neutralisation test suggested variations in antigenicity, however, a meaningful distinction was not identified.

Changes in viral epitopes have historically been mapped using monoclonal antibodies produced by hybridoma cells (Ito et al., 1998). Monoclonal antibodies (mAbs) have a single epitope and display high specificity, hence their use in epitope mapping (Luo et al., 2020). Their

development depends on the inoculation of animals with either: inactivated virus or, for example, with the HA protein expressed in bacteria, at varying time points and then spleen cells are harvested from select animal species. The spleen cells are then fused with immortal myeloma cells to form hybridoma cells that are also immortal. The hybridoma cells are then screened and cloned for the long-term production of antibodies (Mitra and Tomar, 2021). This process is lengthy and necessitates costly animal experiments. Generating ferret antisera for neutralising tests also requires immunising animals and is therefore becoming increasingly discouraged for ethical reasons.

3.1.2 Antibody phage display

This study uses antibody phage display, a method that produces antibodies largely without using animals, instead using bacteriophage to display peptides. The technique uses antibody phage libraries, typically synthetic, to provide a high diversity of random peptides in varying amino acid lengths that can be used to produce antibodies to target antigens (Tsoumpeli et al., 2022). Immune libraries are created by immunizing animals or human B-cells and these libraries produce high quality and high affinity antigen specific antibodies, however it is time consuming and requires a new library for each antigen (Bazan et al., 2012). Naïve libraries are also human, or animal derived however the individual is not immunized against the target antigen so can produce a single library against all antigens in a quicker time frame but will likely be lower affinity to target antigens (Moon et al., 2011). Synthetic

libraries whilst challenging to use, provide many advantages including, avoiding animal testing or immunisation, can be used with non-immunogenic or toxic targets, shorter time to obtain binders and are able to be used in multiple projects (Valdés-Tresanco et al., 2022).

There is a range of antibody formats that can be used in phage display: fragment antigen-binding (Fab), single chain variable fragments (ScFv) and variable domain of heavy chain (VHH) (Figure 3.2) by mutating the CDR2 and CDR3 regions in a single scaffold during library construction. The VHH is the variable domain of the heavy chain, however camelids have heavy chain only antibodies, therefore heavy chains on other antibodies act as antigen-binding sites (Hamers-Casterman et al., 1993). In the VHH there is a change in the complementarity-determining region 3 (CDR3) that makes it longer than a typical CDR3 to compensate for the missing light chain (Bond et al., 2003, Muyldermans et al., 1994), which can be altered in synthetic phage libraries to typically include 12, 16 and 21 amino acid random sequences (Tsoumpeli et al., 2022). As is common amongst phage library designs the CDR1 and CRD2 were left at fixed lengths because not all amino acids are used due to folding constraints (Muyldermans, 2021b).

Limitations in the length of CDR3 regions reduce structural flexibility and remove the ability to form extended loops that have the capacity to identify hidden epitopes (Liu et al., 2022). Target-specific antibodies have a variety of applications including drug delivery and proteomics. This method of antibody production is rapid and animals do not need to be immunized (Aghebat-Maleki et al., 2021).

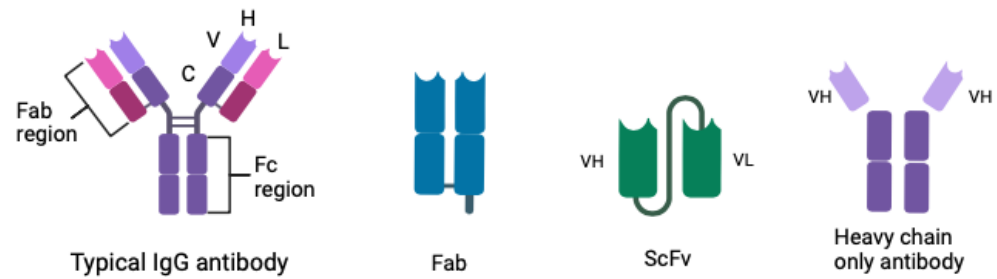


Figure 3.2. Types of antibody format used in phage display. A

typical IgG antibody and the different domains that are used for each antibody format, fragment antigen-binding (Fab), single chain variable fragments (ScFv) and variable domain of heavy chain (VHH). Adapted from André et al. (2022) and created using BioRender.

When performing antibody phage display there are three steps: 1) generation and display of the antibody library; 2) enrichment of the antibodies that bind to the antigen by repeat binding rounds (panning) and amplification; 3) finally, recovery of the antigen-specific antibodies. After the panning rounds, traditionally hundreds of colonies are picked and then tested by ELISA, initially using pooled phage to screen for potential binders and then repeated using individual phage that bound during panning. Alternatively next generation sequencing (NGS) of the phagemids can be used to identify sequences enriched in phage panned against the target antigen. The NGS can be prepared for by purifying the phagemid DNA produced at the end of the panning rounds and then performing 2 rounds of PCR: (1) to amplify the region containing the CDR3 and (2) to attach barcodes that are site compatible with Ion Torrent sequencing so samples can be pooled during

sequencing and then pulled apart during analysis using the barcodes. The DNA is then pooled and sent off to be sequenced.

3.1.3 Project background

The work done prior to starting this used a VHH library created by Tsoumpeli et al. (2022). This library can identify binders to any potential antigen, which is why it was used by a former PhD student in the group (Wu, 2020). The aim of the project was to generate an antibody that could be used to differentiate between the two Florida clades of equine influenza virus using one representative of each clade. To do this, two 7:1 recombinant viruses were made using reverse genetics by Dr Debra Elton and Dr Adam Rash at The Animal Health Trust (now closed). These viruses both had seven genome segments from A/equine/Richmond/07 and the HA from A/Kentucky/1/2014 (rFC1) or A/Devon/1/2011 (rFC2), respectively and are the representatives (Figure 3.3). This enabled a panning strategy to be designed that focused on enriching phage that recognised the HA proteins, as seen attached to the plate in Figure 3.3. Each experiment had either three or five rounds of panning, which included binding the phage to the chosen antigen and washing off any phage that did not bind. The bound phage were eluted and then amplified in bacteria for repeat panning to identify potential binders. Further information on the phage and methods used were described by Wu (2020).

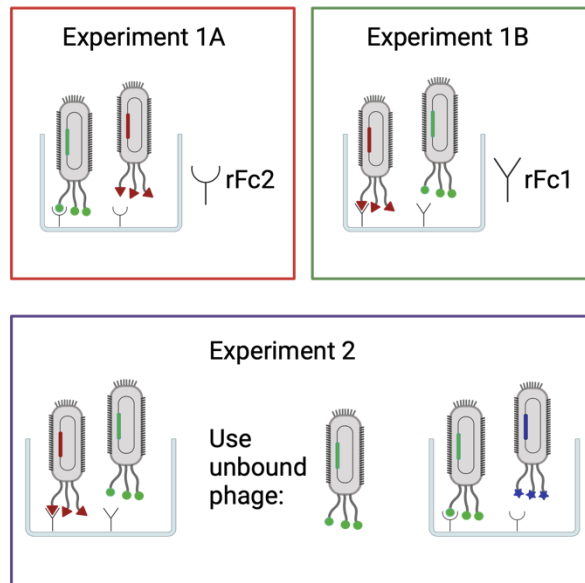


Figure 3.3. A breakdown of the phage display experiments. Three phage display experiments were performed, in the first two (1A and 1B) the VHH library was panned against the representative of FC2 and FC1 attached to the plate signified by curved or triangular shapes respectively. In experiment 2, the library was initially panned against rFc1, then the unbound phage were panned against the rFc2 to identify binders that were specific to rFc2. Image created using BioRender.

Wu (2020) performed the panning, submitted the phage for sequencing and analysed the data. In this project, the data analysis was independently repeated as described below.

3.1.4 Aim

To develop an antibody reagent that can differentiate between the two Florida clades of equine influenza A virus.

3.1.5 Objectives:

- Analyse the next generation phage display data.
- Express soluble maltose binding protein (MBP)-fused VHH antibodies in *E. coli*.
- Analyse the ability of the MBP-fused VHH antibodies to differentiate between the two Florida clades e.g. ELISA or HI.
- Generate Fc fused VHH antibodies.
- Analyse the ability of the Fc fused VHH antibodies to differentiate between the two Florida clades.

3.2 Methods

3.2.1 Next generation phage display analysis

The deep sequencing data was provided as a FASTQ file after Ion Torrent Sequencing by the University of Pennsylvania commercial service. The Perl scripts for use in a Unix-like command line interface were provided by Dr Jon Owen (ADAS Biotechnology) and can be found at https://github.com/UoN-ADAS-KGough/NGS_Scripts01 although some adaptations were made. A list of Ion Torrent barcode sequences was also provided to identify individual samples (Appendix 2). To identify HCDR3 sequences as possible VHH candidates, the HCDR3 sequences first needed to be extracted and then analysed. Two methods were used to determine which phage sequences were positively enriched compared to negative controls in different panning rounds. The first was the Z score (3.2.1.1) and the second the highest

frequency analysis (3.2.1.2). A version of the scripts in table form can be found in Appendix 3.

The first command script converted the FASTQ file to a FASTA file as the raw data was decompressed. The second round of demultiplexing involved the individual barcoded sequences identified in the Ion Torrent barcode (BC) sequence list (Appendix 2). This allowed identification of all 96 specific barcoded sequences, which were then split into individual files. Each file was then reverse complemented to allow for the VHH library being sequenced in reverse. The next script that was run involved translating each reverse complemented FASTA file into three reading frames (-f 1, 2 and 3) producing three output files. The three output files were combined into a single file using the 'cat' Unix standard utility command. Within this pooled file there were motifs bordering the VHH randomised region (CDR3); this iterate command searched for and identified the CDR3 sequence within the file. The left flanking sequence was 'YYCAA', and the right flanking was 'WGQGT'; only sequences with these motifs adjoining them were used in the next step. To reduce the chance of non-functional sequences appearing, a minimum number of four amino acids was required to appear between the flanking motifs. The negative controls for each individual experiment were grouped together so they could be compared with the individual positive barcodes. Each round of panning and experiment had a separate set of negative controls, in this case:

Experiment 1A Round 3: BC49–BC56

Experiment 1A Round 5: BC57–BC6

Experiment 1B Round 5: BC67–BC76

Experiment 2 Round 3: BC77–BC85

Experiment 2 Round 5: BC86–BC95

3.2.1.1 Z-Score analysis

The next step compared the frequencies of the pooled negative controls and the positive barcodes of the .LR.fa file, (file name used after searching for left and right motifs flanking VHH region). This was done by using the positive barcodes for each experiment and round of panning and the negative controls that correspond with each round. The file was output as a table with the ranking of the number of occurrences of each randomised region and percentage. The output table had six different columns of information, the sequence; the number of reads present in the positive sample, the number of reads in the negative control. The Z score is the relative level of each HCDR3 compared to a control sample. A high Z score will be generated when the phage have bound frequently to the target in the target samples, but not in the control sample. The final Z score and the percentages for the reads of the positive samples and negative control samples were also present in the table. This table was then used as the input file to produce new table files with Z score thresholds of ≥ 2 , ≥ 5 , or ≥ 10 . It ranks each sequence based on frequency within the HCDR3 sequences in the target samples but also on its frequency in the negative control. For this analysis, a threshold score of 10 was assigned because there were a

large number of identified binders. The output files from the previous step were then joined together to create one file based on the experimental round. Finally, the pooled samples were sorted numerically in descending order for each peptide that was $Z \geq 10$. The samples with the highest score and the ones enriched across both rounds were identified and taken for further analysis.

3.2.1.2 Highest frequency analysis

The sequences with the highest frequency within each barcode were also identified to test if they might bind to the H3 more broadly rather than to the HA for the specific clades used in the panning round. The following command was used:

```
cat xxxx.LR.fa | grep -v '>' | sort | uniq -c | sort -nr >output.txt
```

This turned each .LR.fa file into a table of results with the sequences in frequency order with the highest at the top. To look across multiple barcodes the files were joined using:

```
cat xxxx.LR.fa yyyy.LR.fa zzzz.LR.fa > joined.LR.fa
```

This produced a table which had all the sequences that occurred at the highest frequency.

3.2.2 Expression of soluble VHH antibodies

Figure 3.4 presents an overview of the steps for expression of the soluble VHH antibodies.

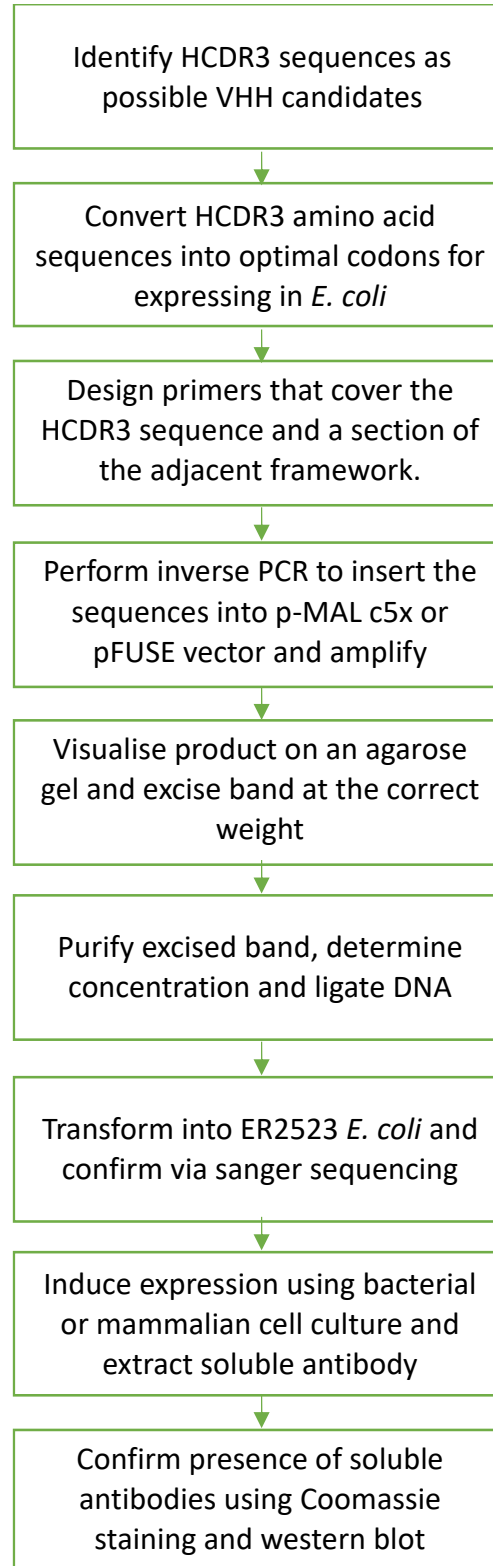


Figure 3.4. Flow diagram of expression of soluble VHH. A

breakdown of the individual steps that were followed once the HCDR3 sequence had been identified.

3.2.2.1 Primer design

The HCDR3 amino acid sequences selected for synthesis, identified during 3.2.1, were converted to optimal nucleotide codons for expressing in *E. coli* using an online conversion tool (www.jcat.de). The *E. coli* strain ‘K12’ was selected as the model organism. The amber stop codons (Klivleyeva et al., 2022) had to be converted to glutamines (CAG or CAA) to resolve potential issues caused by premature stops; the conversion tool performs this process automatically.

There were two design options for the primers. The first option was to design the forward and reverse primers so that they cover half of the HCDR3 sequence as well as each primer covering a section of framework three (F3) and four (F4). The second option was to design a single primer that covers the HCDR3 sequence as well as some of F4 and then design a universal primer that covers a section of F3 (Figure 3.5). Both options require one of the primers to be phosphorylated at synthesis, however the second method which is more cost effective as it only requires one specifically designed primer for each VHH sequence and one universal primer, with this primer being the phosphorylated one. This reduces the overall number of primers that are required.

The primers were designed using a plasmid map of the p-MAL c5x vector on Snapgene 7.2 (Figure 3.6). The universal primer was 5' phosphorylated to ensure efficient ligation of the linear PCR product.

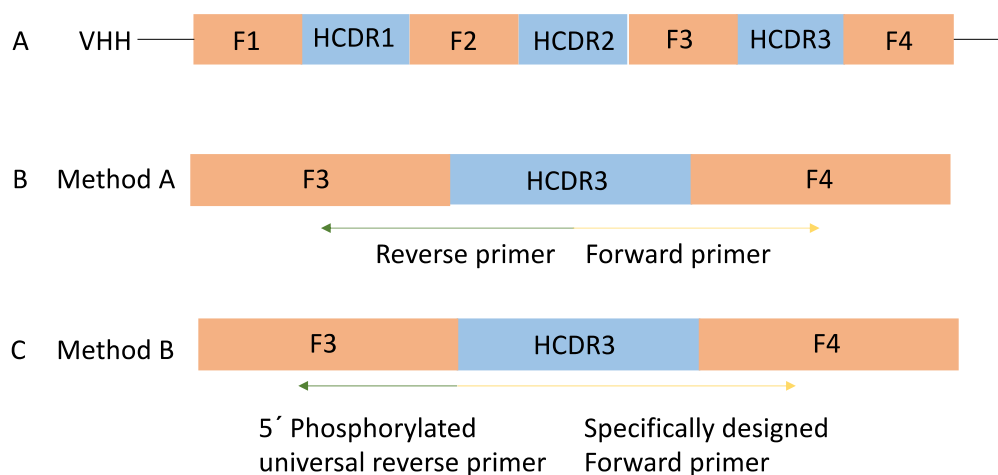


Figure 3.5. Primer design: A) the variable heavy chain region, including HCDR1 and 2 which were not altered B) Method A where the primers cover half of the HCDR3 region each as well as covering several nucleotides in F3 and F4, respectively. C) Method B where a universal 5' phosphorylated reverse primer covering framework three as well as forward primer that must be designed for each sequence, this also covers several nucleotides in framework four.

3.2.2.2 Inverse PCR

The plasmid p-MAL c5x was the target vector and was gifted by Dr Jon Owen as a glycerol stock; it was purified as explained in 2.3.2 and prepared at 10 ng/μl.

The inverse PCR reaction aimed to subclone the HCDR3 sequence into the pMAL c5x vector and amplify the whole construct. In the reaction mixture there was 2.5 µl of 10 ng/µl of DNA template, 0.5 µl Q5 polymerase (New England Biolabs Ltd), 2.5 µl of 10 µM forward and reverse primer, 2 µl of 10 mM dNTPs, 10 µl Q5 enhancer, 10 µl 5X Q5 Buffer and 20 µl of ddH₂O to make the final volume up to 50 µl. The first PCR was run with an initial denaturing step at 95°C for 5 minutes followed by 20 cycles of 95°C for 30 seconds, 52°C for 1 minute and an extension time of 5.5 minutes at 72°C. The following 10 cycles involved 95°C for 30 seconds, 55°C for 1 minute and finally 72°C for 5.5 minutes and a final 10 cycles with 95°C for 30 seconds, 58°C for 1 minute and finally 72°C for 5.5 minutes. The reaction was then held for 10 minutes at 72°C and then chilled at 4°C until removed from the thermal cycler.

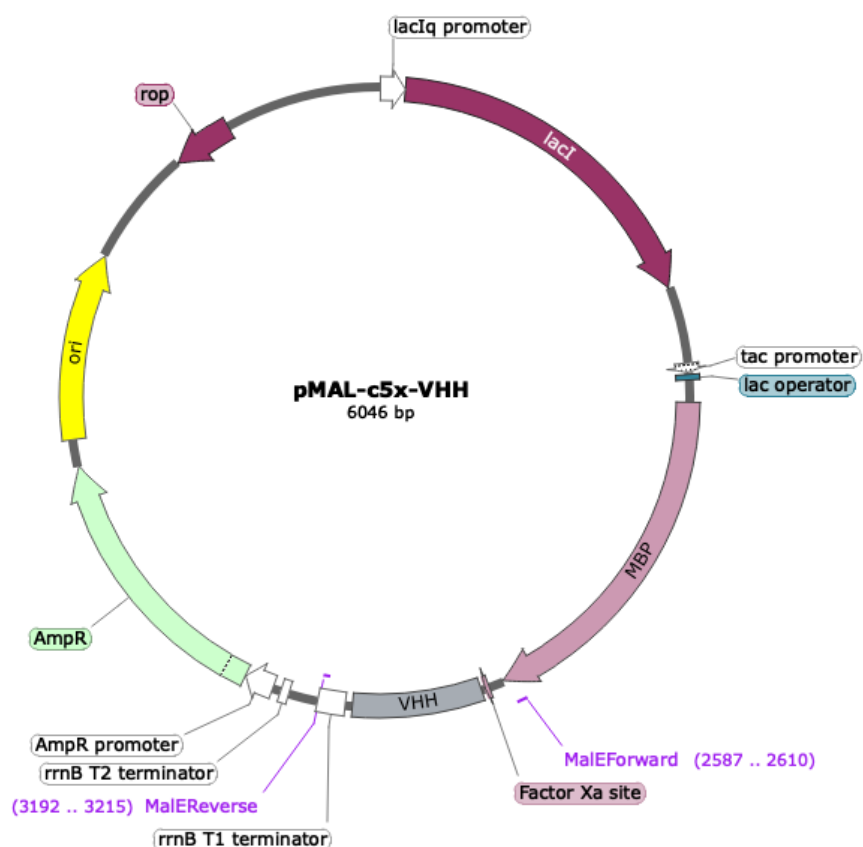


Figure 3.6. Vector map for pMAL-c5x. The target vector used in the inverse PCR to subclone the CDR3 sequence into the VHH section. The vector has an ampicillin resistance gene. It is a bacterial vector for inducible expression of maltose-binding protein (MBP) fusions. The MalEforward and MalERreverse primers are shown on the vector map.

3.2.2.3 Sample visualisation

To visualise the results, 25 µl of each PCR reaction was loaded onto a 1% agarose/TAE gel with 6X gel loading dye (several suppliers used). The agarose gel was stained with Nancy-520 (Merck) and run at 100V for one hour with a 1 kb+ ladder (New England Biolabs Ltd). Bands at around 6 Kb were excised using a scalpel after visualisation using blue

light and were transferred into pre-weighed 1.5 ml microtube. The Macherey-Nagel Nucleospin Gel and PCR clean up kit (Macherey-Nagel #740609.50) was used according to the manufacturer's instructions. The purified samples were analysed by Nanodrop spectrophotometer to determine the DNA concentration.

3.2.2.4 Ligation reaction

The purified DNA underwent ligation prior to transformation. The DNA was added at 50 ng to 1.5 µl of T4 ligase (New England Biolabs Ltd), 3 µl of 10x ligase buffer and then made up to 30 µl with ddH₂O. The reaction mixture was then left to incubate for 72 hours on ice.

3.2.2.5 Transformation into chemically competent cells

The ligation reaction was transformed as described in 2.3.1. The samples were quantified using a Nanodrop spectrophotometer and then sent for Sanger sequencing (Source Biosciences) to confirm the VHH HCDR3 sequences using the MalEforward primer (GGT CGT CAG ACT GTC GAT GAA GCC) and MalERreverse primers (TGT CCT ACT CAG GAG AGC GTT CAC).

3.2.2.6 Protein expression in a trial culture

The target clone was streaked out onto 2xYT plates with 100 µg/ml ampicillin and left to incubate overnight at 37°C. From that plate a single colony was used to inoculate 10 ml of 2xYT broth with 100 µg/ml ampicillin in a 50 ml falcon tube and then left for 2 hours at 37°C. Then

1 ml was removed to check the optical density (OD) OD_{600} . The next day 10 ml cultures were made up and a 1:100 dilution was made up from the overnight culture was added and left to incubate until OD_{600} of 0.6 was reached, a pre-induction control was taken at this point. Isopropyl β -D-1-thiogalactopyranoside (IPTG, several suppliers used) to induce protein expression was added at 1 mM and after 2 hours, 1 ml was collected and centrifuged at 3,500 g for 10 minutes and frozen at -20°C. Another 1 ml sample was collected after 4 hours, spun down and frozen, then a final 1 ml was collected, spun down and frozen following an overnight incubation.

3.2.2.7 Generating electrocompetent cells

Prior to making the electrocompetent cells, SOB was created (2% tryptone, 0.5% yeast, 10 mM NaCl, 2.5 mM KCl, 10 mM $MgCl_2$ and 10 mM $MgSO_4$). From that the SOC media was created (SOB, 20 mM glucose). A single colony of ER2325 was inoculated into 10 ml of SOB in a 125 ml flask and left to incubate for 16–18 hours at 37°C and 250 rpm. Two 1 L flasks with pre-warmed SOB at 37°C were prepared and two drops of overnight culture was added to each flask. The flasks were left to shake at 250 rpm and 37°C until OD_{600} of 0.5–0.7 was reached, the Avanti J-E centrifuge JLA 16.250 (Beckman Coulter) was set to 4°C and 1 L of 10% glycerol (v/v) was placed on ice. Once the appropriate OD_{600} was reached, the flasks were placed on ice for 15 minutes and were poured into chilled 500 ml microcentrifuge bottles and balanced. The bottle was centrifuged at 5,000 rpm for 10 minutes and then put

back on ice, the supernatant was poured off and residual broth was removed. To resuspend the pellet 250 ml of 10% glycerol (v/v) was added to each bottle and then balanced before being returned to the centrifuge for a 10-minute centrifuge at 5,000 rpm. The bottles were then put back on ice, the supernatant removed, and another 250 ml of 10% glycerol was added, the pellet was resuspended and then centrifuged for 10 minutes at 5,000 rpm. The supernatant was removed, leaving a small amount of 10% glycerol and the pellet was resuspended in the residual glycerol, then aliquoted into tubes on ice either at 50 μ l or 100 μ l. It was then transferred to dry ice for 10 minutes before being stored at -80°C.

3.2.2.8 Transformation into ER2523 E. coli

A 50 μ l aliquot of ER2523 cells was thawed on ice and 1 μ l of plasmid was added and mixed. The mixture was put into a pre chilled 1 mm electroporation cuvette and gently tapped on the side and wiped down. The cuvette was put into the module and the Gene pulser Xcell (Bio-Rad) was run using the following options:

- Voltage (V) 1800
- Capacitance (μ F) 25
- Resistance (Ω) 200
- Cuvette (mm) 1

The sample was then pulsed and placed back on ice before 450 μ l of SOC outgrowth media was added into the cuvette and mixed. Then the mixture was moved into a fresh 1.5 ml microtubes. The 1.5 ml tube was

put in the shaking incubator at 37°C and 220 rpm for an hour. Subsequently, 100 µl was added to a 2YT plate with 100 µg/ml ampicillin and streaked out. The plate was left overnight at 37°C and checked for colonies the next day.

3.2.2.9 Protein expression and purification

The target clones were streaked onto 2xYT plates with ampicillin at a final concentration of 100 µg/ml and were left to incubate for approximately 72 hours at 30°C to compensate for the longer incubation time or overnight at 37°C. In a 50 ml falcon tube, 10 ml of 2xYT was inoculated with a single colony and then left to incubate overnight at 37°C and 200 rpm. A 2 L flask with 250 ml 2xYT and 100 µg/ml ampicillin was left overnight at 37°C and an additional 250 ml 2xYT was also left to incubate overnight at 30°C. A 250 ml volume of pre-warmed 2xYT was inoculated with 2.5 ml of overnight culture. The flask was incubated at 37°C and 200 rpm until OD₆₀₀ ~0.6 was reached. When OD₆₀₀ of 0.6 was reached 250 ml pre-warmed 2xYT with 1 mM IPTG and 100 µg/ml ampicillin was added to the culture. Immediately, a 1 ml sample was taken and centrifuged at 3,500 g for 10 minutes and the pellet stored at -20°C until use. The pellet was resuspended in 100 µl 2x Laemmli sample buffer (Sigma Aldrich) and heated to 98°C. The flasks were left to incubate at 30°C for 6 hours at 200 rpm. The remaining culture was centrifuged at 3,500 g for 10 minutes and the pellet stored at -20°C until further use.

The pellet was lysed with 5 ml BugBuster protein extraction reagent per gram (Merck), 0.4 µl of 25 KU benzonase per ml, 1:200 lysozyme and rotated for 30 minutes. Next the samples were centrifuged for 20 minutes at 4°C and 15,000 g and the supernatant was kept at 4°C. The pellet was resuspended in an equivalent volume to the supernatant in column buffer (20 mM Tris 7.4, 200 mM NaCl, 1 mM EDTA) and sonicated at 75% amplitude in 10x10 second pulses. The sonicated sample was centrifuged for 20 minutes at 4°C and 15,000 g and pooled with the supernatant at 4°C. A sample of 10 µl was then added to 10 µl Laemmli sample buffer. A Pierce disposable column was equilibrated with 1 ml of amylose resin and then 2 ml of column buffer was added. The sample was added to the column next and the flow through was collected and a 10 µl sample was taken and added to 10 µl Laemmli sample buffer. Next the column was washed with 40 ml column buffer. A 10 µl sample was taken from the first and last wash and added to 10 µl Laemmli sample buffer. The column was eluted five times with 0.5 ml elution buffer (20 mM Tris 7.4, 200 mM NaCl, 1 mM EDTA, 10 mM maltose) and then a 10 µl sample was taken from each elution and added to 10 µl Laemmli sample buffer. The samples added to Laemmli sample buffer were stored at -20°C and the eluates were stored at 4°C.

3.2.2.10 SDS-PAGE and Coomassie stain of MBP-VHH

For the SDS-PAGE, the samples with Laemmli sample buffer were heated to 98°C for 5 minutes and were processed as described in 2.3.7. The prestained protein ladder was added at 7 µl to be Coomassie

stained. A gel was electrophoresed for each VHH with samples from: the supernatant, flow through, first and last wash and then all five elution steps. The gel was then stained as described in 2.3.8 and imaged.

3.2.3 MBP VHH ELISA

To coat 96-well ELISA plates, the recombinant concentrated viruses used during panning were diluted to 1 µg per well in coating buffer (0.1M sodium carbonate buffer pH 9.6) and then vortexed. Then 100 µl of the diluted viruses was added per well and a plate seal applied. The plate was left to incubate overnight at room temperature. The next day, the soluble antibody extracts from the column purification and the plate were blocked for an hour with 3% skimmed milk in 1x PBS (blocking solution). After an hour, 100 µl of the blocked soluble antibody extract was added per well and left to incubate for an hour at room temperature. Additionally, 100 µl of 3% skimmed milk in 1x PBS without antibody was added as a negative control in duplicate. In addition, post infection ferret antisera raised against A/equine/Kentucky/1/2014 and A/equine/Devon/1/2011 rFC1 and rFC2 respectively, provided by Dr Debra Elton prior to the closure of the Animal Health Trust, were diluted at varying concentrations and included as positive controls. The plate was then washed three times with 1x PBS, three times with 1x PBS with 0.1% Tween 20 (PBS-T) and then patted dry. The anti-MBP monoclonal antibody (NEB # E8032S) was diluted 1:10,000 in blocking solution and 100 µl was added per well and left to incubate for an hour at room

temperature. The plate was washed as described above and then anti-mouse IgG HRP antibody (Cell Signalling Technology #7076) was diluted 1:2,000 in blocking solution. 100 µl was added per well and left to incubate for an hour at room temperature. The plate was then washed as described above and 100 µl of 1 step Ultra TMB ELISA substrate solution (Thermo Fisher Scientific) was added per well and left to incubate for 15 minutes with kitchen foil over the top (Figure 3.7). The reaction was then stopped using 100 µl of 2 M sulphuric acid and the absorbance was read on a Promega Glowmax Explorer at 450 nm.

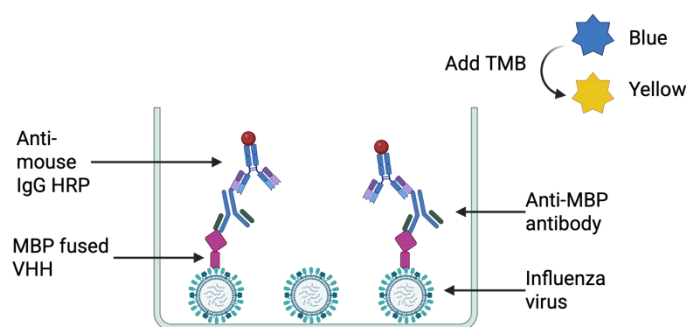


Figure 3.7. MBP fused VHH ELISA. The ELISA method used to detect whether maltose binding protein fused VHH would differentiate between Florida clades of equine influenza A virus. Maltose binding protein (MBP), horseradish peroxidase (HRP) and 3,3',5,5' tetramethylbenzidine (TMB). Image created using BioRender.

3.2.4 Haemagglutination inhibition test

A HI test was performed as described in 2.2.9 substituting the 25 µl of antisera for 25 µl of 50 µg/ml MBP fused VHH. The viruses included were:

- 7:1 recombinant A/equine/Devon/1/2011
- 7:1 recombinant A/equine/Kentucky/1/2014
- A/equine/Shropshire/10
- A/equine/Richmond/07

3.2.5 Expression of Fc fusion VHH antibodies in mammalian cell culture

3.2.5.1 Inverse PCR pFUSE +ss vector

After testing the VHH in the pMAL vector, Fc fusion VHH were generated by inserting the original sequences into a pFUSE vector. The inverse PCR protocol was performed as described in 3.2.2.2 but substituting the pMAL-c5x vector with a pFUSE +ss (Figure 3.8). This vector was modified from a pFUSE-hIgG1-Fc1 by a former PhD student in the lab group (John Bish), to include an II-2 signal sequence and an anti-beta lactamase sequence to be used as a control. The product was visualised as described in 3.2.2.3 and then ligated using the same products but was instead incubated at 16°C overnight and then transformed into electrocompetent cells as described in 3.2.2.8. The media used for bacterial growth was LB. Due to the resistance gene present in the pFUSE vector, the media was supplemented with zeocin at 1:4000. The next day colonies were picked, and overnight cultures were grown. The plasmid DNA was extracted and quantified as described in 2.3.2. The samples were sent for Sanger sequencing using pFUSE_seq_fwd: GGCGCCTACCTGAGA (Figure 3.8) (Source

Biosciences) to confirm the presence of the inserted sequence into the pFUSE vector.

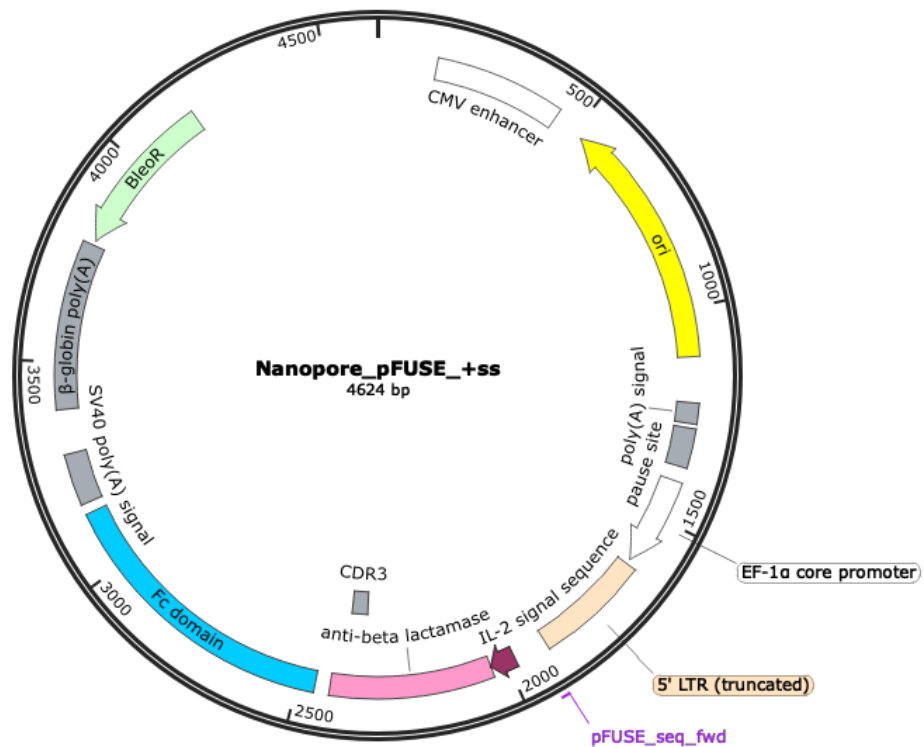


Figure 3.8 pFUSE +ss vector map. This vector has been modified to include an IL-2 signal sequence to assist with solubility of the Fc fusion anti-beta lactamase as it is a protein that is not naturally secreted. The section of the vector adjusted for our sequences was the CDR3 region labelled. The pFUSE_seq_fwd primer was the one used for sanger sequencing to confirm the presence of our sequences. All other sections of the vector were present in the original vector.

3.2.5.2 Plasmid transfection in 293T cells

Initially six-well plates were seeded overnight with 293T cells at 3×10^5 cells per well. To scale up expression, 10cm³ tissue cultures dishes

were seeded with 2.2×10^6 cells per dish. The media was changed to serum-free DMEM an hour prior to transfection. Then 750 μ l OptiMEM and 20 μ l Lipofectamine 2000 were combined according to the manufacturer's instructions and left to incubate for 10 minutes whilst 15 μ g of plasmid DNA was added to 750 μ l OptiMEM. The two solutions were combined and left to incubate for 5 minutes and then added drop wise to the vessel and incubated for 48–72 hours. The supernatant was harvested and stored at -20°C .

3.2.5.3 Protein G purification of harvested supernatant

The harvested supernatant was diluted 1:1 with 0.02M pH 7.0 sodium phosphate buffer (binding buffer). A Pierce Disposable Column was set up with 500 μ l of Pierce Protein G Plus agarose or 1 ml of Pierce Protein G resin and allowed to settle. All the preservative was left to drain. Five column volumes (CV) of binding buffer were added to equilibrate the column prior to the sample being applied to the column. An aliquot of both the supernatant and flow through were collected and then the column was washed with five CVs of binding buffer and aliquots of the first and last washes were collected. Finally, 500 μ l aliquots of 0.1M pH 2.7 Glycine-HCl (elution buffer) were added to the column and collected into 1.5 ml microtubes with 50 μ l of 1M pH 9.0 Tris-HCl (neutralization buffer). The column was regenerated for further use by adding 1 CV of water then 3 CVs of elution buffer followed by two CVs of PBS. The column was then capped at the bottom, 500 μ l of

20% ethanol added and the top sealed. The column was then placed at 4°C for long term storage.

3.2.5.4 Coomassie staining

All the samples taken during the purification were added to 2x Laemmli sample buffer, and heated to 98°C, and then electrophoresed on an SDS-PAGE and Coomassie stained as described in 2.3.7 and 2.3.8. In all gels, 7 µl of pre-stained protein ladder was added so that the product size could be confirmed.

3.2.5.5 Western blot

Samples were also electrophoresed and used for western blot analysis as described in 2.3.9. There was 10 µl of pre-stained protein ladder and a positive control of human sera as the AP antibody used would bind to the sera. The primary antibody used was Anti-human IgG (Fc specific) alkaline phosphatase produced in goat (Sigma #A9544) diluted to 1:5000. The membrane was then washed using PBS-T and then 1-Step NBT/BCIP (Thermo Scientific #34042) was added and left to incubate for no more than 15 minutes or until sufficient colour development. The membranes were then rinsed with water to stop any further colour development.

3.2.6 Fc Fusion VHH ELISA

The ELISA protocol used for the Fc fusion VHH was based on the protocol used in 3.2.3. The 96-well ELISA plates were coated with

concentrated virus at 1 µg/well in sodium carbonate buffer pH 9.6. The plate was incubated overnight at room temperature, and then blocked with 3% skimmed milk in blocking buffer and the Fc fusion VHH were diluted to 10 µg/ml in blocking buffer. Both were incubated for an hour at room temperature along with a negative control containing no VHH. Then, 100 µl of the blocked Fc fusion VHH and negative control were added and incubated for an hour at room temperature. The plate was washed three times with 1X PBS, then three times with PBS-T and patted dry. Anti-human IgG (Fc specific) alkaline phosphatase antibody produced in goats (Sigma #A9544) was diluted 1:5000 in 3% milk in PBS and left to incubate for an hour at room temperature. The plate was washed as described above and 100 µl of pNPP made up from SIGMAFAST pNPP tablets (Sigma) was added per well and then left to incubate for an hour with foil over the top. The plate was then read at 405 nm. The background was removed from all samples.

The viruses used were 7:1 recombinant A/equine/Richmond 07 with the HA from A/Kentucky/1/2014 (rFC1), A/equine/Newmarket/5/03 (FC2), A/equine/Sussex/89 (Eurasian lineage), A/Puerto Rico/8/34 (Human H1N1), A/Canine/Illinois (H3N2) recombinant virus and Schmallerberg virus.

3.2.7 Western blot of transfected cells

To further understand the target of the Fc fusion antibody, 293T/17 cells were seeded onto a 12-well plate at 1×10^5 cells per well in 1.5 ml of complete media. After 24 hours the cells were 65% confluent, and the

complete media was replaced with serum free DMEM. A mix of 7 μ l of lipofectamine 2000 (Thermo Fisher) and 100 μ l of OptiMEM per well were combined in a 1.5 ml tube. In a separate tube 0.5 μ g of plasmid DNA was added to 150 μ l OptiMEM per well. The plasmids used were H3 (A/canine/Illinois/41915/2015), H1(A/Puerto Rico/8/34), NA1 and NP1. The two mixtures were combined and left to incubate for 5–10 minutes and then gently added drop wise to each well, rocked to confirm full coverage and left to incubate for 24 hours at 37°C and 5% CO₂. At the end of the 24 hours, 100 μ l of 2x Laemmli buffer was added per well and transferred into individual tubes prior to heating at 98°C for 10 minutes. SDS-PAGE was performed as described in 2.3.7, followed by western blot performed similarly to the description in 2.3.9. The primary antibody used was the Fc fusion VHH at 10 μ g/ml, which was diluted in 3% milk in PBS-T and rolled at room temperature for an hour. The membrane was washed 5 times with PBS-T, each wash was for 5 minutes. Then anti-human IgG (Fc specific) alkaline phosphatase antibody (Sigma #A9544) was diluted 1:5000 in 3% milk in PBS-T and rolled for an hour at room temperature. The wash step was repeated and then One Step NBT/BCIP (Thermo Scientific) was added and left to develop for no more than 15 minutes, or until sufficient colour development was observed. The membrane was rinsed with water and then visualised using the Invitrogen iBright imager.

3.3 Results

3.3.1 NGS data analysis

From the three panning experiments (1A, 1B and 2), 58 sequences met the Z score criteria described above (3.2.1.1). Several of the sequences were identified in multiple rounds of panning such as RRTLLGFSKPGPRKRK and RRTLWVSKPGPRKRK.

Table 3.1. Sequences identified based on Z-score ≥ 10 . A breakdown of the sequences identified during NGS analysis as explained in 3.2.1.1. The sequences are separated into their individual experiments and the panning round in which they were identified. The sequences surrounded by a box were identified in multiple panning rounds/ experiments. Residues coded by a stop codon were replaced by a lower-case q.

Experiment 1A (Panned against FC2)	
Round 3	Round 5
ACKqPQKLIKPTPAP	EFqLDSCGTLTLRNRK
CITFMSTRKWHIQqIT	EFqLDRLRTLTLRNRK
CPYLqYVWRRPS	EFLAGqLRTLTLRNRK
DYqNTVLVTLEV	RRTLLGFSKPGPRKRK
GPAGqRIDSPRNLRTV	DPYPLIRGVTFCCqAGTTKTK
HHYFRAqVqSAE	
HNSMSTRQRqLHqLLL	
IRKqYRPCRKTQ	
KqTDGTALKRHH	
LKIEqKTVCKFTYALI	
LPTCWADLVNTKTqPG	
NAqRERQ	
NqPTMTWRQWTLGRMR	
NTDqDAVRTVITVTANCMPPq	
PGPPKITNIRARTTTR	
qCVRFRANALSLHLKP	
qLQSPDNNRNRFTSP	
qLSPPYSRSFTPYFGP	
qPISAqAEPNNLMPVR	
qRCRYLLPQSSLQTAK	
qRPRLLLNPGKDYGPQ	
RKLRVPMLWqRQRLMW	
SATSSTYRTLKPTqSH	
SLLARPKDNDLPQqSA	
STYDPLAPENTISIHq	
SWPTRARqQRSIANAL	
TPARKPLSAAqDTALL	
YqPGHLNSHRTVHRNL	
Experiment 1B (Panned against FC1)	

Round 3	Round 5
	SWRVSqSIRKNS
	RRWSNIFETFKNRRTI
	RKHRFKNWSRFRQGLR
	NRRFHRqKWQWRSFFR
	FHYANLRLTQNL
	RRWSNILRLoEqADY
	KRRRFPFGVRRTRQF
	RRRqPFRTWSWRLGRGVKRLT
	RRLVEYFETFKNRRTI
	RRHRRIRGLANRGGRNRKRYA
	SQKLSSqLRRSL
	RRRRPRTWNKFYNKTR
	YKqHPWWPKPWRRPRT
Experiment 2 (Subtracted with FC1, panned against FC2)	
Round 3	Round 5
RRTLLGFSKPGPRKRK	SqGRRRWPFRRARFTV
RRSLLRWTVGRMTRRP	RRTLWVSKPGPRKRK
NqPTMTWRQWTLGRMR	RRTLLGFSKPGPRKRK
AlqRLQPHDPNPQRFR	qTCKYHKPVLPIMLRL
TKGLRFWRYRLRAKL	qRqKSKYLWMWRIRSH
SWKYKTRRAMAqQMGR	WMNWRGqLQRWWAQRRHRNFN
SRGqRDSQRDRFNDqW	RRRLQTWQRFKLPMRS
QRRVqFKTWYIHRSP	AKRKRSPGRLRRRRWL
NMCLHFKNSNNDMGFE	
FqYRFLWTSASRIRAS	
RRTLWVSKPGPRKRK	

3.3.2 Highest frequency analysis

Another 13 sequences were picked because they appeared at a high frequency across all experiments and were hypothesised to be non-specific binders to the HA protein.

Table 3.2. Highest frequency sequences. A list of all the sequences identified during the highest frequency analysis as performed in 3.2.1.2.

Sequences identified
YKqHPWWPKPWRRPRT
PYSRFYDKPYVTRWKH
RRWFRRQIPLRR
VKRRHLINRPSLKRPKSRRSF
SSHLKRWGAWRNKRSR
RGPMGREPqPLRRRRQRWLHR
AKRKRSPGLRRRWL
RSLRPAWWSKLAKRMT
KTRIARWLFP SLRRNARHFYT
LHqPRWRKTLGKSHPR
ARFRSIKIWQRPLQRKRWRF
IKRNLPTAMLKGRWFGMRMR
THQTAAMRMRKARPSLSSqRW

3.3.3 Pilot study

An initial study of 10/71 sequences was performed, due to time and cost restraints. These were picked by choosing the sequences that occurred at multiple panning rounds and were identified by Wu (2020) and myself in individual analyses of the data. The sequences picked from the highest frequency sequences were the first two sequences in the list. The sequences were either 12mers or 16mers in length. Two of the sequences were picked from Table 3.2 as additional candidates. This can be seen in Table 3.3 where the experiment number and round are shown for each sequence.

Table 3.3. Trial experiment sequences and initial primers. A

breakdown of the sequences picked, the experiment and round they originated from, and the primer designed for each one.

Sequences picked	Experiment & round	Primer
AlqRIQPHNDPNPQRFR	2-R3	GCTATCCAGCGTCTGCAGCCGCACGACCCG AACCCGCAGCGTTTCCGTTGGGGACAAGGGA CGCAGGTG
EFLAGqLRTLTLNRK	1A-R5	GAATTCCTGGCTGGTCAGCTGCGTACCCTGA CCCTGCGTAACCGTAAATGGGGACAAGGGAC GCAGGTG
EFqLDRLRTLTLNRK	1A-R5	GAATTCAGCTGGACCGTCTGCGTACCCTGA CCCTGCGTAACCGTAAATGGGGACAAGGGAC GCAGGTG
EFqLDSCGTLTLNRK	1A-R5	GAATTCAGCTGGACTCTTGCGGTACCCTGA CCCTGCGTAACCGTAAATGGGGACAAGGGAC GCAGGTG
HHYFRAqVqSAE	1A-R3	CACCACTACTTCCGTGCTCAGGTTCACTCTG CTGAATGGGGACAAGGGACGCAGGTG
NqPTMTWRQWTLGRMR	2-R5	AACCAGCCGACCATGACCTGGCGTCAGTGGA CCCTGGGTCGTATGCGTTGGGGACAAGGGAC GCAGGTG
PYSRFYDKPYVTRWKH	1B-R5	CCGTACTCTCGTTTCTACGACAAACCGTACGT TACCCGTTGGAAACACTGGGGACAAGGGACG CAGGTG
RRSLLRWTVGRMTRRP	2-R3	CGTCGTTCTCTGCTGCGTTGGACCGTTGGTC GTATGACCCGTCGTCCGTGGGGACAAGGGAC GCAGGTG
RRTLLGFSKPGPRKRK	2-R3&R5	CGTCGTACCCTGCTGGGTTTCTCTAAACCGG GTCCGCGTAAACGTAAATGGGGACAAGGGAC GCAGGTG
YKqHPWWPKPWRRPRT	1B-R5	TACAAACAGCACCCGTGGTGGCCGAAACCGT GGCGTCGTCCGCGTACCTGGGGACAAGGGA CGCAGGTG

The original primers designed for the pilot study used method B from

Figure 3.5. The universal primer not included in this table was:

CGCAGCGCAATAGTAGATCGC. This was used for all initial attempts at inverse PCR before the primers were redesigned.

Table 3.4. The second round of primers designed. The redesigned primers for the seven sequences that did not successfully amplify with the original set of primers in Table 3.3. These primers were designed using method A in Figure 3.5. One of the primers for each sequence was 5' phosphorylated.

Sequences	Primers redesigned
AlqRLQPHDPNPQRFR Forward	TAAACCGGGTCCGCGTAAACGTAAA TGGGGACAAGGGACGCAGGTGACA
AlqRLQPHDPNPQRFR Reverse	GAGAAACCCAGCAGGGTACGACGCGCAGCGCAATAGTAGATCG
EFqLDSCGTLTLRNRK Forward	CCCTGACCCTGCGTAACCGTAAA TGGGGACAAGGGACGCAGGTG
EFqLDSCGTLTLRNRK Reverse	TACGCAGACGGTCCAGCTGGAATCCGCGCAGCGCAATAGTAGATCGC
EFqLDRLRTLTLRNRK Forward	TACCCTGACCCTGCGTAACCGTAAA TGGGGACAAGGGACGCAGGTG
EFqLDRLRTLTLRNRK Reverse	CGCAGCTGACCAGCCAGGAATTCGCGCAGCGCAATAGTAGATCGC
EFLAGqLRTLTLRNRK Forward	TAAACCGGGTCCGCGTAAACGTAAA TGGGGACAAGGGACGCAGGTGACA
EFLAGqLRTLTLRNRK Reverse	GAGAAACCCAGCAGGGTACGACGCGCAGCGCAATAGTAGATCG
RRTLLGFSKPGPRKRK Forward	TCAGTGGACCCTGGGTCTGATGCGTTGGGGACAAGGGACGCAGGTG
RRTLLGFSKPGPRKRK Reverse	CGCCAGGTATGGTTCGGCTGTTTCGCGCAGCGCAATAGTAGATCGC
NqPTMTWRQWTLGRMR Forward	GACCCGAACCCGCGCAGCGTTTCCGT TGGGGACAAGGGACGCAGGTG
NqPTMTWRQWTLGRMR Reverse	GTGCGGCTGCAGACGCTGGATAGCCGCGCAGCGCAATAGTAGATCGC
YKqHPWWPKPWRRPRT Forward	GTGCGGCTGCAGACGCTGGATAGCCGCGCAGCGCAATAGTAGATCGC
YKqHPWWPKPWRRPRT Reverse	CGGCCACCACGGGTGCTGTTGTACGCGCGCAATAGTAGATCG

3.3.4 Inverse PCR

When the inverse PCR was performed, using the first primers designed, only three out of the ten reactions successfully amplified (Figure 3.9). The inverse PCR products were expected to be around 6,000 bp with the VHH added as the pmal-C5X vector is 6,046 bp in length.

Several changes were made to the PCR protocol to attempt to amplify the other seven sequences; the annealing temperatures were increased to 55, 58 and 60°C and then to 60, 62 and 65°C. Neither of these changes yielded amplification and so a gradient inverse PCR was performed. There was no success when performing the gradient inverse PCR and so primers were redesigned using method A in Figure 3.5.

The new primers designed also failed to amplify any products even after making the same modifications to the inverse PCR protocol. The decision was made to continue with the three that worked successfully and revisit the other seven sequences if time allowed. The three successful candidates came from different experiments and were each given an ID (Table 3.5).

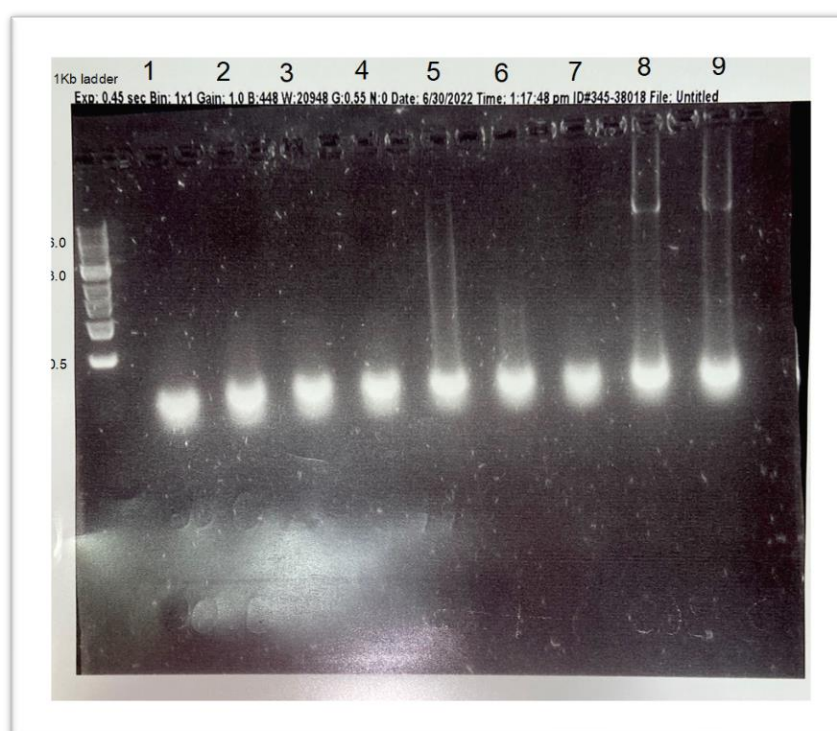


Figure 3.9. Agarose gel of the first nine sequences with bands produced around 6 kb. The products from the first run of the inverse PCR using pmal-C5x as the vector and the primers designed in table 8 were run on a 1% agarose gel with a 1 kb Ladder. The bands for sequences 8 and 9 were at the expected size. Sequence 10 PCR reaction was not run on this gel. Once transformed the mini preps were sent for Sanger sequencing to confirm the presence of the individual HCDR3 sequences (Appendix 4).

Table 3.5. The ID given to the three successful sequences VHH A-C. IDs were given to each sequence that was successfully rescued via inverse PCR.

VHH ID	Amino acid sequence	Experiment & Round	Panning strategy
VHH-A	HHYFRAqVqSAE	1A-R3	Panned against FC2
VHH-B	PYSRFYDKPYVTRWKH	1B-R5	Panned against FC1 Subtracted against FC1 then panned against FC2
VHH-C	RRSLLRWTVGRMTRRP	2-R3	

3.3.5 Trial protein expression

The bands from the agarose gel (Figure 3.9) were successfully excised and cleaned up prior to ligation and transformation into chemically competent cells. The transformed samples were induced using IPTG and then electrophoresed by SDS-PAGE and Coomassie stained (3.2.2.5, 3.2.2.6, 3.2.2.10 without protein purification) (Figure 3.10). The control sample produced visible bands after overnight induction by IPTG, where a band should not have been present. A visible band was expected at 60 kDa however given the presence of a band in the control sample after overnight induction, this was classed as unsuccessful. The decision was made to retransform the samples into electrocompetent cells.

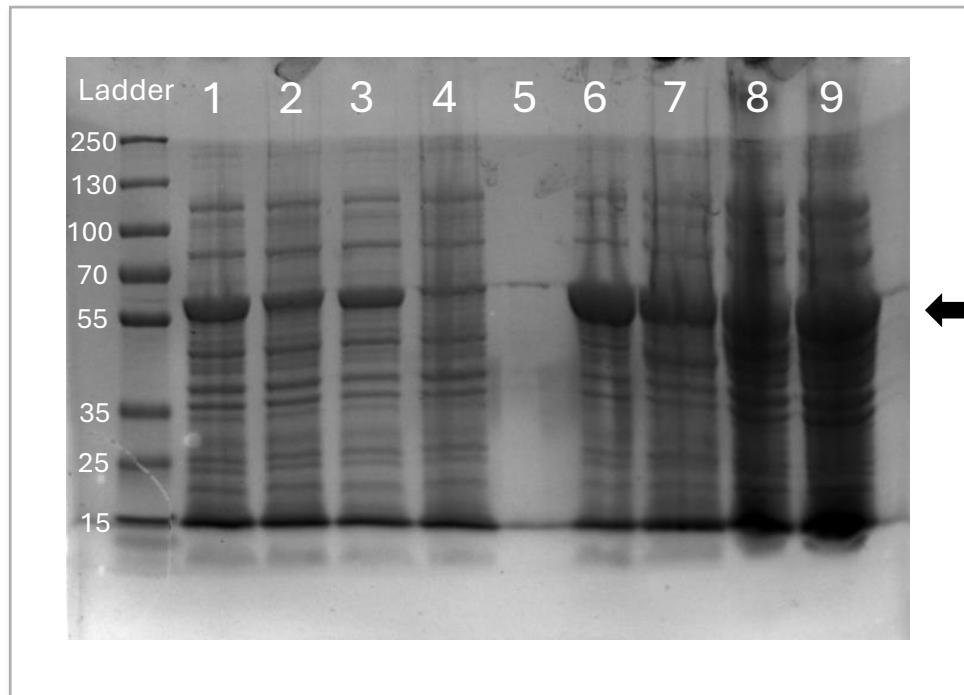


Figure 3.10. Coomassie staining of trial samples after induction by IPTG. Samples were taken after 2 hours and after an overnight incubation post induction with IPTG. Lanes 1–3 are VHH B, C and A, two hours after induction and lane 4 is the two-hour control and lane 5 is empty. Lanes 6–8 are VHH B, C and A after the overnight incubation lane 9 is the control for the overnight samples. The expected band is present at around 60 kDa as shown by the arrow.

3.3.6 Protein expression of retransformed samples

The samples from 3.2.2.5 were used in the retransformation into electrocompetent cells. Transformed cells were induced following the method described in 3.2.2.9. Aliquots were taken during protein induction and stained to check for protein expression (Figure 3.11). There were only bands present in the induced VHH and not the uninduced control. The bands were lower than expected but the large

amount of product made the results difficult to read. The expected molecular weight was ~60 kDa, 45 kDa for the MBP and 15 kDa for the VHH.

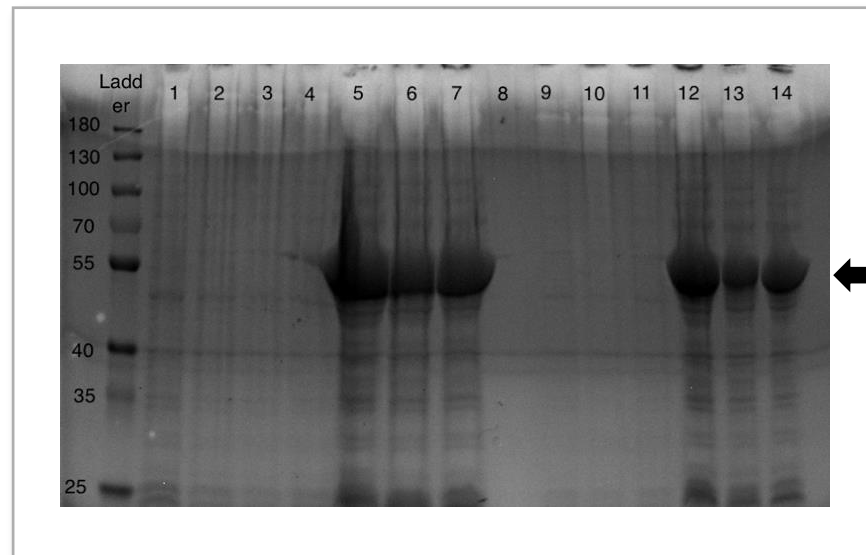


Figure 3.11. Coomassie staining of retransformed VHH B, C and A prior to and during induction. Lanes 1–3 are control samples taken prior to induction, lane 4 is empty, lanes 5–7 are VHH B, C and A 2 hours after induction and lane 8 is empty. Lanes 9–11 are control samples and finally 12–14 are the induced samples after overnight incubation. Bands were present at roughly 50 kDa as indicated by the arrow.

3.3.7 Protein purification of retransformed samples

Samples were taken at set points during the purification process; lysate, flow through, first wash, last wash, and a sample for each elution. Five elutions were performed in total. To confirm the presence of the VHH at each stage, SDS-Page and Coomassie staining was performed (Figure 3.12, Figure 3.13, Figure 3.14).

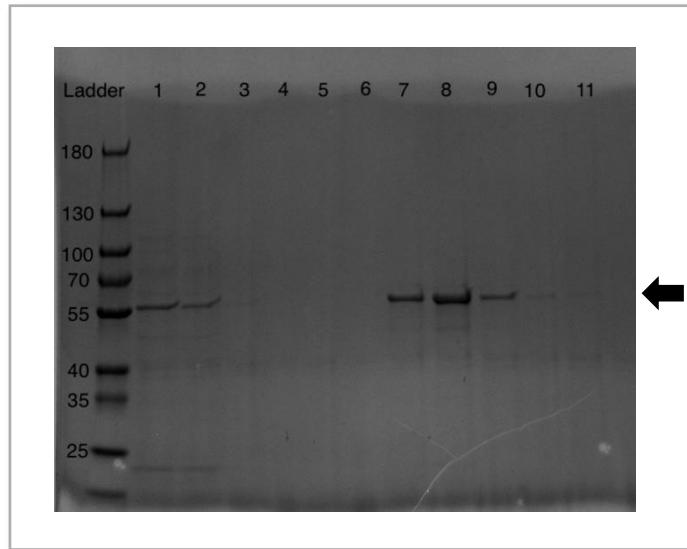


Figure 3.12. Coomassie staining of purified VHH A. The Coomassie shows where the VHH is present during different steps of the purification. Lane 1 is the lysate, 2 is the flow through, 3 is empty and 4 is the first wash. Lane 5 is the last wash and 6 is empty, lanes 7 through to 11 are the elutions. The majority of the VHH is present in the first two elutions at ~60 kDa, indicated by the arrow.

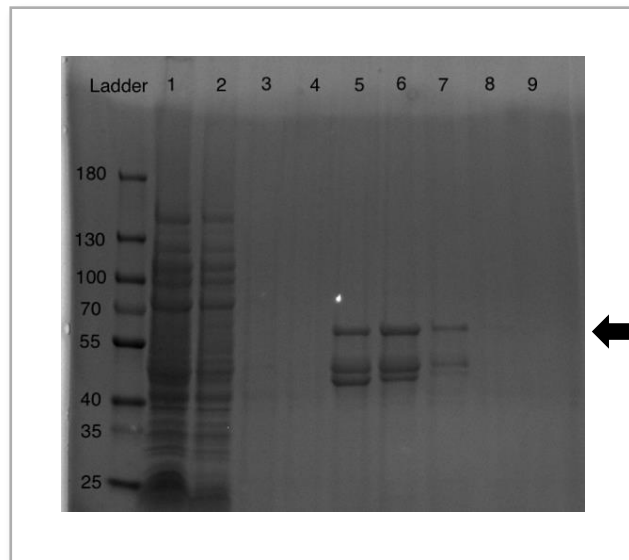


Figure 3.13. Coomassie staining of purified VHH B. The Coomassie shows where the VHH is present during different steps of the purification. Lane 1 is the lysate, 2 is the flow through, 3 is the first wash and 4 is the last wash. Lanes 5 to 9 are the elutions with the majority of the VHH present in elutions 1 and 2. Two bands are present at 60 and 45 KDa, likely the MBP bound VHH (indicated by the arrow) and then an artifact, respectively.

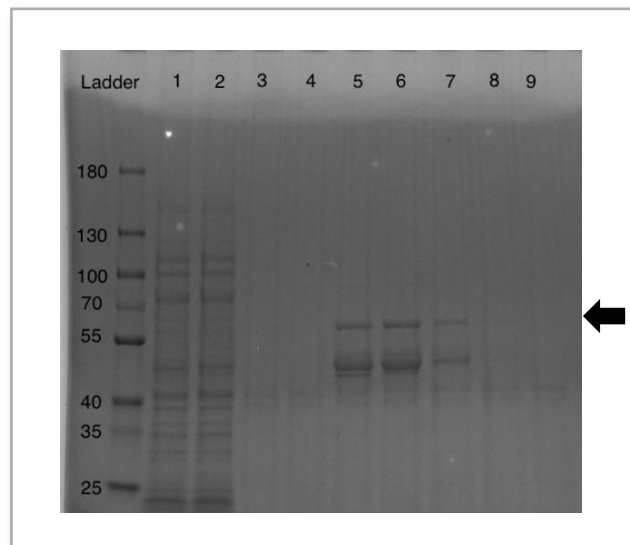


Figure 3.14. Coomassie staining of purified VHH C. The Coomassie shows where the VHH is present during different steps of the purification. Lane 1 is the lysate, 2 is the flow through, 3 is the first wash and 4 is the last wash. Lanes 5 to 9 are the elutions with the majority of the VHH present in elutions 1 and 2. Two bands are present at 60 and 45 KDa, likely the MBP bound VHH (indicated by the arrow) and then an artifact, respectively.

In the lysate and flow through there were many bands present due to the presence of debris from lysing the cells. The lower of the two bands on Figure 3.14 and Figure 3.13 is likely to be an artifact. The band around 60 kDa on Figure 3.14, Figure 3.12 and Figure 3.13 are the MBP fused VHH because the VHH is around 15 kDa in size. All VHH were purified, and their protein concentration was determined as seen in Table 3.6.

Table 3.6. Protein concentration of the MBP VHH. Concentration of each MBP VHH as measured on a nanodrop spectrophotometer.

Soluble VHH ID	Protein concentration (µg/ml)
VHH-A	580
VHH-B	730
VHH-C	790

3.3.8 VHH ELISA

The ELISA protocol was similar to the original panning experiments whereby the FC1 and FC2 representative viruses were bound to the plate at 1 µg per well and incubated overnight at room temperature. Initially 15 µg/ml of the MBP fused VHH was added but all three VHH produced results similar to the negative control. The concentration was increased to 50 µg/ml for the three other ELISA experiments performed where the results varied from the negative control. The ferret antisera dilution was also varied, initially at 1:40 and then 1:100 as seen on Appendix 5 and finally 1:50 as seen in Figure 3.16. All three MBP fused VHH bound better to the rFC2 which aligns with the original panning for MBP fused VHH C and A since they were panned against rFC2, however MBP fused VHH B was panned against rFC1 (Figure 3.15). All repeats of the ELISA showed an increase in binding to the rFC2 compared to the rFC1 (Figure 3.16 and Appendix 5).

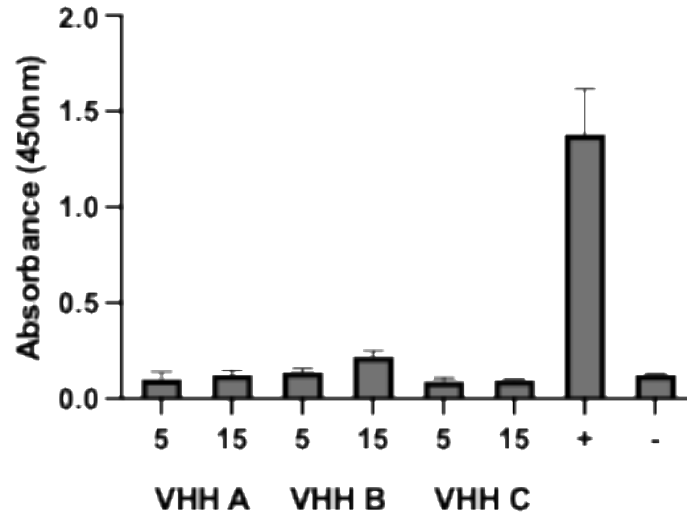


Figure 3.15. MBP VHH ELISA against rFC2. Colorimetric assay comparing the binding of MBP VHH A, B and C against rFC2. The 96-well plates were coated with rFC2 at 1 µg per well and incubated overnight. The MBP fused VHH were run in duplicate at two different concentrations (5 and 15 µg/ml) after they were blocked with 3% milk in 1x PBS. Ferret antisera was included as a positive control (+) to confirm binding of the virus to the plate. The negative control was performed using 3% milk in 1x PBS and then anti-MBP monoclonal antibody was added. Next anti-mouse IgG HRP antibody was added for all wells and Ultra TMB ELISA substrate solution was applied to the plate. Finally, the reaction was stopped using 2M sulphuric acid and absorbance read at 450nm. The mean and standard error mean values were calculated, and the background (duplicate empty wells) was removed to standardise results. The error bars show standard error of the mean of technical replicates performed in duplicate; no biological repeats were performed.

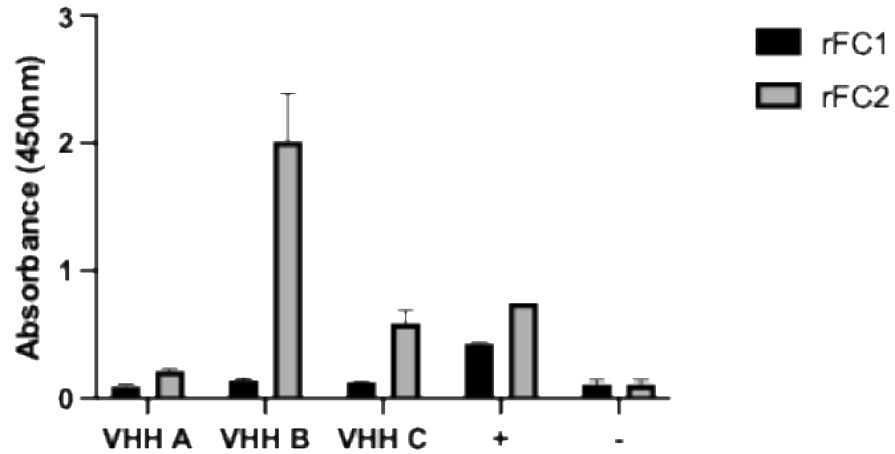


Figure 3.16. MBP VHH ELISA against rFC1 and rFC2. A

representative colorimetric assay comparing the binding of MBP VHH A, B and C against rFC1 and rFC2. The 96-well plates were coated with rFC1 and rFC2 at 1 µg per well and incubated overnight. The MBP fused VHH were diluted to 50 µg/ml then blocked with 3% milk in 1x PBS and added to the plate. Ferret antisera was included as a positive control (+), diluted 1:50 to confirm binding of the virus to the plate. The negative control was performed using 3% milk in 1x PBS and then anti-MBP monoclonal antibody was added. Next anti-mouse IgG HRP antibody was added for all wells and Ultra TMB ELISA substrate solution was applied to the plate. Finally, the reaction was stopped using 2M sulphuric acid and absorbance read at 450nm. The mean and standard error mean values were calculated, and the background (duplicate empty wells) was removed to standardise results. The error bars show standard error of the mean of technical replicates performed in duplicate; no biological repeats were performed. All MBP VHH and the positive control, bound more to the rFC2 than rFC1.

3.3.9 Haemagglutination inhibition test

The soluble antibodies were tested in HI tests with rFC1 and rFC2, however none of the three VHH demonstrated inhibition of haemagglutination at varying dilutions (50–100 µg/ml) of the soluble antibody. All viruses produced a HA titre and PBS controls which demonstrated no reaction in both HA and HI tests. The HI test was also performed with Shropshire/10 and Richmond/07 eIAV and there was no HI.

3.3.10 Anti-beta lactamase in pFUSE 6-well plate transfection

Anti-beta lactamase was used as a trial to confirm that the Fc fused protein would be expressed in static 293T cultures prior to the generation of the Fc fused VHH. An anti-beta lactamase VHH with the Fc domain (Figure 3.8) was expressed by performing transfections of the pFUSE plasmid in 6-well plates with static 293T cells. Half of the supernatant was concentrated, then purified (3.2.2.9) and checked for expression by Coomassie and western blot. The concentrated anti-beta lactamase was primarily present in the supernatant and flow through and not present in any of the elutions (Figure 3.17). This was confirmed in the western blot (Figure 3.18) where there was potentially a droplet present in the supernatant which was likely smaller than expected due to incorrect cutting of the gel used for both the Coomassie and western blot. The expected molecular weight was ~40 kDa, with 25 kDa for the Fc region and 15 kDa for the anti-beta lactamase.

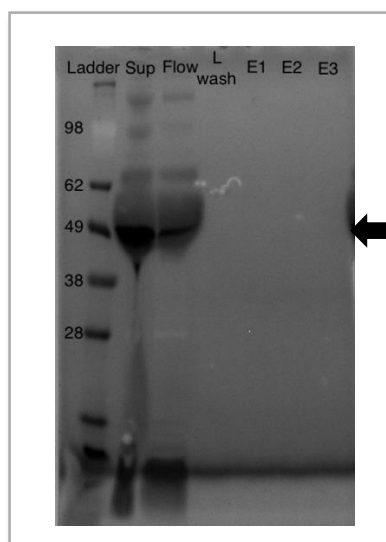


Figure 3.17. Coomassie stain of concentrated and purified anti-beta lactamase Fc. Supernatant harvested from transfection of pFUSE plasmid in 293T cells in a 6-well plate was purified. Aliquots were collected during flow through, first and last wash and all five elutions from the protein G gravity flow column purification. The supernatant (Sup), flow through (Flow), last wash (L wash) and three elutions (E1-E3) were electrophoresed on an SDS-Page and then stained with Coomassie. There was a band present at around 49 kDa in the supernatant and flow through, but this could not be confirmed as the MBP fused VHH was larger than the expected band (40 kDa).

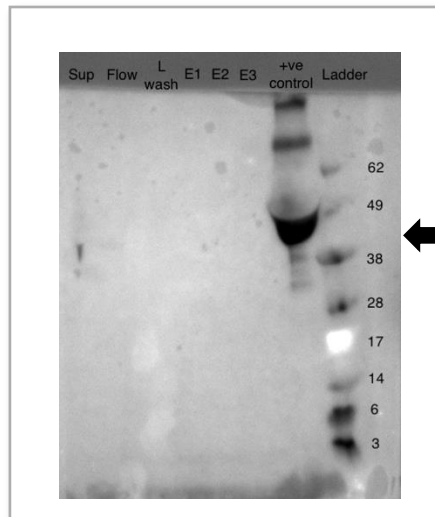


Figure 3.18. Concentrated anti-beta lactamase Fc western blot.

Concentrated supernatant harvested from transfection of pFUSE plasmid in 293T cells in a 6-well plate was protein G gravity flow column purified, and aliquots were collected during flow through, first and last wash and all elutions. Polyclonal human sera was added as a positive control to confirm that the anti-human IgG (Fc specific) antibody was working. Only elutions 1–3 were electrophoresed on this western blot, but protein is only visible in the supernatant (indicated by the arrow).

The second half of the supernatant was purified using the same column without prior concentration. A western blot was performed and as seen in Figure 3.19 there was protein present in elutions 3, 4 and 5. There was also minimal amounts present in the supernatant likely due to the 1:1 dilution of the supernatant.

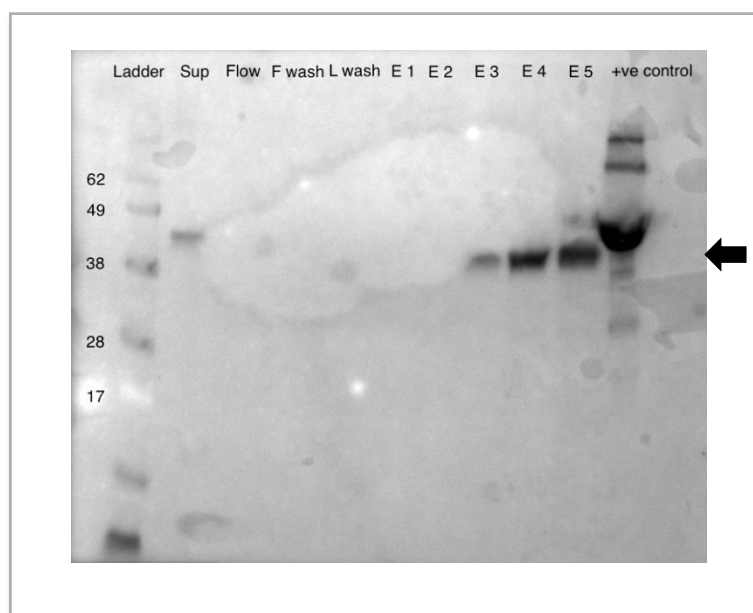


Figure 3.19. Non-concentrated anti-beta lactamase Fc western blot.

Supernatant harvested from transfection of pFUSE plasmid in 293T cells in a 6-well plate was diluted. The diluted supernatant was protein G gravity flow column purified, and aliquots were collected during flow through, first and last wash and all five elutions. Polyclonal human sera was added as a positive control to confirm that the antibody was working. For beta lactamase the soluble protein was present in elutions 3, 4 and 5 but predominantly in elution 4. The expected molecular weight was 40 kDa which was observed in elutions 3, 4 and 5, indicated by the arrow.

3.3.11 Inverse PCR VHH B, C and A in pFUSE

The three sequences that were successful in the 10-sequence trial were then inserted into the pFUSE vector using inverse PCR with the original primers designed. The inverse PCR product containing pFUSE with VHH sequence inserted was electrophoresed on a 1% agarose gel

(Figure 3.20) and visualised, demonstrating that amplification was successful. The plasmid was around 4,600 bp so the band is present at the correct size. The bands produced were excised and then the DNA extracted from them and ligated. After transformation into electrically competent cells the samples were sent for sequencing to confirm incorporation of the sequence into the vector (data not shown).

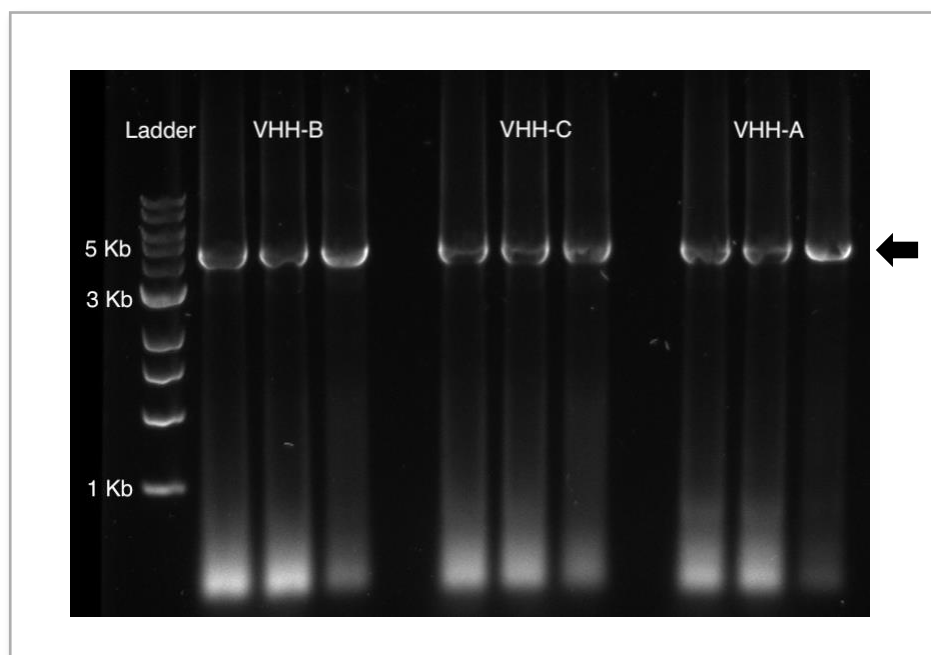


Figure 3.20. Agarose gel following inverse PCR with pFUSE vector.

The products from the inverse PCR were run on a 1% agarose gel with a 1 Kbp ladder. Each well had 20 µl of sample/loading dye so all the product could be loaded and then easily excised from the gel afterwards. All three produced visible bands at around 4.6 Kbp, in keeping with the plasmid size, indicated by the arrow.

3.3.12 Transfection of anti-beta lactamase, VHH A, B and C as Fc fused VHH.

Once it was confirmed that the anti-beta lactamase could be expressed in static 293T cells, the cultures were bulked up to 10 cm dishes and repeated for anti-beta lactamase as well as with the pFUSE plasmids containing VHH A, B and C. Bands were present on all four western blots, primarily in elutions 1 and 2 but a smaller amount was present in elution 3 and 4 however all bands were observed at ~40 kDa

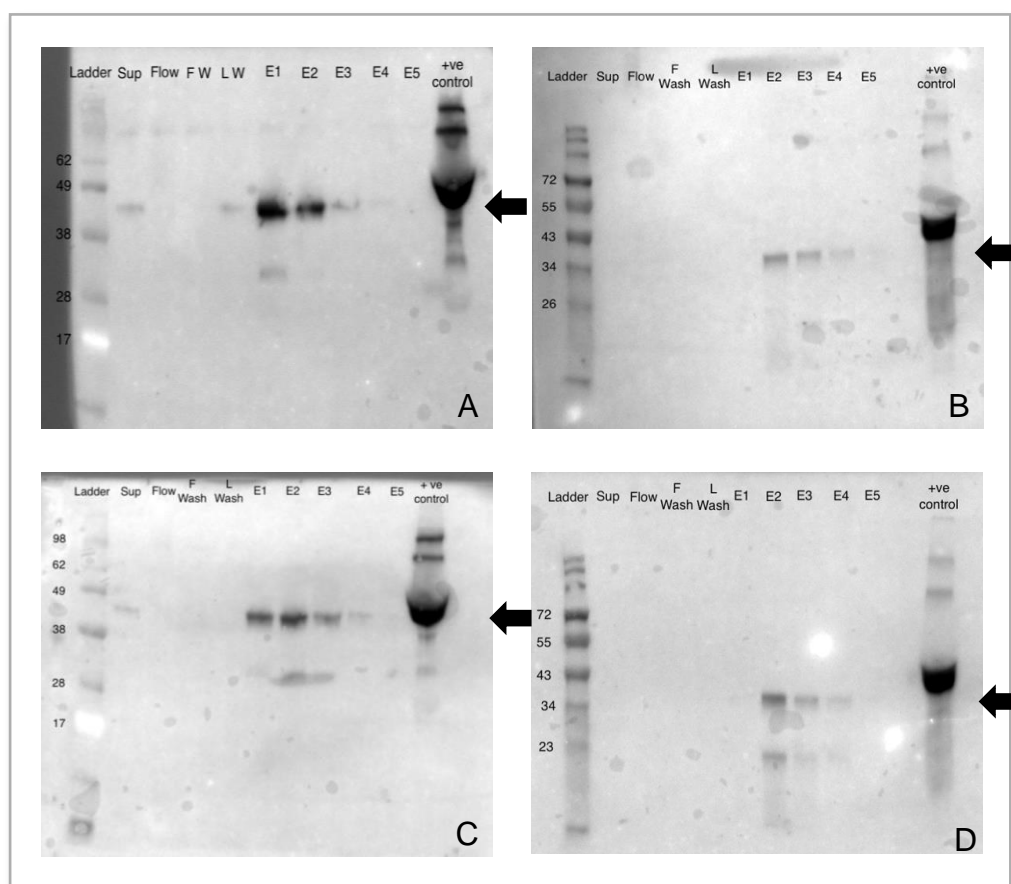


Figure 3.21. Western blots of anti-beta lactamase VHH and pFUSE VHH A, B and C from 10 cm dishes. Supernatant harvested from

transfections of pFUSE with anti-beta lactamase or the three VHH sequences inserted in 10 cm dishes were Protein G gravity flow column purified, and aliquots were collected during flow through (Flow), first (F wash) and last wash (L wash) and all five elutions (E1- E5). Polyclonal human sera was added as a positive control to confirm that the antibody was working. For anti-beta lactamase (A) the soluble protein was present in elutions 1, 2 and 3 but predominantly in elution 1. For VHH A (B), B (C) and C (D), the protein was predominantly present in E2, although the protein was present in E1-E4. The bands were visible at ~40 kDa, the expected molecular weight, indicated by the arrow.

Table 3.7. Protein concentration of Fc fusion VHH. Protein concentration from pooled elutions after protein G gravity flow column purified as measured on a nanodrop spectrophotometer for each Fc fusion VHH.

Fc fusion VHH ID	Protein concentration (µg/ml)
VHH-A	50.44
VHH-B	184.1
VHH-C	89.78

3.3.13 Fc fusion VHH ELISA

Three Fc Fusion VHH ELISAs were run, the first one had the four Fc fused antibodies against 7:1 recombinant Kentucky (rFC1). The anti-beta lactamase produced an absorbance equal to that of the negative control (Figure 3.22). The second ELISA was performed using the three

anti-eIAV Fc fusion antibodies against 7:1 recombinant Kentucky (rFC1), A/equine/Sussex/89 (Eurasian) and A/equine/Richmond/07 (FC2). Fc fusion VHH B produced a signal against all three equine viruses unlike Fc-fused VHH A and C where the absorbance was equal to the negative control (Figure 3.23). The final ELISA focused on Fc fusion VHH B against Schmallenberg virus (SBV) and H1N1 A/Puerto Rico/8/34. As expected, the antibody did not bind to the Schmallenberg virus, but it did bind to the H1N1 virus (Figure 3.24).

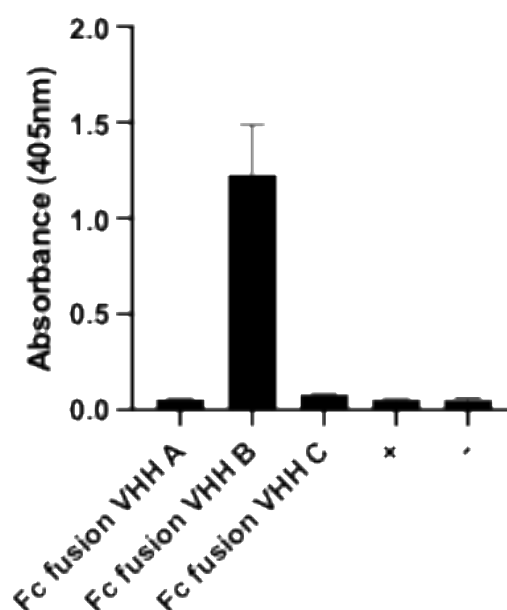


Figure 3.22. Fc fusion VHH ELISA against rFC1. A colorimetric assay comparing the binding of Fc fusion VHH A, B and C against rFC1. The 96-well plates were coated with rFC1 and rFC2 at 1 μ g per well and incubated overnight. The Fc fused VHH were diluted to 10 μ g/ml then blocked with 3% milk in 1x PBS and added to the plate. Fc fused anti-beta lactamase was included as a positive control (+). The negative control was performed using 3% milk in 1x PBS. Then anti-human IgG (Fc specific) alkaline phosphatase antibody was added. Finally, pNPP solution was applied to the plate and left to incubate for an hour and then the absorbance was read at 405nm. The mean and standard error mean values were calculated, and the background (duplicate empty wells) was removed to standardise results. The error bars show standard error of the mean of technical replicates performed in duplicate; no biological repeats were performed.

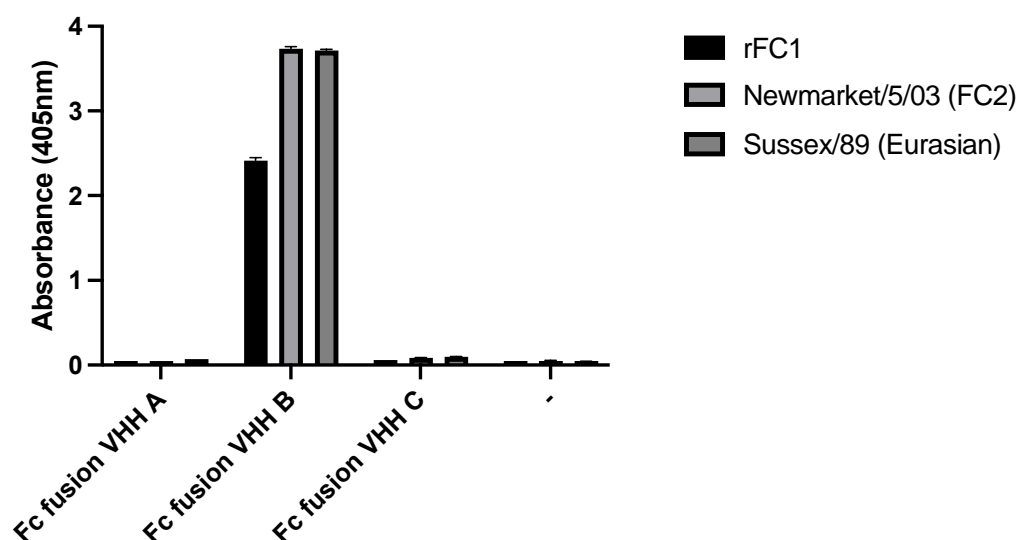


Figure 3.23. Fc fusion VHH ELISA against rFC1 and two additional eIAV. A colorimetric assay comparing the binding of Fc fusion VHH A, B and C against rFC1, Newmarket/5/03 and Sussex/89. The 96-well plates were coated with rFC1 and rFC2 at 1 μ g per well and incubated overnight. The Fc fused VHH were diluted to 10 μ g/ml then blocked with 3% milk in 1x PBS and added to the plate. The negative control was performed using 3% milk in 1x PBS. Then anti-human IgG (Fc specific) alkaline phosphatase antibody was added. Finally, pNPP solution was applied to the plate and left to incubate for an hour and then the absorbance was read at 405nm. The mean and standard error mean values were calculated, and the background (duplicate empty wells) was removed to standardise results. The error bars show standard error of the mean of technical replicates performed in duplicate; no biological repeats were performed.

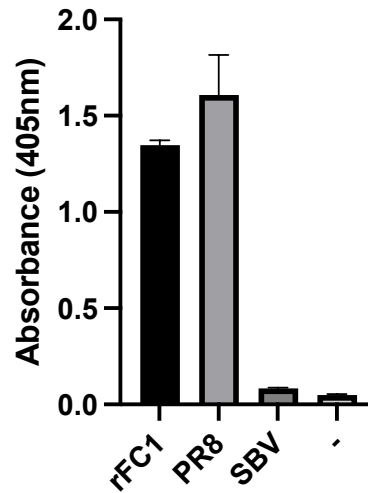


Figure 3.24. Fc fusion VHH ELISA against rFC1, human H1N1 IAV and Schmallerberg virus. A colorimetric assay comparing the binding of Fc fusion VHH A, B and C against rFC1, H1N1 A/Puerto Rico/8/34 and Schmallerberg virus. The 96-well plates were coated with rFC1 and rFC2 at 1 μ g per well and incubated overnight. The Fc fused VHH were diluted to 10 μ g/ml then blocked with 3% milk in 1x PBS and added to the plate. The negative control was performed using 3% milk in 1x PBS. Then anti-human IgG (Fc specific) alkaline phosphatase antibody was added. Finally, pNPP solution was applied to the plate and left to incubate for an hour and then the absorbance was read at 405nm. The mean and standard error mean values were calculated, and the background (duplicate empty wells) was removed to standardise results. The error bars show standard error of the mean of technical replicates performed in duplicate; no biological repeats were performed.

3.3.14 Western blot of transfected cells

To further understand the target of the Fc fusion VHH, 293T/17 cells were transfected with plasmids from the influenza virus that the Fc fusion VHH were likely to bind to. These were the HA from subtypes 3 and 1 as well as the NA and nucleoprotein from subtype 1. When this was blotted, multiple bands were produced between 130 and 250 kDa, which were not expected and suspected to have been caused by the concentration of the primary antibody being too high. Time constraints meant that optimisation could not be performed.

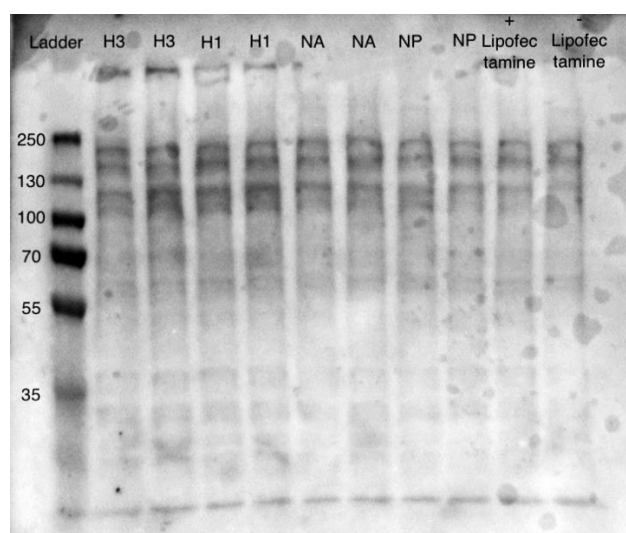


Figure 3.25. 293T/17 cells transfected with HA (H3N2), HA (H1N1), NA (H1N1) and NP (H1N1) expressing plasmids. A western blot of HEK 293T/17 cells that were transfected with plasmids expressing HA, NA, NP, a lipofectamine only control and a no lipofectamine control. The Fc fusion VHH were added at 10 µg/ml, however bands present in the lipofectamine controls suggest a lower concentration may be required.

3.4 Discussion

The aim of this chapter was to develop a reagent that could differentiate between the two Florida clades of equine influenza A virus. This was done using next generation phage display data, expressing soluble and Fc fusion VHH in their respective protein expression systems and then analysing the ability of the VHH to differentiate between the two Florida clades.

In this chapter a large number of potential sequences of interest was identified. The identification of so many potential binders meant that the original experiment plan to generate all the antibodies required revision. The cost of taking all 78 sequences forward was unworkable and so a trial experiment of 10 sequences was performed with the hypothesis that at least one would be a suitable candidate. The probability that one of the 10 trial sequences would work was lower due to the random selection of sequences. The sequences that were identified as being at the highest frequency overall were unlikely to be specific to the rFC1 or rFC2 but could produce a reagent that bound either to a conserved region or more broadly to the influenza HA. This theory was the reason behind including two sequences from the highest frequency list in the trial experiment.

Only three sequences were successfully rescued by inverse PCR, the other seven failed despite repeated attempts at optimisation. This is believed to be due to the large plasmid size (~6 Kb). For the inverse PCR, the protocol was previously optimised for the pMAL plasmid by

the group who provided the plasmid. The protocol provided two PCR programs both with increasing annealing temperatures to increase stringency. The elevation of the annealing temperature during optimisation has been shown to improve the generation of product in inverse PCR (Erster and Liscovitch, 2010). Synthetic generation would negate the need for more optimisation and would reduce production time however this was prohibited by cost limitations. The inverse PCR results could be improved by including only one annealing temperature and performing a gradient PCR to optimise PCR conditions as there may be primer specific temperatures.

The three VHH that were successfully amplified were given the IDs VHH A, B and C and were expressed in bacteria. The MBP is one of the most commonly used tags in protein expression because of its ability to enhance the solubility of target proteins especially when expressed in *E. coli* (Kapust and Waugh, 1999). The MBP does not promote protein aggregation, however it is large at ~45 kDa. The expression of an artifact in VHH B and C was likely reducing the purity of the MBP fused VHH so alternate tags including glutathione S-transferase (GST) and serum albumin could be included (Khersonsky et al., 2023, Reuten et al., 2016). The concentrations produced for each VHH were lower than expected and could potentially have been improved by scaling up the bacterial cultures and cleaving the MBP using the enterokinase site once the VHH were soluble. If the MBP was cleaved, then there may be a drop in yield. Additionally, it would be possible that the VHH may

become insoluble. Alternatively, a different method of protein expression could have been considered. The literature suggests that rather than using bacterial expression, mammalian cultures may improve results, producing yields of up to 5 g/L (Reuten et al., 2016). One disadvantage of mammalian cultures are the cost of generating large volumes of antibody due to plasmid transformation and transfection reagents. There are also some tags that do not express in mammalian cultures, meaning that the expression system is not always the correct choice.

The three expressed VHH were tested by ELISA using the original reverse genetics viruses used in the phage panning rounds. The original concentrations of 15 µg/ml and 5 µg/ml were used based on a previous study by Tsoumpeli et al. (2022). This concentration produced no signal and so the concentration was increased to 50 µg/ml which improved the signal for all three VHH however there was still a large variation between the results for the assays. It is likely that with optimisation either by substituting an alternative blocking buffer or by optimising the antibody concentrations, the ELISA results could be improved. The results differed from the expected result in that VHH B should bind to rFC1 and VHH C and A to rFC2 based on the original panning experiments. This indicated that the VHH were potentially binding to the virus at a conserved region of the HA or on another part of the virus. A hindrance in further assay testing was the limited availability of the reverse genetics viruses used in the original study

subsequent to the closure of the Animal Health Trust. An attempt was made to generate more through inoculation of embryonated hens' eggs, but this was unsuccessful. If further testing had been possible, then the MBP fusion VHH antibodies could also have been tested against other eIAVs from the Florida clades. This would have clarified whether they were indeed binding to the HA or another virus segment.

Hultberg et al. (2011) produced monovalent, bivalent and trivalent VHH as neutralising antibodies against H5N1 Influenza and tested them in HI assays. Only 2 of the monovalent antibodies neutralised pseudotype H5N1, however the bivalent and trivalent antibodies had a higher neutralising potency, although the monovalent inhibited haemagglutination to 156 nM versus 2 nM. As an alternative to the ELISA, HI tests were also used with the intent to further confirm the effectiveness of the VHH MBP fusion. No inhibition was observed, either due to the low purity of the VHH or because they were not binding to the HA. The concentration initially used was 50 µg/ml as in the ELISA, then the concentration was increased to 100 µg/ml however there was still no inhibition. Both concentrations tested were significantly higher than those used in the study by Hultberg et al. (2011). If the conclusion is that the VHH are not binding to the HA then they are likely binding somewhere else on the virus, suggesting that they do not work as initially hypothesised.

There are several methods that can be used for protein expression, which include bacterial, plant and mammalian cell expression. In this thesis I used both bacterial and mammalian cell expression. Both methods were easy to perform and allowed production of antibodies in bulk. Optimisation of both methods would likely improve the concentration and purity of the antibodies produced. For the mammalian cell expression, 293T cells were used as static cultures however there are a range of other cell lines such as Chinese Hamster Ovary cells (CHO) and HEK293-F suspension cultures that could be used as alternatives for recombinant protein expression (Malm et al., 2020, Dahodwala and Lee, 2019).

The pFUSE vector allowed the generation of Fc fused VHH using 293T static cultures, initially in 6-well plates and then in 10 cm dishes. The vector was provided with the anti-beta lactamase sequence already cloned in, which was included as a positive control. Once production of the anti-beta lactamase was confirmed on western blot, the original primers were used to inverse PCR the sequences into the pFUSE vector. Successfully cloned vector was used to transfect 293T cells, with protein expression confirmed by western blot. The concentration of the proteins produced was at least five times lower than that of the bacterial expression. Purifying the proteins using protein G resin in gravity flow columns was slower than with amylose resin, particularly with VHH A and B where the Fc fused VHH concentrations were lower. Repeat transfection and purification would likely improve the

concentration and generate a larger antibody volume. If repeating these experiments, I would investigate changing the cell line to a HEK293-F suspension culture line which can be grown in larger volumes.

The Fc fusion VHH were also tested by ELISA using the same premise as the MBP fusion VHH. Although there was no rFC2 available, all three VHH were tested against the rFC1 and as seen with the MBP VHH it was observed that VHH B bound to the rFC1. The anti-beta lactamase was included in the first Fc fusion VHH ELISA as a positive control however obtaining beta lactamase in a high enough quantity from commercial products was difficult. From this point the experimental focus was on why VHH B bound to rFC1. The following ELISAs showed that VHH B could bind to not only rFC1 but also to other eIAVs and a human H1N1 virus however not to schmallenberg the negative control suggesting that VHH B was not binding to the HA in a way that would differentiate between the Florida clades.

To investigate what protein the VHH B did bind to, cells were transfected with different plasmids from the influenza virus and a western blot was performed. The first attempt showed that further optimisation would be required to identify the correct concentration of VHH to use. The time constraints of this study precluded further optimisation.

The Fc fusion VHH have the potential to be neutralising antibodies, however time limitations to the study meant that this could not be

confirmed. A positive control would be required, which would have already demonstrated neutralising capabilities with influenza A virus, and have the CDR3 sequence available. Son et al. (2023) produced two antibodies that were capable of neutralising human influenza A viruses of H1N1 and H3N2 subtypes. By cloning the sequence into the pFUSE vector we could investigate whether a successful neutralising antibody could be produced with this vector. The benefit of the F fusion VHH is that it has demonstrated binding to several influenza A viruses and therefore has the potential to act as a broadly neutralising antibody against various subtypes of influenza A virus. The neutralising assay could be performed in MDCK cells in keeping with the assay completed by Son et al. (2023), once confirmed it would be carried out in embryonated hen's eggs for equine influenza A viruses.

This study has demonstrated that whilst synthetic phage libraries can identify potential binders to target antigens, their generation and ability to work as intended requires further work and optimisation. The concept of using synthetic phage libraries is still novel and there are many applications for it, although the cost and time to produce a suitable output would need to be calculated before using the method. This study has shown that VHH are a versatile tool that have many applications, and their animal-free ethical production method means their development should continue to be investigated.

Some suggestions for further use of this method include creating a reagent to differentiate between the different subtypes of canine influenza A virus or creating neutralising antibodies against more recent strains of equine influenza A virus. This would create a reagent that is up to date with circulating strains. Studies have been done using a similar method which generated neutralising antibodies for influenza virus, but not as a tool for differentiating between antigenically similar clades of influenza viruses (Chen et al., 2017, Hultberg et al., 2011). Generation of the other VHH sequences identified could provide alternate binders to individual strains of equine influenza A virus, as well as providing stronger binding antibodies.

To conclude, I have been able to generate both soluble MBP fusion VHH and Fc fusion VHH based on next generation phage display data, however their ability to differentiate between the two Florida clades is still indeterminate. The Fc fused VHH bind to influenza viruses however the area of binding remains unknown.

4 Exploring the suitability of canine and equine cell lines in the investigation of the innate immune response and host interactions of influenza A viruses

4.1 Introduction

Equine and canine influenza A viruses are difficult viruses to study *in vitro* as there is a limited number of cell lines that can be infected with either virus. Furthermore, it is unclear and unlikely that those that are currently available produce an immune response similar to *in vivo*. The importance of obtaining the correct cell lines for studying virus-host interactions was reviewed by Hare et al. (2016). In research, immortal cell lines are more commonly used than primary cells. This is because immortal cells are cost effective, an unlimited number of cells are available, and they are convenient to use and obtain (Kaur and Dufour, 2012). Additional advantages of immortal cell lines include ease of use, circumvention of ethical concerns related to use of animal and human tissue and reproducibility of results. Immortal cell lines are obtained in one of four ways: i) physical or chemical induction to destroy regulation of proto-oncogenes or tumour suppressor genes ii) induction of expression of viral oncogenes to help escape the cell cycle control iii) stimulation of cellular telomerase to overcome replicative senescence iv) spontaneous formation (Guo et al., 2022, Irfan Maqsood et al., 2013, Stacey and MacDonald, 2001).

There are several disadvantages to using immortal cell lines. They do not always have the same functions and features of primary cells meaning they are not always directly comparable. Primary cells are considered a better representative of the original tissues. Their limited passage number means they do not change phenotypically. However, in later passages of primary cells, it has been shown that there is a stronger interferon (IFN) response when infected with viruses due to an increased basal level of IFN- β (Hata et al., 2001). This can therefore make it difficult to study virus-host interactions in primary cells.

4.1.1 Primary cell and *ex vivo* culture

Primary cell culture has been a long-used method in the study of human influenza virus. Primary human cells can be easily purchased, and a wide range of cell types are available, from companies including American Tissue Culture Collection (ATCC), cells-online and Merck . They can also be obtained from biopsies (Triana-Baltzer et al., 2010). A review was carried out by Chan et al. (2013b) comparing different culture types and several factors relating to IAV pathogenicity. They concluded that *ex vivo* cultures alone were useful however the combination of primary cells, differentiated cultures and *ex vivo* cultures created an all-round picture into transmission and pathogenesis of influenza viruses.

A study was carried out by Powe and Castleman (2009) used macrophages from the lungs of laboratory maintained, cadaver and

community shelter dogs and macrophages from peripheral blood monocytes. These were then inoculated with H3N8 A/canine/Florida/43/2004, the RNA was extracted, and RT-PCR was performed to look at tumour necrosis factor- α (TNF) and interleukin-10 (IL) response. The supernatant was also quantified by ELISA. The TNF- α response was elevated more than the IL-10 response in both the ELISA and the reverse transcriptase quantitative polymerase chain reaction (RT-qPCR), suggesting that the macrophages were responding to the virus infection with the production of TNF- α . A different study performed by Lee et al. (2011) looked at chemokines and cytokines by ELISA in the sera and lungs of beagles infected with H3N2. Whilst they only observed changes in IL-8 and interferon- γ (IFN) in the sera, the profile in the lungs was different. They observed increased levels of IFN- γ and TNF- α . This study looked at a longer time scale (3–9 days) compared to *in vitro* studies that typically used a 24-hour period.

4.1.2 Explanted tracheal cultures

Explant models mimic *in vivo* situations, because of their 3D structure and preservation of receptors and cilia (Vandekerckhove et al., 2009). Explant tissues can be obtained from animals that have been euthanised (e.g. due to a broken leg) but were otherwise healthy. The tracheal explants can be split into many smaller explants, increasing the number of experiments that can be performed from a single piece of tissue. Additionally, a range of tissues from different areas of the respiratory tract can be obtained and studied. Equine tracheal and

nasal tissues can be obtained from recently euthanised horses and established in cell culture. Chambers et al. (2013) infected equine explant tracheal epithelium with aIAV and concluded that avian influenza viruses were able to replicate in the explanted tracheal epithelium although they could not replicate within living horses. This suggests that equine tracheal explant models may be a poor predictor of aIAV infectivity. Lin et al. (2001) successfully infected explants with equine H3N8 and demonstrated their ability to mimic the natural host. This was further reinforced by Amat et al. (2021) who infected explants with A/equine/Miami/1963 and A/equine/Ohio/1/2003 and identified higher viral titres with the 2003 virus in comparison to the 1963 virus.

Feng et al. (2015) infected equine and canine tracheal explants with canine influenza A virus (cIAV), equine influenza A virus (eIAV) and recombinant cIAV and eIAV with the alternate species glycoproteins. All four viruses were able to replicate in the canine tracheal explants to a similar level however in the equine explants, the cIAV viruses replicated to between 1 and 2 log₁₀ lower titre. Additional studies performed by Gonzalez et al. (2014) showed similar results in the canine explants with a cIAV and an eIAV from a similar time point to the Feng study. Equine viruses circulating in 1963 were able to infect the explants however the replication was significantly lower than the 2003 eIAV. The results from both studies contradict a study done by Yamanaka et al. (2012b) that kept experimentally infected dogs alongside healthy horses and observed no clinical signals, seroconversion or lesions in the

respiratory tract or lungs. The reason behind this is that a single dog is unlikely to be able to infect a horse, however the canine explants have shown that they do act like the natural host, additionally there is a difference between explant infection and natural transmission.

4.1.3 Madin-Darby canine kidney cells

Madin-Darby canine kidney (MDCK) cells are commonly used as a cell model for epithelial cells (Capellini et al., 2020). For human IAV growth the viruses propagated in MDCK cells alone appear to be more representative of the natural virus than those grown in chicken eggs as there are less mutations selected. For replication to occur in MDCK cells exogenous trypsin is required (Genzel et al., 2004) as it facilitates virus infection by proteolytic activation of the viral HA (Seitz et al., 2012). Additionally, it has been concluded that IFN expression is not a limiting factor for influenza virus replication in MDCK cells, partially caused by a lack of anti-influenza activity by canine Mx proteins, that exhibit antiviral activity against influenza viruses by blocking viral replication and transcription (Seitz et al., 2010). MDCK cells are very efficient at human influenza A virus growth at high titres, however the physiology of the cell line is not considered sufficiently representative of the natural host tissue.

MDCK cells have also been used in production of human influenza vaccines (Ganguly et al., 2020). Both $\alpha 2,3$ and $\alpha 2,6$ sialic acid receptors are expressed on the surface of MDCK cells, however when

compared to human respiratory cells the number of $\alpha 2,6$ receptors is lower (Ito et al., 1997, Matrosovich et al., 2003). Most equine IAVs replicate very inefficiently in MDCK cells and are usually propagated in embryonated hens' eggs. When eIAVs are passaged in MDCK cells, they are more likely to select variants with mutations in the HA and NA genes, in comparison to human IAVs where variants with mutations in the glycoproteins are more likely to be selected in embryonated hens eggs (Chambers et al., 2014). A study performed by Spruit et al. (2021) they used MDCK cells to compare growth kinetics between two strains of equine influenza. In MDCK cells viral replication was greater with the more recent isolate of eIAV although no statistical significance difference was observed.

4.1.4 DH82 α cells

DH82 α cells were derived in 1985 from bone marrow from a golden retriever that died from malignant histiocytosis. Their morphology is similar to that of macrophages, and they can phagocytose latex particles. This cell line has been used to study a number of different diseases including equine infectious anaemia virus (Hines and Maury, 2001), canine distemper virus, bluetongue, epizootic haemorrhagic disease virus (Howerth et al., 2004) and *Ehrlichia* pathogens (Liu et al., 2011). On the cell surface, Fc-gamma receptors are expressed as observed on human macrophages (Junker et al., 2020, Wellman et al., 1988). Additional similarities to typical canine macrophages include producing similar amounts of TNF and expressing mRNA of cytokines

expressed by macrophages: IL-8, IL-12, and TNF (Grone et al., 1999, Heinrich et al., 2015). There are some differences to canine macrophages including reduced expression of IL-1 and increased expression of IL-6 (Barnes et al., 2000).

4.1.5 Alternate canine cells

Park and co-workers (2015) developed an immortalized canine tracheal epithelial cell line (KU-CBE). The cell line is highly susceptible and permissive to cIAV H3N2 infection (Park et al., 2015). Two other studies were completed with this cell line studying response to infection with canine H3N2, one looking at signalling pathways and the other to observe the antiviral effects of IFN- λ 3 (Kim et al., 2021, Park et al., 2021). The study by Park et al. (2015) compared their immortalized canine tracheal epithelial cells with MDCK cells and observed that the cytokine profile was different between the two. They saw a greater fold increase in TNF- α in their cell line compared to MDCK cells when quantified by RT-qPCR. The ELISA data showed that in MDCK cells no TNF- α was observed however in their cell line it was present at all time points. Levels of IFN- β were marginally higher when detected by RT-qPCR however were lower when observed by ELISA. The levels of IL-4 were higher in MDCK cells in both the RT-qPCR and ELISA although minimal levels were observed for the immortalized canine tracheal epithelial cell lines. This cell line is not available on the ATCC website and very limited information is available other than that published above, hence it not being included in this study.

4.1.6 Equine cell lines

There are very few immortal equine cell lines, these are limited to: Fetal Horse Kidney (FHK) cells, E. derm and extEqFL.

Equine dermal (E. derm) cells exhibit morphology similar to that of fibroblast cells and whilst they were the first equine cell line established they grow slowly and are limited to around 40 passages (Maeda et al., 2007). E. derm cells were shown to be interferon competent whereas MDCK cells are not (Crispell, 2018).

It has been shown by Crispell (2018) that E. derm cells were more selective therefore fewer influenza viruses were able to replicate effectively in them. The cells were infected with A/canine/New York/dog23/2009 (cIAV 09 H3N8) and viral replication was significantly lower when compared to A/equine/Ohio/1/03. The addition of an exogenous protease such as TPCK trypsin was shown to not be required when infected with equine influenza however it was required for E. derm infected with cIAV. The conclusion was that E. derm may be a useful cell line for the study of equine influenza virus, but less so for canine influenza virus. A previous student of the group, Shona MacRae, also infected E. derm cells with equine influenza virus and observed limited growth of Sussex/89 and Newmarket/2/93 viruses suggesting that influenza replication was not efficient in these cells (MacRae, 2010). MacRae (2010) also looked at IFN- α protein production by ELISA following infection of E. derm cells and noted that the

absorbance values were less than the lowest concentrations in the standard curve confirming the suboptimal nature of the cell line. The same experiment was performed with equine tracheal organ cultures and there was a significant increase in IFN- α concentration at 24 hours (MacRae, 2010).

Fetal horse kidney cells are primary cells from fetal tissue and therefore obtaining a constant supply of fresh cells is difficult. They were developed into an immortal cell line however as with E. derm cells they could only be passaged 40 times maximum (Maeda et al., 2007). A previous undergraduate student of the group, Lorna Beeley, performed cytopathic staining, haemagglutination (HA) tests and immunocytochemical staining on FHK cells. There was no obvious cytopathic effect between mock cells and infected cells at varying virus concentrations suggesting that infection did not occur (unpublished data). Additionally, the results from the HA test were negative for all dilutions and there was no difference in staining after immunocytochemical staining (unpublished data).

The equine lung cell line (extEqFL) was derived from a 5-month-old equine fetus and were transduced to become an established immortal cell line. The cells were transduced at passage 2 with non-replicating retrovirus carrying the PA317 LXSHPV16E6E7 vector (Thorsteinsdóttir et al., 2016). The extended lifespan of these cells means they can be passaged about 40 times, compared to 10–12 times

for primary cells. Current published research using this cell line is limited to equine gammaherpes viruses (Thorsteinsdóttir et al., 2016).

4.1.7 Human embryonic kidney 293T cells

The human cell line (HEK) 293T originated from the kidney of an aborted human female embryo in 1973. It was immortalized by the integration of a 4 Kb adenoviral 5 genome fragment, which inhibits apoptosis and disrupts transcription (Graham et al., 1977, Louis et al., 1997). This cell line is extensively used for generating pseudotype viruses and recombinant viruses using reverse genetics. This is because HEK293T cells are highly susceptible to transfection, although the HEK293T/17 variant is more capable of producing high titre influenza pseudotypes (Carnell et al., 2015). When titrating pseudotype viruses, an alternate cell line is usually used as the target for transduction/ infection, however since there are a limited number of equine specific cell lines, 293T cells have been used as they produced a higher titre than E. derm cells (Scott et al., 2016).

When recombinant viruses are produced using reverse genetics, a co-culture of 293T and MDCK cells is required. The combination of the two cell lines makes use of the benefits that each cell line provides: 293T cells being highly susceptible to DNA transfection and MDCK cells being able to effectively support replication of IAVs (Bdeir et al., 2019).

4.1.8 Requirements of a cell line for studying canine and equine influenza A virus

The limited availability of *ex vivo* or explant cultures means that one of the key requirements for a cell line is that it is immortal. This is so that experiments can be repeated without acquiring new cells and without changes to the interferon response. As described in 1.4 and 1.16.1, sialic acid receptors are important for understanding interspecies transmission of IAVs. A cell line for studying cIAV and eIAV must have receptors that correspond as closely as possible to those of the natural host. Currently there is only published data using E. derm cells (Crispell, 2018), which discusses the issues of using this cell line. Published research does not exist for DH82 α and extEqFL cells and their response to eIAV and cIAV and these are therefore the focus of this chapter.

4.1.9 Aim

To determine whether there is a suitable cell line for the study of equine and canine influenza A virus.

4.1.10 Objectives

- To determine whether α 2,3 and α 2,6 sialic acid receptors are present on DH82 α , E. derm and extEqFL cells.
- To investigate viral growth kinetics across set time points for DH82 α and extEqFL cells infected with cIAVs.

- Analyse the differences in cytokine response between DH82 α cells and extEqFL cells.
- Perform RNA sequencing for DH82 α cells infected with cIAV.

4.2 Methods

4.2.1 Cell lines

The cell lines used in this chapter were HEK293T, MDCK, DH82 α , E. derm and extEqFL cells. They were maintained using the media and cell culture methods described in 2.1.1.–2.1.4 and summarised in Table 2.1.

4.2.2 Viruses

The equine influenza viruses used were A/equine/Newmarket/5/03 (H3N8) referenced from now as Nm/5/03 H3N8. The canine influenza viruses used were A/canine/New York/51864/2008 (H3N8) referenced from now as Can NY H3N8 and a recombinant A/canine/Illinois/41915/2015 (H3N2) referenced from now as Can II H3N2 generated as described in 2.2.7.

4.2.3 Reverse genetics

Reverse genetics was performed as described in 2.2.7 using an 8-plasmid system (provided by Professor Colin Parish) to generate an A/canine/Illinois/41915/2015 (H3N2) recombinant virus. The titre was determined by performing a HA test as described in 2.2.8.

4.2.4 Lectin staining

Staining of α 2,3 and α 2,6 sialic acids was performed on: DH82 α , HEK293T, MDCK, extEqFL and E. derm cells. The coverslips were placed into 12 or 24-well plates. Cells were grown to a density of 1×10^5 cells per coverslip onto 1 M HCL etched coverslips for 24 hours. Prior to fixation the coverslips were rinsed carefully with TRIS-buffered saline (TBS). The coverslips were then covered with acetone and left to soak for 10 minutes at 20°C followed by a repeat rinse in TBS. Streptavidin and biotin blocking solutions (Vector Laboratories), were sequentially added to the coverslips, both were left to incubate for 15 minutes after which they were rinsed with TBS. Two lectins were used: *Maackia Amuensis* Lectin II biotinylated (α 2,3 SA) (Vector Laboratories #B-1265-1) and *Sambucus Nigra* Lectin Fluorescein (α 2,6 SA) (Vector Laboratories #FL-1301-2) and both were diluted 1:200 in TBS, added drop by drop to the coverslips and left to incubate overnight at 4°C in a dark humid chamber. The next day the coverslips were rinsed with TBS, 3 times for 5 minutes, before 250 μ l of diluted (1:500) streptavidin-Alexa-Fluor594 (Thermo Fisher #S32356) was added and left to incubate for 2 hours. The TBS wash step was repeated, the coverslips were attached to slides using Prolong Gold with DAPI (Invitrogen) and left to cure for 24 hours in the dark at room temperature. The cells were then observed and imaged under a fluorescent microscope (Leica).

4.2.5 50% Tissue culture infectious dose (TCID₅₀)

The TCID₅₀ was performed as described in 2.2.10. The supernatant was harvested and stored at -20°C, and a HA test was performed as described in 2.2.8. The TCID₅₀ values for the Can NY H3N8 and Can II H3N2 were determined in DH82α, extEqFL and E. derm and the Nm/5/03 H3N8 in extEqFL and E. derm. The TCID₅₀ for Nm/5/03 H3N8 in DH82α cells was completed by Askar Alshammari (Lab group member).

4.2.6 Viral replication kinetics

Infection was performed as described in 2.2.11 using 24-well plates, with timed collections at 6, 12, 24, 48, 72 and 96 hours. Viral replication kinetics was performed on DH82α and extEqFL cells infected with Can NY H3N8 and Can II H3N2.

4.2.7 Infection with influenza A virus

Infections were performed as described in 2.2.11 using 24-well plates, with individual plates for each cell type and virus strain. The DH82α cells were infected with the same viruses as named above, although the extEqFL and E. derm were only infected with the two cIAV. The supernatant and cell suspension were harvested at 6-, 12- and 24 hours post infection as described in 2.2.11.1 and stored at -20°C for further use.

4.2.8 M gene and cytokine mRNA quantification by RT-qPCR

RNA extractions were performed as described in 2.3.3 and samples were stored at -20°C short term or -80°C long term. A subset of samples underwent M gene RT-qPCR as described in 2.3.4 to confirm infection of cells. To analyse the cycle threshold (Ct, the number of cycles at which a sample reaction crosses the threshold line) values, the known M gene copy number was plotted on a log₁₀ scale against Ct value (Figure 4.4). All samples were RNA extracted then reverse transcribed as described in 2.3.5. They then underwent qPCR as described in 2.3.6 with the primers in Table 2.6. For the canine DH82α cells hydroxymethylbilane synthase (HMBS) and glyceraldehyde 3-phosphate dehydrogenase (GAPDH) were used as the housekeeping gene control and for the equine cells, beta actin was used.

4.2.9 RNA sequencing

The work done up to and including sending the samples for RNA sequencing was performed by Askar Alshammari. For the RNA sequencing DH82α cells were infected with recombinant A/canine/Illinois/41915/2015 (H3N2). The extracted RNA was quantified by Qubit quantification and then prepared to be shipped at ≥ 500 ng. The samples were shipped to Novogene for long non-coding RNA (LncRNA) sequencing. The samples were quality checked after arrival and then the RNA library was prepared and quality checked again prior to sequencing. Novogene use Illumina Novaseq platforms using a paired end 150 bp strategy (Novogene).

4.2.10 RNA sequencing quality and assembly

The data from the RNA sequencing was received as fastq files for each replicate and the RNA seq read qualities were checked using FastQC software (<https://www.bioinformatics.babraham.ac.uk/projects/fastqc>).

At each step MultiQC (v1.22.3) was used to check the analysis by creating an HTML report. FastP (v0.23.4) was used to trim the adapters and to remove short or poor-quality reads. The final step was to use Salmon (v1.10.1) to align the reads to the transcriptome. This was done by generating a decoy genome from the genome (ROS_Cfam_1.0, GCA014441545.1, labrador retriever), from the NCBI genome database.

4.2.11 Differential expression and pathway analysis

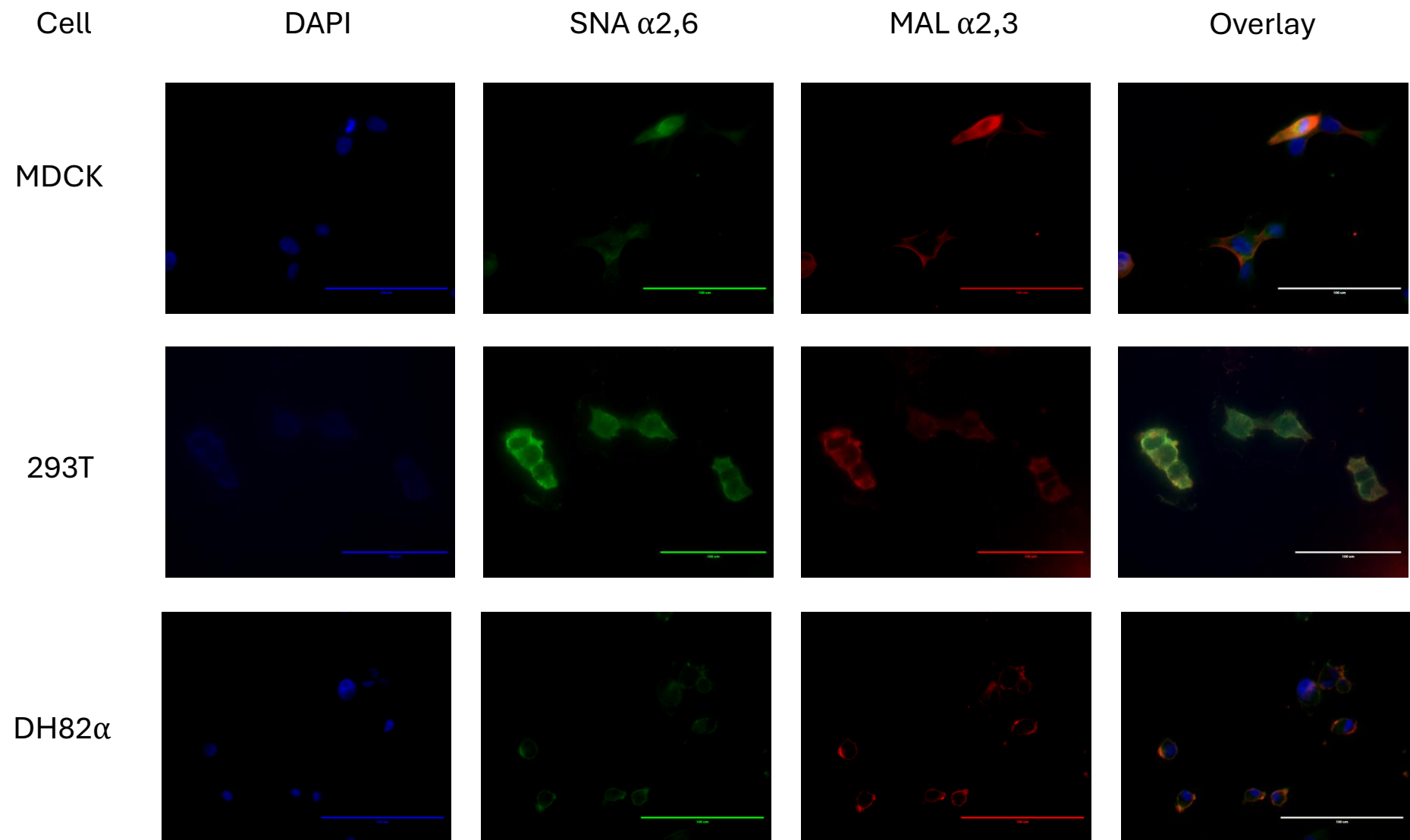
All further analysis was completed in R (v4.4.1) mostly using packages from Bioconductor (v1.30.23). Tximport (v1.32.0) was used to import the results after processing with Salmon. The data were separated into time point and strain vs mock to perform analysis using DESeq2 (v1.44.0). DESeq2 provided the methods to test for differential gene expression using negative binomial generalized linear models to estimate dispersion and log fold changes. All figures were produced in R studio (v2024.04.2). Principal component analysis (PCA) of variance stabilising transformation (VST) was performed using plotPCA from the DESeq2 package. The package pheatmap (v1.0.12) was used for the heatmaps generated. All volcano plots were generated using the

EnhancedVolcano (v1.22.0) package available on R studio. Gene ontology (GO) analysis for biological process, cellular component and molecular function was explored using GOstats. Kyoto encyclopedia of genes and genomes (KEGG) pathway enrichment analysis was performed using clusterProfiler (v4.12.0) a package available on R. The package Pathview (v3) was used to view pathway analysis.

4.3 Results

4.3.1 Lectin staining

All five cell lines showed staining for both α 2,6 and α 2,3 sialic acids however there was variation between them (Figure 4.1). The MDCK cells showed more staining for α 2,3 sialic acids, although there was staining of the α 2,6 sialic acids. Staining was predominantly around the outside and unexpectedly around the nuclear material, in particular for α 2,6 sialic acid receptors. The 293T cells showed more staining for α 2,6 when compared to α 2,3. The DH82 α cells show slightly more of a balance of both receptors, however there was slightly more staining for the α 2,3 sialic acid receptors as can be seen on the overlay. For the equine cell lines there was a preference for α 2,6 sialic acids although that was only marginal. The two cell lines showed minimal staining around the outside of the cell compared to MDCK and HEK293T cells, with the extEqFL cells showing more staining for α 2,3 sialic acids around the nuclear material. The E. derm results were unremarkable, demonstrating low levels for both sialic acids.



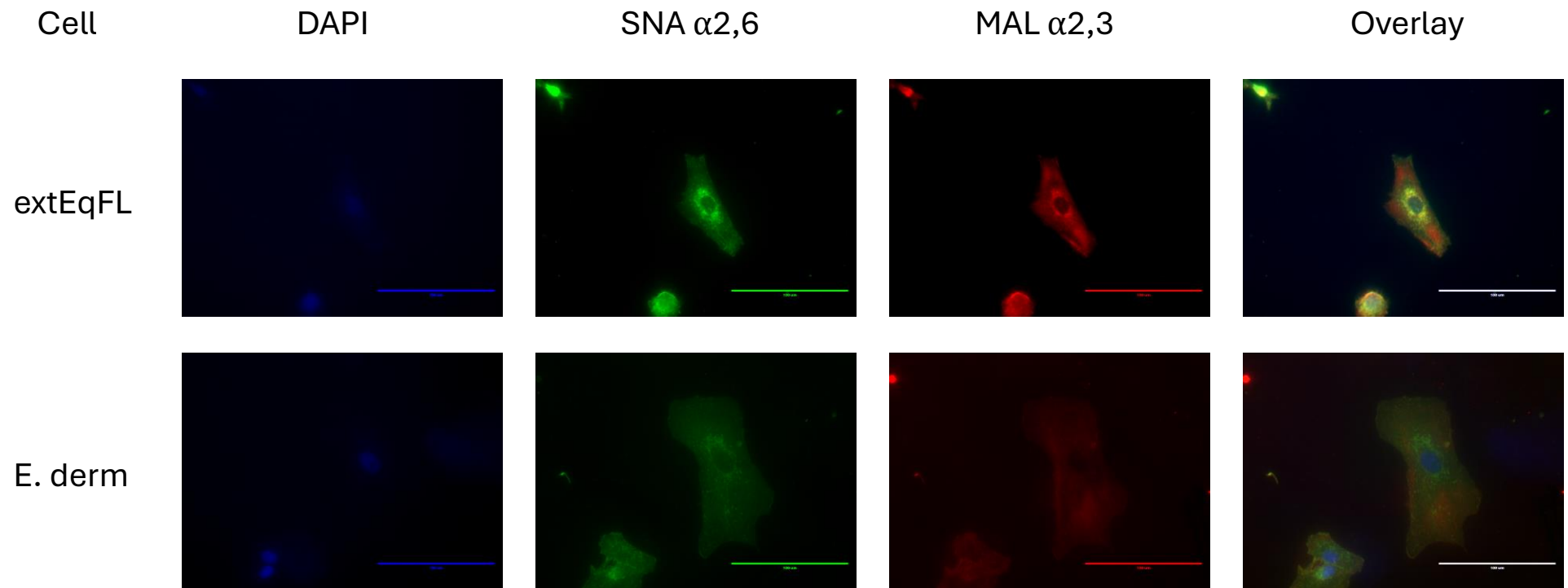


Figure 4.1. Receptor staining of the five cell lines of interest. The immunofluorescent images show the varying presence of α 2,3 and α 2,6 sialic acid receptors of the five chosen cell lines. The first column highlights the nucleus inside the cell using DAPI stain. The second column is fluorescein-conjugated *Sambucus Nigra* (SNA) to identify the α 2,6 sialic acid receptors present. The

third column is a representation of α 2,3 sialic acid receptors stained red by the combination of *Maackia Amuensis* (MA) biotinylated lectin and streptavidin-Alexa-Fluor594. The final column is an overlay of the three images.

4.3.2 Generation of canine H3N2 virus by reverse genetics

Plasmid stocks were generated and used to transfect 293T and MDCK co-cultures. Canine H3N2 reverse genetics virus was cultured in hens' eggs and tested using HA tests, with titre readings of 1/128 and 1/32 meaning it can cause haemagglutination up to a 1/128 or 1/132 dilution. These were then cultured in another batch of hen's eggs to increase the volume. Repeat HA tests after the second round of culture produced HA titre results of 1/128. These results confirmed successful production of reverse genetics influenza viruses.

4.3.3 Cytokine response experiment

4.3.3.1 Tissue culture infectious dose 50%

Three cell lines were taken forward: DH82 α , extEqFL and E. derm. All three cell lines showed visible cytopathic effect with each virus except Can NY H3N8 with DH82 α cells, for which there was no visible cytopathic effect observed. Additionally, when an HA test was performed there was no haemagglutination observed.

Table 4.1. TCID₅₀/ml for each virus and cell line.

	DH82 α	extEqFL	E. derm
Nm/5/03 H3N8	10 ^{5.8}	10 ^{4.5}	10 ^{3.2}
Can NY H3N8	N/A	10 ^{5.5}	10 ^{4.2}
Can II H3N2	10 ^{6.5}	10 ^{5.2}	10 ^{3.5}

4.3.3.2 RNA extraction

RNA extractions were performed on all samples infected. The results of the equine derm cells were repeated twice as the RNA concentrations were too low.

Table 4.2. RNA quantification.

		RNA (ng/μl)		
	Infection	DH82α	extEqFL	E. derm
6 hours	Can II H3N2	17.41	36.78	10.61
	Can II H3N2	36.22	38.86	10.86
	Can NY H3N8	32.44	54.11	11.16
	Can NY H3N8	20.48	63.37	12.84
	Mock	10.61	53.40	8.37
24 hours	Can II H3N2	28.53	21.82	5.38
	Can II H3N2	56.35	31.29	4.45
	Can NY H3N8	36.30	42.43	5.70
	Can NY H3N8	66.49	40.07	5.27
	Mock	97.13	34.81	4.96

4.3.3.3 M-gene RT-qPCR

The E. derm samples were tested for the influenza M gene from viral RNA. The results were comparable to the mock and demonstrated no presence of the M gene. This was performed to confirm unsuccessful infection of the E. derm cells. It was concluded that the E. derm cells would not sufficiently infect to measure the cytokine response. Samples of DH82α and extEqFL cells were infected with cIAV H3N2 and H3N8 and the presence of the M gene was tested. There was no standard performed with these data, so the Ct value was used for the y axis. For DH82α cells, both viruses demonstrated an increase in the presence of the M gene at 48 hours before plateauing. The curves for both viruses

were comparable suggesting similar replication efficiency in the DH82 α cells. In the extEqFL cells the cIAV H3N2 demonstrated replication efficiency that was more similar to the DH82 α cells, however, the Ct values were not as low, suggesting reduced replication efficiency. The extEqFL cells infected with cIAV H3N8 did not show signs of efficient replication as the Ct values were comparable to that of the mock samples (mock not shown). For extEqFL cells the error bars suggest a large variation between individual samples and biological replicates would have been beneficial.

4.3.3.1 Viral replication kinetics

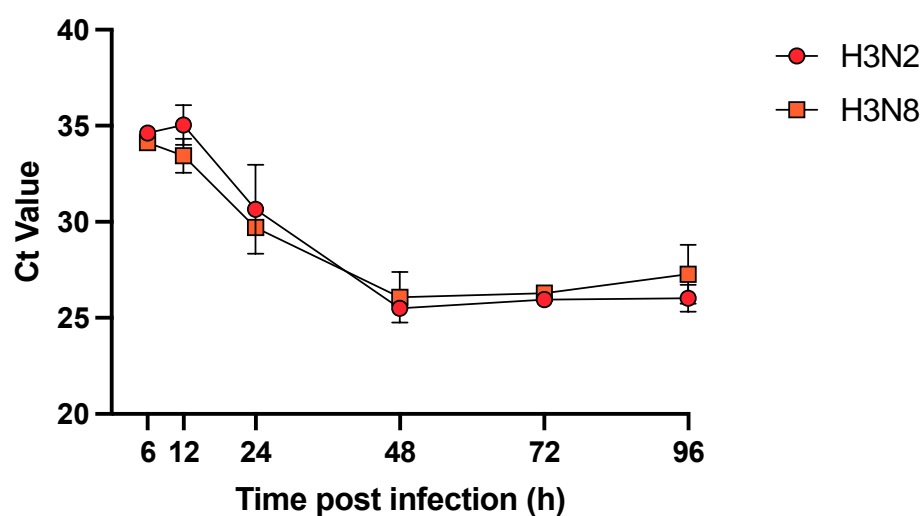


Figure 4.2. Viral replication kinetics of cIAV H3N2 and H3N8 in DH82 α cells. DH82 α cells were infected with cIAV H3N2 and H3N8 and the M gene was measured at 6 time-points. All samples were tested in duplicate technical replicates, and biological replicates were not performed. The mean is plotted on the graph, with the standard deviation plotted as error bars.

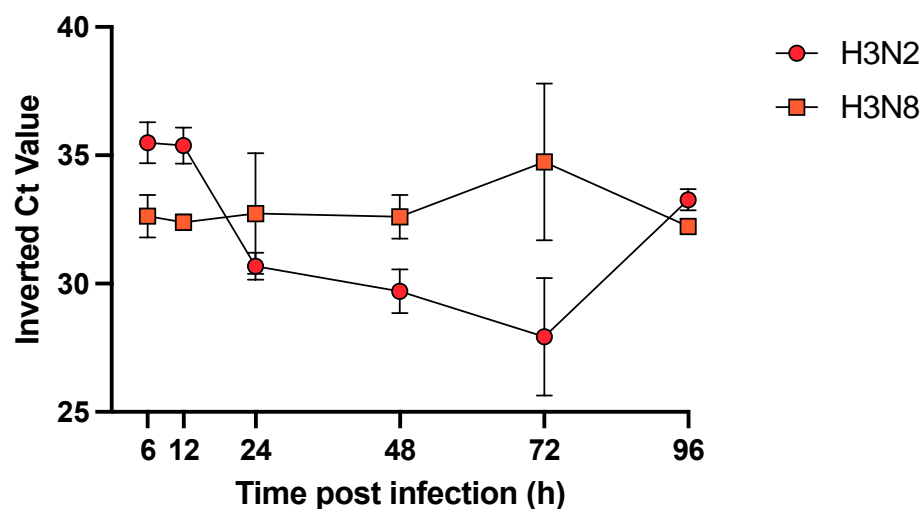


Figure 4.3. Viral replication kinetics of cIAV H3N2 and H3N8 in extEqFL cells. As above, extEqFL cells were infected with cIAV H3N2 and H3N8 and the M gene was measured at 6 time-points. All samples were tested in duplicate technical replicates and biological replicates were not performed. The mean is shown on the graph with the standard deviation plotted as error bars.

4.3.3.2 Reverse transcription and qPCR

Efficiency curves were attempted for beta actin (reference gene), equine IL-6 and equine TNF- α however only beta actin produced results when run by qPCR. The Ct values for IL-6 were recorded at 36 for the neat dilution and 37 for the 1 in 4 dilution. For TNF- α there were no recorded Ct values. The decision was made not to continue to investigate the cytokine response in extEqFL cells.

4.3.4 RNA sequencing experiment

4.3.4.1 Tissue culture infectious dose 50%

The TCID₅₀ results were the same as seen above in 4.3.3.1. The result for this was converted into focus forming units (FFU) by adding $10^{0.7}$ to the TCID₅₀/ml so that DH82α cells could be infected at a multiplicity of infection (MOI) of 0.1 for RNA sequencing. The result was $10^{-5.8}$ for the Can II H3N2 virus.

4.3.4.2 RNA extraction

Table 4.3. RNA extraction results for RNA sequencing samples.

The nanodrop measurement of RNA for DH82α cells infected with Can II H3N2 or treated as a mock infection. All samples were repeated in triplicate.

Time point	RNA (ng/μl)	
	Can II H3N2	Mock
6 hours	95.0	100.3
	133.3	146.6
	131.6	115.1
24 hours	72.1	82.0
	140.5	193.8
	120.9	189.1

4.3.4.3 M gene RT-qPCR

The results from the M gene RT-qPCR (Table 4.4) show that the Can II H3N2 infected samples at both 6 and 24 hours were positive for the M gene. The mock results at 6 hours are at the lowest level of detection in the M gene RT-qPCR..

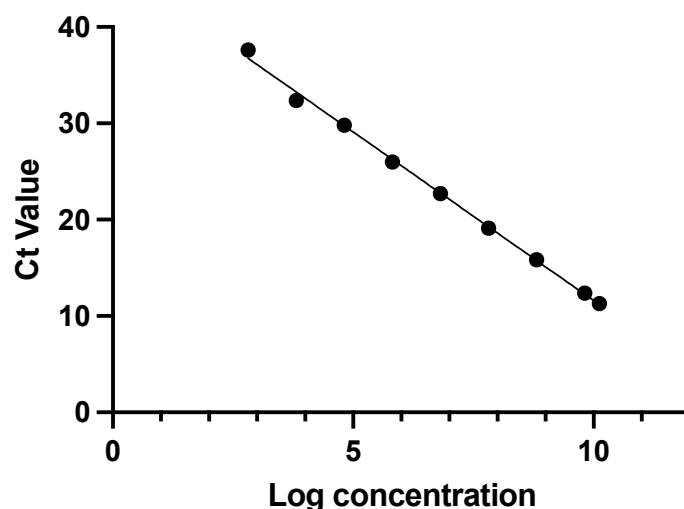


Figure 4.4. M gene standard curve for influenza virus. The mean Ct values for the standard M gene copy number, shown as log concentration. The R^2 is 0.9976 and the $y = -3.499X + 46.60$.

Table 4.4. M-gene RT-qPCR results. A breakdown of the M gene copy number for the mock samples and the DH82 α cells infected with Can II H3N2 at 6 and 24 hours. Three samples were taken for each infection and were calculated from the M gene standard curve Figure 4.4.

	Sample 1	Sample 2	Sample 3
Mock 6 hour	457.6	457.6	457.6
Can II H3N2 6 hour	1.04×10^7	5.39×10^6	2.26×10^6
Mock 24 hour	457.6	800.6	550.2
Can II H3N2 24 hour	1.64×10^7	2.53×10^7	4.01×10^7

4.3.4.4 RNA sequencing

The sample variation is shown in Figure 4.5 by principal component analysis (PCA) and demonstrates larger variance in principal component (PC) 1 than PC2 for both mock vs 6 hours and mock vs 24 hours. There is a greater % variance between the infected samples

than there is between the mock samples particularly at 24 hours for both PC1 and PC2. There was minimal difference between the number of differentially expressed genes (DEGs) at both time points. It was also noted that there were a smaller number of down-regulated genes than expected (Table 4.5).

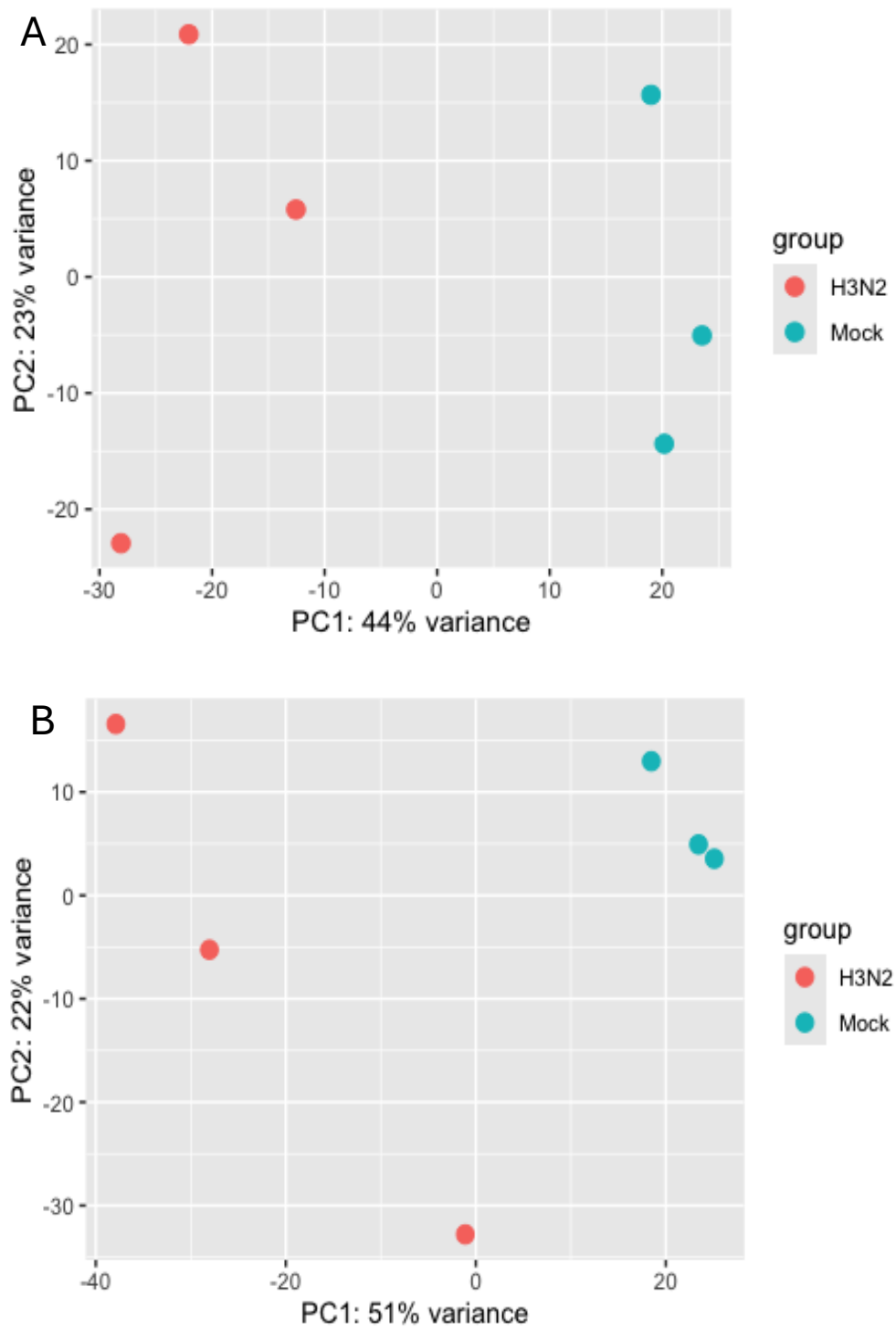


Figure 4.5. Principal component analysis (PCA) plot. A) PCA plot of mock vs H3N2 at 6 hours, B) PCA plot of mock vs H3N2 at 24 hours. Each individual dot represents a single sample.

Table 4.5. Differentially expressed genes in DH82 α cells. The number of differentially expressed genes identified at their individual time points. All samples had a $p < 0.05$ and the p adjusted was also set to $p < 0.05$.

Strain	Time	Up	Down	Total
Can II H3N2	6hr	109	2	111
	24hr	129	15	144

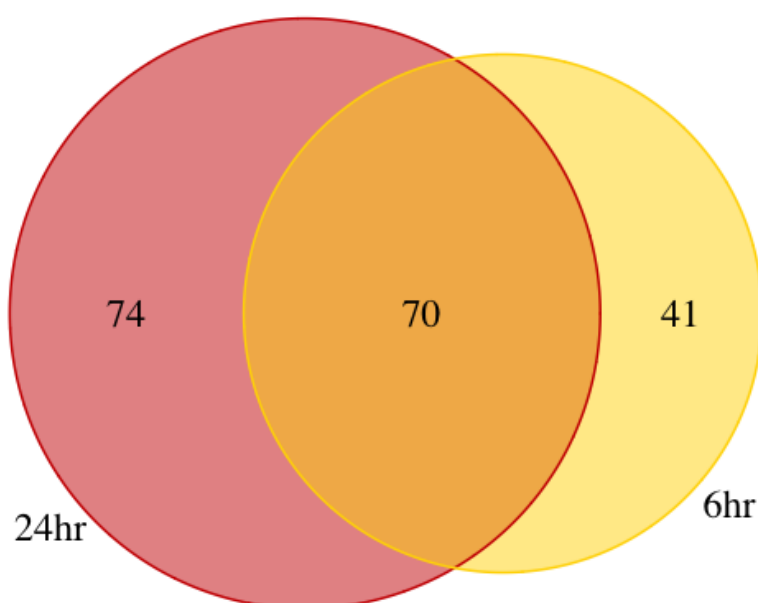


Figure 4.6. Venn diagram of the differentially expressed genes. A Venn diagram showing the shared and individual differentially expressed genes at 6 hours and 24 hours for DH82 α cells infected with reverse genetics cIAV H3N2.

The Venn diagram (Figure 4.6) showed that over half of the DEGs were shared across both time points $n = 70$. There were no down-regulated genes that were seen at both time points (data not shown). Both volcano plots skew to the right (Figure 4.7), indicating that there are more up-regulated genes than down-regulated genes, which is in

keeping with the Venn diagram (Figure 4.6). Only one of the down-regulated genes has a log 2-fold change and p value above the thresholds (EDNRB). The heat maps highlight the difference between each replicate and the normalised counts (Figure 4.8). The two time points are not easily comparable on a heatmap because the mocks are time point specific. Additionally, within that figure there is a lot of variation between the individual samples, which likely relates to the low log 2-fold change values. There are some notable genes such as HERC5 and OAS1 which were found at both time points.

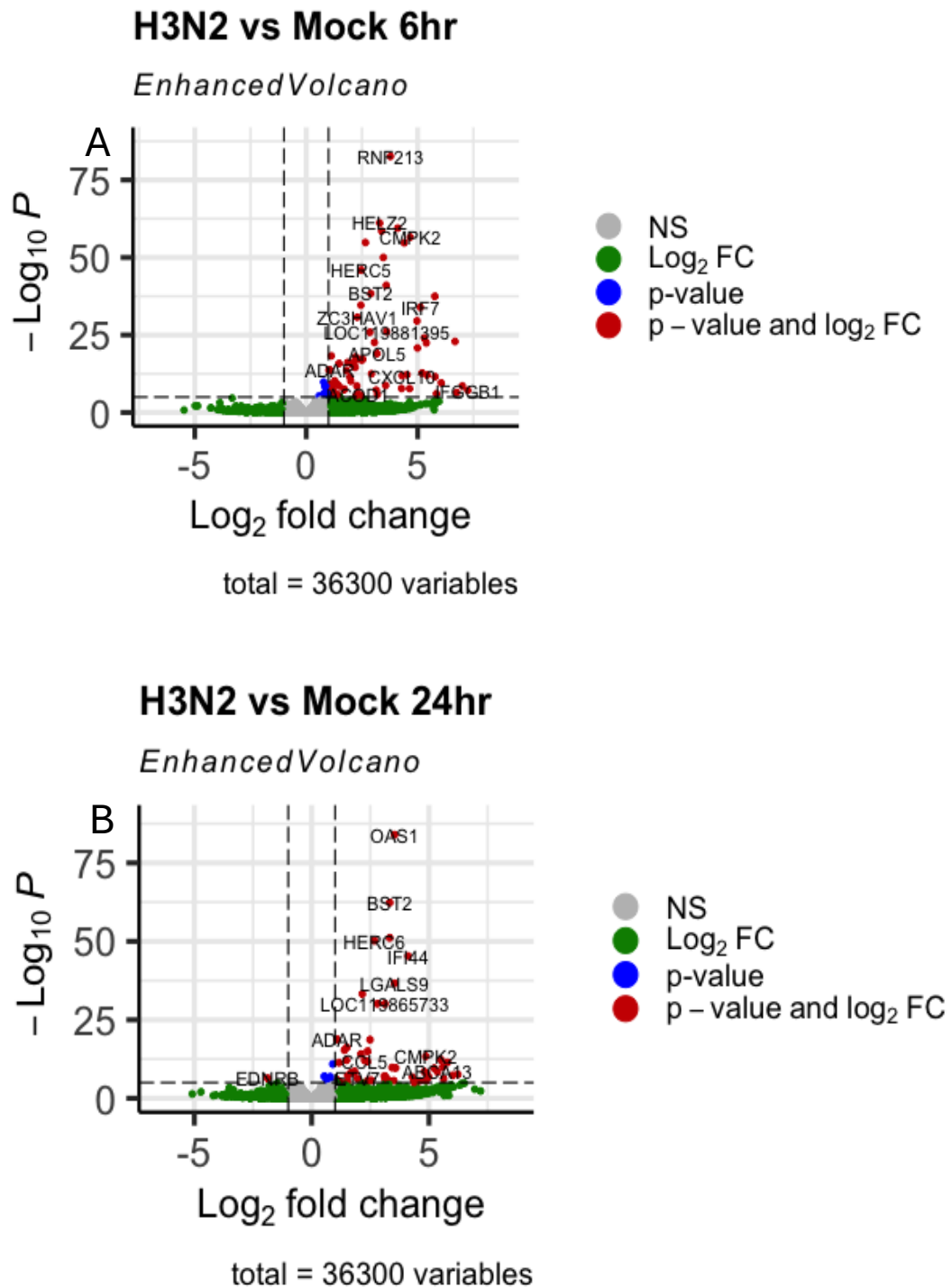


Figure 4.7. Enhanced volcano plots of the two time points.

Enhanced volcano plots of the differentially expressed genes at the two time points, A) 6 hours and B) 24 hours. The two plots skew to the right,

with only the 24-hour showing a single down-regulated gene that had a significant p-value and log 2-fold change (EDNRB).

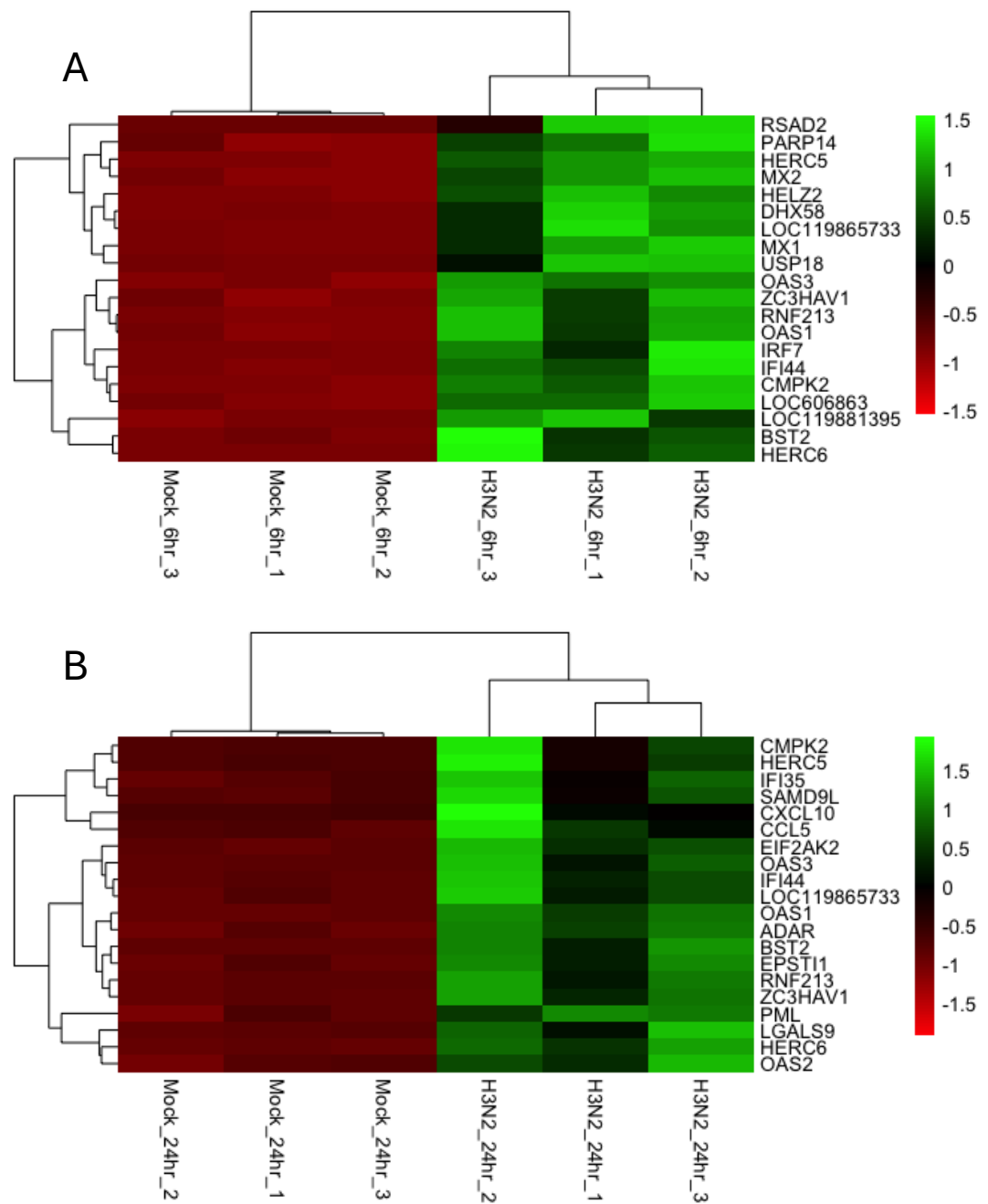


Figure 4.8. Heat maps for the top 20 differentially expressed genes.

Two heat maps showing the top 20 differentially expressed genes at 6 hours and 24 post infection based on the normalized count. A) 6 hours and B) 24 hours.

Therefore Figure 4.9 shows the top 20 DEGs for each time point, with 10 DEGs seen at both time points. The normalized counts for the 10 seen at both time points, do not vary significantly, with the greatest count difference between the two time points of 151 seen with interferon-induced protein 44 (IFI44). This figure backs up the results seen in Figure 4.8 where there are some similarities of genes between the two time-points however their log 2-fold changes are low.

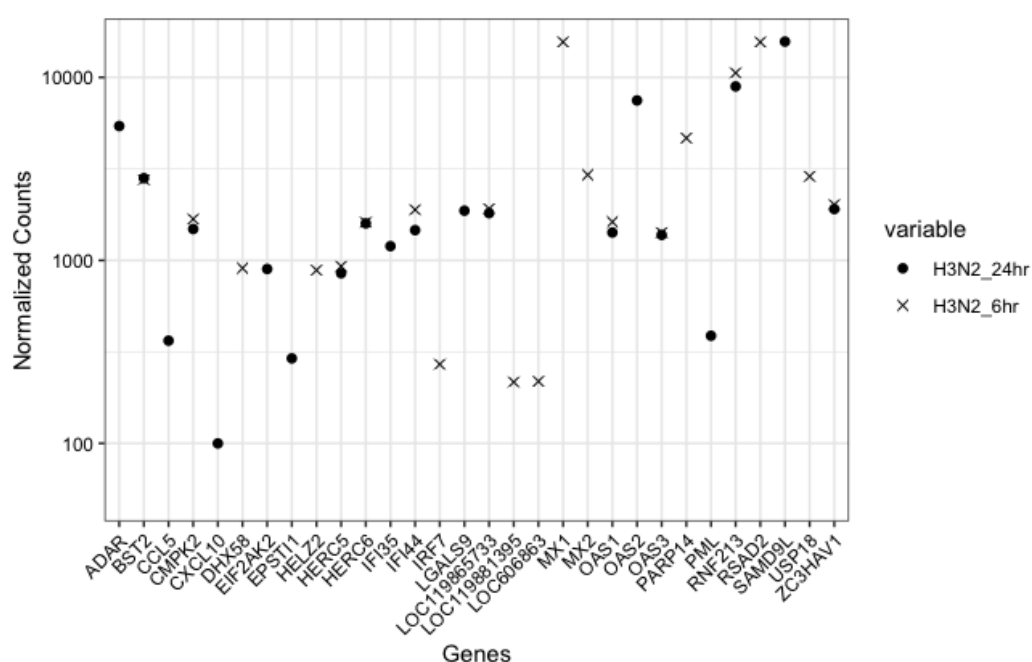


Figure 4.9. A dot plot of the top 20 differentially expressed genes.

A dot plot showing the top 20 differentially expressed genes at 6 hours and 24 hours post infection based of the normalised count data.

To determine the biological interactions and functional network of DEGs, gene ontology (GO) analysis was performed using GOstat. Gene ontology enrichment analysis was performed for all three ontologies: biological processes (BP), molecular function (MF) and cellular component (CC) for both the up and down regulated genes at

24 hours. There were no results for the CC analysis for the up regulated genes. Only 4 GO terms were identified for the down regulated genes, all coming from the molecular function ontology.

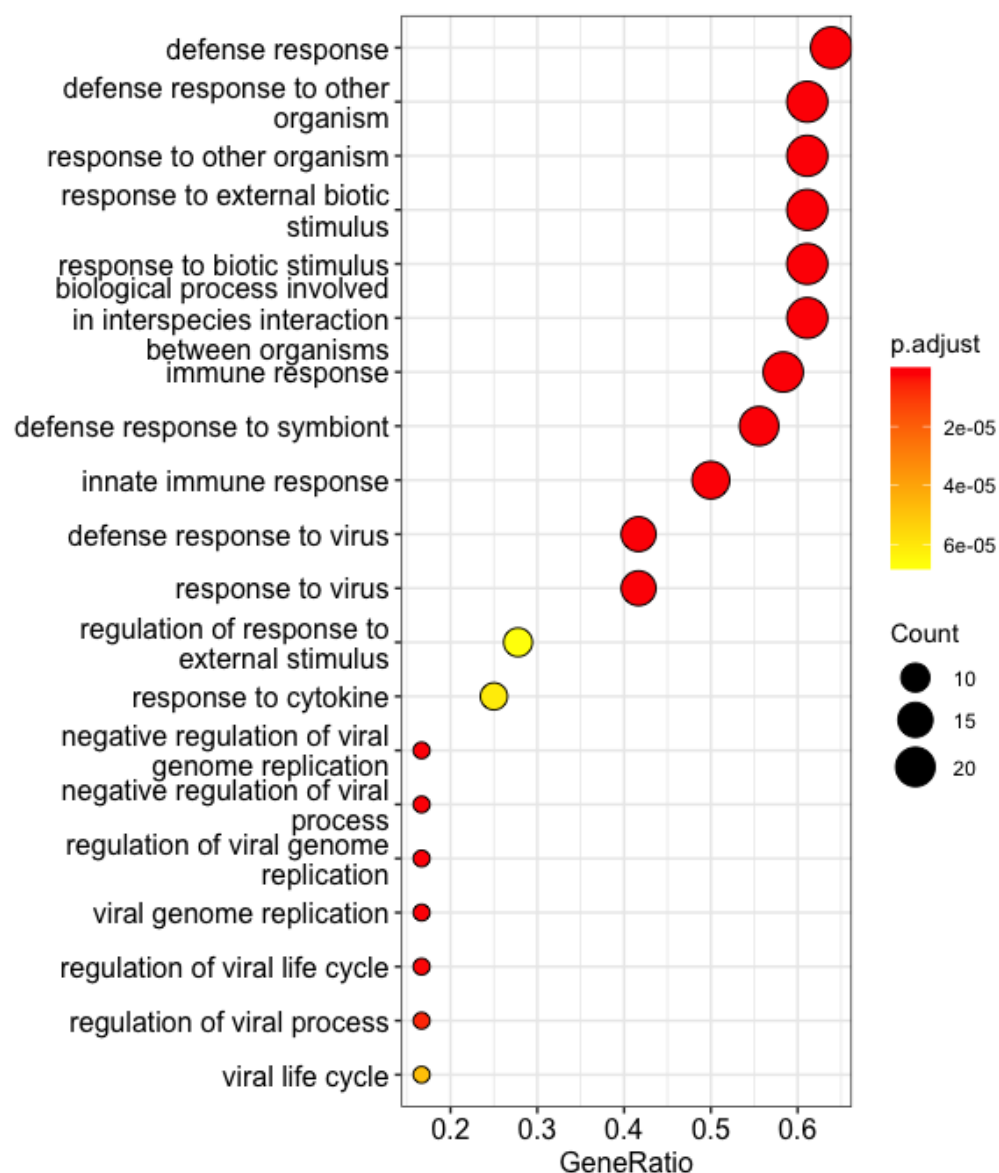


Figure 4.10. Dot plot of the biological processes (BP) at 24 hours.

Gene ontology of the upregulated genes at 24 hours and the biological processes involved with them and the p-adjust value for each term (colour). The larger the dot the greater number of genes associated with that term. The plot displays the top 20 GO terms by gene ratio (the number of genes related to the GO term/total number of significant genes).

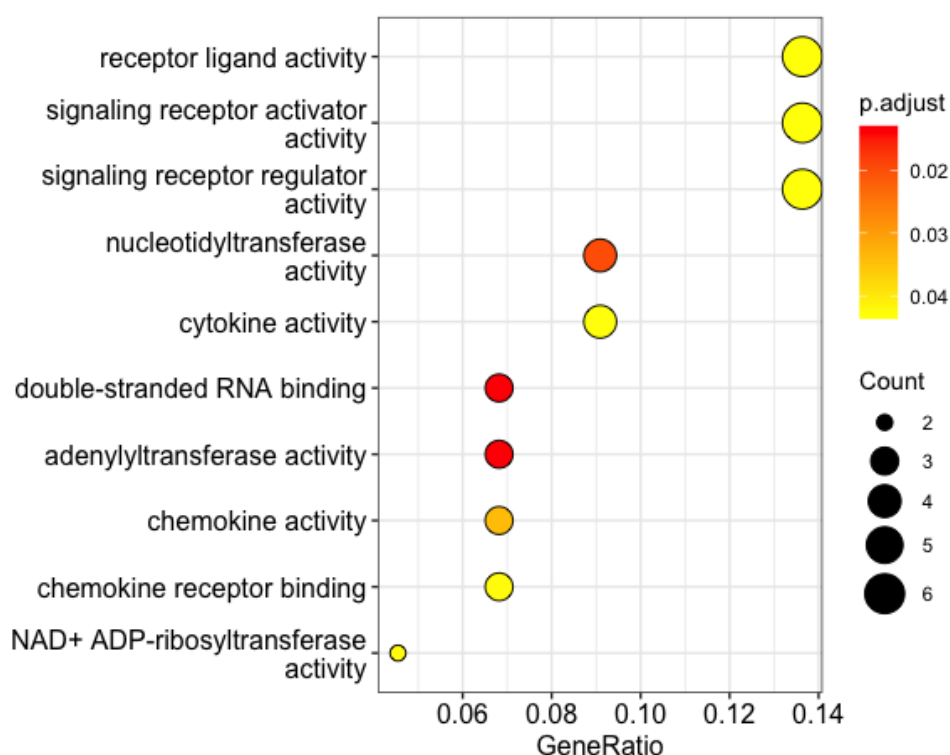


Figure 4.11. Dot plot of the molecular function (MF) at 24 hours.

Gene ontology of the upregulated genes at 24 hours and the molecular function involved with them and the p-adjust value for each term (colour). The larger the dot the greater number of genes associated with that term. The plot displays the top 20 GO terms by gene ratio (the number of genes related to the GO term/total number of significant genes).

Kyoto encyclopedia of genes and genomes (KEGG) analysis using clusterProfile and KEGG organism *Canis lupus familiaris* was performed at 6 and 24 hours. The top six pathways were either from the human infectious disease category with subcategory viral (top 4), or from the organismal systems category with the subcategory immune system. The gene ratio for the top pathway, influenza A (Figure 4.12)

was 21/74 with the lowest p-value <0.0001 . The next three pathways were other viral diseases and then the nucleotide-binding oligomerization domain (NOD)-like receptor signalling pathway with a gene ratio of 14/74 and the RIG-I-like receptor signalling pathway with 10/74. There were no down-regulated genes present in either pathway.

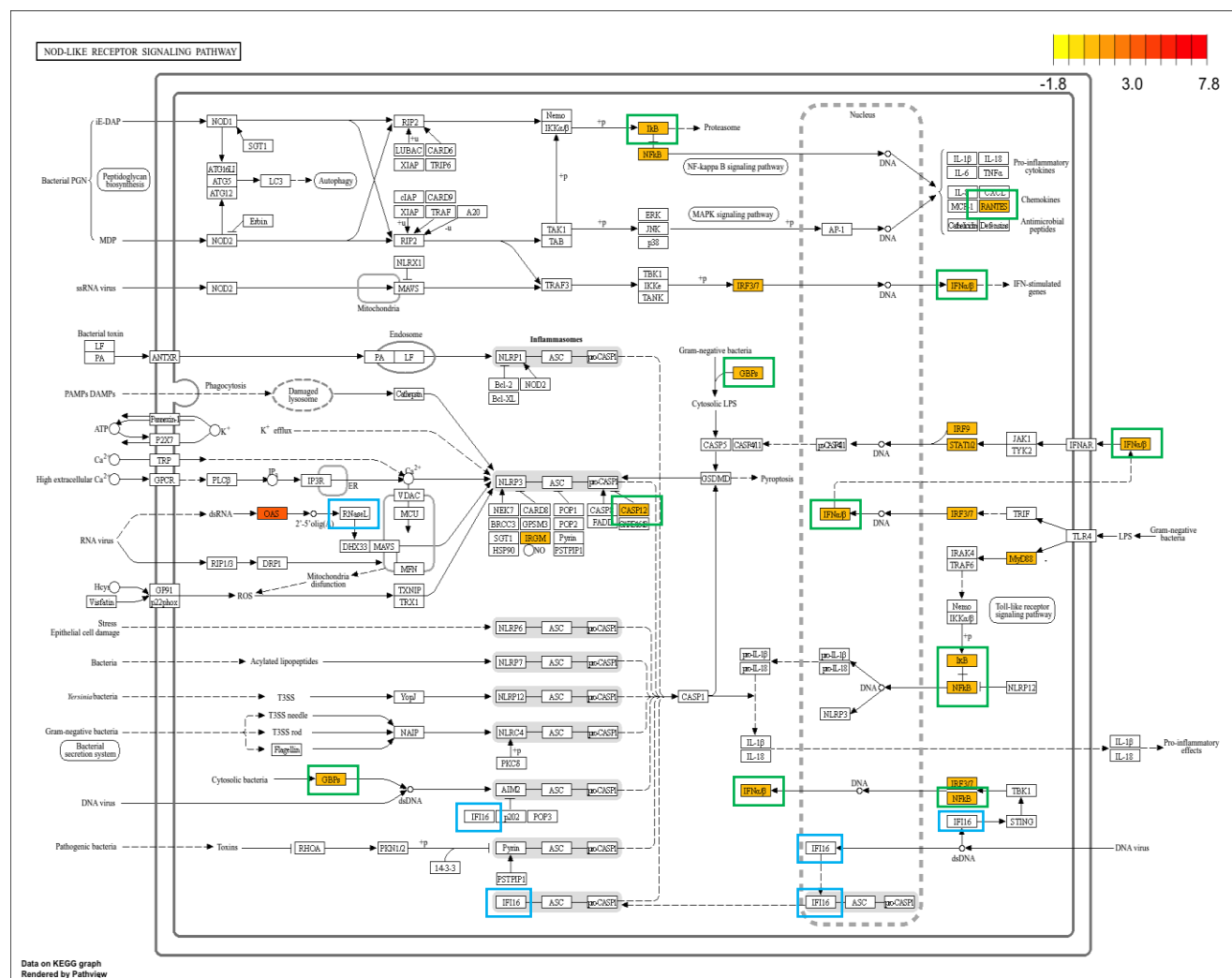


Figure 4.13. KEGG pathway analysis of the NOD-like receptor signalling pathway at 24 hours post infection. KEGG pathway analysis of NOD-like receptor pathway at 24 hours post infection showing minimal enrichment. The colour gradient shows the log 2-fold change. Only genes identified during analysis are highlighted. All genes surrounded by a blue box were present at 6 hours but not at 24, and all genes with a green box were present at 24 hours but not at 6.

4.3.4.5 Cytokine response DH82 α cells

To confirm upregulation of IFN- β but not TNF- α in the RNA sequencing analysis, mRNA of these cytokines was measured by qPCR in DH82 α cells infected with cIAV H3N2. Infection with cIAV H3N8 was included in this experiment for comparison. There was no significant difference in delta Ct values for TNF- α between cIAV-infected and mock-infected cells (Figure 4.14). However, there was a statistically significant but small increase in IFN- β in the H3N8-infected cells only, p value= 0.0496 (Figure 4.15).

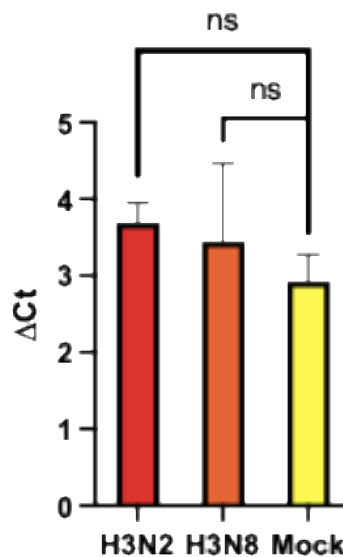


Figure 4.14. Cytokine response of TNF- α in DH82 α cells infected with cIAV H3N2 and H3N8 at 24 hours. The cytokine response of TNF- α measuring the Δ Ct by qPCR from DH82 α cells infected with cIAV H3N2, H3N8 and mock infected. The error bars demonstrate the standard deviation, and ns signifies non-significant values.

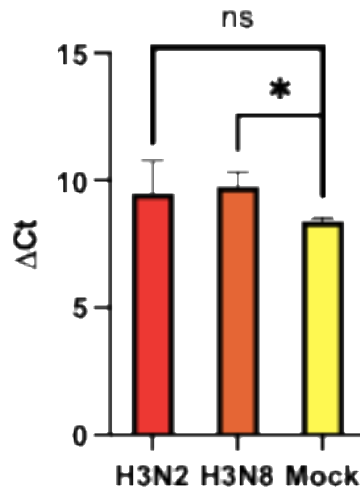


Figure 4.15. Cytokine response of IFN- β in DH82 α cells infected with cIAV H3N2 and H3N8 at 24 hours. The cytokine response of IFN- β measuring the ΔC_t by qPCR from DH82 α cells infected with cIAV H3N2, H3N8 and mock infected. The error bars demonstrate standard deviation. The star signifies the level of significance, the p value was 0.0496 and ns signifies no statistical significance.

4.4 Discussion

The aim of this chapter was to determine whether there was a suitable cell line for the study of equine and canine influenza A viruses. Three cell lines were explored, and their differences investigated.

The first way this was explored was by comparing the receptors present on the surface of the cell lines in comparison to the cell lines currently used for IAV research. The MDCK cells and 293T cells showed sialic acid linkages as expected: MDCK had both $\alpha 2,3$ and $\alpha 2,6$ sialic acids

and 293Ts only had $\alpha 2,6$ SA, as was demonstrated by Nelson et al. (2019) and Guo et al. (2009), respectively. The mix of receptors and preference for $\alpha 2,3$ SAs on MDCKs does not correlate to replication as the receptor preference is only required for attachment, not for replication. The first cell line of interest was DH82 α cells a canine macrophage cell line already used to investigate canine and equine viral diseases. The cell line demonstrated a more equal mix of the two receptors with slightly more $\alpha 2,3$ SAs. The relative abundance of $\alpha 2,3$ receptors made them a good candidate for investigating equine and canine influenza viruses that both demonstrate a preference for $\alpha 2,3$ SAs (1.16.1).

The two other cell lines were from equines: extEqFL (equine lung) and E. derm (equine dermal) cells. Neither cell line demonstrated either receptor in abundance on the cell surface especially in comparison to the other cell line. The results for E. derm cells were unremarkable, demonstrating minimal staining for both receptors however DAPI staining was visible and suggested that they would not be ideal for IAV research. The extEqFL whilst lacking receptors on the outside, had a strong staining for $\alpha 2,6$ surrounding the nucleus and $\alpha 2,3$ within the cytoplasm. This was expected as Scocco and Pedini (2008) demonstrated that MAA and SNA lectins do not bind to alveolar cells from the lungs.

The method used for the staining was effective and although the MAL was detected using direct immunofluorescence this did not heavily affect the staining ability as demonstrated by the strong staining present in the MDCK, 293T and extEqFL cells. The reason the staining was anticipated to potentially be affected by the conjugated antibody was that direct detection has a lower sensitivity and signal amplification than indirect immunofluorescence. Initially the method was performed using acetone at -20°C as the fixative however switching to 4% paraformaldehyde made the fixation process work more effectively. Another issue identified was that the results were qualitative rather than quantitative resulting in a subjectivity that may vary per person and the perceived brightness of red vs green may also vary. The alternative method for this was flow cytometry which could more accurately indicate the presence of sialic acid receptors however would not distinguish between on the surface and internally. Additionally, proteomics could be completed for each cell line to look at protein expression, particularly on the cell surface. This could then be further investigated using flow cytometry and lectin staining (Geiger et al., 2012, Wojdyla et al., 2020). This would identify a base line of protein expression for cell lines that are not currently well researched or understood.

Reverse genetics cIAV H3N2 was successfully generated and was included as an alternative subtype of canine IAV to compare in the cell lines. The H3N2 subtype has a different species origin than the H3N8

and has sustained transmission unlike the H3N8 subtype. Therefore, there may be an alternative cytokine response to the equine origin H3N8.

The TCID₅₀/ml was performed to measure the infectious viral titre so that the infectivity of each virus could be determined. The E. derm cells produced lower TCID₅₀/ml for all three viruses when compared to the DH82α or extEqFL cells. This was to be expected as it has been shown that even after optimisation the highest percentage of cells that could be infected was 46% (Crispell, 2018) therefore without optimisation the percentage could be expected to be significantly lower. This was confirmed when E. derm infected with both canine IAVs gave a low RNA concentration and when the samples were checked for the presence of the M gene they were comparable to the mock. Although Crispell (2018) used this cell line and did transcriptomic analysis with it for eIAVs from 1963 and 2003, the decision was made to not continue with this cell line in this study as the combination of the receptor staining and low infectivity did not make them a good candidate for researching equine and canine IAVs.

Although the results for the DH82α cells infected with canine H3N8 demonstrated no visible cytopathic effect or haemagglutination in an HA test the decision was made to continue investigating the response of the cells to the virus because it was a subtype of interest, and its equine origin meant it would respond differently to the cIAV H3N2. The

TCID₅₀/ml showed that in the extEqFL a higher amount per ml of the equine H3N8 was required to obtain an equivalent MOI. The expectation was that the equine virus would require a lower viral titre to infect equine cells. The viral replication kinetics showed that both equine and avian origin cIAVs could replicate successfully in DH82 α cells however the anticipated peak in replication was observed at 48 hours rather than 24 hours. The viral replication kinetics were also performed on the extEqFL cells, however there was very little replication for H3N2 and no significant replication from cIAV H3N8. This concurs with a study done by Yamanaka et al. (2012b) where experimentally infected dogs did not infect horses. This was in contradiction to Feng et al. (2015) who successfully infected equine tracheal explants, albeit 2 logs lower with cIAV than eIAV so replication is shown as less efficient. Additionally, tracheal explants have been previously shown to be a poor predictor of IAV infectivity (Chambers et al., 2013).

Whilst the extEqFL cells responded well in the TCID₅₀, the cytokine response was not able to be performed as efficiency curves could not be produced for either IL-6 or TNF- α from pooled samples. Future work would involve obtaining alternative primers such as IFN- α and IFN- β and focusing on cIAV H3N8 only samples. The cytokines were investigated with this cell line using efficiency curves and only one reference gene to limit the amount of material required and to determine whether the primers would work with the samples.

Since extEqFL and E. derm cells were ruled out as above, DH82 α cells became the focus of this study. An MOI of 0.1 was selected based on researching other papers that performed RNA sequencing analysis. A paper by Tao et al. (2019) was of particular interest as they used MDCKs with canine H3N2 and performed RNA sequencing also with an MOI of 0.1.

The PCA analysis showed that there was a large variation between the three samples as well as between the mocks at 6 hours but not at 24 hours. This was seen again in the heat maps where there was variation seen between the individual replicates. When samples are at the lower limit of detection, there is a greater chance stochastic variation has an impact.

Long non-coding RNA sequencing was used rather than mRNA sequencing as it provides a larger bank of data and more thorough investigation into gene expression, protein-protein interactions, lncRNA identification and lncRNA target prediction. Long non-coding RNA sequencing was chosen because it allows investigation into coding mRNA, viral transcripts and lncRNAs. The difference between mRNA sequencing and lncRNA sequencing by Novogene is that it is rRNA depleted rather than poly A enriched which does not remove non-coding RNAs. Tao et al. (2019) investigated whole transcriptome RNA sequencing of MDCK cells infected with two subtypes of cIAV where a

total of 2,464 were differentially expressed with 181 in lncRNAs in cells infected with H3N2 cIAV. In our study the number of DEGs expressed at both time points were lower than expected, particularly for the number of down regulated genes. As expected, the lower number of down-regulated genes meant the volcano plots all skewed to the right, however this highlighted the number of upregulated genes that were significant and had a log 2-fold change value greater than 1 for both 6 and 24 hours. As discussed above, the heat maps showed the variation between each sample and highlighted the grouping of the genes. For the 24-hour time point, there were lower numbers of normalised counts for the first replicate in a large portion of the genes. This suggests that infection was not as successful with the first replicate, which would correlate with the M gene being marginally lower.

Whilst the volcano plot and heat map allowed the identification of the top DEGs, it was not clear and had the MOI been higher it would be likely that the results would be better. The dot plot whilst based on the normalized count data, highlighted the top 20 genes for both time-points and unsurprisingly 10 DEGs were seen at both time points. Of the 10, BST2, CXCL10, HERC5, HERC6, IFI44 and OAS1 have all been identified during IAV infection with five different subtypes across two cell lines (Dissanayake et al., 2020, Zhou et al., 2021). To further understand the interactions and functions of the DEGs, GO analysis was performed and the highest results in the biological processes were related to defence and response to stimulus, as would be expected in

response to viral infection. As with the biological processes, the molecular function relates back to genes such as OAS1 and CXCL10 that are involved with the influenza A virus pathway. This links with the KEGG analysis that identified the influenza A virus pathway as the top result however there was a gene ratio of 21/74 genes, suggesting that infection was not efficient in the DH82 α cells at 24 hours. The inclusion of RIG-I-like receptor signalling pathway and the NOD-like receptor signalling pathway which are highlighted in the influenza A virus pathway show that some pathways are more efficient than others. The RIG-I pathway plays an important role in innate immune evasion. Activation of the RIG-I like receptors prior to viral entry, induce a spectrum of antiviral responses, including expression of type I and III interferons by the binding of TRIM25 and upregulation of Mx proteins, 2'5'-oligoadenylate synthetase 1 (OAS1) and protein kinase RNA-activated (PKR). Once a cell is infected RIG-I becomes it works as pre-cell infection (Coch et al., 2017). RIG-I is expressed in all cell types however it is crucial in epithelial cells and alveolar macrophages when infected (Malik and Zhou, 2020). NOD-like-receptors are expressed by a smaller number of cell types, typically myeloid cell types and also by human bronchial epithelial cells (Pothlichet et al., 2013). NOD-like receptors form an inflammasome complex that upon activation causes a change of procaspase 1 to caspase 1 which then produces IL-1 β and IL-18 (Figure 4.12 and Figure 4.13) (Goraya et al., 2015).IL-18 is crucial for antibody and T cell responses whereas IL-1 β attracts innate

and adaptive immune cells and is involved in tissue inflammation (Lapiente et al., 2018).

There were some genes expected to have been highlighted, which were not, these include: IFN- α , interferon-induced transmembrane protein (IFITM); RIG-1; and TNF- α that are typically highlighted in relation to influenza A virus infection. Until recently the role of IFITM was not understood and now its role in restricting viral replication has been shown in lung tissue, MDCK and A549 cells (Lu et al., 2021). There were no interleukins or toll like receptors, in particular IL-6 which was previously identified as being expressed upon infection with lipopolysaccharide (LPS) (Barnes et al., 2000). There were two genes identified at 6 hours but not seen at 24 hours, these were RNaseL and TRIM25. RNaseL has been identified as playing a role in regulating type 1 IFN production, specifically IFN- β (Chakrabarti et al., 2015) which was not present at 6 hours but was at 24 hours in our study. The presence of TRIM25 at 6 hours is likely one of the triggers for the presence of NF- κ B at 24 hours due to its role in the RIG-I pathway (Choudhury et al., 2022). A paper by Kang et al. (2013) performed DNA microarray on lung tissue from euthanised cIAV H3N2 infected dogs which highlighted a large range of genes associated with different cells, receptors and processes. In comparing the results there were 26 genes that were present from our 24-hour samples that were present in the dogs 5 days post infection, these were primarily associated with IFN. Although DH82 α cells are a macrophage like cell line, there were no genes that

Kang et al. (2013) associated with macrophages that were present in this study, potentially due to the reduced level of infection observed.

The two cytokines investigated were TNF- α and IFN- β . As mentioned above, TNF- α was expected to be identified during RNA sequencing. The role of TNF- α as a pro-inflammatory cytokine in influenza infection has long been known as it has been shown to exacerbate inflammation and enhance morbidity, however TNF- α neutralization can reduce lung injury and reduce pulmonary infiltration (DeBerge et al., 2014, Peper and Van Campen, 1995). Powe and Castleman (2009) showed that canine alveolar macrophages induce TNF- α production, hence the expectation that it would be observed in the macrophage like cell line. The cytokine response by qPCR suggests that there is a lower level of expression in infected cells, than compared to mock however this was not significant. There is limited research on IFN- β response in cells infected with cIAV H3N2 except for work done by Park et al. (2015). As discussed in 4.1.5 they compared MDCKs and the immortalised canine tracheal epithelial cells they generated. At 24 hours there was a reduced fold change compared to at 12 and 18 hours for both cell lines however in this chapter the IFN- β response was higher than the mock at 24 hours, but only significantly with cIAV H3N8. The validity of these results, specifically the IFN- β RT-qPCR, is unclear as the ΔC_t values are high. Future work would be to repeat the qPCR experiments and infect MDCK cells with the same viruses and compare the cytokine RT-qPCR response. Additionally, performing cytokine ELISAs and

luciferase immunoassays for cytokine detection in cells may additionally confirm whether there is a cytokine response. Canines infected *in vivo* have also shown increases in TNF- α , IFN- γ and MCP-1 levels at 3–9 days post infection (Lee et al., 2011). All three genes were not identified during RNA sequencing. Although cytokine expression analysis of DH82 α cells infected with eIAV has not been performed during this study, the cell line has still been investigated for eIAV infection. Equines show increased expression of IFN- α , IL- β , IL-6 and TNF- α , all of which were not identified during RNA sequencing (Quinlivan et al., 2007).

There were some changes that could have improved results. The MOI of the experiment was set to 0.1, however increasing it to 1 may have highlighted more genes. There is additionally an argument for changing the mock time point to zero hours to act as a comparison for the two sample sets combined, and including the individual time point specific mocks. The virus replication curves suggest that having an additional time point at 48 hours, might show a different response as viral replication was at its highest at this timepoint. If repeating this, then changing the sequencing to mRNA rather than LncRNA sequencing may highlight more DEGs as shown by Tao et al. (2019). The quality and assembly analysis was performed using programs regularly used and there were no issues highlighted, although there may be alternative programs that do the same analysis. The genome used was from a Labrador retriever and was the closest to the cell line breed (golden

retriever) however, there could have been some differences between the breeds.

The analysis was performed with DESeq2. Alternatively, it could have been performed using edgeR or limma. Limma uses a linear model for statistics and can be applied to all gene expression technologies whilst edgeR and DESeq2 use statistical methods based on negative binomial distribution and typically obtain more DEGs than limma (Love et al., 2014, Ritchie et al., 2015, Robinson et al., 2009, Smyth, 2004). One of the disadvantages of DESeq2 and edgeR is that they are known to produce a large number of false positives, however they remain the preferred methods for sequencing data analysis (Liu et al., 2021). The programs used on R were reliable and simple to work with except pathview. The small number of down-regulated genes meant that the data was not considered bidirectional and therefore only two colours could be applied to the scale, rather than three (one for positive, one for negative and one for zero). This made visual analysis harder to achieve on the KEGG pathway.

Throughout this chapter, DH82 α cells were shown to be the best cell line out of those explored. The similarity to host receptor staining, and the high TCID₅₀/ml results for equine and canine IAVs demonstrated good infectivity and similarity to the natural host. However, the cytokine and RNA sequencing results were not reflective of the natural host response likely related to methodological issues, although limited

studies demonstrate the latter response limiting the validity of this conclusion. DH82 α cells may still prove to be a suitable cell line to investigate the innate immune response with further investigation in the form of repeat studies and the inclusion of eIAV infection as this study only investigated two cIAVs.

5 Potential influence of receptor binding changes on transmission of equine influenza A virus to dogs

5.1 Introduction

Equine influenza A virus demonstrated transmission to dogs on two independent occasions, once in Florida in greyhounds in 2004 (Crawford et al., 2005) and then it was retrospectively identified in 2002 in Foxhounds in the UK (Daly et al., 2008). The breakout in Florida then spread across the United States, whilst it has not been observed since 2015, there were two independent breakouts, suggesting the possibility of further transmission events. This suggests the need for better understanding of viral transmission, especially in equines and the mutations previously identified that potentially influenced receptor binding changes causing the independent outbreaks. Binding to sialic acid (SA) receptors is required for almost all subtypes of influenza A virus (IAV). The exceptions are H17, H18 and hypothetically H19. These instead utilise the major histocompatibility complex (MHC) class II molecule as a host receptor (Karakus et al., 2019, Karakus et al., 2024). Binding happens between the receptor binding site (RBS) of the haemagglutinin (HA) glycoprotein, and the SA receptor found on the target cell surface. There are more than 50 types of sialic acids, with 5-N-acetylneuraminic acid (Neu5Ac) and 5-N-glycoylneuraminic acid (Neu5Gc) being the two most common (Sriwilaijaroen and Suzuki, 2012). The Neu5Gc modification is created by hydroxylation of an N-

acetyl moiety, however some mammals have lost the ability for the cytidine monophosphate-N-acetyl neuraminic acid hydroxylase (CMAH) to work and therefore predominately express Neu5Ac (Broszeit et al., 2019). Horses and pigs still express a functional CMAH enzyme, however humans, ferrets, dogs, and a range of other mammals do not (Ng et al., 2014, Spruit et al., 2021). The H7N7 equine virus predominantly bound to Neu5Gc whereas equine H3N8 virus binds Neu5Ac (Gambaryan et al., 2012). Broszeit et al. (2019) showed this using a glycan microarray for Neu5Ac and Neu5Gc.

As introduced in 1.7.1, antigenic drift causes single point mutations within viral epitopes of the HA and neuraminidase (NA) (Woodward et al., 2015). Typically, mutations introduce minor changes to viral proteins or create nonviable progeny (Fitch et al., 1991, Kim et al., 2018b, Treanor, 2004, Webby and Webster, 2001). Single point mutations in the viral glycoproteins can also contribute to changes in receptor binding (Petrova and Russell, 2018, van de Sandt et al., 2012a). As discussed in de Vries et al, (2020) it is more complicated than the introduction of several mutations in the HA solely causing a switch from α 2,3 to α 2,6 SA receptor binding. There are individual preferences to sulphation, sialylation and fucosylation that can change between viruses with a single mutational difference (Stevens et al., 2006a).

Within the sialic acid binding site, mutations that may affect receptor binding reside within the 130-loop, the 190- α helix and the 220-loop

where the sialic acid binding site is (Figure 5.1) (Sriwilaijaroen and Suzuki, 2012). The most important switch in receptor binding is from α 2,3 SA to α 2,6, adapting the virus to bind to the human respiratory tract. This switch was conferred by Q226L and G228S substitutions both in the 220-loop in H3 HAs (Connor et al., 1994, Rogers et al., 1983). There are currently three HA subtypes that have human pandemic potential: H1, H2 and H3 (Saunders-Hastings and Krewski, 2016, Webby and Webster, 2003). In H1 viruses, two amino acid residues have been recognised as critical in the switch from avian to human receptor binding specificity, these are D190 and G225 (Lazniewski et al., 2018). The H3 subtype was shown to demonstrate interactions with side chains of sialic acids through hydrogen bonds at positions Y98, W153, E190, Y195 and H183 (Eisen et al., 1997, Weis et al., 1988). This suggests that mutations, especially at 190 where interactions with sialic acids have been exhibited, are likely to play a larger role in receptor binding.

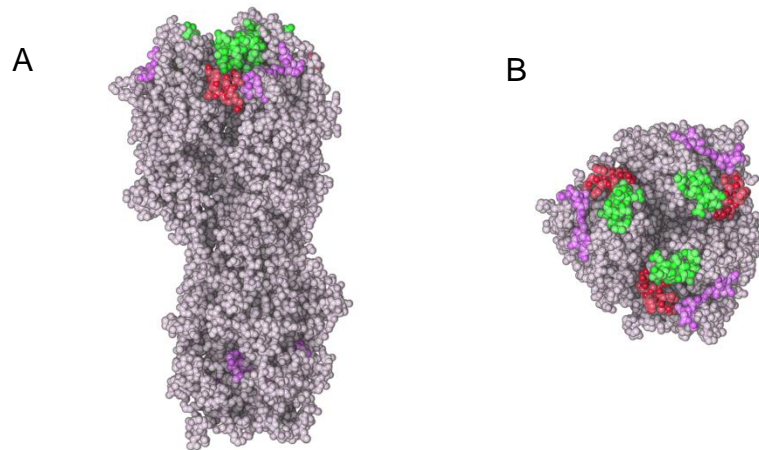


Figure 5.1. Receptor binding sites on the H3 glycoprotein. The 3D protein imaging model of H3 as a trimer (2HMG.pdb) with the three loops that make up the receptor binding site. A) is the side on view and B) is the top-down view. The pink denotes the 130-loop, the green is the 190-loop, and the red is the 220-loop.

5.1.1 Canine and equine influenza receptor binding

Canine influenza A virus (cIAV) has demonstrated two jumps of the interspecies barrier within only a few years. The two events were independent and originated from different species, the H3N8 event was an equine to canine jump (Crawford et al., 2005) and the H3N2 event was an avian to canine jump (Song et al., 2008). Representative viruses of equine influenza A virus (eIAV) prior to transmission into dogs, and cIAV from several years after transmission were compared phylogenetically and by molecular methods. This comparison showed that although the sequences varied phylogenetically, there was very little difference in their infectivity, receptor binding and cleavage efficiency so they were biologically similar (Feng et al., 2015). Collins et

al. (2014) compared the HA structures of Eurasian lineage eIAV, Florida lineage eIAV and a cIAV virus, using biolayer interferometry (BLI) to compare receptor binding and x-ray crystallography to compare HA structure. As discussed in 1.13 and 1.16, a tryptophan to leucine mutation at residue 222 was highlighted. The study by Collins et al. (2014) highlighted that this was the key mutational change in the receptor binding site of the canine virus and was likely responsible for any changes to receptor binding.

5.1.2 Current methods to study receptor binding

Receptor binding to SAs has been investigated using several methods since its importance in binding and therefore viral replication was identified. These methods include the solid-phase receptor binding assay (Matrosovich and Gambaryan, 2012), BLI and glycan microarray. Flow cytometry can also be used to measure SA binding of viruses in cells by using fluorescence. Ramos et al. (2011) infected MDCK cells with wild-type and mutated virus and compared the difference in SA binding using flow cytometry. The MDCK cells when infected with wild-type A/Vietnam/1203/2004 H5N1 demonstrated binding to 2,3 SAs but not α 2,6 however when two mutations at 226 and 228 were introduced there was a reduction in binding to α 2,3 and an increase in α 2,6. This was confirmed in solid-phase binding assays where the same results were observed.

5.1.2.1 Solid phase receptor binding

The solid phase receptor binding assay described by Matrosovich and Gambaryan (2012) is technically a simple assay, similar to a standard ELISA that can be completed with a relatively basic lab set up. The assay can be used with a range of lectins and an array of influenza A viruses, although it is not the most precise and is prone to human error in pipetting and plate washing if done manually. One of the limitations of the assay is the availability of lectins as those lectins used in previous studies are no longer available.

5.1.2.2 Biolayer interferometry

A newer method that is very similar is BLI, which is a way to measure biomolecular interactions by analyses of interference patterns of white light reflecting off two surfaces (Petersen, 2017). There are different size options for the octet (4-, 8-, 16- and 96-channel), all of which can be used to perform this assay and other kinetic analysis methods. The machine requires sensors with immobilised ligands on the biosensor surface that then detect changes in interference patterns once other molecules are bound to the sensor.. There is a broad array of sensors available, and it is possible to work with companies to develop personalised sensors if the commercially available ones are not appropriate. The biosensors can be used several times if regenerated correctly. The raw data can be adjusted using controls for signal drift and non-specific binding. Other benefits of using BLI versus ELISA or flow-cytometry are the real time aspect, and the label/tag-free

technology (Murali et al., 2022). Label-free technology is a popular advantage as it enables better characterisation of biological interactions, preparation is faster, interference is reduced and experiments can be performed in a range of media that may be more typical of the natural environment (Easthope, 2023). There are a few limitations involved with BLI: samples can evaporate over time and constant agitation is required, although the equipment has this step included. Another issue seen with BLI is non-specific binding, which can be adjusted for using controls or by introducing detergents to the buffer. BLI has been utilized for several studies to look at receptor binding. Peacock et al. (2021) looked at binding preferences of H9N2 and introduced mutations to see if single point mutations affected receptor binding.

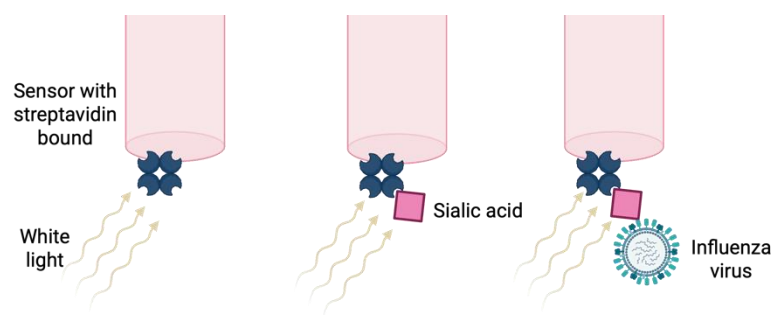


Figure 5.2. Biolayer interferometry. A visual representation of biolayer interferometry (BLI) using streptavidin sensors and influenza A virus. Image created using BioRender.

5.1.2.3 Glycan microarray

Glycan microarray has been used since 2002 to look at glycan binding proteins with their glycan ligands. Since then, the technology has developed and microarrays that are suited for influenza viruses have

been developed by the Consortium for Functional Glycomics (Blixt et al., 2004). Analysis using glycan microarrays have focused on using recombinant HA or whole virus (Stevens et al., 2006b). One of the limitations of glycan microarrays is the array of glycans available. Since receptor specificity is not limited to just $\alpha 2,3$ and $\alpha 2,6$ sialic acid receptors, there is a requirement to test against as many glycans as possible to narrow down further changes in the glycan structure. To perform all these assays recombinant reverse genetics viruses, live whole viruses, pseudotype viruses (PV) or expressed HAs are required.

5.1.3 Equine influenza pseudotype viruses

Dr Rebecca Kinsley used PVs to investigate the eight amino acids changes between the HA1 sequences of *A/equine/Newmarket/1/93* (N/1/93) and *A/equine/Newmarket/5/03* (N/5/03) (Kinsley, 2017). Dr Kinsley focused on understanding antigenic drift and serosurveillance using PVs to introduce mutations in the HA1 where the amino acid changes were identified (Figure 5.3). The two virus strains were picked because of their differing lineages, one prior to the divergence of the American lineage N/1/93 and the other after N/5/03. It was also shown that horses vaccinated against N/1/93 were not protected against the N/5/03 strain (Newton et al., 2006). Three of the mutations were identified in antigenic sites: I48M (isoleucine substituted for methionine), Q190E (glutamine substituted for glutamic acid) and E193K (glutamic acid substituted for lysine). These changes can be seen in the

alignment of the sequences in Figure 5.3 and their position within the structure of the H3 in Figure 5.4.

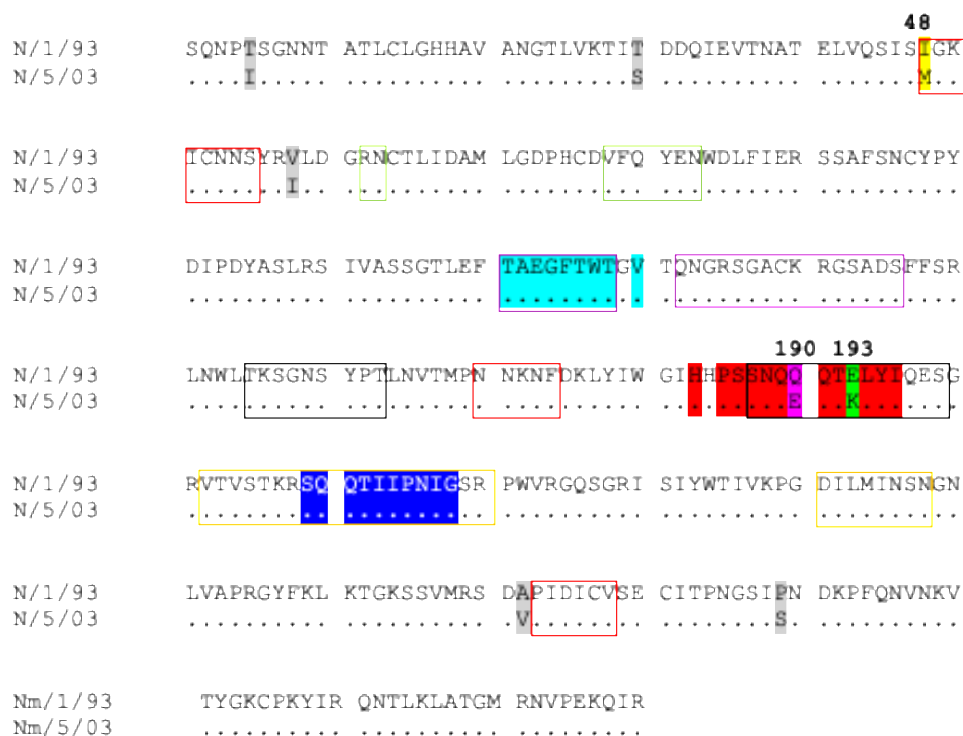


Figure 5.3. HA alignment. The alignment of the HA1 regions of A/equine/Newmarket/1/93 (GenBank accession number CAA59415.3) and Newmarket/5/03 (GenBank accession number ACI48804.1). The eight amino acid changes are highlighted in grey (outside antigenic sites), gold (I48M), pink (Q190E) and green (E193K). The turquoise section is the 130-loop, the red is the 190-loop, and the dark blue is the 220-loop. The antigenic sites are boxed in purple (site A), black (site B), red (site C), yellow (site D) and green (site E). There are gaps between the boxes because the antigenic sites can be linear (a continuous

sequence of amino acids) or conformational epitopes (discontinuous amino acid sequences joined together during protein folding).

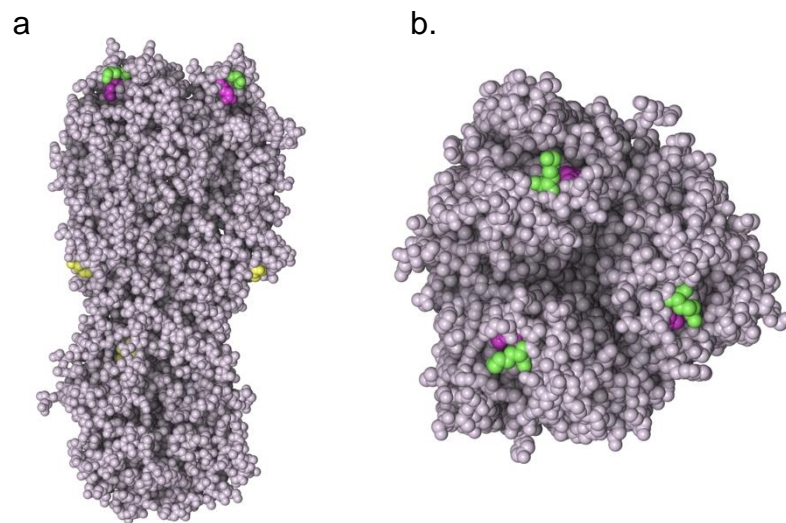


Figure 5.4. 3D structure of the HA glycoprotein as a trimer. a) A side view of H3 (2HMG.pbd) and b) a top-down view. The gold signifies residue 48, the pink is 190 and the green is 193.

Dr Kinsley produced pseudotypes with a maximum titre of 4.3×10^9 RLU/ml for the N/1/93 with the 190E mutation (Figure 5.5). Two of the mutations (190 and 193) were positioned in antigenic site B and the 190-loop that makes up the receptor binding site. Altering the amino acids at these positions caused a decrease in titre for N/1/93 (193K) and N/5/03 (190Q). They theorised that the two positions were complementary as when they introduced both mutations into the N/5/03, the titre was restored to the wild-type N/5/03 level. They were however unable to produce the double mutation in the N/1/93. The titre reduction in the N/1/93 193K and N/5/03 190Q mutation may have been caused by changes to the receptor binding of the virus. The mutational changes

may have be the pre-determining factor for interspecies transmission from horses to dogs.

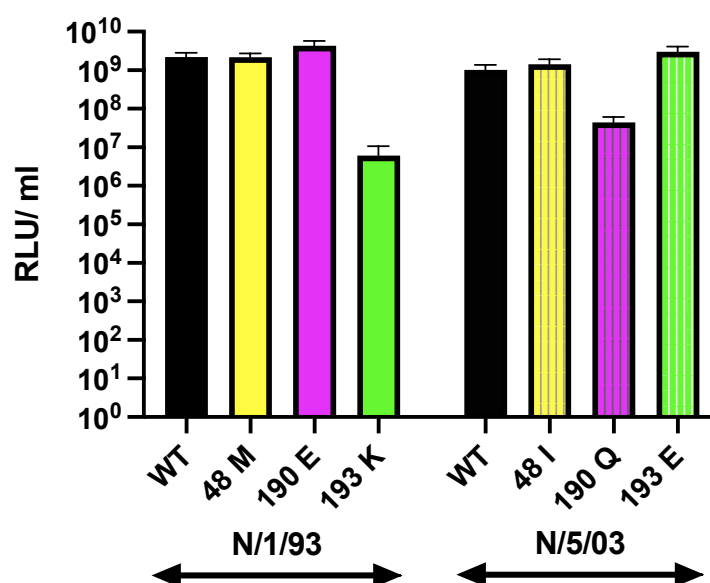


Figure 5.5. The titres for pseudotype viruses of Nm/1/93 and N/5/03. The titres for the PVs produced by Dr Kinsley for A/equine/Newmarket/1/93 and A/equine/Newmarket/5/03 for the wild type (WT) and the HA mutants, expressed in relative luminescence units (RLU/ml) adapted from Kinsley (2017). The bars are plotted with the mean of 8 replicates with the error bars representative of the standard error mean.

5.1.4 Aim

To understand whether amino acid changes in the HA of recent eIAV isolates modify receptor binding arising as a result of antigenic drift which could explain interspecies transmission from horses to dogs.

5.1.5 Objectives:

- Generate recombinant viruses with the mutated HAs using reverse genetics.
- Generate pseudotype viruses with the mutated HA plasmids.
- Complete solid phase binding assays to compare receptor binding of viruses.
- Perform BLI with the pseudotype viruses to observe receptor binding kinetics.

5.2 Materials and methods

5.2.1 Prediction of mutational effects

PolyPhen-2 a structural homology-based prediction program was used to predict the effect that mutations have on protein structure and function (Adzhubei et al., 2010). Sequences for A/equine/Newmarket/5/03 (ACI48804) and A/equine/Newmarket/1/93 (AGB08293) were downloaded from the NCBI database and altered to include the mutations named in Table 5.1. The software produces a report suggesting the effect the mutation would have.

Sorting intolerant from tolerant (SIFT) uses sequence homology and physical properties to determine the effect amino acid substitutions have on the protein function and was used in the same way as above (Ng and Henikoff, 2003). The NCBI sequences used for PolyPhen-2 were inputted into SIFT in a FASTA format and the substitutions of interest were inputted below in X#Y format where X is the original amino acid, # is the position and Y is the new amino acid. The results

are then outputted with the tolerance level and a score between 0 and 1, anything >0.05 is tolerated and anything equal to or smaller than is predicted to be damaging. Additionally, a number between 0 and 4.32 is given to predict how closely related the sequences are, an ideal result would be between 2.75 and 3.5.

5.2.2 Molecular modelling

Robetta (<https://robetta.bakerlab.org/submit.php>) was used to build a three-dimensional model of the structure of the individual HAs with the mutations introduced (Kim et al., 2004). This was done using comparative modelling to PDB structure 4UO0. The monomers were then downloaded and inputted into 3D protein imaging to highlight the mutations (Tomasello et al., 2020).

5.2.3 Cell lines

The cell lines used in this chapter were 293T/17 HEK cells, DH82 α cells, MDCK cells and E. derm cells which were cultured, counted, and thawed as described in 2.1.1–2.1.4.

5.2.4 Viruses

The viruses used for the receptor specificity assay were A/equine/Shropshire/10 (H3N8), A/Puerto Rico/8/34 (H1N1) and A/equine/Newmarket/5/03 (H3N8). The viruses used for the BLI were A/Puerto Rico/8/34 (H1N1), A/equine/Newmarket/5/03 (H3N8), A/equine/Newmarket/1/93 (H3N8), A/equine/Newmarket/2/93 (H3N8),

A/equine/Sussex/89 (H3N8) and A/canine/Illinois/41915/2015 (H3N2 reverse genetics). A high titre A/avian/Vietnam/1194/2004 (H5N1) pseudotype virus was also used for the BLI.

5.2.5 Plasmid transformation

Plasmids with mutations in the HA were kindly supplied by Dr Simon Scott and Dr Rebecca Kinsley. The plasmids were transformed as described in 2.3.1.

Table 5.1. HA plasmids from A/equine/Newmarket/93 and A/equine/Newmarket/5/03 with mutations introduced. The HA plasmids from either A/equine/Newmarket/93 or A/equine/Newmarket/5/03 either as wild-type or with mutations introduced at key positions in the receptor binding site.

HA	Mutation
N/93	WT
N/93	190E
N/93	193K
N/03	WT
N/03	190Q
N/03	193E
N/03	190Q + 193E

5.2.6 Plasmid DNA purification and quantification

The plasmid DNA was purified and quantified as described in 2.3.2.

5.2.7 Reverse genetics

The reverse genetics was performed as described in 2.2.7, using a 12 plasmid H1N1 Puerto Rico 8 system (provided by Dr Holly Shelton) that the HA plasmids would be substituted into. The reverse genetics viruses were tested using HA assay as described in 2.2.8. The 8 plasmid H3N2 system was also used as an alternative system to substitute the HA plasmids into (Rodriguez et al., 2017).

5.2.8 Pseudotyped viruses

The pseudotype viruses were kindly generated by Dr Ola Elbohy after extensive attempts to generate non-mutated PVs. I concentrated the PVs using Lenti-X concentrator. Pseudotype viruses were generated as described in 2.2.5 with either N2, N8 plasmids or exogenous NA (Table 5.2). The psPAX2 plasmid was substituted for P8.91 which had been shown previously to produce higher titres with these plasmids (Kinsley, 2017). Issues with PV production meant that they were only produced in 6-well plates. The PVs were concentrated using Lenti-X Concentrator, by combining 1 volume of Lenti-X concentrator with 3 volumes of clarified supernatant. The mixture was gently inverted several times and then placed at 4°C to incubate for 2 hours. The sample was then centrifuged at 1,500 g at 4°C for 45 minutes. This produced an off-white pellet, that was resuspended in 1/10th–1/100th of the original volume of PBS.

Table 5.2. Neuraminidase options for pseudotype viruses.

Neuraminidase	Quantity 6-well plate
N2 plasmid	125ng
N8 plasmid	125ng
Exogenous NA	15 mU/ ml

5.2.9 Pseudotype titration

The titration was performed as described in 2.2.6 using 293T/17, MDCK, DH82 α and E. derm cells as target cells. The alternative titration method performed by Dr Ola Elbohy used 100 μ l of each reagent instead of 50 μ l and left the plate for 24 hours instead of 48 hours as the protocol was optimised when Rift Valley pseudotype viruses were generated.

5.2.10 Sucrose gradient ultracentrifugation

All viruses used for BLI were ultracentrifuged down a sucrose gradient as described in 2.2.4. They were resuspended in 200 μ l of PBS and stored at -80°C until further use.

5.2.11 Receptor specificity assay

The receptor specificity assay was performed as described in 2.2.13. Variations were made to the protocol to attempt to improve the results including changing the peroxidase labelled streptavidin and decreasing the time after the labelled streptavidin was added. The steps for the protocol can be seen below (Figure 5.6).

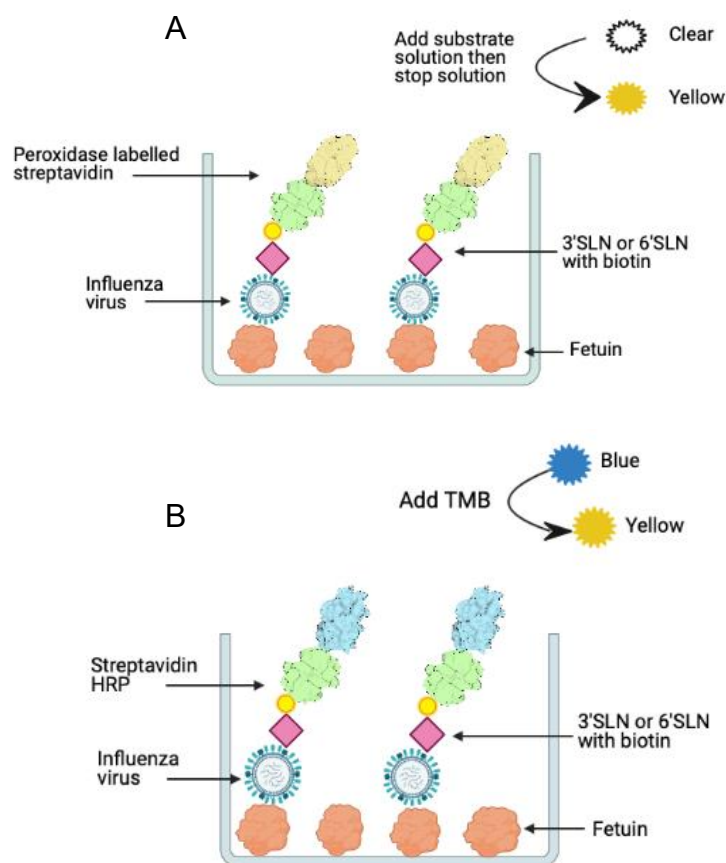


Figure 5.6. Receptor binding assay. The two methods used for the receptor specificity assay A uses peroxidase labelled streptavidin and shows a colour change from clear to yellow and B uses streptavidin HRP with TMB as the substrate solution producing a colour change of blue to yellow. Horseradish peroxidase (HRP) and 3,3',5,5' tetramethylbenzidine (TMB). Image created using BioRender.

5.2.12 Anti-NP ELISA

The Anti-NP ELISA was performed to quantify the virus concentration, using the method described in 2.2.12.

5.2.13 Bradford protein assay

The protein concentration for each virus was measured using a Bradford protein assay as described in 2.3.10. Each virus was run in duplicate and then was plotted on a graph to calculate the protein concentration compared to BSA.

5.2.14 Biolayer interferometry

An array of assays were performed using the methods described in 2.2.14. The qualitative assay (2.2.14.1) was performed to confirm which lectin each virus bound to so that the quantitative assay (2.2.14.2) could be performed. The raw graphs produced for the BLI, varied in presentation. Figure 5.7 and Figure 5.8 are representative examples of raw data graphs obtained from BLI measurements. Upon data processing as described in 2.2.14.3, the data was presented as in Figure 5.9 and Figure 5.10, assay dependent. The label on the y axis nm is a name for wavelength shift seen during the experiment.

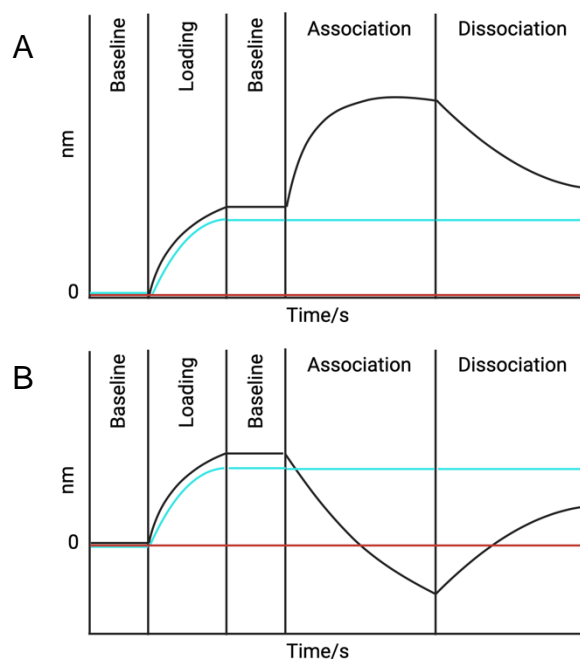


Figure 5.7. Mock graph of results produced from the qualitative assay by BLI. The two mock graphs are for the qualitative assay, and demonstrate binding to the lectins however if the absorbance was too large it dropped below 0 as demonstrated in B. The data could be flipped (negative result to positive) during processing to produce a positive result. The turquoise line is the no-signal drift control included in each assay. The red line is the negative control to confirm that the virus was not binding without the presence of the lectins, this was also included in every assay. Image created using BioRender.

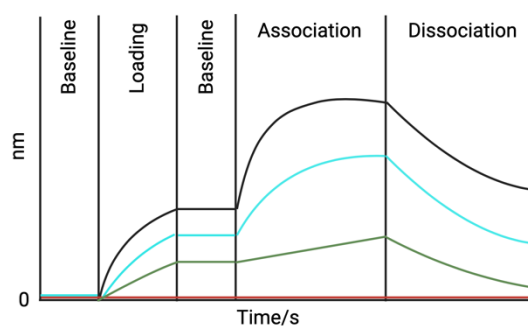


Figure 5.8. Mock graph of results produced from the quantitative assay by BLI. The mock graph demonstrates the results produced from the quantitative assay, where the lectins are introduced at varying concentrations. The black line is the highest concentration, and the turquoise and green lines are the lower concentrations. The red line is the negative control to confirm that the virus was not binding without the presence of the lectins and was included in every assay. Image created using BioRender.

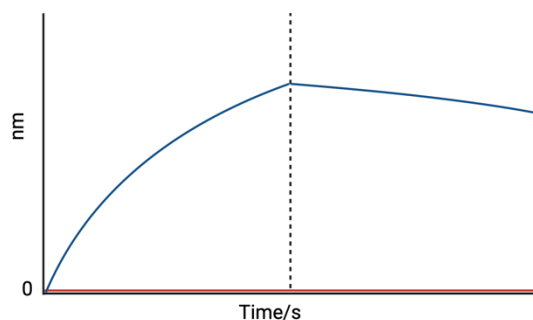


Figure 5.9. Mock graph of processed qualitative assay. The mock graph demonstrates the processed graph from the qualitative assay, that has been corrected. The graph only includes the association and dissociation steps. The red line would be an example of the virus not binding, and the blue line would be an example of the virus binding to the lectin. Image created using BioRender.

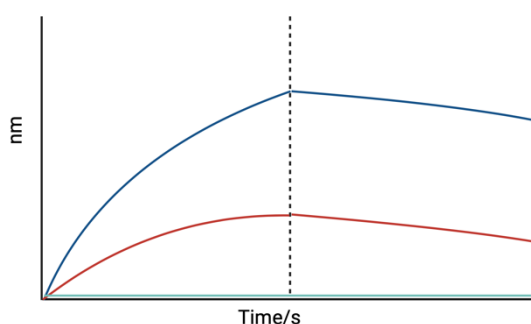


Figure 5.10. Mock graph of processed quantitative assay. The mock graph demonstrates the processed graph from the quantitative assay, that has been corrected. The graph only includes the association and dissociation steps. The dark blue line would be an example of the highest concentration of lectin the virus bound. The red and turquoise lines are the reduction in concentration of each lectin and the associated binding/ dissociation. Image created using BioRender.

5.3 Results

5.3.1 Predicted effects of mutations on the protein function and structure

5.3.1.1 PolyPhen-2 results

For N/1/93 190E, 193K and N/5/03 193E the mutations were predicted to have no effect on the structure and function with a score of 0 (Table 5.3). The whole HA sequences for N/1/93 were found to align with cIAV sequences rather than eIAV. The multiple sequence alignment for the N/5/03 sequences aligned with eIAV sequences rather than cIAV. The 190Q mutation in N/5/03 was predicted to probably be damaging to the structure and function with a score of 0.96 (Table 5.3).

Table 5.3. PolyPhen-2 score results. The table shows the strains and mutations associated with them and the score generated by PolyPhen-2 to indicate the effect on protein structure and function. The sensitivity and specificity for each result is also included.

Strain and mutation	Score	Sensitivity	Specificity
N/1/93 190E	0.00	1.00	0.00
N/1/93 193K	0.00	1.00	0.00
N/5/03 190Q	0.96	0.78	0.95
N/5/03 193E	0.00	1.00	0.00

5.3.1.2 SIFT results

As a comparison the sequences with the mutations were tested using SIFT, the result for N/5/03 with the 190Q mutation was that it would affect the protein function with a score of 0 (Table 5.4). The 193E

mutation in N/5/03 and the N/1/93 with the 190E and 193K mutation were all predicted to be tolerated.

Table 5.4. SIFT results for each strain with mutations. The results from the analysis using SIFT, including a score between 1.00 and 0.00 to predict amino acid substitution damage and the median sequence conservation which measures the diversity of the sequences.

Strain and mutation	Score	Median sequence conservation
N/1/93 190E	1.00	3.19
N/1/93 193K	0.52	3.19
N/5/03 190Q	0.00	3.07
N/5/03 193E	0.42	3.07

5.3.1.3 3D protein structure

All six structures were generated using comparative modelling against known structure 4UO0 (A/equine/Richmond/07 H3). A considerable level of variation between each structure was observed. All the structures have variations in roughly the first 50 residues (the lower half of the structure). There was a greater similarity in the top half of the corresponding strain structures, particularly between the 193E and double mutation of N/5/03. These structures were just the monomer structure, rather than the complete structure seen as a trimer in the wild type (Figure 5.4). There is some variation in the orientation of each structure, however the three N/1/93 structures were superimposed separately to the N/5/03 to keep consistency amongst the strains.

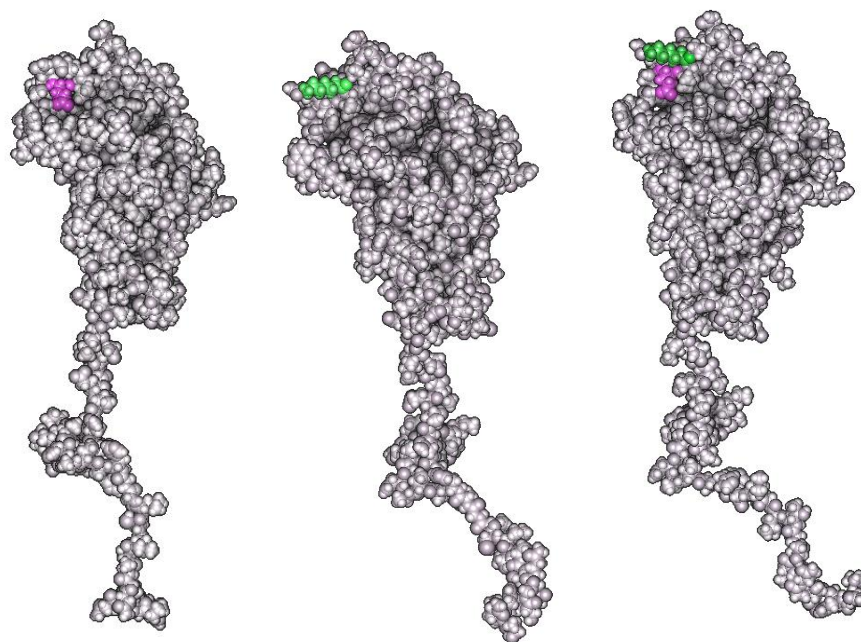


Figure 5.11. N/1/93 3D protein structures with mutations. The 3D structure of the HA monomer for N/1/93 with 190E (left, pink), 193K (middle, green) and both (right, pink and green) mutations using the predicted structure from Robetta.

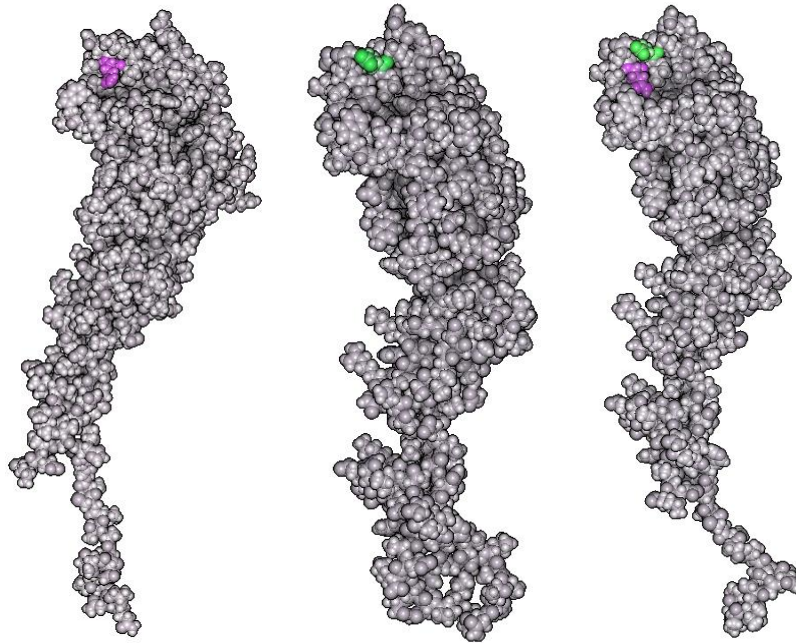


Figure 5.12. N/5/03 3D protein structures with mutations. The 3D structure of the HA monomer for N/5/03 with 190Q (left, pink), 193E (middle, green) and both (right, pink and green) mutations using the predicted structure from Robetta.

5.3.2 Reverse genetics & HA test

An attempt was made to generate recombinant PR8, however this was unsuccessful as the HA test performed gave a result of zero. Several attempts to repeat the generation of canine H3N2 (4.3.2) with the mutated HAs were unsuccessful when a HA test was performed. The conclusion from this was that it would be more beneficial to pursue generating pseudotype viruses.

5.3.3 Pseudotype viruses

Prior to pseudotyping with the mutated HA plasmids, several months were spent learning to generate pseudotypes with an equine H3 wild

type plasmid. The titres produced were never greater than 10^5 , equal to the Δ envelope. During this time, both exogenous neuraminidase and several neuraminidase plasmids were tested to attempt to improve results. When the mutated HA plasmids were obtained titration assays revealed successful production of N/1/93 WT, 190E and 193K mutations in 293T/17 target cells (Figure 5.13). There was also successful production albeit at a lower titre for N/5/03 WT, 193E and the double mutation (190Q +193E) (Figure 5.14). All PVs were compared to their respective delta envelope controls. A positive control using VSV-G was developed in parallel to confirm successful transfection. All pseudotypes were measured in relative light units (RLU)/ml. The N/1/93 193K PV was also titrated with MDCK, DH82 α and E. derm cells as target cells (Figure 5.15). All three cell lines produced a titre that was equivalent or lower than the Δ envelope suggesting that the cells were not good target cell lines however HEK control produced titres higher than the Δ envelope. The N/5/03 WT PV was included as an additional comparison and the titre in DH82 α cells was comparable to the HEK293T/17 cell titre potentially demonstrating strain specific differences, however it was less than 1-log fold higher than the Δ envelope. The titres in the 293T/17 cells were lower than seen by Dr Kinsley (Figure 5.5) but were greater than the three other cell lines. The pseudotypes were generated with an N2 plasmid as the titre was higher than with an N8 plasmid. Attempts to generate the pseudotypes with p8.91 produced titres only increasing by less than 1-log fold than with psPAX2 (data not shown).

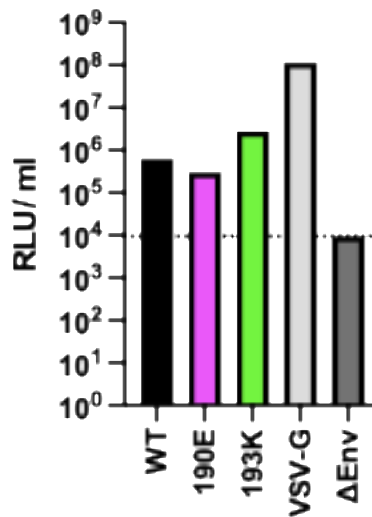


Figure 5.13. Pseudotype titration of N/1/93 pseudotypes. The pseudotype titration results for the mutated and wild type plasmids for N/1/93 with the N2 plasmid as well as the positive (VSV-G) and negative (Δ envelope) controls. The titration was performed using HEK293T/17 cells as the target cells.

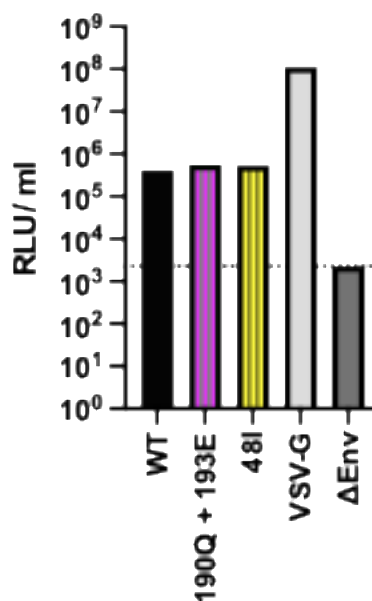


Figure 5.14. Pseudotype titration of N/5/03 pseudotypes. The pseudotype titration results for the mutated and wild type plasmids for N/5/03 with the N2 plasmid as well as the positive (VSV-G) and negative (Δ envelope) controls. The titration was performed using HEK293T/17 cells as the target cells.

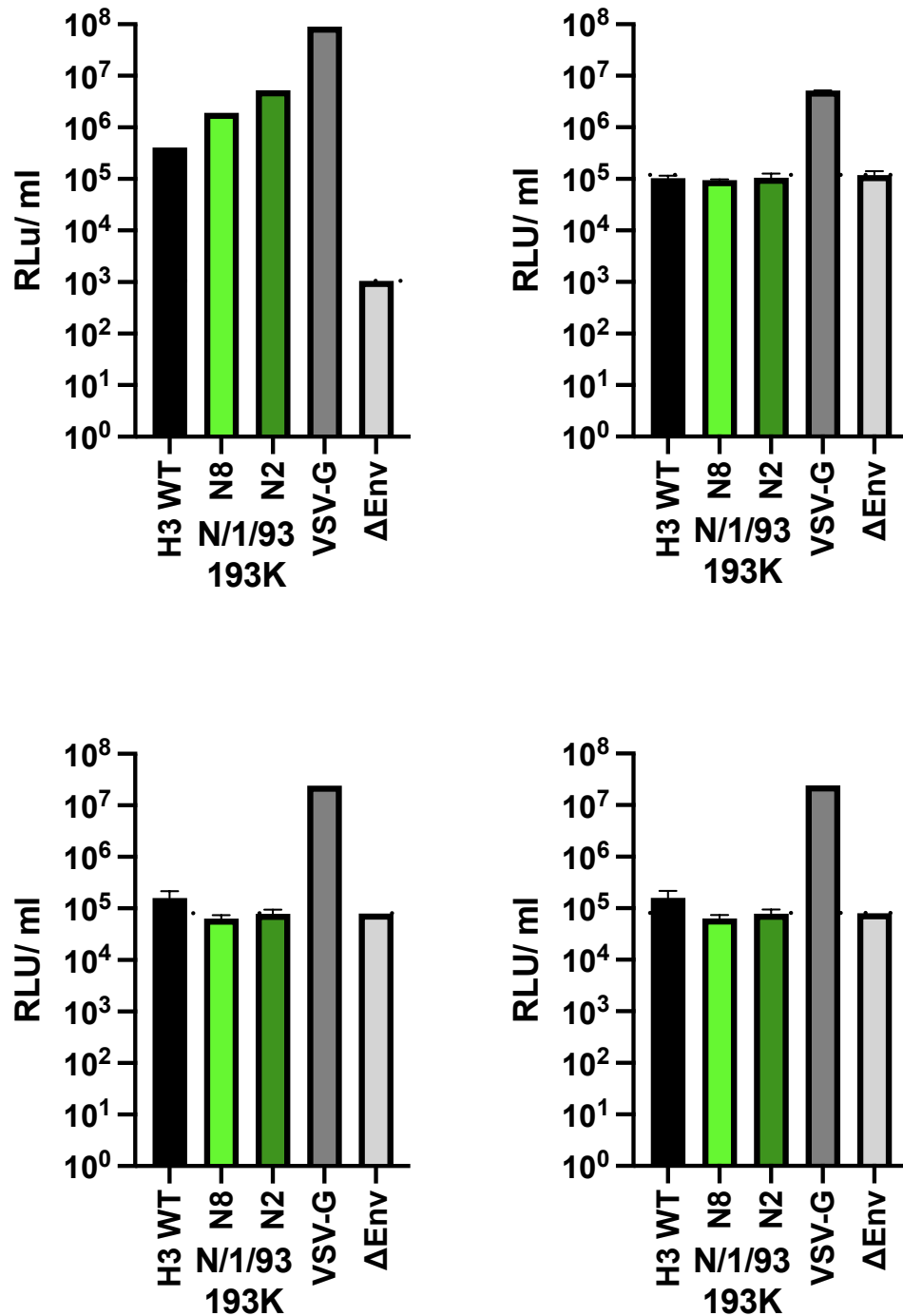


Figure 5.15. Pseudotype virus titres in four different target cells.

The pseudotype titration results for the N/1/93 193K mutated and H3 WT (N/5/03) pseudotype viruses against three different target cells. A) 293T/17 cells, B) MDCK cells and C) DH82α cells, D) E. derm cells.

The positive (VSV-G) and negative (Δ envelope) controls were

included. Each pseudotype (other than in 293T/17 cells) was run in duplicate and error bars are representative of standard error of mean.

5.3.4 Receptor specificity assay results

The two viruses chosen for the development of solid phase assays were A/equine/Newmarket/5/03 and A/Puerto Rico/8/34, wild-type viruses. Although repeated multiple times, neither virus demonstrated specific binding to the expected lectins ($\alpha 2,6$ for H1N1 PR8 and $\alpha 2,3$ for N/5/03) (Figure 5.16 and Figure 5.17). As the results were inconsistent, alternative methods were sought.

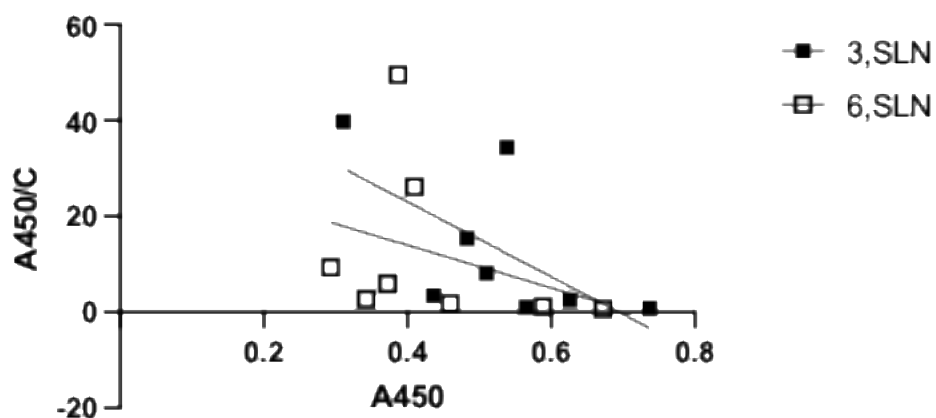


Figure 5.16. Receptor specificity assay- receptor binding of N/5/03.

A representative attempt at determining the receptor binding of N/5/03 against 3'SLN and 6'SLN lectins using solid phase receptor binding assays. The trend lines attempt to demonstrate the correlation between the results, if positive then trend lines would follow samples and it would be at 0 for 6'SLN and a positive correlation between A450 and A450/C.

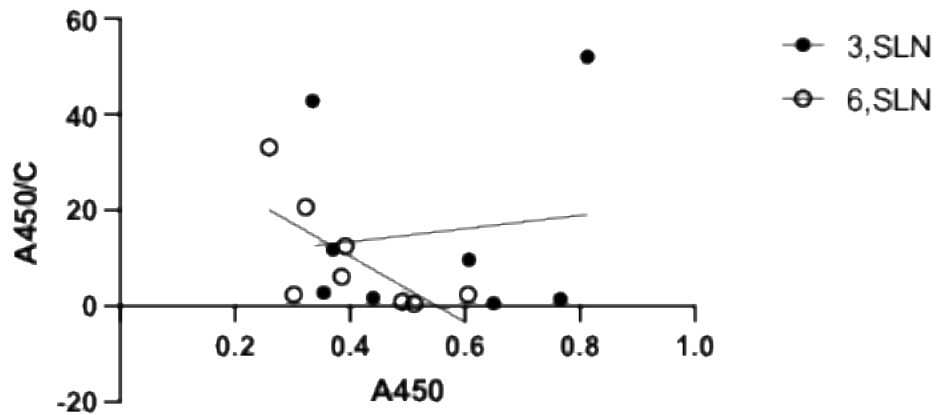


Figure 5.17. Receptor specificity assay- receptor binding of PR8. A representative attempt at determining the receptor binding of H1N1 A/Puerto Rico/8/34 against 3'SLN and 6'SLN lectins using solid phase receptor binding assays. The trend lines attempt to demonstrate the correlation between the results.

5.3.5 Biolayer interferometry

Initial development of the method used wild-type A/equine/Sussex/89 (H3N8) virus. The virus bound the $\alpha 2,3$ sialic acid and did not bind the $\alpha 2,6$ as seen in Figure 5.18 A. The Sussex/89 virus showed good positive binding to the lectins with the absorbance measured at > 4 at the peak of association. Following the success with the wild-type virus, the highest titre influenza pseudotype virus available in the lab (H5) was concentrated and tested by BLI (Figure 5.19).

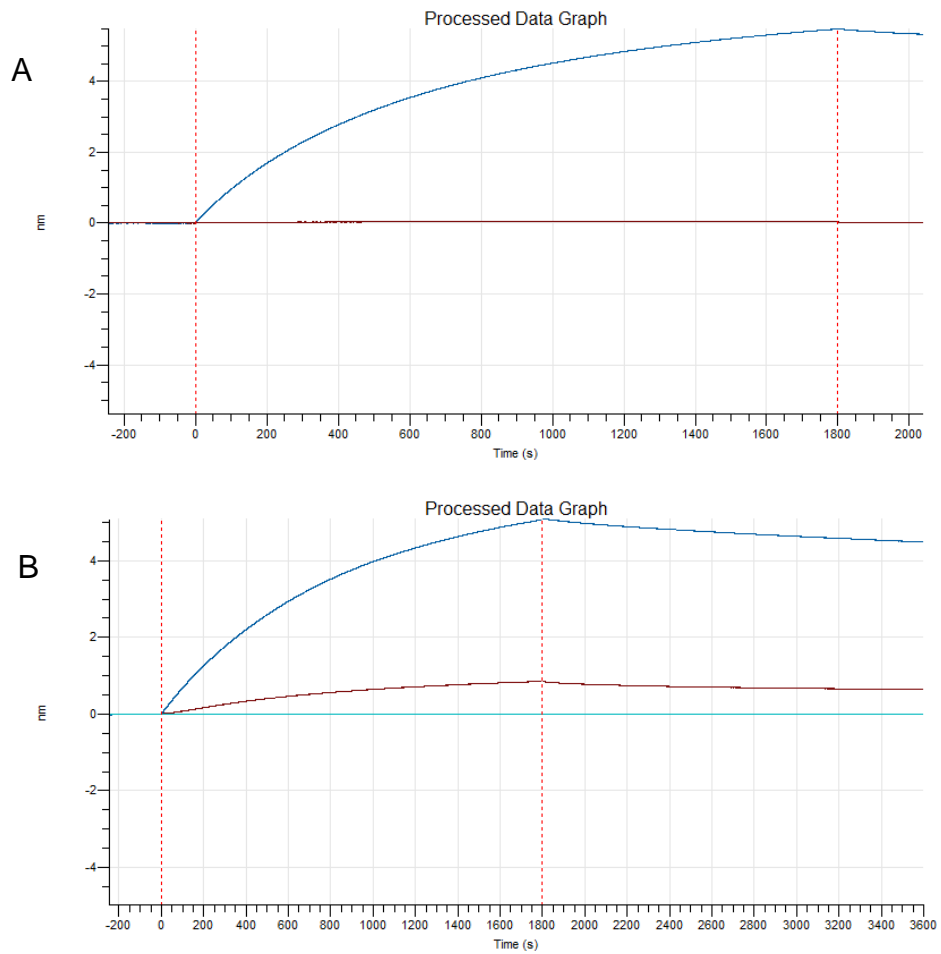


Figure 5.18. Biolayer interferometry- receptor binding of Sussex/89. Figure A demonstrates receptor binding of Sussex/89 to 3'SLN shown in blue and 6'SLN shown in red. Figure B demonstrates receptor binding of Sussex/89 at varying concentrations (0.2 (blue), 0.02 (red) and 0.002 µg/ml (turquoise)). The dotted vertical red lines represent the different steps.

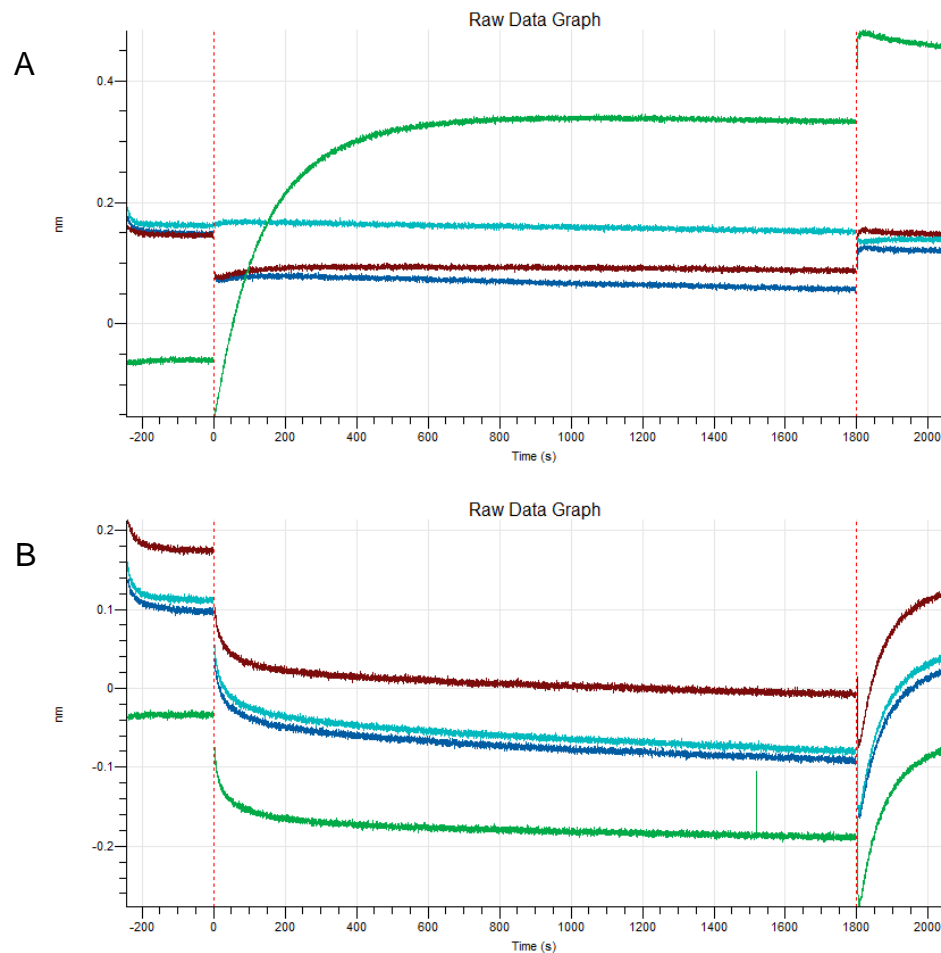


Figure 5.19. Biolayer interferometry- receptor binding of concentrated H5 pseudotype virus. Figure A demonstrates receptor binding of concentrated H5 pseudotype virus against 3'SLN shown in blue and 6'SLN shown in red. The line shown in green was included as a non-specific binding control and shows a high reading and the turquoise line was to control for baseline shift (the shift if it was different to the baseline value). Figure B uses the same lectins, but concentrated H5 PV had 0.05% tween 20 added to the buffer to remove/reduce the non-specific binding seen in the graph above. The same controls were included. The dotted vertical red lines represent the different steps.

The raw data could not be processed because there was significant non-specific binding as seen in Figure 5.19 A as seen by the green line going above the pseudotype specific lines suggesting that any binding observed would be non-specific. To compensate for this, 0.05% tween 20 was added to the virus buffer. This reduced non-specific binding however there was still a significant amount of non-specific binding observed but the results could not be flipped to demonstrate this. Additionally, the control for base line shift (lectin added but no pseudotype virus) showed binding at the same absorbance to the PVs. The absorbance measured was also significantly lower than would be classified as successful binding.

The A/equine/Newmarket/1/93 and A/equine/Newmarket/5/03 viruses were assessed using BLI to determine whether there were differences in receptor binding. The viruses were added at the same concentration as determined by the Bradford protein assay as the quantification of the NP by Anti-NP ELISA could not be confirmed without a virus of known concentration. Both viruses were added at 15 µg/ml however the virus quantity was likely different given the difference in absorbance measured (Figure 5.20) since the Bradford protein assay measures all proteins and does not specify viral proteins. Neither virus bound to the lectin fully in the association time provided or produced a curved shaped line as seen on Figure 5.18 A. Additionally, cIAV H3N2 reverse genetics virus generated in chapter 4, was included in the BLI experiments. Similarly to the two Newmarket viruses, the virus did not

bind fully however it did demonstrate preferential binding to $\alpha 2,3$ (Figure 5.21). In Figure 5.21 there is some binding observed with the $\alpha 2,6$ lectin, which was not observed with any other virus.

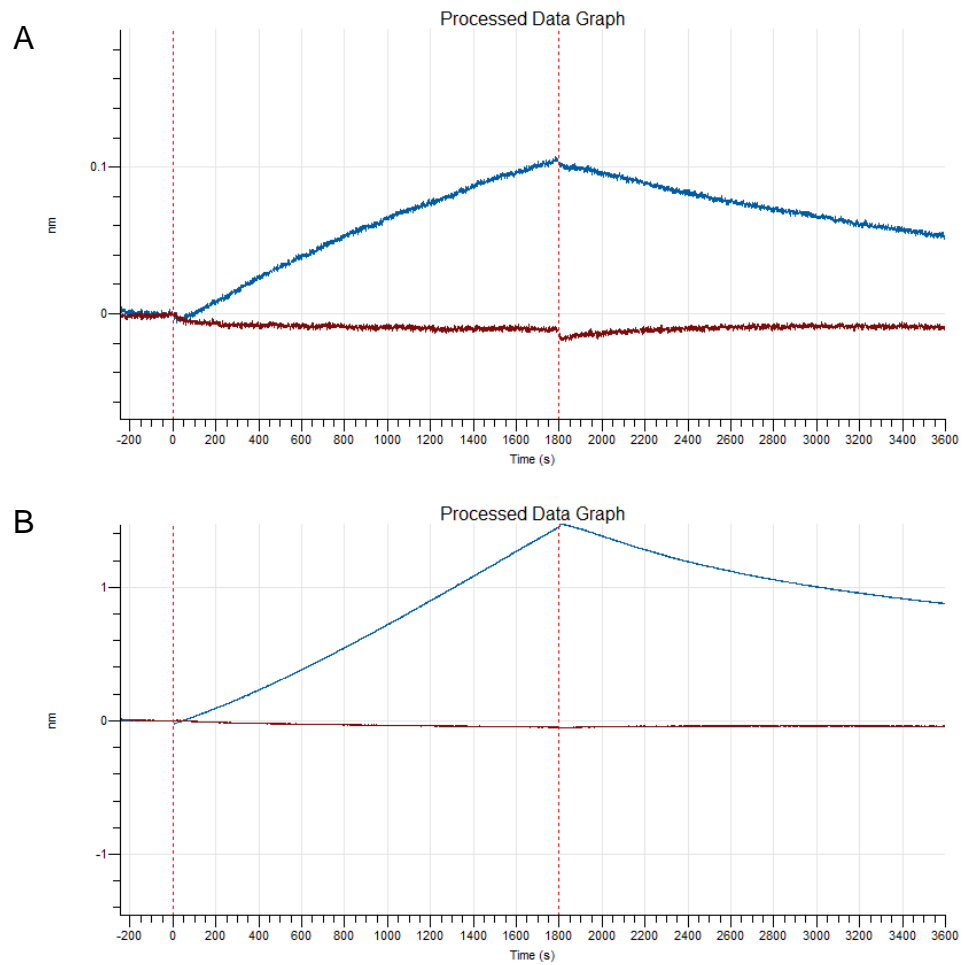


Figure 5.20. Biolayer interferometry- receptor binding of Newmarket/1/93 (A) and Newmarket/5/03 (B). Figure A demonstrates receptor binding of Newmarket/1/93 against 3'SLN show in blue and 6'SLN shown in red. Figure B uses the same lectins but with Newmarket/5/03. The data was corrected for the two controls however binding was significantly lower than seen on Figure 5.18 with Sussex/89 because the nm value was lower. The dotted vertical red lines represent the different steps.

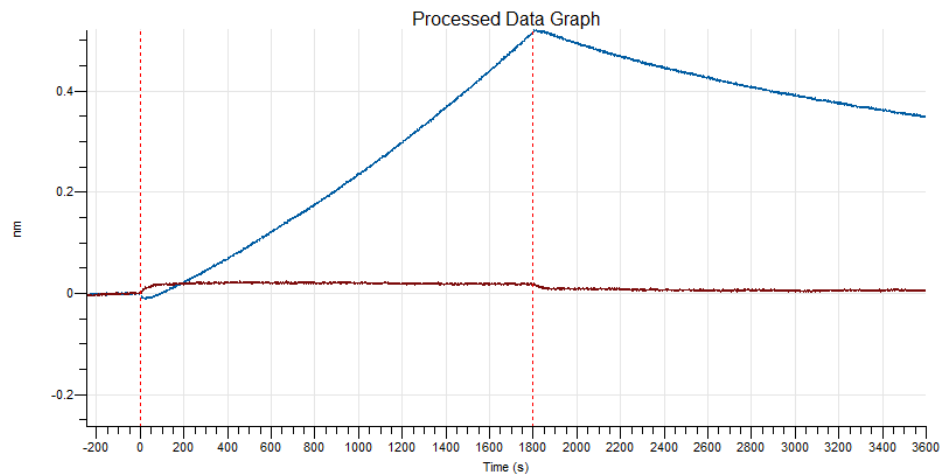


Figure 5.21. Biolayer interferometry - receptor binding of cIAV H3N2 reverse genetics virus. The figure demonstrates receptor binding of cIAV H3N2 reverse genetics virus against 3'SLN show in blue and 6'SLN shown in red. The data was corrected for the two controls. The dotted vertical red lines represent the different steps.

5.4 Discussion

The aim of this chapter was to understand whether amino acid changes in recent eIAV isolates modify receptor binding. Following on from the issues Dr Kinsley identified during development of the pseudotypes, the mutations introduced were checked to confirm whether they may affect the protein function. The N/5/03 190Q and N/1/93 193K mutations were expected to affect the function due to lower titres in the pseudotypes generated by Dr Kinsley however only the 190Q was predicted to be detrimental based on the PolyPhen-2 results. Since this was predicted by both software programs PolyPhen-2 and SIFT, it is likely that the reason for the lower pseudotype titre relates to the effect the mutation has on the structure/function. The N/1/93 193K mutation whilst not

predicted to influence the function may alter the structure and therefore the results were repeated using a secondary piece of software: SIFT. Another issue related to the use of PolyPhen-2 is that it is designed for human proteins which our eIAV strains are not, and therefore the specificity of the results is not clear. To circumvent this issue, SIFT analysis was also performed since this software was not designed specifically to test human proteins. Nevertheless, the results were comparable to that of PolyPhen-2. The SIFT results showed that whilst the 190Q mutation would affect the protein function, the three other mutations would not affect it, however the score heavily varied. The highest score 1.00 was achieved by only one mutation, the results for the two other mutations, whilst not near the lower boundary of 0.05, are not at the highest confidence interval.

Robetta has several methods for predicting the structure. RoseTTAFold is the suggested method on the website used as it is the most accurate, however upon using this method to generate the double mutation N/5/03 the confidence interval was limited to 0.73 out of 1. The decision was made to use comparative modelling so the mutated sequences could be compared back to a known structure. Whilst the monomer could be easily predicted, the trimer formation could not be performed as available 3D structures were generated by crystallization and x-ray crystallography. These methods were not considered as there were already trimer structures available for eIAV. One of the limitations of using Robetta to predict the structure was the lack of availability of

equine HA structures. There are two PDB structures available for eIAV H3, 4UO0 (A/equine/Richmond/07) and 4UNW (A/equine/Newmarket/2/93). The Richmond strain was isolated 4 years after the N/5/03 and is from the same clade (Florida Clade 2) and therefore the most phylogenetically similar structure available. The Richmond strain was not as similar as N/1/93 which was isolated 14 years prior to Richmond/07. Additionally, the Newmarket/2/93 structure was not chosen as it was pre-divergence into the American lineage subclades, and it was a strain from the Eurasian clade. The differences between the two clades meant that the 4UO0 structure had to be used for the comparative modelling despite its likely differences to the strains of interest.

The Robetta results, once downloaded and inputted into 3D protein imaging, could be visually observed. This highlighted the differences between the mutated sequences. The highest variation in structure was seen in the N-termini, which is made up of the first and last 20 residues. The last 20 residues make up the stem fragment that interacts with HA2 and potentially explains the variations seen between the structures. 3D protein imaging only superimposes two structures at once, making comparison between several structures difficult.

It was intended to use reverse genetics viruses generated with the mutated HA plasmids produced by Dr Kinsley. Two reverse genetics systems were attempted, one using 8 plasmids, a H3N2 canine

backbone which had successfully produced recombinant WT cIAV (chapter 4.3.2) and the other a 12-plasmid system with a H1N1 backbone. The 12-plasmid system was originally established in 1999 which included 4 polymerase II plasmids encoding the viral PB2, PB1, PA and NP as well as 8 polymerase I plasmids for the eight segments because to generate vRNA *in vivo* from cDNA RNA polymerase was required to initiate and terminate transcription without additional nucleotides (Fodor et al., 1999, Neumann et al., 1999). The invention of the 8-plasmid system using ambisense/bidirectional plasmids was more successful due to the reduction in the number of plasmids required (Hoffmann et al., 2000a, Hoffmann et al., 2000b, Nogales and Martínez-Sobrido, 2016). The complex combination of plasmids and two cell lines can be challenging to achieve and after several attempts at making each system work, the decision was made to move to pseudotype viruses which use a maximum of five plasmids.

Similar issues were encountered with the pseudotype viruses, in that for successful production of PVs the correct ratio of plasmids is needed (Ruiz-Jiménez et al., 2021). Initially this was attempted using wild type H3 plasmids, with different types of neuraminidase (N2, N8 or exogenous neuraminidase) and this was not successful. One potential reason for this was that there was an issue with the H3 plasmid as PVs have since been generated with the neuraminidases and the other core plasmids. Once the mutated plasmids were acquired, generation was tried again and pseudotypes were successfully produced. The titres were not as

high as produced by Dr Kinsley, possibly due to the use of pCAGGS-HAT instead of pCAGGS-TMPRSS2 as only the pCAGGS-HAT was available at the time of PV generation. Also, unlike Dr Kinsley, the highest titre produced was from the N/1/93 with the 193K mutation. To improve the titres a different promoter could have been substituted into the system such as murine leukemia virus or vesicular stomatitis virus, both have been used to produce pseudotype viruses (Carnell et al., 2015). Alternatively, the addition of polybrene or a centrifugation step during transduction may increase the efficacy of transduction or changing the transfection reagent to PEI (Denning et al., 2013, Le Doux et al., 2001, Swaney et al., 1997).

One method to looking at variations in the receptor binding used in this study was the solid phase binding assay. This method is well established and has been proven to be consistent in looking at receptor binding. In this study, the results were unreliable and inconsistent after many attempts with viruses grown in hens' eggs. The human H1N1 PR8 virus should have shown specific binding to 6'SLN and this was not observed across any of the repeats. Similarly, the N/5/03 should have shown specific binding to 3'SLN, but the results were inconsistent. Potential explanations for this are that the manual plate washing may not have been thorough enough, or the viruses were not at a sufficient concentration. Pseudotypes viruses are less concentrated than egg grown viruses and therefore would not improve the results.

The solid phase binding assay used in this study was adapted by Kamiki et al. (2022) and Sekine et al. (2024) who initially incubated the plates with streptavidin before addition of the lectins. The virus was then incubated overnight and then serum or mouse anti-H3N8 cIAV antibody was added. Anti-mouse secondary and HRP were added and then the assay was continued as described in this study. This was done to reduce nonspecific reactions which would be beneficial with the pseudotype viruses where non-specific binding was observed. The limitations to performing this experiment would be in obtaining serum or cIAV antibody. The adaptations to this method were published after establishing that other methods may provide more accurate results. If this study was repeated, then the adaptations suggested above would be included.

As conducted above, prior to BLI being performed with the PVs, it was trialled with egg grown viruses. The first issue encountered was in virus quantification. The absence of a virus of known concentration meant the anti-NP ELISA could not be quantified. At the time of starting this work, this was not something the lab possessed and therefore other methods were investigated to quantify the virus. Initially a BSA protein assay was performed, however it became clear that this was not precise enough and only factored in protein concentration and not amount of virus present. Nonetheless, egg grown viruses were tested by BLI, however curves of the fractional saturation vs sugar loading could not be produced. The Sussex/89 virus, a predecessor of the eIAV strains of

interest, demonstrated specific receptor binding to the 3'SLN lectin used. Similarly, egg grown N/1/93 and N/5/03 wild type and reverse genetics cIAV H3N2 demonstrated the same pattern of binding, however this was at a much lower absorbance, likely due to the virus not being concentrated enough. The cIAV H3N2 virus also demonstrated a very small initial binding to $\alpha 2,6$, which was unlikely to be significant binding.

The PVs were generated with two different neuraminidase plasmids for N/1/93 193K and were used for the PV titration with different target cells. The HAs are from equine IAV strains and therefore if there are changes to the receptor binding, the titration might demonstrate a preference towards cell lines expressing $\alpha 2,3$ receptors. From the titration assay only HEK 293T/17 cells as target cells expressing $\alpha 2,3$ and $\alpha 2,6$ sialic acids produced a successful titre. Investigation into whether the other PVs in particular the N/5/03 double mutation, may alter the titres was not performed however would help to confirm whether the alternate cell lines would be better target cells. If repeated, extEqFL cells (an equine lung cell line) would also be included, as the most similar cell type to the natural host.

Although this was observed, several attempts were made at using the most concentrated pseudotypes available in the lab. Initially a large amount of non-specific binding was observed, and so Tween 20 was added to compensate. This reduced the amount observed, but did not

remove it completely and once the non-specific binding and drift controls were subtracted from the data there was no binding observed. From this it was concluded that, as with the solid phase binding assay it was unlikely that the PVs would be concentrated enough to demonstrate receptor binding. Additionally, the anti-NP ELISA could not be performed on the PVs making it increasingly difficult to quantify them.

Future research would use glycan microarray to demonstrate differential receptor binding. This would mean that the viruses with mutations introduced could have been observed interacting with a larger range of sialic acid receptors. Similarly to the BLI and the ELISA, it is unlikely that the PVs would work successfully. The reverse genetics viruses, or alternatively the expression of HAs in mammalian cells, would work successfully on glycan microarray. Stevens et al. (2006b) compared whole-virus and recombinant HA, and noted that there was a decreased biosafety concern, longer sample preparation and weaker avidity for the recombinant HA and therefore concluded reverse genetics viruses should be used.

Although the PVs with the mutations were successfully generated, the difference in receptor binding could not be confirmed as the methods used in this study required the virus at higher concentrations than were produced. There is no current literature that discusses the use of PVs in receptor binding studies and this work has confirmed their inefficacy in

the methods attempted. The study has also shown that receptor binding can be observed using BLI on wild-type and reverse genetics viruses and that the strains tested bind to the expected receptors. Further work would include additional attempts to generate recombinant viruses using reverse genetics for use in BLI or glycan microarray.

6 Conclusion

This thesis presents an investigation into new approaches to study canine influenza A virus (cIAV) and equine influenza A virus (eIAV). The first results chapter focused on the production of single domain antibodies (sdAb) for differentiation between the two Florida clades of eIAV. The second chapter centred on the suitability of cell lines to investigate the innate immune response and host interactions with a focus on cIAV. The final chapter focused on understanding receptor binding and whether changes to recent eIAV isolates may affect receptor binding and subsequently enabled transmission into dogs.

Phage display, a method used in this thesis, has the potential to generate specific sdAbs to any chosen target. A synthetic phage library was used to provide a high diversity of potential binders that produce antibodies to target antigens. The two target antigens used were recombinant eIAVs each with the haemagglutinin (HA) from one of the two Florida subclades. Two types of antibodies were successfully generated: maltose binding protein (MBP) fused VHH and Fc fused VHH. Their relatively small size makes them an ideal format. The VHH were expressed using mammalian and bacterial expression however if repeated plant expression or mammalian suspension culture, which provide their own advantages, should be considered (Nosaki et al., 2021). Plant expression has mainly been used for vaccine and therapeutic production however it demonstrates a reduced chance of pathogen contamination, is a more economical method and has the

capacity to assemble large multimeric proteins, which would benefit recombinant protein expression (Nosaki et al., 2021). The generation of Fc fused antibodies using this method would also ensure that the antibodies were generated in keeping with the 3 Rs (replacement, reduction and refinement). Although neither antibody format could differentiate between the two Florida subclades, they did bind specifically to influenza viruses, and they have the potential to work as broader influenza targeting antibodies. The limits to this study were time and financial cost meaning that only a small number of potential targets were investigated. Therefore, the potential remains that a better candidate could be identified in the other 60 identified binders. Future work would be to demonstrate the neutralising capabilities of the Fc fused VHH already generated and then to produce more antibodies using this method. This approach could be used to generate neutralising antibodies to influenza A viruses with therapeutic potential in equines and canines (Daly et al., 2023, Dong et al., 2020). This process of generating antibodies could be used in a wider context against any target antigen and would be beneficial for future pandemics as a process of quickly developing antibodies in any format.

As part of exploring the suitability of cell lines, reverse genetics canine H3N2 virus was generated to provide an additional H3 virus that underwent interspecies transmission into dogs. The H3N2 cIAV circulated at the same time and may have reassorted with the H3N8 potentially supporting the sustained transmission of H3N2. The virus

was also utilised in the third results chapter to look at receptor binding using BLI. The three cell lines explored were: DH82 α a canine macrophage like cell line, extEqFL and E. derm, equine lung and dermal cell lines respectively. The E. derm cells appeared deficient of clear staining patterns in the lectin staining and the TCID₅₀ results were low suggesting inefficient replication of equine and canine IAVs, which was in keeping with previous research into the cell line (Crispell, 2018, MacRae, 2010). The extEqFL cells required a lower TCID₅₀/ml than the E. derm cells although the lectin staining did not highlight receptors on the cell surface. The viral growth kinetics for cIAV subtypes demonstrated the inability of this cell line for efficient cIAV replication. The cells were not tested further with eIAV and there are currently no published papers that discuss this cell line in reference to eIAV, therefore further research should be performed. Scocco and Pedini (2008) showed that equine lung cells had no staining for α 2,3 or α 2,6 however there was moderate staining in the tracheal sub mucosal glandular cells. This would suggest that a more appropriate cell line to be investigated would be from the sub mucosal tracheal gland.

DH82 α cells stained positively for both receptors and exhibited efficient viral replication for both cIAV subtypes and were further explored by RNA sequencing. In combination with the cytokine response data DH82 α cells demonstrated minimal activation of the immune response at the time points studied in comparison to studies in other cell lines and to the natural host response (Kang et al., 2013, Tao et al., 2019).

Although the RNA sequencing experiments were performed on the DH82 α cells infected with cIAV H3N2, the cells also demonstrated replication of eIAV N/5/03 by TCID₅₀. The lectin staining of DH82 α cells demonstrated the presence of α 2,3 SAs the receptor targeted by eIAV therefore DH82 α cells have the potential to be used for research into eIAV as well as cIAV. The methods used in this chapter could be applied to a range of cell lines to further investigate their use in research. The RNA sequencing in particular could be used with any cell line, immortal or primary cells and for cells from explant tissues, but has also been used for cancer research.

The receptor binding of recent H3N8 isolates could not be observed in detail as the appropriate viral tool to display the mutated HAs could not be developed. There was no prior research demonstrating the use of pseudotype viruses by biolayer interferometry (BLI). The PVs did not produce reliable results by BLI because of a high level of non-specific binding that could not be controlled. PVs could not be used for BLI or solid phase binding assays to investigate receptor binding and further research into the mutations should be completed using reverse genetics generated viruses. The BLI assays performed demonstrated that the wild type eIAV and cIAV viruses tested, all demonstrated binding to the α 2,3 SA receptor as expected.

As discussed in chapter 3.4, although the antibodies generated in this thesis focused on equine influenza A virus, this method could be

replicated for cIAV, with the alternative focus of differentiating between subtypes of cIAV. The binding ability of the antibodies generated could be investigated by BLI. Alternatively, the reverse genetics virus system used in 4.3.2 could be used to generate cIAVs as target antigens in the phage display system. An area not explored herein was the interaction of the PVs, WT or reverse genetics cIAV H3N2 with the cell lines investigated in chapter 4 using immunohistochemistry.

The work completed above is preliminary work that could be developed to further our understanding of these tools. The VHH antibody development will be continued into a publishable study by testing whether the antibodies have neutralising capacity and could therefore identify escape mutants. The antibody has already demonstrated binding to several influenza A virus subtypes potentially suggesting a broad antibody which are in less abundance (Doud et al., 2018). In combination with further characterisation of the antibody by x-ray crystallography and cryo-electron microscopy as well as kinetic analysis using the octet this additional work would generate a publishable study from the preliminary work of chapter 3.

For chapter 4 to become complete, repeat RNA sequencing analysis would be required using a higher MOI, a zero-hour time-point and the inclusion of extEqFL cells. Further RT-qPCR experiments and potentially cytokine ELISAs to back up the analysis would further confirm the immune response demonstrated by the cell lines.

Additionally with the inclusion of controls such as equine/ canine tracheal explants or primary cell culture of equine/canine cells, this would generate a complete study exploring canine and equine cell lines.

Chapter 5 began to introduce the influence of receptor binding changes. To further explore this, computational HA trimer structures would be generated with the individual mutations introduced, as well as the double mutation. Ligand docking would then be performed to investigate the interaction of the mutated trimers with the sialic acids. In combination with glycan array studies and octet analysis using recombinant HA proteins the influence of receptor binding changes would be further investigated. The methods described could be applied to any influenza virus, especially when investigating changes in amino acids between clades circulating simultaneously to identify targets for vaccine design. BLI also has uses in kinetic studies in chemistry and in any protein-protein interaction, which in combination with computational modelling makes a powerful tool.

Equine and canine influenza A viruses are both considered neglected influenza viruses and research into them, especially cIAV, is limited. The work presented demonstrates the generation of a new potential reagent and the suggestion of a cell line to research both viruses. Although differences between recent isolates of eIAV could not be observed, the individual binding preferences of wild type eIAVs and cIAV H3N2 were confirmed, and the method demonstrated the inability

of PVs using that platform. The work completed here has further improved the understanding of approaches that can be applied to equine and canine influenza A viruses.

7 References

- ADEYEFA, C., MCCAULEY, J., DANEJI, A. I., KALEJAIYE, O., BAKARE, A. & ASHIMOLOWO, O. 1997. Cellular Immune Recognition of Influenza A Viruses in Equines: in vitro and in vivo Studies on the Immunogenicity of Equine Influenza Viruses. *Acta Veterinaria Brno*, 66, 39-49.
- ADZHUBEI, I. A., SCHMIDT, S., PESHKIN, L., RAMENSKY, V. E., GERASIMOVA, A., BORK, P., KONDRASHOV, A. S. & SUNYAEV, S. R. 2010. A method and server for predicting damaging missense mutations. *Nature Methods*, 7, 248-249.
- AGHEBATI-MALEKI, A., BARADARAN, B., HAJIASGHARZADEH, K., BAKHSHINEJAD, B. & AGHEBATI-MALEKI, L. 2021. The Application of Next Generation Sequencing in Phage Display: A Short Review. *ImmunoAnalysis*, 1, 7-7.
- AHMED, B. M., BAYOUMI, M. M., FARRAG, M. A., ELGAMAL, M. A., DALY, J. M. & AMER, H. M. 2022. Emergence of equine influenza virus H3Nx Florida clade 2 in Arabian racehorses in Egypt. *Virology Journal*, 19, 185.
- ALFORD, R. H., KASEL, J. A., LEHRICH, J. R. & KNIGHT, V. 1967. Human responses to experimental infection with influenza A/equi 2 virus. *American Journal of Epidemiology*, 86, 185-192.
- ALLEN, J. D. & ROSS, T. M. 2018. H3N2 influenza viruses in humans: Viral mechanisms, evolution, and evaluation. *Hum Vaccin Immunother*, 14, 1840-1847.

AMAT, J. A. R., PATTON, V., CHAUCHÉ, C., GOLDFARB, D., CRISPELL, J., GU, Q., COBURN, A. M., GONZALEZ, G., MAIR, D., TONG, L., MARTINEZ-SOBRIDO, L., MARSHALL, J. F., MARCHESI, F. & MURCIA, P. R. 2021. Long-term adaptation following influenza A virus host shifts results in increased within-host viral fitness due to higher replication rates, broader dissemination within the respiratory epithelium and reduced tissue damage. *PLOS Pathogens*, 17, e1010174.

ANDRÉ, A. S., MOUTINHO, I., DIAS, J. N. R. & AIRES-DA-SILVA, F. 2022. In vivo Phage Display: A promising selection strategy for the improvement of antibody targeting and drug delivery properties. *Frontiers in Microbiology*, 13.

ASHA, K. & KUMAR, B. 2019. Emerging Influenza D Virus Threat: What We Know so Far! *Journal of Clinical Medicine*, 8, 192.

ASHTON, L. V., CALLAN, R. L., RAO, S. & LANDOLT, G. A. 2010. In Vitro Susceptibility of Canine Influenza A (H3N8) Virus to Nitazoxanide and Tizoxanide. *Vet Med Int*, 2010.

BANCROFT, C. T. & PARSLOW, T. G. 2002. Evidence for segment-nonspecific packaging of the influenza A virus genome. *Journal of virology*, 76, 7133-7139.

BARBA, M. & DALY, J. M. 2016. The Influenza NS1 Protein: What Do We Know in Equine Influenza Virus Pathogenesis? *Pathogens (Basel, Switzerland)*, 5, 57.

BARDOR, M., NGUYEN, D. H., DIAZ, S. & VARKI, A. 2005. Mechanism of Uptake and Incorporation of the Non-human Sialic Acid

N-Glycolylneuraminic Acid into Human Cells *.</sup>

Journal of Biological Chemistry, 280, 4228-4237.

BARNARD, K. N., WASIK, B. R., ALFORD-LAWRENCE, B. K.,
HAYWARD, J. J., WEICHERT, W. S., VOORHEES, I. E. H., HOLMES,
E. C. & PARRISH, C. R. 2020. Influenza A viruses serially passaged in
different MDCK cell lines exhibit limited sequence variation across their
genomes, with the exception of the hemagglutinin gene. *bioRxiv*,
2020.02.20.959015.

BARNES, A., BEE, A., BELL, S., GILMORE, W., MEE, A., MORRIS, R.
& CARTER, S. D. 2000. Immunological and inflammatory
characterisation of three canine cell lines: K1, K6 and DH82. *Veterinary
Immunology and Immunopathology*, 75, 9-25.

BAZAN, J., CAIKOSIŃSKI, I. & GAMIAN, A. 2012. Phage display--a
powerful technique for immunotherapy: 1. Introduction and potential of
therapeutic applications. *Hum Vaccin Immunother*, 8, 1817-28.

BDEIR, N., ARORA, P., GÄRTNER, S., HOFFMANN, M., REICHL, U.,
PÖHLMANN, S. & WINKLER, M. 2019. A system for production of
defective interfering particles in the absence of infectious influenza A
virus. *PLoS One*, 14, e0212757.

BEAN, W. J. 1984. Correlation of influenza A virus nucleoprotein genes
with host species. *Virology*, 133, 438-442.

BLIXT, O., HEAD, S., MONDALA, T., SCANLAN, C., HUFLEJT, M. E.,
ALVAREZ, R., BRYAN, M. C., FAZIO, F., CALARESE, D., STEVENS,
J., RAZI, N., STEVENS, D. J., SKEHEL, J. J., VAN DIE, I., BURTON,
D. R., WILSON, I. A., CUMMINGS, R., BOVIN, N., WONG, C.-H. &

- PAULSON, J. C. 2004. Printed covalent glycan array for ligand profiling of diverse glycan binding proteins. *Proceedings of the National Academy of Sciences*, 101, 17033-17038.
- BOND, C. J., MARSTERS, J. C. & SIDHU, S. S. 2003. Contributions of CDR3 to VHH Domain Stability and the Design of Monobody Scaffolds for Naive Antibody Libraries. *Journal of Molecular Biology*, 332, 643-655.
- BORLAND, S., GRACIEUX, P., JONES, M., MALLET, F. & YUGUEROS-MARCOS, J. 2020. Influenza A Virus Infection in Cats and Dogs: A Literature Review in the Light of the "One Health" Concept. *Frontiers in Public Health*, 8, 8.
- BOUVIER, N. M. & PALESE, P. 2008. The biology of influenza viruses. *Vaccine*, 26 Suppl 4, D49-D53.
- BRAUER, R. & CHEN, P. 2015. Influenza virus propagation in embryonated chicken eggs. *J Vis Exp*.
- BROSZEIT, F., TZARUM, N., ZHU, X., NEMANICHVILI, N., EGGINK, D., LEENDERS, T., LI, Z., LIU, L., WOLFERT, M. A., PAPANIKOLAOU, A., MARTÍNEZ-ROMERO, C., GAGARINOV, I. A., YU, W., GARCÍA-SASTRE, A., WENNEKES, T., OKAMATSU, M., VERHEIJE, M. H., WILSON, I. A., BOONS, G.-J. & DE VRIES, R. P. 2019. N-Glycolylneuraminic Acid as a Receptor for Influenza A Viruses. *Cell reports*, 27, 3284-3294.e6.
- BRYANT, N. A., RASH, A. S., RUSSELL, C. A., ROSS, J., COOKE, A., BOWMAN, S., MACRAE, S., LEWIS, N. S., PAILLOT, R., ZANONI, R., MEIER, H., GRIFFITHS, L. A., DALY, J. M., TIWARI, A., CHAMBERS,

- T. M., NEWTON, J. R. & ELTON, D. M. 2009. Antigenic and genetic variations in European and North American equine influenza virus strains (H3N8) isolated from 2006 to 2007. *Veterinary Microbiology*, 138, 41-52.
- BUI, M., WHITTAKER, G. & HELENIUS, A. 1996. Effect of M1 protein and low pH on nuclear transport of influenza virus ribonucleoproteins. *Journal of Virology*, 70, 8391-8401.
- BULLOUGH, P. A., HUGHSON, F. M., SKEHEL, J. J. & WILEY, D. C. 1994. Structure of influenza haemagglutinin at the pH of membrane fusion. *Nature*, 371, 37-43.
- BUTLER, D. 2006. Thai dogs carry bird-flu virus, but will they spread it? *Nature*, 439, 773-773.
- BYRD-LEOTIS, L., CUMMINGS, R. D. & STEINHAEUER, D. A. 2017. The Interplay between the Host Receptor and Influenza Virus Hemagglutinin and Neuraminidase. *International journal of molecular sciences*, 18, 1541.
- CAPELLINI, F. M., VENCIA, W., AMADORI, M., MIGNONE, G., PARISI, E., MASIELLO, L., VIVALDI, B., FERRARI, A. & RAZZUOLI, E. 2020. Characterization of MDCK cells and evaluation of their ability to respond to infectious and non-infectious stressors. *Cytotechnology*, 72, 97-109.
- CARNELL, G. W., FERRARA, F., GREHAN, K., THOMPSON, C. P. & TEMPERTON, N. J. 2015. Pseudotype-based neutralization assays for influenza: a systematic analysis. *Frontiers in immunology*, 6, 161-161.

- CAULDWELL, A. V., LONG, J. S., MONCORGÉ, O. & BARCLAY, W. S. 2014. Viral determinants of influenza A virus host range. *Journal of General Virology*, 95, 1193-1210.
- CDC. 2024. *CDC A (H5N1) Bird Flu Response Update June 28, 2024* [Online]. Available: <https://www.cdc.gov/bird-flu/spotlights/h5n1-response-06282024.html> [Accessed 03/07/2024 2024].
- CHAKRABARTI, A., BANERJEE, S., FRANCHI, L., LOO, Y.-M., GALE, M., NÚÑEZ, G. & SILVERMAN, ROBERT H. 2015. RNase L Activates the NLRP3 Inflammasome during Viral Infections. *Cell Host & Microbe*, 17, 466-477.
- CHAMBERS, B. S., LI, Y., HODINKA, R. L. & HENSLEY, S. E. 2014. Recent H3N2 influenza virus clinical isolates rapidly acquire hemagglutinin or neuraminidase mutations when propagated for antigenic analyses. *J Virol*, 88, 10986-9.
- CHAMBERS, T. M. 2020a. A Brief Introduction to Equine Influenza and Equine Influenza Viruses. In: SPACKMAN, E. (ed.) *Animal Influenza Virus: Methods and Protocols*. New York, NY: Springer US.
- CHAMBERS, T. M. 2020b. Equine Influenza. *Cold Spring Harbor Perspectives in Medicine*.
- CHAMBERS, T. M., BALASURIYA, U. B. R., REEDY, S. E. & TIWARI, A. 2013. Replication of avian influenza viruses in equine tracheal epithelium but not in horses. *Influenza and Other Respiratory Viruses*, 7, 90-93.

CHAMBERS, T. M. & REEDY, S. E. 2014. Equine Influenza Culture Methods. *In*: SPACKMAN, E. (ed.) *Animal Influenza Virus*. New York, NY: Springer New York.

CHAN, J. F.-W., TO, K. K.-W., TSE, H., JIN, D.-Y. & YUEN, K.-Y. 2013a. Interspecies transmission and emergence of novel viruses: lessons from bats and birds. *Trends in microbiology*, 21, 544-555.

CHAN, R. W., CHAN, M. C., NICHOLLS, J. M. & MALIK PEIRIS, J. S. 2013b. Use of ex vivo and in vitro cultures of the human respiratory tract to study the tropism and host responses of highly pathogenic avian influenza A (H5N1) and other influenza viruses. *Virus Res*, 178, 133-45.

CHEN, I. C., CHIU, Y. K., YU, C. M., LEE, C. C., TUNG, C. P., TSOU, Y. L., HUANG, Y. J., LIN, C. L., CHEN, H. S., WANG, A. H. & YANG, A. S. 2017. High throughput discovery of influenza virus neutralizing antibodies from phage-displayed synthetic antibody libraries. *Sci Rep*, 7, 14455.

CHEN, M., LYU, Y., WU, F., ZHANG, Y., LI, H., WANG, R., LIU, Y., YANG, X., ZHOU, L., ZHANG, M., TONG, Q., SUN, H., PU, J., LIU, J. & SUN, Y. 2023. Increased public health threat of avian-origin H3N2 influenza virus caused by its evolution in dogs. *eLife*, 12, e83470.

CHEN, R. & HOLMES, E. C. 2008. The Evolutionary Dynamics of Human Influenza B Virus. *Journal of Molecular Evolution*, 66, 655.

CHEN, Y., ZHONG, G., WANG, G., DENG, G., LI, Y., SHI, J., ZHANG, Z., GUAN, Y., JIANG, Y., BU, Z., KAWAOKA, Y. & CHEN, H. 2010. Dogs are highly susceptible to H5N1 avian influenza virus. *Virology*, 405, 15-9.

CHIBA, S., KONG, H., NEUMANN, G. & KAWAOKA, Y. 2023. Influenza H3 hemagglutinin vaccine with scrambled immunodominant epitopes elicits antibodies directed toward immunosubdominant head epitopes. *mBio*, 14, e00622-23.

CHOU, Y.-Y., HEATON, N. S., GAO, Q., PALESE, P., SINGER, R. & LIONNET, T. 2013. Colocalization of Different Influenza Viral RNA Segments in the Cytoplasm before Viral Budding as Shown by Single-molecule Sensitivity FISH Analysis. *PLOS Pathogens*, 9, e1003358.

CHOUDHURY, N. R., TRUS, I., HEIKEL, G., WOLCZYK, M., SZYMANSKI, J., BOLEMBACH, A., DOS SANTOS PINTO, R. M., SMITH, N., TRUBITSYNA, M., GAUNT, E., DIGARD, P. & MICHLEWSKI, G. 2022. TRIM25 inhibits influenza A virus infection, destabilizes viral mRNA, but is redundant for activating the RIG-I pathway. *Nucleic Acids Res*, 50, 7097-7114.

CHUTIWITOONCHAI, N. & AIDA, Y. 2016. NXT1, a Novel Influenza A NP Binding Protein, Promotes the Nuclear Export of NP via a CRM1-Dependent Pathway. *Viruses*, 8, 209.

COCH, C., STÜMPEL, J. P., LILIEN-WALDAU, V., WOHLLEBER, D., KÜMMERER, B. M., BEKEREDJIAN-DING, I., KOCHS, G., GARBI, N., HERBERHOLD, S., SCHUBERTH-WAGNER, C., LUDWIG, J., BARCHET, W., SCHLEE, M., HOERAUF, A., BOOTZ, F., STAEHEL, P., HARTMANN, G. & HARTMANN, E. 2017. RIG-I Activation Protects and Rescues from Lethal Influenza Virus Infection and Bacterial Superinfection. *Mol Ther*, 25, 2093-2103.

COLLINS, P. J., VACHIERI, S. G., HAIRE, L. F., OGRODOWICZ, R. W., MARTIN, S. R., WALKER, P. A., XIONG, X., GAMBLIN, S. J. & SKEHEL, J. J. 2014. Recent evolution of equine influenza and the origin of canine influenza. *Proceedings of the National Academy of Sciences*, 111, 11175-11180.

CONNOR, R. J., KAWAOKA, Y., WEBSTER, R. G. & PAULSON, J. C. 1994. Receptor Specificity in Human, Avian, and Equine H2 and H3 Influenza Virus Isolates. *Virology*, 205, 17-23.

CRAWFORD, P. C., DUBOVI, E. J., CASTLEMAN, W. L., STEPHENSON, I., GIBBS, E. P., CHEN, L., SMITH, C., HILL, R. C., FERRO, P., POMPEY, J., BRIGHT, R. A., MEDINA, M. J., JOHNSON, C. M., OLSEN, C. W., COX, N. J., KLIMOV, A. I., KATZ, J. M. & DONIS, R. O. 2005. Transmission of equine influenza virus to dogs. *Science*, 310, 482-5.

CRISPELL, J. 2018. *Investigating equine host barriers to infection with influenza A viruses.*, University of Glasgow.

CROS, J. F. & PALESE, P. 2003. Trafficking of viral genomic RNA into and out of the nucleus: influenza, Thogoto and Borna disease viruses. *Virus Research*, 95, 3-12.

CULLINANE, A. & NEWTON, J. R. 2013. Equine influenza—A global perspective. *Veterinary Microbiology*, 167, 205-214.

DAHODWALA, H. & LEE, K. H. 2019. The fickle CHO: a review of the causes, implications, and potential alleviation of the CHO cell line instability problem. *Curr Opin Biotechnol*, 60, 128-137.

DALY, J., WU, G., NORMAN, F., PRESTON, T., KYDD, J., JENGARN, J., SCOTT, S., TEMPERTON, N., RASH, A. & ELTON, D. 2021. Limited evidence for exposure of UK horses to influenza D virus. *Equine Vet. J.*, 53, 10.1111.

DALY, J. M., BLUNDEN, A. S., MACRAE, S., MILLER, J., BOWMAN, S. J., KOLODZIEJEK, J., NOWOTNY, N. & SMITH, K. C. 2008. Transmission of equine influenza virus to English foxhounds. *Emerg Infect Dis*, 14, 461-4.

DALY, J. M., LAI, A. C. K., BINNS, M. M., CHAMBERS, T. M., BARRANDEGUY, M. & MUMFORD, J. A. 1996. Antigenic and genetic evolution of equine H3N8 influenza A viruses. *Journal of General Virology*, 77, 661-671.

DALY, J. M., LIM, T. S. & GOUGH, K. C. 2023. Therapeutic Phage Display-Derived Single-Domain Antibodies for Pandemic Preparedness. *Antibodies (Basel)*, 12.

DALY, J. M., WHITWELL, K. E., MILLER, J., DOWD, G., CARDWELL, J. M. & SMITH, K. C. 2006. Investigation of equine influenza cases exhibiting neurological disease: coincidence or association? *J Comp Pathol*, 134, 231-5.

DALZIEL, B. D., HUANG, K., GEOGHEGAN, J. L., ARINAMINPATHY, N., DUBOVI, E. J., GRENFELL, B. T., ELLNER, S. P., HOLMES, E. C. & PARRISH, C. R. 2014. Contact Heterogeneity, Rather Than Transmission Efficiency, Limits the Emergence and Spread of Canine Influenza Virus. *PLOS Pathogens*, 10, e1004455.

DAVIS, J., GARNER, M. G. & EAST, I. J. 2009. Analysis of Local Spread of Equine Influenza in the Park Ridge Region of Queensland. *Transboundary and Emerging Diseases*, 56, 31-38.

DAWOOD, F. S., JAIN, S., FINELLI, L., SHAW, M. W., LINDSTROM, S., GARTEN, R. J., GUBAREVA, L. V., XU, X., BRIDGES, C. B. & UYEKI, T. M. 2009. Emergence of a novel swine-origin influenza A (H1N1) virus in humans. *N Engl J Med*, 360, 2605-15.

DE VLUGT, C., SIKORA, D. & PELCHAT, M. 2018. Insight into Influenza: A Virus Cap-Snatching. *Viruses*, 10, 641.

DE VRIES, E., DU, W., GUO, H. & DE HAAN, C. A. M. 2020. Influenza A Virus Hemagglutinin-Neuraminidase-Receptor Balance: Preserving Virus Motility. *Trends Microbiol*, 28, 57-67.

DEBERGE, M. P., ELY, K. H. & ENELOW, R. I. 2014. Soluble, but not transmembrane, TNF- α is required during influenza infection to limit the magnitude of immune responses and the extent of immunopathology. *J Immunol*, 192, 5839-51.

DENNING, W., DAS, S., GUO, S., XU, J., KAPPES, J. C. & HEL, Z. 2013. Optimization of the transductional efficiency of lentiviral vectors: effect of sera and polycations. *Mol Biotechnol*, 53, 308-14.

DIALLO, A. A., SOULEY, M. M., ISSA IBRAHIM, A., ALASSANE, A., ISSA, R., GAGARA, H., YAOU, B., ISSIAKOU, A., DIOP, M., BA DIOUF, R. O., LO, F. T., LO, M. M., BAKHOUM, T., SYLLA, M., SECK, M. T., MESEKO, C., SHITTU, I., CULLINANE, A., SETTYPALLI, T. B. K., LAMIEN, C. E., DUNDON, W. G. & CATTOLI, G. 2021. Transboundary spread of equine influenza viruses (H3N8) in West and

Central Africa: Molecular characterization of identified viruses during outbreaks in Niger and Senegal, in 2019. *Transbound Emerg Dis*, 68, 1253-1262.

DIONÍSIO, L., MEDEIROS, F., PEQUITO, M. & FAUSTINO-ROCHA, A. I. 2021. Equine influenza: a comprehensive review from etiology to treatment. *Anim Health Res Rev*, 22, 56-71.

DISSANAYAKE, T. K., SCHäUBLE, S., MIRHAKKAK, M. H., WU, W. L., NG, A. C., YIP, C. C. Y., LÓPEZ, A. G., WOLF, T., YEUNG, M. L., CHAN, K. H., YUEN, K. Y., PANAGIOTOU, G. & TO, K. K. 2020. Comparative Transcriptomic Analysis of Rhinovirus and Influenza Virus Infection. *Front Microbiol*, 11, 1580.

DONG, J., HUANG, B., JIA, Z., WANG, B., GALLOLU KANKANAMALAGE, S., TITONG, A. & LIU, Y. 2020. Development of multi-specific humanized llama antibodies blocking SARS-CoV-2/ACE2 interaction with high affinity and avidity. *Emerg Microbes Infect*, 9, 1034-1036.

DOU, D., REVOL, R., ÖSTBYE, H., WANG, H. & DANIELS, R. 2018. Influenza A Virus Cell Entry, Replication, Virion Assembly and Movement. *Frontiers in Immunology*, 9.

DOUD, M. B., LEE, J. M. & BLOOM, J. D. 2018. How single mutations affect viral escape from broad and narrow antibodies to H1 influenza hemagglutinin. *Nature Communications*, 9, 1386.

DRISKELL, E. 2014. Influenza in Animals. In: MCMANUS, L. M. & MITCHELL, R. N. (eds.) *Pathobiology of Human Disease*. San Diego: Academic Press.

DU, W. J., WOLFERT, M. A., PEETERS, B., VAN KUPPEVELD, F. J. M., BOONS, G. J., DE VRIES, E. & DE HAAN, C. A. M. 2020. Mutation of the second sialic acid-binding site of influenza A virus neuraminidase drives compensatory mutations in hemagglutinin. *Plos Pathogens*, 16, 20.

DUBOVI, E. J. & NJAA, B. L. 2008. Canine Influenza. *Veterinary Clinics of North America: Small Animal Practice*, 38, 827-835.

EASTHOPE, E. 2023. Principle and applications of label-free detection. Available: <https://www.biocompare.com/Bench-Tips/597403-Principles-Applications-of-Label-Free-Detection/> [Accessed 26/07/24].

EISEN, M. B., SABESAN, S., SKEHEL, J. J. & WILEY, D. C. 1997. Binding of the Influenza A Virus to Cell-Surface Receptors: Structures of Five Hemagglutinin–Sialyloligosaccharide Complexes Determined by X-Ray Crystallography. *Virology*, 232, 19-31.

EISFELD, A. J., NEUMANN, G. & KAWAOKA, Y. 2015a. At the centre: influenza A virus ribonucleoproteins. *Nature Reviews Microbiology*, 13, 28-41.

EISFELD, A. J., NEUMANN, G. & KAWAOKA, Y. 2015b. At the centre: influenza A virus ribonucleoproteins. *Nature reviews. Microbiology*, 13, 28-41.

ELTON, D., SIMPSON-HOLLEY, M., ARCHER, K., MEDCALF, L., HALLAM, R., MCCAULEY, J. & DIGARD, P. 2001. Interaction of the Influenza Virus Nucleoprotein with the Cellular CRM1-Mediated Nuclear Export Pathway. *Journal of Virology*, 75, 408-419.

ERSTER, O. & LISCOVITCH, M. 2010. A Modified Inverse PCR Procedure for Insertion, Deletion, or Replacement of a DNA Fragment in a Target Sequence and Its Application in the Ligand Interaction Scan Method for Generation of Ligand-Regulated Proteins. *In*: BRAMAN, J. (ed.) *In Vitro Mutagenesis Protocols: Third Edition*. Totowa, NJ: Humana Press.

FENG, K. H., GONZALEZ, G., DENG, L., YU, H., TSE, V. L., HUANG, L., HUANG, K., WASIK, B. R., ZHOU, B., WENTWORTH, D. E., HOLMES, E. C., CHEN, X., VARKI, A., MURCIA, P. R. & PARRISH, C. R. 2015. Equine and Canine Influenza H3N8 Viruses Show Minimal Biological Differences Despite Phylogenetic Divergence. *Journal of virology*, 89, 6860-6873.

FEREIDOUNI, S., STARICK, E., KARAMENDIN, K., GENOVA, C. D., SCOTT, S. D., KHAN, Y., HARDER, T. & KYDYRMANOV, A. 2023. Genetic characterization of a new candidate hemagglutinin subtype of influenza A viruses. *Emerg Microbes Infect*, 12, 2225645.

FITCH, W. M., LEITER, J. M., LI, X. Q. & PALESE, P. 1991. Positive Darwinian evolution in human influenza A viruses. *Proceedings of the National Academy of Sciences*, 88, 4270-4274.

FODOR, E., DEVENISH, L., ENGELHARDT, O. G., PALESE, P., BROWNLEE, G. G. & GARCÍA-SASTRE, A. 1999. Rescue of Influenza A Virus from Recombinant DNA. *Journal of Virology*, 73, 9679-9682.

FONI, E., CHIAPPONI, C., BAIONI, L., ZANNI, I., MERENDA, M., ROSIGNOLI, C., KYRIAKIS, C. S., LUINI, M. V., MANDOLA, M. L., BOLZONI, L., NIGRELLI, A. D. & FACCINI, S. 2017. Influenza D in

Italy: towards a better understanding of an emerging viral infection in swine. *Scientific Reports*, 7, 11660.

FUJII, Y., GOTO, H., WATANABE, T., YOSHIDA, T. & KAWAOKA, Y. 2003. Selective incorporation of influenza virus RNA segments into virions. *Proceedings of the National Academy of Sciences of the United States of America*, 100, 2002-2007.

FUJIOKA, Y., KASHIWAGI, S., YOSHIDA, A., SATOH, A. O., FUJIOKA, M., AMANO, M., YAMAUCHI, Y. & OHBA, Y. 2022. A method for the generation of pseudovirus particles bearing SARS coronavirus spike protein in high yields. *Cell Struct Funct*, 47, 43-53.

GAMBARYAN, A., WEBSTER, R. & MATROSOVICH, M. 2002. Differences between influenza virus receptors on target cells of duck and chicken. *Archives of Virology*, 147, 1197-1208.

GAMBARYAN, A. S., MATROSOVICH, T. Y., PHILIPP, J., MUNSTER, V. J., FOUCHIER, R. A. M., CATTOLI, G., CAPUA, I., KRAUSS, S. L., WEBSTER, R. G., BANKS, J., BOVIN, N. V., KLENK, H. D. & MATROSOVICH, M. N. 2012. Receptor-Binding Profiles of H7 Subtype Influenza Viruses in Different Host Species. *Journal of Virology*, 86, 4370-4379.

GANGULY, M., YEOLEKAR, L., TYAGI, P., SAGAR, U., NARALE, S., ANASPURE, Y., TUPE, S., WADKAR, K., INGLE, N., DHERE, R., SCORZA, F. B. & MAHMOOD, K. 2020. Evaluation of manufacturing feasibility and safety of an MDCK cell-based live attenuated influenza vaccine (LAIV) platform. *Vaccine*, 38, 8379-8386.

GARCÍA-SASTRE, A. 2006. Antiviral response in pandemic influenza viruses. *Emerg Infect Dis*, 12, 44-7.

GEIGER, T., WEHNER, A., SCHAAB, C., COX, J. & MANN, M. 2012. Comparative proteomic analysis of eleven common cell lines reveals ubiquitous but varying expression of most proteins. *Mol Cell Proteomics*, 11, M111.014050.

GENZEL, Y., BEHRENDT, I., KÖNIG, S., SANN, H. & REICHL, U. 2004. Metabolism of MDCK cells during cell growth and influenza virus production in large-scale microcarrier culture. *Vaccine*, 22, 2202-8.

GIRARD, M. P., TAM, J. S., ASSOSSOU, O. M. & KIENY, M. P. 2010. The 2009 A (H1N1) influenza virus pandemic: A review. *Vaccine*, 28, 4895-4902.

GONZALEZ, G., MARSHALL, J., MORRELL, J., ROBB, D., MCCAULEY, J., PEREZ, D., PARRISH, C. & MURCIA, P. 2014. Infection and Pathogenesis of Canine, Equine, and Human Influenza Viruses in Canine Tracheas. *Journal of Virology*, 88, 9208 - 9219.

GORAYA, M. U., WANG, S., MUNIR, M. & CHEN, J.-L. 2015. Induction of innate immunity and its perturbation by influenza viruses. *Protein & Cell*, 6, 712-721.

GOSTIC, K. M., AMBROSE, M., WOROBEY, M. & LLOYD-SMITH, J. O. 2016. Potent protection against H5N1 and H7N9 influenza via childhood hemagglutinin imprinting. *Science*, 354, 722-726.

GOVORKOVA, E. A., LENEVA, I. A., GOLOUBEVA, O. G., BUSH, K. & WEBSTER, R. G. 2001. Comparison of efficacies of RWJ-270201, zanamivir, and oseltamivir against H5N1, H9N2, and other avian

influenza viruses. *Antimicrobial Agents and Chemotherapy*, 45, 2723-2732.

GRAHAM, F. L., SMILEY, J., RUSSELL, W. C. & NAIRN, R. 1977. Characteristics of a human cell line transformed by DNA from human adenovirus type 5. *J Gen Virol*, 36, 59-74.

GRONE, A., FONFARA, S., MARKUS, S. & BAUMGARTNER, W. 1999. RT-PCR Amplification of Various Canine Cytokines and Socalled House-keeping Genes in a Species-Specific Macrophage Cell Line (DH82) and Canine Peripheral Blood Leukocytes. *Journal of Veterinary Medicine, Series B*, 46, 301-310.

GUAN, M., OLIVIER, A. K., LU, X., EPPERSON, W., ZHANG, X., ZHONG, L., WATERS, K., MAMALIGER, N., LI, L., WEN, F., TAO, Y. J., DELIBERTO, T. J. & WAN, X. F. 2022. The Sialyl Lewis X Glycan Receptor Facilitates Infection of Subtype H7 Avian Influenza A Viruses. *J Virol*, 96, e0134422.

GUO, D., ZHANG, L., WANG, X., ZHENG, J. & LIN, S. 2022. Establishment methods and research progress of livestock and poultry immortalized cell lines: A review. *Frontiers in Veterinary Science*, 9.

GUO, F., ROY, A., WANG, R., YANG, J., ZHANG, Z., LUO, W., SHEN, X., CHEN, R.-A., IRWIN, D. M. & SHEN, Y. 2021. Host Adaptive Evolution of Avian-Origin H3N2 Canine Influenza Virus. *Frontiers in Microbiology*, 12.

GUO, Y., RUMSCHLAG-BOOMS, E., WANG, J., XIAO, H., YU, J., WANG, J., GUO, L., GAO, G. F., CAO, Y., CAFFREY, M. & RONG, L.

2009. Analysis of hemagglutinin-mediated entry tropism of H5N1 avian influenza. *Virology journal*, 6, 39-39.

GUO, Y., WANG, M., KAWAOKA, Y., GORMAN, O., ITO, T., SAITO, T. & WEBSTER, R. G. 1992. Characterization of a new avian-like influenza A virus from horses in China. *Virology*, 188, 245-55.

GUO, Y., WANG, M., ZHENG, G. S., LI, W. K., KAWAOKA, Y. & WEBSTER, R. G. 1995. Seroepidemiological and molecular evidence for the presence of two H3N8 equine influenza viruses in China in 1993-94. *J Gen Virol*, 76 (Pt 8), 2009-14.

GUTHRIE, A. J., STEVENS, K. B. & BOSMAN, P. P. 1999. The circumstances surrounding the outbreak and spread of equine influenza in South Africa. *Revue Scientifique et Technique (International Office of Epizootics)*, 18, 179-185.

HAMERS-CASTERMAN, C., ATARHOUCHE, T., MUYLDERMANS, S., ROBINSON, G., HAMMERS, C., SONGA, E. B., BENDAHMAN, N. & HAMMERS, R. 1993. Naturally occurring antibodies devoid of light chains. *Nature*, 363, 446-448.

HAMILTON, B. S., WHITTAKER, G. R. & DANIEL, S. 2012. Influenza Virus-Mediated Membrane Fusion: Determinants of Hemagglutinin Fusogenic Activity and Experimental Approaches for Assessing Virus Fusion. *Viruses*, 4, 1144-1168.

HARE, D., COLLINS, S., CUDDINGTON, B. & MOSSMAN, K. 2016. The Importance of Physiologically Relevant Cell Lines for Studying Virus-Host Interactions. *Viruses*, 8.

HATA, N., SATO, M., TAKAOKA, A., ASAGIRI, M., TANAKA, N. & TANIGUCHI, T. 2001. Constitutive IFN- α / β signal for efficient IFN- α / β gene induction by virus. *Biochem Biophys Res Commun*, 285, 518-25.

HAYWARD, J. J., DUBOVI, E. J., SCARLETT, J. M., JANECKO, S., HOLMES, E. C. & PARRISH, C. R. 2010. Microevolution of canine influenza virus in shelters and its molecular epidemiology in the United States. *J Virol*, 84, 12636-45.

HE, W., LI, G., WANG, R., SHI, W., LI, K., WANG, S., LAI, A. & SU, S. 2019. Host-range shift of H3N8 canine influenza virus: a phylodynamic analysis of its origin and adaptation from equine to canine host. *Veterinary Research*, 50, 87.

HEINRICH, F., CONTIOSO, V. B., STEIN, V. M., CARLSON, R., TIPOLD, A., ULRICH, R., PUFF, C., BAUMGÄRTNER, W. & SPITZBARTH, I. 2015. Passage-dependent morphological and phenotypical changes of a canine histiocytic sarcoma cell line (DH82 cells). *Veterinary Immunology and Immunopathology*, 163, 86-92.

HEROLD, S., BECKER, C., RIDGE, K. M. & BUDINGER, G. R. S. 2015. Influenza virus-induced lung injury: pathogenesis and implications for treatment. *European Respiratory Journal*, 45, 1463-1478.

HERRLER, G. & KLENK, H. D. 1991. Structure and function of the HEF glycoprotein of influenza C virus. *Advances in virus research*, 40, 213-234.

- HINES, R. & MAURY, W. 2001. DH82 cells: a macrophage cell line for the replication and study of equine infectious anemia virus. *Journal of Virological Methods*, 95, 47-56.
- HOFFMANN, E., NEUMANN, G., HOBOM, G., WEBSTER, R. G. & KAWAOKA, Y. 2000a. "Ambisense" Approach for the Generation of Influenza A Virus: vRNA and mRNA Synthesis from One Template. *Virology*, 267, 310-317.
- HOFFMANN, E., NEUMANN, G., KAWAOKA, Y., HOBOM, G. & WEBSTER, R. G. 2000b. A DNA transfection system for generation of influenza A virus from eight plasmids. *Proc Natl Acad Sci U S A*, 97, 6108-13.
- HOWERTH, E. W., PARLAVANTZAS, G. S. & STALLKNECHT, D. E. 2004. Replication of epizootic haemorrhagic disease and bluetongue viruses in DH82 cells. *Vet Ital*, 40, 520-4.
- HULTBERG, A., TEMPERTON, N. J., ROSSEELS, V., KOENDERS, M., GONZALEZ-PAJUELO, M., SCHEPENS, B., IBAÑEZ, L. I., VANLANDSCHOOT, P., SCHILLEMANS, J., SAUNDERS, M., WEISS, R. A., SAELENS, X., MELERO, J. A., VERRIPS, C. T., VAN GUCHT, S. & DE HAARD, H. J. 2011. Llama-Derived Single Domain Antibodies to Build Multivalent, Superpotent and Broadened Neutralizing Anti-Viral Molecules. *PLOS ONE*, 6, e17665.
- HUSSAIN, M., GALVIN, H., HAW, T., NUTSFORD, A. & HUSAIN, M. 2017. Drug resistance in influenza A virus: the epidemiology and management. *Infection and Drug Resistance*, 10, 121-134.

ILOBI, C. P., HENFREY, R., ROBERTSON, J. S., MUMFORD, J. A., ERASMUS, B. J. & WOOD, J. M. 1994. Antigenic and molecular characterization of host cell-mediated variants of equine H3N8 influenza viruses. *Journal of General Virology*, 75, 669-673.

ILOBI, C. P., NICOLSON, C., TAYLOR, J., MUMFORD, J. A., WOOD, J. M. & ROBERTSON, J. S. 1998. Direct sequencing of the HA gene of clinical equine H3N8 influenza virus and comparison with laboratory derived viruses. *Arch Virol*, 143, 891-901.

IRFAN MAQSOOD, M., MATIN, M. M., BAHRAMI, A. R. & GHASROLDASHT, M. M. 2013. Immortality of cell lines: challenges and advantages of establishment. *Cell Biology International*, 37, 1038-1045.

ITO, T., COUCEIRO, J. N., KELM, S., BAUM, L. G., KRAUSS, S., CASTRUCCI, M. R., DONATELLI, I., KIDA, H., PAULSON, J. C., WEBSTER, R. G. & KAWAOKA, Y. 1998. Molecular basis for the generation in pigs of influenza A viruses with pandemic potential. *Journal of virology*, 72, 7367-7373.

ITO, T., KAWAOKA, Y., OHIRA, M., TAKAKUWA, H., YASUDA, J., KIDA, H. & OTSUKI, K. 1999. Replacement of internal protein genes, with the exception of the matrix, in equine 1 viruses by equine 2 influenza virus genes during evolution in nature. *J Vet Med Sci*, 61, 987-9.

ITO, T., SUZUKI, Y., TAKADA, A., KAWAMOTO, A., OTSUKI, K., MASUDA, H., YAMADA, M., SUZUKI, T., KIDA, H. & KAWAOKA, Y. 1997. Differences in sialic acid-galactose linkages in the chicken egg

amnion and allantois influence human influenza virus receptor specificity and variant selection. *J Virol*, 71, 3357-62.

IWASAKI, A. & PILLAI, P. S. 2014. Innate immunity to influenza virus infection. *Nature reviews. Immunology*, 14, 315-328.

JANEWAY, C. A. J., TRAVERS, P., WALPORT, M. & SCLOMCHIK, M. J. 2001a. Immunobiology: The Immune System in Health and Disease. *T cell-mediated cytotoxicity*. 5th ed. New York: Garland Science.

JANEWAY, C. A. J., TRAVERS, P., WALPORT, M. & SCLOMCHIK, M. J. 2001b. Immunobiology: The Immune System in Health and Disease. *Antigen Recognition by T cells*. 5th ed. New York: Garland Science.

JANKE, B. H. 2014. Influenza A Virus Infections in Swine: Pathogenesis and Diagnosis. *Veterinary Pathology*, 51, 410-426.

JENKINSON, E. J., JENKINSON, W. E., ROSSI, S. W. & ANDERSON, G. 2006. The thymus and T-cell commitment: the right niche for Notch? *Nat Rev Immunol*, 6, 551-5.

JEOUNG, H.-Y., LIM, S.-I., SHIN, B.-H., LIM, J.-A., SONG, J.-Y., SONG, D.-S., KANG, B.-K., MOON, H.-J. & AN, D.-J. 2013. A novel canine influenza H3N2 virus isolated from cats in an animal shelter. *Veterinary microbiology*, 165, 281-286.

JIMENEZ-BLUHM, P., SEPULVEDA, A., BAUMBERGER, C., DI PILLO, F., RUIZ, S., SALAZAR, C., MARAMBIO, V., BERRIOS, F., GALDAMES, P., AMARO, A., TAPIA, D., SHARP, B., FREIDEN, P., MELIOPOULOS, V., SCHULTZ-CHERRY, S. & HAMILTON-WEST, C. 2021. Evidence of influenza infection in dogs and cats in central Chile. *Preventive Veterinary Medicine*, 191, 105349.

JUNKER, F., GORDON, J. & QURESHI, O. 2020. Fc Gamma Receptors and Their Role in Antigen Uptake, Presentation, and T Cell Activation. *Frontiers in Immunology*, 11.

KAMIKI, H., MURAKAMI, S., NISHIKAZE, T., HIONO, T., IGARASHI, M., FURUSE, Y., MATSUGO, H., ISHIDA, H., KATAYAMA, M., SEKINE, W., MURAKI, Y., TAKAHASHI, M., TAKENAKA-UEMA, A. & HORIMOTO, T. 2022. Influenza A Virus Agnostic Receptor Tropism Revealed Using a Novel Biological System with Terminal Sialic Acid Knockout Cells. *J Virol*, 96, e0041622.

KANG, Y. M., KIM, H. M., KU, K. B., PARK, E. H., YUM, J. & SEO, S. H. 2013. H3N2 canine influenza virus causes severe morbidity in dogs with induction of genes related to inflammation and apoptosis. *Veterinary Research*, 44, 92.

KAPUST, R. B. & WAUGH, D. S. 1999. Escherichia coli maltose-binding protein is uncommonly effective at promoting the solubility of polypeptides to which it is fused. *Protein Science*, 8, 1668-1674.

KARAKUS, U., MENA, I., KOTTUR, J., EL ZAHED, S. S., SEOANE, R., YILDIZ, S., CHEN, L., PLANCARTE, M., LINDSAY, L., HALPIN, R., STOCKWELL, T. B., WENTWORTH, D. E., BOONS, G.-J., KRAMMER, F., STERTZ, S., BOYCE, W., DE VRIES, R. P., AGGARWAL, A. K. & GARCÍA-SASTRE, A. 2024. H19 influenza A virus exhibits species-specific MHC class II receptor usage. *Cell Host & Microbe*.

KARAKUS, U., THAMAMONGOOD, T., CIMINSKI, K., RAN, W., GÜNTHER, S. C., POHL, M. O., ELETTO, D., JENEY, C., HOFFMANN, D., REICHE, S., SCHINKÖTHE, J., ULRICH, R., WIENER, J., HAYES,

M. G. B., CHANG, M. W., HUNZIKER, A., YÁNGÜEZ, E., AYDILLO, T., KRAMMER, F., ODERBOLZ, J., MEIER, M., OXENIUS, A., HALENIUS, A., ZIMMER, G., BENNER, C., HALE, B. G., GARCÍA-SASTRE, A., BEER, M., SCHWEMMLE, M. & STERTZ, S. 2019. MHC class II proteins mediate cross-species entry of bat influenza viruses. *Nature*, 567, 109-112.

KAUR, G. & DUFOUR, J. M. 2012. Cell lines. *Spermatogenesis*, 2, 1-5.

KHERSONSKY, O., GOLDSMITH, M., ZARETSKY, I., HAMER-ROGOTNER, S., DYM, O., UNGER, T., YONA, M., FRIDMANN-SIRKIS, Y. & FLEISHMAN, S. J. 2023. Stable Mammalian Serum Albumins Designed for Bacterial Expression. *Journal of Molecular Biology*, 435, 168191.

KIM, D.-H., PARK, B.-J., AHN, H.-S., GO, H.-J., KIM, D.-Y., KIM, J.-H., LEE, J.-B., PARK, S.-Y., SONG, C.-S., LEE, S.-W. & CHOI, I.-S. 2021. Canine interferon lambda 3 expressed using an adenoviral vector effectively induces antiviral activity against canine influenza virus. *Virus Research*, 296, 198342.

KIM, D. E., CHIVIAN, D. & BAKER, D. 2004. Protein structure prediction and analysis using the Robetta server. *Nucleic Acids Research*, 32, W526-W531.

KIM, H., WEBSTER, R. G. & WEBBY, R. 2018a. Influenza Virus: Dealing with a Drifting and Shifting Pathogen. *Viral Immunology*, 31, 174-183.

KIM, H., WEBSTER, R. G. & WEBBY, R. J. 2018b. Influenza Virus: Dealing with a Drifting and Shifting Pathogen. *Viral Immunology*, 31, 174-183.

KINSLEY, R. 2017. *Development of lentiviral pseudotypes for surveillance studies on animal influenza viruses*. PhD, University of Kent.

KLIVLEYEVA, N. G., GLEBOVA, T. I., SHAMENOVA, M. G. & SAKTAGANOV, N. T. 2022. Influenza A viruses circulating in dogs: A review of the scientific literature. *Open veterinary journal*, 12, 676-687.

KOELLE, K., COBEY, S., GRENFELL, B. & PASCUAL, M. 2006. Epochal Evolution Shapes the Phylodynamics of Interpandemic Influenza A (H3N2) in Humans. *Science*, 314, 1898-1903.

KRUG, R. M. 1981. Priming of influenza viral RNA transcription by capped heterologous RNAs. *Curr Top Microbiol Immunol*, 93, 125-49.

KUCHIPUDI, S. V., NELLI, R., WHITE, G. A., BAIN, M., CHANG, K. C. & DUNHAM, S. 2009. Differences in influenza virus receptors in chickens and ducks: Implications for interspecies transmission. *Journal of molecular and genetic medicine : an international journal of biomedical research*, 3, 143-151.

KUMAR, N., BERA, B. C., GREENBAUM, B. D., BHATIA, S., SOOD, R., SELVARAJ, P., ANAND, T., TRIPATHI, B. N. & VIRMANI, N. 2016. Revelation of Influencing Factors in Overall Codon Usage Bias of Equine Influenza Viruses. *PLOS ONE*, 11, e0154376.

LAKADAMYALI, M., RUST, M. J., BABCOCK, H. P. & ZHUANG, X. 2003. Visualizing infection of individual influenza viruses. *Proceedings of the National Academy of Sciences*, 100, 9280-9285.

LAPUENTE, D., STORCKSDIECK GENANNT BONSMANN, M., MAASKE, A., STAB, V., HEINECKE, V., WATZSTEDT, K., HEß, R., WESTENDORF, A. M., BAYER, W., EHRHARDT, C. & TENBUSCH, M. 2018. IL-1 β as mucosal vaccine adjuvant: the specific induction of tissue-resident memory T cells improves the heterosubtypic immunity against influenza A viruses. *Mucosal Immunology*, 11, 1265-1278.

LATTIMER, J., ROBERTS, H., BARNARD, M., PATERSON, A., BELL, I., HEPPLER, R., HOLLAND, S. & GEORGE, A. 2020. Investigating an outbreak of equine viral arteritis at two connected premises. *Veterinary Record*, 187, e113-e113.

LAZNIEWSKI, M., DAWSON, W. K., SZCZEPINSKA, T. & PLEWCZYNSKI, D. 2018. The structural variability of the influenza A hemagglutinin receptor-binding site. *Briefings in functional genomics*, 17, 415-427.

LE DOUX, J. M., LANDAZURI, N., YARMUSH, M. L. & MORGAN, J. R. 2001. Complexation of Retrovirus with Cationic and Anionic Polymers Increases the Efficiency of Gene Transfer. *Human Gene Therapy*, 12, 1611-1621.

LEE, Y.-N., LEE, H.-J., LEE, D.-H., KIM, J.-H., PARK, H.-M., NAHM, S.-S., LEE, J.-B., PARK, S.-Y., CHOI, I.-S. & SONG, C.-S. 2011. Severe canine influenza in dogs correlates with hyperchemokinaemia and high viral load. *Virology*, 417, 57-63.

LEUNG, C., KING, A. N., BARKER, P. R. A., ALSHALLAL, A. D., LEE, J. Y. & SU, L. 2024. Global seroprevalence and prevalence of infection of influenza in dogs (*Canis familiaris*): A systematic review and meta-analysis. *Reviews in Medical Virology*, 34, e2542.

LEWIS, N. S., DALY, J. M., RUSSELL, C. A., HORTON, D. L., SKEPNER, E., BRYANT, N. A., BURKE, D. F., RASH, A. S., WOOD, J. L., CHAMBERS, T. M., FOUCHIER, R. A., MUMFORD, J. A., ELTON, D. M. & SMITH, D. J. 2011. Antigenic and genetic evolution of equine influenza A (H3N8) virus from 1968 to 2007. *J Virol*, 85, 12742-9.

LI, S., SHI, Z., JIAO, P., ZHANG, G., ZHONG, Z., TIAN, W., LONG, L. P., CAI, Z., ZHU, X., LIAO, M. & WAN, X. F. 2010. Avian-origin H3N2 canine influenza A viruses in Southern China. *Infect Genet Evol*, 10, 1286-8.

LI, X., GU, M., ZHENG, Q., GAO, R. & LIU, X. 2021a. Packaging signal of influenza A virus. *Virology Journal*, 18, 36.

LI, X., LIU, J., QIU, Z., LIAO, Q., PENG, Y., CHEN, Y. & SHU, Y. 2021b. Host-Adaptive Signatures of H3N2 Influenza Virus in Canine. *Frontiers in veterinary science*, 8, 740472-740472.

LI, Y., ZHANG, X., LIU, Y., FENG, Y., WANG, T., GE, Y., KONG, Y., SUN, H., XIANG, H., ZHOU, B., FANG, S., XIA, Q., HU, X., SUN, W., WANG, X., MENG, K., LV, C., LI, E., XIA, X., HE, H., GAO, Y. & JIN, N. 2021c. Characterization of Canine Influenza Virus A (H3N2) Circulating in Dogs in China from 2016 to 2018. *Viruses*, 13.

LIN, C., HOLLAND JR, R. E., WILLIAMS, N. M. & CHAMBERS, T. M. 2001. Cultures of equine respiratory epithelial cells and organ explants

as tools for the study of equine influenza virus infection. *Archives of Virology*, 146, 2239-2247.

LIU, C., LIN, H., CAO, L., WANG, K. & SUI, J. 2022. Research progress on unique paratope structure, antigen binding modes, and systematic mutagenesis strategies of single-domain antibodies. *Front Immunol*, 13, 1059771.

LIU, S., WANG, Z., ZHU, R., WANG, F., CHENG, Y. & LIU, Y. 2021. Three Differential Expression Analysis Methods for RNA Sequencing: limma, EdgeR, DESeq2. *JoVE*, e62528.

LIU, Y., ZHANG, Z., JIANG, Y., ZHANG, L., POPOV, V. L., ZHANG, J., WALKER, D. H. & YU, X.-J. 2011. Obligate intracellular bacterium *Ehrlichia* inhibiting mitochondrial activity. *Microbes and infection*, 13, 232-238.

LOUIS, N., EVELEGH, C. & GRAHAM, F. L. 1997. Cloning and sequencing of the cellular-viral junctions from the human adenovirus type 5 transformed 293 cell line. *Virology*, 233, 423-9.

LOVE, M. I., HUBER, W. & ANDERS, S. 2014. Moderated estimation of fold change and dispersion for RNA-seq data with DESeq2. *Genome Biology*, 15, 550.

LU, G., OU, J., CAI, S., LAI, Z., ZHONG, L., YIN, X. & LI, S. 2021. Canine Interferon-Inducible Transmembrane Protein Is a Host Restriction Factor That Potently Inhibits Replication of Emerging Canine Influenza Virus. *Front Immunol*, 12, 710705.

LUO, S., DENG, X., XIE, Z., HUANG, J., ZHANG, M., LI, M., XIE, L., LI, D., FAN, Q., WANG, S., ZENG, T., ZHANG, Y. & XIE, Z. 2020.

Production and identification of monoclonal antibodies and development of a sandwich ELISA for detection of the H3-subtype avian influenza virus antigen. *AMB Express*, 10, 49.

MAAS, R., TACKEN, M., RUULS, L., KOCH, G., VAN ROOIJ, E. & STOCKHOFE-ZURWIEDEN, N. 2007. Avian influenza (H5N1) susceptibility and receptors in dogs. *Emerg Infect Dis*, 13, 1219-21.

MACRAE, S. 2010. *Pathogenicity and transmissibility of H3N8 equine influenza viruses*. The Open University.

MAEDA, K., YASUMOTO, S., TSURUDA, A., ANDOH, K., KAI, K., OTOI, T. & MATSUMURA, T. 2007. Establishment of a novel equine cell line for isolation and propagation of equine herpesviruses. *J Vet Med Sci*, 69, 989-91.

MALIK, G. & ZHOU, Y. 2020. Innate Immune Sensing of Influenza A Virus. *Viruses*, 12.

MALM, M., SAGHALEYNI, R., LUNDQVIST, M., GIUDICI, M., CHOTTEAU, V., FIELD, R., VARLEY, P. G., HATTON, D., GRASSI, L., SVENSSON, T., NIELSEN, J. & ROCKBERG, J. 2020. Evolution from adherent to suspension: systems biology of HEK293 cell line development. *Scientific Reports*, 10, 18996.

MARSHALL, J. S., WARRINGTON, R., WATSON, W. & KIM, H. L. 2018. An introduction to immunology and immunopathology. *Allergy, Asthma & Clinical Immunology*, 14, 49.

MARTIN, K. & HELENIUST, A. 1991. Nuclear transport of influenza virus ribonucleoproteins: The viral matrix protein (M1) promotes export and inhibits import. *Cell*, 67, 117-130.

- MATROSOVICH, M., HERRLER, G. & KLENK, H. D. 2015. Sialic Acid Receptors of Viruses. *Topics in current chemistry*, 367, 1-28.
- MATROSOVICH, M. & KLENK, H. D. 2003. Natural and synthetic sialic acid-containing inhibitors of influenza virus receptor binding. *Rev Med Virol*, 13, 85-97.
- MATROSOVICH, M., MATROSOVICH, T., CARR, J., ROBERTS, N. A. & KLENK, H. D. 2003. Overexpression of the alpha-2,6-sialyltransferase in MDCK cells increases influenza virus sensitivity to neuraminidase inhibitors. *J Virol*, 77, 8418-25.
- MATROSOVICH, M., TUZIKOV, A., BOVIN, N., GAMBARYAN, A., KLIMOV, A., CASTRUCCI, M. R., DONATELLI, I. & KAWAOKA, Y. 2000. Early Alterations of the Receptor-Binding Properties of H1, H2, and H3 Avian Influenza Virus Hemagglutinins after Their Introduction into Mammals. *Journal of Virology*, 74, 8502-8512.
- MATROSOVICH, M. N. & GAMBARYAN, A. S. 2012. Solid-phase assays of receptor-binding specificity. *Methods Mol Biol*, 865, 71-94.
- MATROSOVICH, M. N., MATROSOVICH, T. Y., GRAY, T., ROBERTS, N. A. & KLENK, H. D. 2004. Neuraminidase is important for the initiation of influenza virus infection in human airway epithelium. *J Virol*, 78, 12665-7.
- MATSUZAKI, Y., SUGAWARA, K., FURUSE, Y., SHIMOTAI, Y., HONGO, S., OSHITANI, H., MIZUTA, K. & NISHIMURA, H. 2016. Genetic Lineage and Reassortment of Influenza C Viruses Circulating between 1947 and 2014. *Journal of Virology*, 90, 8251-8265.

MCAULEY, J. L., GILBERTSON, B. P., TRIFKOVIC, S., BROWN, L. E. & MCKIMM-BRESCHKIN, J. L. 2019. Influenza Virus Neuraminidase Structure and Functions. *Frontiers in Microbiology*, 10.

MERCER, M. A. 2022. *Miscellaneous Antiviral Agents Used in Animals* [Online]. MSD Manual Veterinary Manual. Available: <https://www.msdsvetmanual.com/pharmacology/antiviral-agents/miscellaneous-antiviral-agents-used-in-animals> [Accessed 24.06.24 2024].

MIBAYASHI, M., MARTÍNEZ-SOBRIDO, L., LOO, Y.-M., CÁRDENAS, W. B., GALE, M. & GARCÍA-SASTRE, A. 2007. Inhibition of Retinoic Acid-Inducible Gene I-Mediated Induction of Beta Interferon by the NS1 Protein of Influenza A Virus. *Journal of Virology*, 81, 514-524.

MITRA, S. & TOMAR, P. C. 2021. Hybridoma technology; advancements, clinical significance, and future aspects. *J Genet Eng Biotechnol*, 19, 159.

MOGHADAMI, M. 2017. A Narrative Review of Influenza: A Seasonal and Pandemic Disease. *Iranian journal of medical sciences*, 42, 2-13.

MOON, S. A., KI, M. K., LEE, S., HONG, M. L., KIM, M., KIM, S., CHUNG, J., RHEE, S. G. & SHIM, H. 2011. Antibodies against non-immunizing antigens derived from a large immune scFv library. *Mol Cells*, 31, 509-13.

MORENS, D. M. & TAUBENBERGER, J. K. 2010. Historical thoughts on influenza viral ecosystems, or behold a pale horse, dead dogs, failing fowl, and sick swine. *Influenza and Other Respiratory Viruses*, 4, 327-337.

MOSTAFA, A., ABDELWHAB, E. M., METTENLEITER, T. C. & PLESCHKA, S. 2018. Zoonotic Potential of Influenza A Viruses: A Comprehensive Overview. *Viruses*, 10, 497.

MURALI, S., RUSTANDI, R. R., ZHENG, X., PAYNE, A. & SHANG, L. 2022. Applications of Surface Plasmon Resonance and Biolayer Interferometry for Virus-Ligand Binding. *Viruses*, 14.

MURCIA, P. R., WOOD, J. L. N. & HOLMES, E. C. 2011. Genome-Scale Evolution and Phylodynamics of Equine H3N8 Influenza A Virus. *Journal of Virology*, 85, 5312-5322.

MUYLDERMANS, S. 2021a. Applications of Nanobodies. *Annual Review of Animal Biosciences*, 9, 401-421.

MUYLDERMANS, S. 2021b. A guide to: generation and design of nanobodies. *Febs j*, 288, 2084-2102.

MUYLDERMANS, S., ATARHOUCHE, T., SALDANHA, J., BARBOSA, J. A. & HAMERS, R. 1994. Sequence and structure of VH domain from naturally occurring camel heavy chain immunoglobulins lacking light chains. *Protein Eng*, 7, 1129-35.

NAKAKIDO, M., KINOSHITA, S. & TSUMOTO, K. 2024. Development of novel humanized VHH synthetic libraries based on physicochemical analyses. *Scientific Reports*, 14, 19533.

NELSON, S. W., LORBACH, J. N., NOLTING, J. M., STULL, J. W., JACKWOOD, D. J., DAVIS, I. C. & BOWMAN, A. S. 2019. Madin-Darby canine kidney cell sialic acid receptor modulation induced by culture medium conditions: Implications for the isolation of influenza A virus. *Influenza Other Respir Viruses*, 13, 593-602.

NEMOTO, M., OHTA, M., YAMANAKA, T., KAMBAYASHI, Y., BANNAI, H., TSUJIMURA, K., YAMAYOSHI, S., KAWAOKA, Y. & CULLINANE, A. 2021. Antigenic differences between equine influenza virus vaccine strains and Florida sublineage clade 1 strains isolated in Europe in 2019. *The Veterinary Journal*, 272, 105674.

NEMOTO, M., YAMAYOSHI, S., BANNAI, H., TSUJIMURA, K., KOKADO, H., KAWAOKA, Y. & YAMANAKA, T. 2019. A single amino acid change in hemagglutinin reduces the cross-reactivity of antiserum against an equine influenza vaccine strain. *Archives of Virology*, 164, 2355-2358.

NEUMANN, G., WATANABE, T., ITO, H., WATANABE, S., GOTO, H., GAO, P., HUGHES, M., PEREZ, D. R., DONIS, R., HOFFMANN, E., HOBOM, G. & KAWAOKA, Y. 1999. Generation of influenza A viruses entirely from cloned cDNAs. *Proc Natl Acad Sci U S A*, 96, 9345-50.

NEWBURY, S., GODHARDT-COOPER, J., POULSEN, K. P., CIGEL, F., BALANOFF, L. & TOOHEY-KURTH, K. 2016. Prolonged intermittent virus shedding during an outbreak of canine influenza A H3N2 virus infection in dogs in three Chicago area shelters: 16 cases (March to May 2015). *Journal of the American Veterinary Medical Association*, 248, 1022-1026.

NEWTON, J. R., DALY, J. M., SPENCER, L. & MUMFORD, J. A. 2006. Description of the outbreak of equine influenza (H3N8) in the United Kingdom in 2003, during which recently vaccinated horses in Newmarket developed respiratory disease. *Veterinary Record*, 158, 185-192.

NG, P. C. & HENIKOFF, S. 2003. SIFT: predicting amino acid changes that affect protein function. *Nucleic Acids Research*, 31, 3812-3814.

NG, P. S. K., BÖHM, R., HARTLEY-TASSELL, L. E., STEEN, J. A., WANG, H., LUKOWSKI, S. W., HAWTHORNE, P. L., TREZISE, A. E. O., COLOE, P. J., GRIMMOND, S. M., HASELHORST, T., VON ITZSTEIN, M., PATON, A. W., PATON, J. C. & JENNINGS, M. P. 2014. Ferrets exclusively synthesize Neu5Ac and express naturally humanized influenza A virus receptors. *Nature Communications*, 5, 5750.

NING, Z.-Y., WU, X.-T., CHENG, Y.-F., QI, W.-B., AN, Y.-F., WANG, H., ZHANG, G.-H. & LI, S.-J. 2012. Tissue distribution of sialic acid-linked influenza virus receptors in beagle dogs. *Journal of veterinary science*, 13, 219-222.

NOAH, D. L., TWU, K. Y. & KRUG, R. M. 2003. Cellular antiviral responses against influenza A virus are countered at the posttranscriptional level by the viral NS1A protein via its binding to a cellular protein required for the 3' end processing of cellular pre-mRNAs. *Virology*, 307, 386-395.

NOGALES, A., AYDILLO, T., ÁVILA-PÉREZ, G., ESCALERA, A., CHIEM, K., CADAGAN, R., DEDIEGO, M. L., LI, F., GARCÍA-SASTRE, A. & MARTÍNEZ-SOBRIDO, L. 2019. Functional Characterization and Direct Comparison of Influenza A, B, C, and D NS1 Proteins in vitro and in vivo. *Frontiers in Microbiology*, 10.

- NOGALES, A. & MARTÍNEZ-SOBRIDO, L. 2016. Reverse Genetics Approaches for the Development of Influenza Vaccines. *Int J Mol Sci*, 18.
- NOSAKI, S., HOSHIKAWA, K., EZURA, H. & MIURA, K. 2021. Transient protein expression systems in plants and their applications. *Plant Biotechnol (Tokyo)*, 38, 297-304.
- NOVOGENE. *Long Non-coding RNA Sequencing (lncRNA-seq)* [Online]. Available: <https://www.novogene.com/eu-en/services/research-services/transcriptome-sequencing/non-coding-rna-sequencing/long-non-coding-rna-sequencing-lncrna-seq/> [Accessed 23/04/25 2025].
- ODUOYE, M. O., WECHULI, P. N., ABDULKAREEM, H. A., JAVED, B., ZUBAIRU, A. Z. & GHARAIBEH, R. S. 2023. Re-emergence of canine influenza in the United States of America; a call for One Health approach; a letter to the editor. *IJS Global Health*, 6.
- OIE. 2020. *Expert Surveillance Panel on Equine Influenza Vaccine Composition* [Online]. World Organisation for Animal Health. Available: https://doc.woah.org/dyn/portal/digidoc.xhtml?statelessToken=v1GSG3HrdDdi3EyrPCMjDjDL_Oer_eehU46vIToSC7c=&actionMethod=dyn%2Fportal%2Fdigidoc.xhtml%3AdownloadAttachment.openStateless [Accessed].
- OIE. 2022. *Expert surveillance panel on equine influenza vaccine composition. Conclusions and Recommendations* [Online]. World Organisation for Animal Health. Available: <https://www.woah.org/app/uploads/2022/10/expert-surveillance-panel->

[on-equine-influenza-vaccine-composition.pdf](#) [Accessed 18/09/2023

2023].

OIE 2024. Manual of Diagnostic Tests and Vaccines for Terrestrial Animals. *Equine influenza (Infection with equine influenza virus)*. 13th ed.: The World Organisation for Animal Health (WOAH).

OLADUNNI, F. S., OSENI, S. O., MARTINEZ-SOBRIDO, L. & CHAMBERS, T. M. 2021. Equine Influenza Virus and Vaccines. *Viruses*, 13, 1657.

OSTERHAUS, A. D. M. E., RIMMELZWAAN, G. F., MARTINA, B. E. E., BESTEBROER, T. M. & FOUCHIER, R. A. M. 2000. Influenza B Virus in Seals. *Science*, 288, 1051-1053.

PARK, W.-J., PARK, B.-J., SONG, Y.-J., LEE, D.-H., YUK, S.-S., LEE, J.-B., PARK, S.-Y., SONG, C.-S., LEE, S.-W. & CHOI, I.-S. 2015. Analysis of cytokine production in a newly developed canine tracheal epithelial cell line infected with H3N2 canine influenza virus. *Archives of Virology*, 160, 1397-1405.

PARK, W. J., HAN, S. H., KIM, D. H., SONG, Y. J., LEE, J. B., PARK, S. Y., SONG, C. S., LEE, S. W. & CHOI, I. S. 2021. Induction of IFN- β through TLR-3- and RIG-I-Mediated Signaling Pathways in Canine Respiratory Epithelial Cells Infected with H3N2 Canine Influenza Virus. *J Microbiol Biotechnol*, 31, 942-948.

PARRISH, C. R. & VOORHEES, I. E. H. 2019. H3N8 and H3N2 Canine Influenza Viruses: Understanding These New Viruses in Dogs. *Veterinary Clinics of North America: Small Animal Practice*, 49, 643-649.

PAYUNGORN, S., CRAWFORD, P. C., KOUO, T. S., CHEN, L.-M., POMPEY, J., CASTLEMAN, W. L., DUBOVI, E. J., KATZ, J. M. & DONIS, R. O. 2008. Influenza A virus (H3N8) in dogs with respiratory disease, Florida. *Emerging infectious diseases*, 14, 902-908.

PEACOCK, T. P., SEALY, J. E., HARVEY, W. T., BENTON, D. J., REEVE, R. & IQBAL, M. 2021. Genetic Determinants of Receptor-Binding Preference and Zoonotic Potential of H9N2 Avian Influenza Viruses. *Journal of Virology*, 95, 10.1128/jvi.01651-20.

PEPER, R. L. & VAN CAMPEN, H. 1995. Tumor necrosis factor as a mediator of inflammation in influenza A viral pneumonia. *Microbial Pathogenesis*, 19, 175-183.

PETERSEN, R. L. 2017. Strategies Using Bio-Layer Interferometry Biosensor Technology for Vaccine Research and Development. *Biosensors (Basel)*, 7.

PETROVA, V. N. & RUSSELL, C. A. 2018. The evolution of seasonal influenza viruses. *Nature Reviews Microbiology*, 16, 47-60.

PILLAI, S. P. S. & LEE, C. W. 2010. Species and age related differences in the type and distribution of influenza virus receptors in different tissues of chickens, ducks and turkeys. *Virology journal*, 7, 5-5.

PINTO, L. H. & LAMB, R. A. 2006. The M2 Proton Channels of Influenza A and B Viruses *. *Journal of Biological Chemistry*, 281, 8997-9000.

PINTO, R. M., LYCETT, S., GAUNT, E. & DIGARD, P. 2021. Accessory Gene Products of Influenza A Virus. *Cold Spring Harbor Perspectives in Medicine*, 11.

POTHLICHET, J., MEUNIER, I., DAVIS, B. K., TING, J. P., SKAMENE, E., VON MESSLING, V. & VIDAL, S. M. 2013. Type I IFN triggers RIG-I/TLR3/NLRP3-dependent inflammasome activation in influenza A virus infected cells. *PLoS Pathog*, 9, e1003256.

POWE, J. R. & CASTLEMAN, W. L. 2009. Canine Influenza Virus Replicates in Alveolar Macrophages and Induces TNF- α . *Veterinary Pathology*, 46, 1187-1196.

POWELL, D. G., WATKINS, K. L., LI, P. H. & SHORTRIDGE, K. F. 1995. Outbreak of equine influenza among horses in Hong Kong during 1992. *Vet Rec*, 136, 531-6.

PROMED. 2022. *Canine influenza- North America: USA (Texas, Alabama, Michigan, North/South Carolina, Oklahome, Tennessee)* [Online]. Available: <https://promedmail.org> [Accessed 14/12/2022 2022].

PROMED. 2023a. *Canine influenza- North America: USA (California)* [Online]. Available: <https://promedmail.org> [Accessed 06/08/2023 2023].

PROMED. 2023b. *Canine influenza- North America: USA (District of Columbia)* [Online]. Available: <https://promedmail.org> [Accessed 10/08/2023 2023].

PROMED. 2023c. *Canine influenza- North America: USA (Maryland)* [Online]. Available: <https://promedmail.org> [Accessed 18/08/2023 2023].

PROMED. 2023d. *Canine influenza- North America: USA (Minnesota)* [Online]. Available: <https://promedmail.org> [Accessed 07/04/2023 2023].

PROMED. 2023e. *Canine influenza- North America: USA (North Carolina)* [Online]. Available: <https://promedmail.org> [Accessed 06/11/23 2023].

PROMED. 2023f. *Canine influenza- North America: USA (Oklahoma)* [Online]. Available: <https://promedmail.org> [Accessed 22/08/2023 2023].

PROMED. 2024. *Canine influenza- North America: USA (Florida, Nevada)* [Online]. Available: <https://promedmail.org> [Accessed 21/02/2024 2024].

PULIT-PENALOZA, J. A., SIMPSON, N., YANG, H., CREAGER, H. M., JONES, J., CARNEY, P., BELSER, J. A., YANG, G., CHANG, J., ZENG, H., THOR, S., JANG, Y., KILLIAN, M. L., JENKINS-MOORE, M., JANAS-MARTINDALE, A., DUBOVI, E., WENTWORTH, D. E., STEVENS, J., TUMPEY, T. M., DAVIS, C. T. & MAINES, T. R. 2017. Assessment of Molecular, Antigenic, and Pathological Features of Canine Influenza A(H3N2) Viruses That Emerged in the United States. *J Infect Dis*, 216, S499-s507.

QUINLIVAN, M., NELLY, M., PRENDERGAST, M., BREATHNACH, C., HOROHOV, D., ARKINS, S., CHIANG, Y. W., CHU, H. J., NG, T. & CULLINANE, A. 2007. Pro-inflammatory and antiviral cytokine expression in vaccinated and unvaccinated horses exposed to equine influenza virus. *Vaccine*, 25, 7056-64.

RAMOS, I., BERNAL-RUBIO, D., DURHAM, N., BELICHA-VILLANUEVA, A., LOWEN, A. C., STEEL, J. & FERNANDEZ-SESMA, A. 2011. Effects of Receptor Binding Specificity of Avian Influenza Virus on the Human Innate Immune Response. *Journal of Virology*, 85, 4421-4431.

RENDLE, D., IVENS, P., BOWEN, P., LAWRENCE, H., NEWTON, R., MARR, C., PAILLOT, R. & RASH, A. 2019. Equine influenza: A current reference for vets in practice in the UK. *UK-Vet Equine*, 3, 1-13.

REUTEN, R., NIKODEMUS, D., OLIVEIRA, M. B., PATEL, T. R., BRACHVOGEL, B., BRELOY, I., STETEFELD, J. & KOCH, M. 2016. Maltose-Binding Protein (MBP), a Secretion-Enhancing Tag for Mammalian Protein Expression Systems. *PLoS One*, 11, e0152386.

RITCHIE, M. E., PHIPSON, B., WU, D., HU, Y., LAW, C. W., SHI, W. & SMYTH, G. K. 2015. limma powers differential expression analyses for RNA-sequencing and microarray studies. *Nucleic Acids Research*, 43, e47-e47.

ROBINSON, M. D., MCCARTHY, D. J. & SMYTH, G. K. 2009. edgeR: a Bioconductor package for differential expression analysis of digital gene expression data. *Bioinformatics*, 26, 139-140.

RODRIGUEZ, L., NOGALES, A., REILLY, E. C., TOPHAM, D. J., MURCIA, P. R., PARRISH, C. R. & MARTINEZ SOBRIDO, L. 2017. A live-attenuated influenza vaccine for H3N2 canine influenza virus. *Virology*, 504, 96-106.

ROGERS, G. N., PAULSON, J. C., DANIELS, R. S., SKEHEL, J. J., WILSON, I. A. & WILEY, D. C. 1983. Single amino acid substitutions in influenza haemagglutinin change receptor binding specificity. *Nature*, 304, 76-78.

ROSENTHAL, P. B., ZHANG, X., FORMANOWSKI, F., FITZ, W., WONG, C. H., MEIER-EWERT, H., SKEHEL, J. J. & WILEY, D. C.

1998. Structure of the haemagglutinin-esterase-fusion glycoprotein of influenza C virus. *Nature*, 396, 92-6.

RUIZ-JIMÉNEZ, F., PÉREZ-OLAIS, J. H., RAYMOND, C., KING, B. J., MCCLURE, C. P., URBANOWICZ, R. A. & BALL, J. K. 2021.

Challenges on the development of a pseudotyping assay for Zika glycoproteins. *J Med Microbiol*, 70.

SARTORIUS. *Biolayer Interferometry for Label-Free Biomolecular Interaction Analysis* [Online]. Available:

<https://www.sartorius.com/en/products/biolayer-interferometry>

[Accessed 2025].

SAUNDERS-HASTINGS, P. R. & KREWSKI, D. 2016. Reviewing the History of Pandemic Influenza: Understanding Patterns of Emergence and Transmission. *Pathogens*, 5, 66.

SCOCCO, P. & PEDINI, V. 2008. Localization of influenza virus sialoreceptors in equine respiratory tract. *Histol Histopathol*, 23, 973-8.

SCOTT, S. D., KINSLEY, R., TEMPERTON, N. & DALY, J. M. 2016. The Optimisation of Pseudotyped Viruses for the Characterisation of Immune Responses to Equine Influenza Virus. *Pathogens*, 5.

SEITZ, C., FRENSING, T., HÖPER, D., KOCHS, G. & REICHL, U. 2010. High yields of influenza A virus in Madin–Darby canine kidney cells are promoted by an insufficient interferon-induced antiviral state. *Journal of General Virology*, 91, 1754-1763.

SEITZ, C., ISKEN, B., HEYNISCH, B., RETTKOWSKI, M., FRENSING, T. & REICHL, U. 2012. Trypsin promotes efficient influenza vaccine

production in MDCK cells by interfering with the antiviral host response.

Appl Microbiol Biotechnol, 93, 601-11.

SEKINE, W., KAMIKI, H., ISHIDA, H., MATSUGO, H., OHIRA, K., LI, K., KATAYAMA, M., TAKENAKA-UEMA, A., MURAKAMI, S. & HORIMOTO, T. 2024. Adaptation potential of H3N8 canine influenza virus in human respiratory cells. *Sci Rep*, 14, 18750.

SHAFIUDDIN, M. & BOON, A. C. M. 2019. RNA Sequence Features Are at the Core of Influenza A Virus Genome Packaging. *Journal of Molecular Biology*, 431, 4217-4228.

SHAO, W., LI, X., GORAYA, M. U., WANG, S. & CHEN, J. L. 2017. Evolution of Influenza A Virus by Mutation and Re-Assortment. *Int J Mol Sci*, 18.

SHI, Y., WU, Y., ZHANG, W., QI, J. & GAO, G. F. 2014. Enabling the 'host jump': structural determinants of receptor-binding specificity in influenza A viruses. *Nature Reviews Microbiology*, 12, 822-831.

SHINYA, K., EBINA, M., YAMADA, S., ONO, M., KASAI, N. & KAWAOKA, Y. 2006. Influenza virus receptors in the human airway. *Nature*, 440, 435-436.

SINGH, R. K., DHAMA, K., KARTHIK, K., KHANDIA, R., MUNJAL, A., KHURANA, S. K., CHAKRABORTY, S., MALIK, Y. S., VIRMANI, N., SINGH, R., TRIPATHI, B. N., MUNIR, M. & VAN DER KOLK, J. H. 2018. A Comprehensive Review on Equine Influenza Virus: Etiology, Epidemiology, Pathobiology, Advances in Developing Diagnostics, Vaccines, and Control Strategies. *Frontiers in Microbiology*, 9.

- SLATER, J. & HANNANT, D. 2000. Equine Immunity to Viruses. *Veterinary Clinics of North America: Equine Practice*, 16, 49-68.
- SMITH, D. J., LAPEDES, A. S., DE JONG, J. C., BESTEBROER, T. M., RIMMELZWAAN, G. F., OSTERHAUS, A. D. M. E. & FOUCHIER, R. A. M. 2004. Mapping the Antigenic and Genetic Evolution of Influenza Virus. *Science*, 305, 371-376.
- SMYTH, G. K. 2004. Linear models and empirical bayes methods for assessing differential expression in microarray experiments. *Stat Appl Genet Mol Biol*, 3, Article3.
- SON, S., AHN, S. B., KIM, G., JANG, Y., KO, C., KIM, M. & KIM, S. J. 2023. Identification of broad-spectrum neutralizing antibodies against influenza A virus and evaluation of their prophylactic efficacy in mice. *Antiviral Research*, 213, 105591.
- SONG, D., KANG, B., LEE, C., JUNG, K., HA, G., KANG, D., PARK, S., PARK, B. & OH, J. 2008. Transmission of avian influenza virus (H3N2) to dogs. *Emerging infectious diseases*, 14, 741-746.
- SONG, D., MOON, H., JUNG, K., YEOM, M., KIM, H., HAN, S., AN, D., OH, J., KIM, J., PARK, B. & KANG, B. 2011. Association between nasal shedding and fever that influenza A (H3N2) induces in dogs. *Virology*, 8, 1.
- SONGSEEM, T., AMONSIN, A., JAM-ON, R., SAE-HENG, N., PARIYOTHORN, N., PAYUNGORN, S., THEAMBOONLERS, A., CHUTINIMITKUL, S., THANAWONGNUWECH, R. & POOVORAWAN, Y. 2006. Fatal avian influenza A H5N1 in a dog. *Emerg Infect Dis*, 12, 1744-7.

SPRINGER, S. A., DIAZ, S. L. & GAGNEUX, P. 2014. Parallel evolution of a self-signal: humans and new world monkeys independently lost the cell surface sugar Neu5Gc. *Immunogenetics*, 66, 671-674.

SPRUIT, C. M., NEMANICHVILI, N., OKAMATSU, M., TAKEMATSU, H., BOONS, G.-J. & DE VRIES, R. P. 2021. N-Glycolylneuraminic Acid in Animal Models for Human Influenza A Virus. *Viruses*, 13, 815.

SREENIVASAN, C. C., UPRETY, T., REEDY, S. E., TEMEEYASEN, G., HAUSE, B. M., WANG, D., LI, F. & CHAMBERS, T. M. 2022. Experimental Infection of Horses with Influenza D Virus. *Viruses*, 14, 661.

SRIWILAIJAROEN, N. & SUZUKI, Y. 2012. Molecular basis of the structure and function of H1 hemagglutinin of influenza virus. *Proc Jpn Acad Ser B Phys Biol Sci*, 88, 226-49.

STACEY, G. & MACDONALD, C. 2001. Immortalisation of Primary Cells. *Cell Biology and Toxicology*, 17, 231-246.

STACK, J. C., MURCIA, P. R., GRENFELL, B. T., WOOD, J. L. N. & HOLMES, E. C. 2013. Inferring the inter-host transmission of influenza A virus using patterns of intra-host genetic variation. *Proceedings. Biological sciences*, 280, 20122173-20122173.

STEGMANN, T. 2000. Membrane Fusion Mechanisms: The Influenza Hemagglutinin Paradigm and its Implications for Intracellular Fusion. *Traffic*, 1, 598-604.

STEINHAEUER, D. A. 1999. Role of Hemagglutinin Cleavage for the Pathogenicity of Influenza Virus. *Virology*, 258, 1-20.

STEINHAUER, D. A., DOMINGO, E. & HOLLAND, J. J. 1992. Lack of evidence for proofreading mechanisms associated with an RNA virus polymerase. *Gene*, 122, 281-8.

STEVENS, J., BLIXT, O., GLASER, L., TAUBENBERGER, J. K., PALESE, P., PAULSON, J. C. & WILSON, I. A. 2006a. Glycan Microarray Analysis of the Hemagglutinins from Modern and Pandemic Influenza Viruses Reveals Different Receptor Specificities. *Journal of Molecular Biology*, 355, 1143-1155.

STEVENS, J., BLIXT, O., PAULSON, J. C. & WILSON, I. A. 2006b. Glycan microarray technologies: tools to survey host specificity of influenza viruses. *Nature Reviews Microbiology*, 4, 857-864.

SU, S., FU, X., LI, G., KERLIN, F. & VEIT, M. 2017. Novel Influenza D virus: Epidemiology, pathology, evolution and biological characteristics. *Virulence*, 8, 1580-1591.

SUN, H., BLACKMON, S., YANG, G., WATERS, K., LI, T., TANGWANGVIVAT, R., XU, Y., SHYU, D., WEN, F., COOLEY, J., SENTER, L., LIN, X., JARMAN, R., HANSON, L., WEBBY, R., WAN, X.-F. & JUNG, J. U. 2017. Zoonotic Risk, Pathogenesis, and Transmission of Avian-Origin H3N2 Canine Influenza Virus. *Journal of Virology*, 91, e00637-17.

SUN, Y. P., HU, Z., ZHANG, X. X., CHEN, M. Y., WANG, Z., XU, G. L., BI, Y. H., TONG, Q., WANG, M. Y., SUN, H. L., PU, J., IQBAL, M. & LIU, J. H. 2020. An R195K Mutation in the PA-X Protein Increases the Virulence and Transmission of Influenza A Virus in Mammalian Hosts. *Journal of Virology*, 94, 20.

SUZUKI, A. 2006. Genetic basis for the lack of N-glycolylneuraminic acid expression in human tissues and its implication to human evolution. *Proc Jpn Acad Ser B Phys Biol Sci*, 82, 93-103.

SWANEY, W. P., SORGI, F. L., BAHNSON, A. B. & BARRANGER, J. A. 1997. The effect of cationic liposome pretreatment and centrifugation on retrovirus-mediated gene transfer. *Gene Therapy*, 4, 1379-1386.

TAO, P., NING, Z., HAO, X., LIN, X., ZHENG, Q. & LI, S. 2019. Comparative Analysis of Whole-Transcriptome RNA Expression in MDCK Cells Infected With the H3N2 and H5N1 Canine Influenza Viruses. *Front Cell Infect Microbiol*, 9, 76.

TE VELTHUIS, A. J. W. 2019. Flu transcription captured in action. *Nature Structural & Molecular Biology*, 26, 393-395.

THERMO FISHER SCIENTIFIC. 2024. *Useful Numbers for Cell Culture* [Online]. Thermo Fisher Scientific. Available: <https://www.thermofisher.com/uk/en/home/references/gibco-cell-culture-basics/cell-culture-protocols/cell-culture-useful-numbers.html> [Accessed 10/06/24 2024].

THORSTEINSDÓTTIR, L., TORSTEINSDÓTTIR, S. & SVANSSON, V. 2016. Establishment and characterization of fetal equine kidney and lung cells with extended lifespan. Susceptibility to equine gammaherpesvirus infection and transfection efficiency. *In Vitro Cellular & Developmental Biology - Animal*, 52, 872-877.

TOMASELLO, G., ARMENIA, I. & MOLLA, G. 2020. The Protein Imager: a full-featured online molecular viewer interface with server-side HQ-rendering capabilities. *Bioinformatics*, 36, 2909-2911.

TONG, S., ZHU, X., LI, Y., SHI, M., ZHANG, J., BOURGEOIS, M., YANG, H., CHEN, X., RECUENCO, S., GOMEZ, J., CHEN, L.-M., JOHNSON, A., TAO, Y., DREYFUS, C., YU, W., MCBRIDE, R., CARNEY, P. J., GILBERT, A. T., CHANG, J., GUO, Z., DAVIS, C. T., PAULSON, J. C., STEVENS, J., RUPPRECHT, C. E., HOLMES, E. C., WILSON, I. A. & DONIS, R. O. 2013. New World Bats Harbor Diverse Influenza A Viruses. *PLOS Pathogens*, 9, e1003657.

TONOZZI, C. C. 2022. *Canine Influenza (Flu)* [Online]. MSD Manual Veterinary Manual. Available: <https://www.msdsvetmanual.com/respiratory-system/respiratory-diseases-of-small-animals/canine-influenza-flu> [Accessed 24.06.24 June 2024].

TREANOR, J. 2004. Influenza Vaccine — Outmaneuvering Antigenic Shift and Drift. *New England Journal of Medicine*, 350, 218-220.

TRIANA-BALTZER, G. B., BABIZKI, M., CHAN, M. C., WONG, A. C., ASCHENBRENNER, L. M., CAMPBELL, E. R., LI, Q. X., CHAN, R. W., PEIRIS, J. S., NICHOLLS, J. M. & FANG, F. 2010. DAS181, a sialidase fusion protein, protects human airway epithelium against influenza virus infection: an in vitro pharmacodynamic analysis. *J Antimicrob Chemother*, 65, 275-84.

TSOUMPELI, M. T., GRAY, A., PARSONS, A. L., SPILIOTOPOULOS, A., OWEN, J. P., BISHOP, K., MADDISON, B. C. & GOUGH, K. C. 2022. A Simple Whole-Plasmid PCR Method to Construct High-Diversity Synthetic Phage Display Libraries. *Molecular Biotechnology*.

UYEKI, T. M., MILTON, S., HAMID, C. A., WEBB, C. R., PRESLEY, S. M., SHETTY, V., ROLLO, S. N., MARTINEZ, D. L., RAI, S., GONZALES, E. R., KNISS, K. L., JANG, Y., FREDERICK, J. C., CRUZ, J. A. D. L., LIDDELL, J., DI, H., KIRBY, M. K., BARNES, J. R. & DAVIS, C. T. 2024. Highly Pathogenic Avian Influenza A(H5N1) Virus Infection in a Dairy Farm Worker. *New England Journal of Medicine*, 0.

VALDÉS-TRESANCO, M. S., MOLINA-ZAPATA, A., POSE, A. G. & MORENO, E. 2022. Structural Insights into the Design of Synthetic Nanobody Libraries. *Molecules*, 27.

VAN DE SANDT, C. E., KREIJTZ, J. H. & RIMMELZWAAN, G. F. 2012a. Evasion of influenza A viruses from innate and adaptive immune responses. *Viruses*, 4, 1438-76.

VAN DE SANDT, C. E., KREIJTZ, J. H. C. M. & RIMMELZWAAN, G. F. 2012b. Evasion of Influenza A Viruses from Innate and Adaptive Immune Responses. *Viruses*, 4, 1438-1476.

VAN MAANEN, C. & CULLINANE, A. 2002. Equine influenza virus infections: an update. *Vet Q*, 24, 79-94.

VANDEKERCKHOVE, A., GLORIEUX, S., BROECK, W. V. D., GRYSPEERDT, A., VAN DER MEULEN, K. M. & NAUWYNCK, H. J. 2009. In vitro culture of equine respiratory mucosa explants. *The Veterinary Journal*, 181, 280-287.

VINES, A., WELLS, K., MATROSOVICH, M., CASTRUCCI, M. R., ITO, T. & KAWAOKA, Y. 1998. The Role of Influenza A Virus Hemagglutinin Residues 226 and 228 in Receptor Specificity and Host Range Restriction. *Journal of Virology*, 72, 7626-7631.

VIRMANI, N., BERA, B., GULATI, B., KARUPPUSAMY, S., SINGH, B.,
 VAID, R., KUMAR, S., KUMAR, R., MALIK, P., KHURANA, S., SINGH,
 J., MANUJA, A., DEDAR, R., GUPTA, A., YADAV, S., CHUG, P.,
 NARWAL, P., THANKUR, V., KAUL, R. & SINGH, R. 2010. Descriptive
 epidemiology of equine influenza in India (2008-2009): Temporal and
 spatial trends. *Veterinaria italiana*, 46, 449-58.

VOORHEES, I., GLASER, A., TOOHEY-KURTH, K., NEWBURY, S.,
 DALZIEL, B., DUBOVI, E., POULSEN, K., LEUTENEGGER, C.,
 WILLGERT, K., BRISBANE-COHEN, L., RICHARDSON-LOPEZ, J.,
 HOLMES, E. & PARRISH, C. 2017. Spread of Canine Influenza
 A(H3N2) Virus, United States. *Emerging Infectious Diseases*, 23.

VOORHEES, I. E. H., DALZIEL, B. D., GLASER, A., DUBOVI, E. J.,
 MURCIA, P. R., NEWBURY, S., TOOHEY-KURTH, K., SU, S., KRITI,
 D., VAN BAKEL, H., GOODMAN, L. B., LEUTENEGGER, C., HOLMES,
 E. C. & PARRISH, C. R. 2018. Multiple Incursions and Recurrent
 Epidemic Fade-Out of H3N2 Canine Influenza A Virus in the United
 States. *Journal of Virology*, 92, e00323-18.

WADDELL, G., TEIGLAND, M. & SIGEL, M. 1963. A new influenza
 virus associated with equine respiratory disease. *Journal of the
 American Veterinary Medical Association*, 143, 587–590.

WAGNER, R., MATROSOVICH, M. & KLENK, H. D. 2002. Functional
 balance between haemagglutinin and neuraminidase in influenza virus
 infections. *Rev Med Virol*, 12, 159-66.

WASIK, B. R., ROTHSCHILD, E., VOORHEES, I. E. H., REEDY, S. E.,
 MURCIA, P. R., PUSTERLA, N., CHAMBERS, T. M., GOODMAN, L.

B., HOLMES, E. C., KILE, J. C. & PARRISH, C. R. 2023. Understanding the divergent evolution and epidemiology of H3N8 influenza viruses in dogs and horses. *Virus Evol*, 9, vead052.

WASIK, B. R., VOORHEES, I. E. H. & PARRISH, C. R. 2021. Canine and Feline Influenza. *Cold Spring Harb Perspect Med*, 11.

WATTRANG, E., JESSETT, D. M., YATES, P., FUXLER, L. & HANNANT, D. 2003. Experimental Infection of Ponies with Equine Influenza A2 (H3N8) Virus Strains of Different Pathogenicity Elicits Varying Interferon and Interleukin-6 Responses. *Viral Immunology*, 16, 57-67.

WEBBY, R. J. & WEBSTER, R. G. 2001. Emergence of Influenza A Viruses. *Philosophical Transactions: Biological Sciences*, 356, 1817-1828.

WEBBY, R. J. & WEBSTER, R. G. 2003. Are We Ready for Pandemic Influenza? *Science*, 302, 1519-1522.

WEBSTER, R. G., BEAN, W. J., GORMAN, O. T., CHAMBERS, T. M. & KAWAOKA, Y. 1992. Evolution and ecology of influenza A viruses. *Microbiological Reviews*, 56, 152-179.

WEBSTER, R. G., SHORTRIDGE, K. F. & KAWAOKA, Y. 1997. Influenza: interspecies transmission and emergence of new pandemics. *FEMS immunology and medical microbiology*, 18, 275-279.

WEIS, W., BROWN, J. H., CUSACK, S., PAULSON, J. C., SKEHEL, J. J. & WILEY, D. C. 1988. Structure of the influenza virus haemagglutinin complexed with its receptor, sialic acid. *Nature*, 333, 426-31.

WELLMAN, M. L., KRAKOWKA, S., JACOBS, R. M. & KOCIBA, G. J. 1988. A macrophage-monocyte cell line from a dog with malignant histiocytosis. *In Vitro Cell Dev Biol*, 24, 223-9.

WEN, F., BLACKMON, S., OLIVIER, A. K., LI, L., GUAN, M., SUN, H., WANG, P. G. & WAN, X.-F. 2018a. Mutation W222L at the Receptor Binding Site of Hemagglutinin Could Facilitate Viral Adaption from Equine Influenza A(H3N8) Virus to Dogs. *Journal of virology*, 92, e01115-18.

WEN, F., BLACKMON, S., OLIVIER, A. K., LI, L., GUAN, M. H., SUN, H. L., WANG, P. G. & WAN, X. F. 2018b. Mutation W222L at the Receptor Binding Site of Hemagglutinin Could Facilitate Viral Adaption from Equine Influenza A(H3N8) Virus to Dogs. *Journal of Virology*, 92, 13.

WHITE, J., HELENIUS, A. & GETTING, M.-J. 1982. Haemagglutinin of influenza virus expressed from a cloned gene promotes membrane fusion. *Nature*, 300, 658-659.

WHO, OIE & FAO. 2011. *Updated unified nomenclature system for the highly pathogenic H5N1 avian influenza viruses* [Online]. Available: https://cdn.who.int/media/docs/default-source/influenza/global-influenza-surveillance-and-response-system/nomenclature/updated_nomenclature_system_h5n1_avian_influenza_viruses.pdf?sfvrsn=73b9d9a6_8 [Accessed 2025].

WILLE, M., TOLF, C., LATORRE-MARGALEF, N., FOUCHIER, R. A. M., HALPIN, R. A., WENTWORTH, D. E., RAGWANI, J., PYBUS, O. G., OLSEN, B. & WALDENSTRÖM, J. 2022. Evolutionary features of a

prolific subtype of avian influenza A virus in European waterfowl. *Virus Evolution*, 8.

WILSON, I. A., SKEHEL, J. J. & WILEY, D. C. 1981. Structure of the haemagglutinin membrane glycoprotein of influenza virus at 3 Å resolution. *Nature*, 289, 366-73.

WOJDYLA, K., COLLIER, A. J., FABIAN, C., NISI, P. S., BIGGINS, L., OXLEY, D. & RUGG-GUNN, P. J. 2020. Cell-Surface Proteomics Identifies Differences in Signaling and Adhesion Protein Expression between Naive and Primed Human Pluripotent Stem Cells. *Stem Cell Reports*, 14, 972-988.

WOODWARD, A., RASH, A. S., MEDCALF, E., BRYANT, N. A. & ELTON, D. M. 2015. Using epidemics to map H3 equine influenza virus determinants of antigenicity. *Virology*, 481, 187-198.

WU, G. 2020. *Development of diagnostic assays for emergent RNA viruses*. PhD, University of Nottingham.

WU, N. C. & ELLEBEDY, A. H. 2024. Targeting neuraminidase: the next frontier for broadly protective influenza vaccines. *Trends Immunol*, 45, 11-19.

WU, Y., WU, Y., TEFSSEN, B., SHI, Y. & GAO, G. F. 2014a. Bat-derived influenza-like viruses H17N10 and H18N11. *Trends in Microbiology*, 22, 183-191.

WU, Y., WU, Y., TEFSSEN, B., SHI, Y. & GAO, G. F. 2014b. Bat-derived influenza-like viruses H17N10 and H18N11. *Trends Microbiol*, 22, 183-91.

XU, R., KRAUSE, J. C., MCBRIDE, R., PAULSON, J. C., CROWE, J. E. & WILSON, I. A. 2013. A recurring motif for antibody recognition of the receptor-binding site of influenza hemagglutinin. *Nature Structural & Molecular Biology*, 20, 363-370.

YAMANAKA, T., BANNAI, H., NEMOTO, M., TSUJIMURA, K., KONDO, T., MURANAKA, M., HOBO, S., MINAMIJIMA, Y.-H., YAMADA, M. & MATSUMURA, T. 2012a. Efficacy of a single intravenous dose of the neuraminidase inhibitor peramivir in the treatment of equine influenza. *The Veterinary Journal*, 193, 358-362.

YAMANAKA, T., CULLINANE, A., GILDEA, S., BANNAI, H., NEMOTO, M., TSUJIMURA, K., KONDO, T. & MATSUMURA, T. 2015. The potential impact of a single amino-acid substitution on the efficacy of equine influenza vaccines. *Equine Veterinary Journal*, 47, 456-462.

YAMANAKA, T., NEMOTO, M., BANNAI, H., TSUJIMURA, K., KONDO, T., MATSUMURA, T., MURANAKA, M., UENO, T., KINOSHITA, Y., NIWA, H., HIDARI, K. I. & SUZUKI, T. 2012b. No evidence of horizontal infection in horses kept in close contact with dogs experimentally infected with canine influenza A virus (H3N8). *Acta Vet Scand*, 54, 25.

YAMANAKA, T., TSUJIMURA, K., KONDO, T., HOBO, S. & MATSUMURA, T. 2006. Efficacy of Oseltamivir Phosphate to Horses Inoculated with Equine Influenza A Virus. *Journal of Veterinary Medical Science*, 68, 923-928.

YANG, G., LI, S., BLACKMON, S., YE, J., BRADLEY, K. C., COOLEY, J., SMITH, D., HANSON, L., CARDONA, C., STEINHAUER, D. A., WEBBY, R., LIAO, M. & WAN, X. F. 2013. Mutation tryptophan to

leucine at position 222 of haemagglutinin could facilitate H3N2 influenza A virus infection in dogs. *J Gen Virol*, 94, 2599-2608.

YANG, X., STEUKERS, L., FORIER, K., XIONG, R., BRAECKMANS, K., VAN REETH, K. & NAUWYNCK, H. 2014. A beneficiary role for neuraminidase in influenza virus penetration through the respiratory mucus. *PLoS One*, 9, e110026.

YAO, Q., MAI, W., LIAN, Y., ZHANG, M., YAO, Q., HUANG, C., GE, Y. & ZHAO, Z. 2022. Emergence and Evolution of Novel Canine-Avian Reassortant H3N2 Influenza A Viruses in Duck in Leizhou Peninsula, China. *Frontiers in microbiology*, 13, 857800-857800.

YIN, X., LU, G., GUO, W., QI, T., MA, J., ZHU, C., ZHAO, S., PAN, J. & XIANG, W. 2014. Identification of equine influenza virus infection in Asian wild horses (*Equus przewalskii*). *Archives of Virology*, 159, 1159-1162.

YONDON, M., ZAYAT, B., NELSON, M. I., HEIL, G. L., ANDERSON, B. D., LIN, X., HALPIN, R. A., MCKENZIE, P. P., WHITE, S. K., WENTWORTH, D. E. & GRAY, G. C. 2014. Equine influenza A(H3N8) virus isolated from Bactrian camel, Mongolia. *Emerg Infect Dis*, 20, 2144-7.

YOON, K. J., COOPER, V. L., SCHWARTZ, K. J., HARMON, K. M., KIM, W. I., JANKE, B. H., STROHBEHN, J., BUTTS, D. & TROUTMAN, J. 2005. Influenza virus infection in racing greyhounds. *Emerg Infect Dis*, 11, 1974-6.

YUANJI , G., FENGGEN, J., PING, W., MIN, W. & JIMING , Z. 1983. Isolation of Influenza C Virus from Pigs and Experimental Infection of Pigs with Influenza C Virus. *Journal of General Virology*, 64, 177-182.

ZEBEDEE, S. L. & LAMB, R. A. 1988. Influenza A virus M2 protein: monoclonal antibody restriction of virus growth and detection of M2 in virions. *Journal of virology*, 62, 2762-2772.

ZHOU, A., DONG, X., LIU, M. & TANG, B. 2021. Comprehensive Transcriptomic Analysis Identifies Novel Antiviral Factors Against Influenza A Virus Infection. *Frontiers in Immunology*, 12.

ZHU, H., DAMDINJAV, B., GONZALEZ, G., PATRONO, L. V., RAMIREZ-MENDOZA, H., AMAT, J. A. R., CRISPELL, J., PARR, Y. A., HAMMOND, T.-A., SHIILEGDAMBA, E., LEUNG, Y. H. C., PEIRIS, M., MARSHALL, J. F., HUGHES, J., GILBERT, M. & MURCIA, P. R. 2019. Absence of adaptive evolution is the main barrier against influenza emergence in horses in Asia despite frequent virus interspecies transmission from wild birds. *PLOS Pathogens*, 15, e1007531.

ZHU, H., HUGHES, J. & MURCIA, P. R. 2015. Origins and Evolutionary Dynamics of H3N2 Canine Influenza Virus. *Journal of Virology*, 89, 5406-5418.

ZOLOTAROVA, O., BUDZANIVSKA, I., LEIBENKO, L., RADCHENKO, L. & MIRONENKO, A. 2019. Antigenic Site Variation in the Hemagglutinin of Pandemic Influenza A(H1N1)pdm09 Viruses between 2009-2017 in Ukraine. *Pathogens*, 8.

8 Appendix

Appendix 1. Buffers and media.

Name	Constituents	Use
Complete media	Dulbecco's Modified Eagle Medium (DMEM) 10% (v/v) fetal calf serum 1% (v/v) Penicillin-streptomycin made up of 10,000 U penicillin and 10 mg streptomycin/ ml 1% (v/v) L-glutamine	Tissue culture
Minimum Eagle's essential media (EMEM)	EMEM 5% FCS 1% (v/v) Penicillin-streptomycin made up of 10,000 U penicillin and 10 mg streptomycin/ ml 1% (v/v) L-glutamine 1% Non-essential amino acids	Tissue culture
Freezing media	10% DMSO 45% FBS 45% Complete medium	Tissue culture
Diluting fluid	PBS Tryptose phosphate broth Penicillin-streptomycin made up of 10,000 U penicillin and 10 mg streptomycin/ ml	Virus growth in embryonated hen's eggs
Trypsin maintenance media	125 µg/ml TPCK-trypsin Serum free DMEM	TCID ₅₀ Pseudotyping
Reduced FBS DMEM	DMEM 2% FCS 1% (v/v) Penicillin-streptomycin 1% (v/v) L-glutamine	Pseudotyping
Serum-free media	Dulbecco's Modified Eagle Medium (DMEM) 1% (v/v) Penicillin-streptomycin made up of 10,000 U penicillin and 10 mg streptomycin/ ml 1% (v/v) L-glutamine	TCID ₅₀ Pseudotyping

Coating buffer	15 mM sodium carbonate 35 mM sodium bicarbonate PBS	Anti-NP ELISA
ELISA wash buffer	PBS 0.1% Tween-20	Anti-NP ELISA
Triton X-100	PBS 0.2% Triton X-100	Anti-NP ELISA
Receptor assay coating buffer	PBS Fetuin	Receptor specificity assay
Receptor assay wash buffer	PBS 0.01% Tween 80	Receptor specificity assay
Receptor assay blocking buffer	PBS 0.1% BSA-NA	Receptor specificity assay
Receptor assay reaction buffer	PBS 0.02% Tween 80 0.1% BSA-NA 1 μ M Oseltamivir	Receptor specificity assay
HBS-EP buffer	10 mM HEPES pH 7.4 150 mM sodium chloride 3 mM EDTA 0.005% tween-20	Biolayer interferometry
LB broth	1 L ddH ₂ O 25 g LB broth (Miller)	Plasmid transformation
LB agar with ampicillin	483 ml ddH ₂ O 1.68 g tablet 100 μ g/ml ampicillin	Plasmid transformation
Tris-glycine running buffer	100 ml 10X Tris glycine 890 ml ddH ₂ O 10 ml 10% SDS	SDS-PAGE
Transfer buffer	Deionised water 10x Transfer buffer	Western blot

SOB	2% tryptone 0.5% yeast 10 mM sodium chloride 2.5 mM potassium chloride 10 mM magnesium chloride 10 mM magnesium sulphate	Making electrocompetent cells
SOC	SOB 20 mM glucose	Making electrocompetent cells
Column buffer	20 mM Tris 7.4 200 mM sodium chloride 1 mM EDTA	Protein expression and purification
Elution buffer	20 mM Tris 7.4 200 mM sodium chloride 1 mM EDTA 10 mM maltose	Protein expression and purification
Regeneration buffer	ddH ₂ O 0.1% (v/v) SDS	Protein expression and purification
VHH ELISA coating buffer	Distilled water 15 mM sodium carbonate 35 mM sodium bicarbonate	MBP VHH ELISA and Fc fused VHH ELISA
Milk blocking buffer	PBS 3% skimmed milk	MBP VHH ELISA
Binding buffer	Distilled water 12 mM sodium phosphate dibasic heptahydrate 8 mM sodium phosphate monobasic monohydrate	Protein G purification
Elution buffer	Glycine Distilled water 0.1M HCl	Protein G purification
Neutralisation buffer	Distilled water 20 mM Tris 1M HCl	Protein G purification

Appendix 2. Ion torrent barcode sequences.

Barcode ID	Sequence	Barcode ID	Sequence
>BC01	CTAAGGTAAC	>BC49	TCCTAACATAAC
>BC02	TAAGGAGAAC	>BC50	CGGACAATGGC
>BC03	AAGAGGATTC	>BC51	TTGAGCCTATTC
>BC04	TACCAAGATC	>BC52	CCGCATGGAAC
>BC05	CAGAAGGAAC	>BC53	CTGGCAATCCTC
>BC06	CTGCAAGTTC	>BC54	CCGGAGAATCGC
>BC07	TTCGTGATTC	>BC55	TCCACCTCCTC
>BC08	TTCCGATAAC	>BC56	CAGCATTAATTC
>BC09	TGAGCGGAAC	>BC57	TCTGGCAACGGC
>BC10	CTGACCGAAC	>BC58	TCCTAGAACAC
>BC11	TCCTCGAATC	>BC59	TCCTTGATGTTC
>BC12	TAGGTGGTTC	>BC60	TCTAGCTCTTC
>BC13	TCTAACGGAC	>BC61	TCACTCGGATC
>BC14	TTGGAGTGTC	>BC62	TTCCTGCTTCAC
>BC15	TCTAGAGGTC	>BC63	CCTTAGAGTTC
>BC16	TCTGGATGAC	>BC64	CTGAGTTCCGAC
>BC17	TCTATTCGTC	>BC65	TCCTGGCACATC
>BC18	AGGCAATTGC	>BC66	CCGCAATCATC
>BC19	TTAGTCGGAC	>BC67	TTCCTACCAGTC
>BC20	CAGATCCATC	>BC68	TCAAGAAGTTC
>BC21	TCGCAATTAC	>BC69	TTCAATTGGC
>BC22	TTCGAGACGC	>BC70	CCTACTGGTC
>BC23	TGCCACGAAC	>BC71	TGAGGCTCCGAC
>BC24	AACCTCATTC	>BC72	CGAAGGCCACAC
>BC25	CCTGAGATAC	>BC73	TCTGCCTGTC
>BC26	TTACAACCTC	>BC74	CGATCGGTTC
>BC27	AACCATCCGC	>BC75	TCAGGAATAC
>BC28	ATCCGGAATC	>BC76	CGGAAGAACCTC
>BC29	TCGACCACTC	>BC77	CGAAGCGATTC
>BC30	CGAGGTTATC	>BC78	CAGCCAATTCTC
>BC31	TCCAAGCTGC	>BC79	CCTGGTTGTC
>BC32	TCTTACACAC	>BC80	TCGAAGGCAGGC
>BC33	TTCTCATTGAAC	>BC81	CCTGCCATTTCGC
>BC34	TCGCATCGTTC	>BC82	TTGGCATCTC
>BC35	TAAGCCATTGTC	>BC83	CTAGGACATTC
>BC36	AAGGAATCGTC	>BC84	CTTCCATAAC
>BC37	CTTGAGAATGTC	>BC85	CCAGCCTCAAC

>BC38	TGGAGGACGGAC	>BC86	CTTGGTTATTC
>BC39	TAACAATCGGC	>BC87	TTGGCTGGAC
>BC40	CTGACATAATC	>BC88	CCGAACACTTC
>BC41	TTCCACTTCGC	>BC89	TCCTGAATCTC
>BC42	AGCACGAATC	>BC90	CTAACCACGGC
>BC43	CTTGACACCGC	>BC91	CGGAAGGATGC
>BC44	TTGGAGGCCAGC	>BC92	CTAGGAACCGC
>BC45	TGGAGCTTCCTC	>BC93	CTTGTCCAATC
>BC46	TCAGTCCGAAC	>BC94	TCCGACAAGC
>BC47	TAAGGCAACCAC	>BC95	CGGACAGATC
>BC48	TTCTAAGAGAC	>BC96	TTAAGCGGTC

Appendix 3. Scripts run for analysis of next generation sequencing data.

Step	Script name	Function	Details
1	Demultiplex.sh	Converting a fastq file to a fasta file	Seqtk seq -a Ge.fastq > Ge.fasta
2	Demultiplex2.sh	Demultiplexing a barcoded fasta file using the exact matches for the barcode sequences	Cat Ge.fasta grep -E -B 1 '^.{0,5}CTAAGGTAAC' grep - -v '—' > split_barcode_BC01.fasta
3	Reverse_complement.sh	Reverse complementing fasta files	Seqtk seq -r split_barcode01.fasta > split_barcode_BC01.rev.fasta
4	Translate.sh	Translating a single fasta file into the three reading frames	Perl translate.pl -i split_barcode_BC01.rev.fasta -s opq -f 1 > Ge_BC01.frame1.fasta Perl translate.pl -i split_barcode_BC01.rev.fasta -s opq -f 2 > Ge_BC01.frame2.fasta

			Perl translate.pl -i split_barcode_BC01.rev.fasta -s opq -f 3 > Ge_BC01.frame3.fasta
5	Cat.sh	Joining all the files into a single file	Cat Ge_BC01.frame1.fasta Ge_BC01.frame2.fasta Ge_BC01.frames.fasta >Ge_BC01.frames.fasta
6	Iterate.sh	Search for left and right motifs flanking the VHH randomised region	perl iterate_motifs.pl Ge_BC01.frames.fasta 4
7	Make_pool.sh	Pooling the negative controls for a single experiment/ round of panning to be compared against individual positive barcodes	Cat Ge_BC49.frames.fasta.LR.fa Ge_BC50.frames.fasta.LR.fa Ge_BC51.frames.fasta.LR.fa Ge_BC52.frames.fasta.LR.fa Ge_BC53.frames.fasta.LR.fa Ge_BC54.frames.fasta.LR.fa Ge_BC55.frames.fasta.LR.fa Ge_BC56.frames.fasta.LR.fa >exp1R3pDsK.pool.LR.fa

8	Comparison.sh	Comparing the frequencies of the LR.fa files defined by the user/ ranking occurrences of identical randomised regions into a table	Perl compare_collapsed_Zscore_v2.0_percentages.pl -p Ge_BC01.frames.fasta.LR.fa exp1R3pDsk.pool.LR.fa >01.table
9	Awk_Z10.sh	Filtering table data based on Z scores	awk ' NR>1 && \$4>=10 {print\$1;}' 01.table >01Z10
10	Cat2.sh	Joining all filtered tables according to their experimental rounds	cat 01Z10 02Z10 03Z10 04Z10 05Z10 06Z10 07Z10 08Z10 09Z10 >exp1R3_screen_Z10
11	Sort.sh	Determining the frequencies of each peptide $Z \geq 10$ in all the pannings and	cat exp1R3_screen_Z10 sort uniq -c sort -nr sed 's/^[t]*//' >exp1R3_screen_sorted_Z10

		sorting them numerically in descending order	
--	--	---	--

All file names are used as examples, input your own names as necessary and change the barcoded sequences in step 2 as appropriate. Make sure to change the negative controls in step 7 to match up with your own.

**Appendix 4. Sequencing of inserted VHH sequence using
MalEForward and MalEReverse primers.**

VHH A:

CAACAACAACAATAACAATAACAACAACCTCGGGATCGAGGGAAG
GATTTACATATGTCCATGGCCCAAGTTCAATTGGTAGAGTCTGGA
GGAGGTAGCGTTCAGGCGGGCGGAAGCCTGCGTTTATCGTGTAC
GGCAAGTGGGGGGTCCGAATATAGCTACAGTACGTTCTCGCTGGG
CTGGTTCCGTCAAGCGCCAGGCCAAGAGCGCGAAGCGGTGGCCG
CCATTGCAAGCATGGGGGGCCTGACATACTATGCAGATTCGGTAA
AGGGCCGCTTCACAATCAGCCGTGATAATGCTAAAAATACAGTTAC
GCTGCAAATGAACAATTTGAAGCCGGAAGACACCGCGATCTACTA
TTGCGCTGCGCACCACTACTTCCGTGCTCAGGTTCAGTCTGCTGA
ATGGGGACAAGGGACGCAGGTGACAGTTTCCTCTGGTTCTTGAGA
ATTCCCTGCAGGTAATTAAATAAGCTTCAAATAAAACGAAAGGCTC
AGTCGAAAGACTGGGCCTTTCGTTTTATCTGTTGTTTGTGCGGTGAA
CGCTCTCCTGAGTAGGACA

VHH B:

AACAATAACAATAACAACAACCTCGGGATCGAGGGAAGGATTTAC
ATATGTCCATGGCCCAAGTTCAATTGGTAGAGTCTGGAGGAGGTA
GCGTTCAGGCGGGCGGAAGCCTGCGTTTATCGTGTACGGCAAGT
GGGGGGTCCGAATATAGCTACAGTACGTTCTCGCTGGGCTGGTTC
CGTCAAGCGCCAGGCCAAGAGCGCGAAGCGGTGGCCGCCATTGC
AAGCATGGGGGGCCTGACATACTATGCAGATTCGGTAAAGGGCCG
CTTCACAATCAGCCGTGATAATGCTAAAAATACAGTTACGCTGCAA

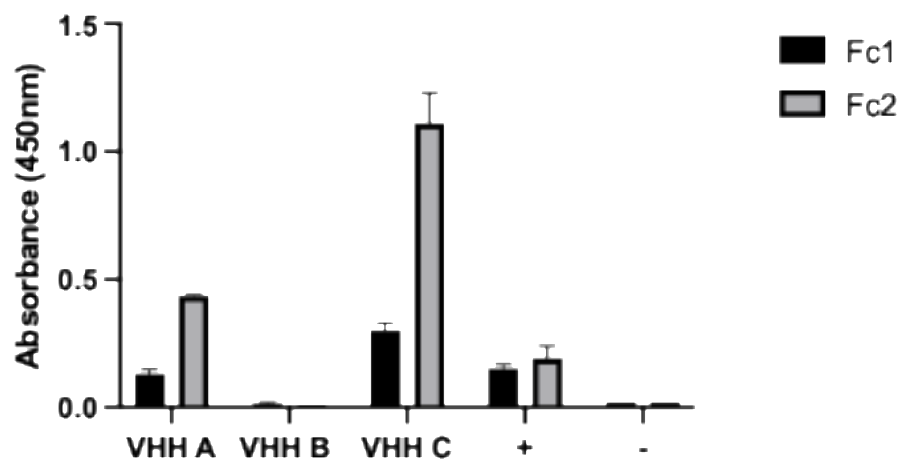
ATGAACAATTTGAAGCCGGAAGACACCGCGATCTACTATTGCGCT
GCGCCGTACTCTCGTTTTCTACGACAAACCGTACGTTACCCGTTGG
AAACACTGGGGACAAGGGACGCAGGTGACAGTTTCCTCTGGTTCT
TGAGAATTCCCTGCAGGTAATTAAATAAGCTTCAAATAAAACGAAA
GGCTCAGTCGAAAGACTGGGCCTTTCGTTTTATCTGTTGTTTGTCG
GTGAACGCTCTCCTGAGTAGGACA

VHH C:

CAGTACGTTCTCGCTGGGCTGGTTCCGTCAAGCGCCAGGCCAAGA
GCGCGAAGCGGTGGCCGCCATTGCAAGCATGGGGGGCCTGACAT
AATGCAGATTCTCGGTAAAGGGCCGCTTCACAATCAGCCGTGATA
ATGCTAAAAATACAGTTACGCTGCAAATGAACAATTTGAAGCCGGA
AGACACCGCGATCTACTATTGCGCTGCGCGTCGTTCTCTGCTGCG
TTGGACCGTTGGTCGTATGACCCGTCGTCCGTGGGGACAAGGGA
CGCAGGTGACAGTTTCCTCTGGTTCTTGAGAATTCCCTGCAGGTAA
TTAAATAAGCTTCAAATAAAACGAAAGGCTCAGTCGAAAGACTGGG
CCTTTCGTTTTATCTGTTGTTTGTCGGTGAACGCTCTCCTGAGTAG
GACA

Appendix 5. MBP VHH ELISA against rFC1 and rFC2 with ferret antisera diluted 1:100.

Colorimetric assay comparing the binding of MBP VHH A, B and C against rFC1 and rFC2. The 96-well plates were coated with rFC2 at 1 µg per well and incubated overnight. The MBP fused VHH were run in duplicate at 50 µg/ml after they were blocked with 3% milk in 1x PBS. Ferret antisera diluted 1:100 was included as a positive control (+) to confirm binding of the virus to the plate. The negative control was performed using 3% milk in 1x PBS and then anti-MBP monoclonal antibody was added. Next anti-mouse IgG HRP antibody was added for all wells and Ultra TMB ELISA substrate solution was applied to the plate. Finally, the reaction was stopped using 2M sulphuric acid and absorbance read at 450nm. The mean and standard error mean values were calculated, and the background (duplicate empty wells) was removed to standardise results. The error bars show standard error of the mean of technical replicates performed in duplicate; no biological repeats were performed.



Appendix 6. PIP reflection statement.

I spent my PIP at the Animal Plant and Health Agency (APHA) in Woking. The APHA is a government funded laboratory that falls under Department for environment food and rural affairs (DEFRA's) jurisdiction. Their focus is on surveillance and diagnostics for a range of animal related diseases. I was working in the Vector-borne diseases group. Their attention is on diseases transmitted primarily by mosquitoes and ticks. The focus of the project was tick-borne diseases and started off with processing and testing deer sera for tick-borne encephalitis virus (TBEV) and other tick-borne diseases. The first week was primarily focused on reading around the subject and then I started to extract DNA and run ELISAs on the deer samples. In the next few weeks, I processed and tested over 60 canine sera samples and 270 deer samples. The focus was on tick-borne encephalitis virus due to its importance as an emerging virus and there are growing concerns about transmission into humans especially towards those who are clinically vulnerable. During the project three cases of TBEV in humans were confirmed in the UK between 2019-2022 demonstrating the importance of surveillance.

We identified eight positive deer samples for TBEV and 20 more samples that were borderline so would require further testing to confirm. From the canine samples three produced borderline results and the rest were negative. We also tested for piroplasmosis in the DNA of the deer and identified nine positive cases of Babesiosis out of 76 samples.

Eight of which were *Babesia divergens* a parasite well documented in cattle.

The skills I worked on whilst on placement include scientific writing, problem solving, working independently and perfecting a range of laboratory-based skills. I worked on a range of methods including DNA extraction, end point PCR, q-PCR and ELISAs. I was also given the opportunity to present the data in front of colleagues within the vector-borne diseases group. The work will also be presented to members of an early career research group within the School of Veterinary Medicine and Science at Nottingham. In preparation for potential publication of this work, I also got to develop my skills using statistics and generating phylogenetic trees, a skill that will prove helpful when continuing with my PhD.

This placement has encouraged me to consider a career outside of academia. Not only has the atmosphere been friendly from within the team I have been part of but also from other teams on site. I also enjoyed studying an area that is different to that of my PhD and has encouraged me to look at other areas of virology not just influenza post PhD. The APHA also has some bonuses in that they do in house sequencing which reduces wait times on results. There is also the opportunity to get training to work in containment and work within the insectary. I have also enjoyed doing surveillance of diseases not just focusing on the research behind diseases.

The work from this placement will be reported back to stakeholders on Exmoor to inform them of the prevalence of tick-borne diseases on Exmoor within the deer population. It will also help with monitoring tick-borne diseases on Exmoor as a whole because deer can be reservoirs for disease, can act as transport vessels for ticks and provide a feeding source for ticks. All the data from this project will also link with other projects within the vector-borne diseases group looking at surveillance of tick-borne diseases.